

R.H.C. LIBRARY	
Class	541
No.	.4
ACC. No.	HOD
Date ACQ.	6.16.114

CHEMICAL IONIZATION MASS SPECTROMETRIC  
ANALYSIS OF LUBRICATING OILS AND THE  
KINETICS OF SOME ASSOCIATED ION-MOLECULE  
REACTIONS.

A Thesis submitted for the  
degree of Doctor of Philosophy  
of the University of London.

by

Michael Graham Hodges.

Chemistry Department  
Royal Holloway College  
University of London.

April 1984.

ProQuest Number: 10097861

All rights reserved

INFORMATION TO ALL USERS

The quality of this reproduction is dependent upon the quality of the copy submitted.

In the unlikely event that the author did not send a complete manuscript and there are missing pages, these will be noted. Also, if material had to be removed, a note will indicate the deletion.



ProQuest 10097861

Published by ProQuest LLC(2016). Copyright of the Dissertation is held by the Author.

All rights reserved.

This work is protected against unauthorized copying under Title 17, United States Code.  
Microform Edition © ProQuest LLC.

ProQuest LLC  
789 East Eisenhower Parkway  
P.O. Box 1346  
Ann Arbor, MI 48106-1346

ABSTRACT

Selection of suitable reagent gases and ion-source pressures can lead to formation of mono-ionic plasmas for chemical ionization. If sample ionization occurs by a single mechanism, discrimination between chemically different components in mixtures is possible. This has permitted the analysis of specific components in lubricating base oils. Ammonia chemical ionization of esters, at ammonia pressures, ca. 0.6 Torr, leads only to the formation of the cluster ions  $(M.NH_4)^+$ . These conditions have been used to analyse aviation lubricant esters.

A method for ion-source pressure determination, of ammonia, directly from the abundance of  $NH_2^+$ ,  $NH_3^+$  and  $NH_4^+$  plasma ions was developed from data obtained in a study of ion-molecule reactions consequent upon its electron-impact ionization.

The collision-stabilized  $NO^+$  ion, generated from nitrogen-nitric oxide mixtures was used to ionize synthetic hydrocarbon lubricants; semi-quantitative determination of components were obtained. Aromatic components in mineral oils, with ionization potentials  $<9.1$  eV, were preferentially ionized by the fluorobenzene molecular ion. The rates of reaction of selected aromatic compounds with fluorobenzene molecular-ion have been determined to permit quantitation. Good agreement

with calculated collision rates (ADO) suggests a direct charge transfer mechanism.

The dependence of ion-abundances of primary ions derived from several fluorinated benzenes have been investigated at ion-source pressures between 0.01 and 0.25 Torr.

ACKNOWLEDGEMENTS

I wish to thank my supervisor, Dr R A Hancock for his unflagging support, encouragement and enthusiasm for the work.

The research would not have been possible without modification and maintenance of the mass spectrometer.

I am grateful to Mr Brian Smethurst, Ray Lane and all the workshop staff for their excellent work in this area. The support of the SERC and Burmah Castrol

is gratefully acknowledged, and in particular Dr S R Wallis and Dr H Askew for the industrial connection.

I am grateful to Mrs S Partin for typing a seemingly never ending manuscript.

I also wish to express my gratitude to my parents for their continual encouragement, and in particular my father for drawing many of the diagrams.

Last but not least, I thank Sian for her continual support and proof reading of the thesis.

CONTENTS

	<u>Page</u>
1. INTRODUCTION	
1.1 <u>Industrial Introduction</u>	
1.1.1. Lubrication and the composition of fluids used as lubricant base oils.	20
1.1.2. Composition and physical properties of fluids used as lubricant base oils.	26
1.1.3. Methods currently used in the analysis of lubricant base oils.	33
1.1.3.1. Mass spectrometric methods excluding GCMS.	36
1.1.3.2. Methods requiring prior separation.	38
1.2 <u>General Aspects of ion-molecule interactions</u>	
1.2.1. The use of mass spectrometers in the generation, analysis and detection of ions.	41
1.2.2. Reaction between ions and molecules in the gas phase.	45
1.2.3. Chemical ionization mass spectrometry.	48
1.2.4. Some current mechanisms of bimolecular ion-molecule reactions.	51
1.2.4.1. Fast exchange reactions,	52
1.2.4.2. Slow exchange reactions.	52
1.2.4.3. Association reactions,	54
1.2.5. Study of ion-molecule reactions and evaluation of rate coefficients.	
1.2.5.1. Reasons for the study of ion-molecule reactions.	55
1.2.5.2. Methods for the study of the kinetics of ion-molecule reactions.	56
1.2.5.3. The use of continuous ion-extraction mass spectrometry for the evaluation of rate coefficients of ion-molecule reactions.	56
1.3 <u>Chemical ionization mass spectrometry in the analysis of complex mixtures without the need for prior separation.</u>	61
1.3.1. Mixtures containing compounds of the same chemical type.	61

CONTENTS (continued) -	<u>Page</u>
1.3.1.1. The use of methane, nitric oxide and nitric oxide/nitrogen mixtures as reagent gases in the chemical ionization of hydrocarbons.	62
1.3.1.2. Ammonia chemical ionization reagent gas.	64
1.3.2. Mixtures containing compounds of more than one chemical type.	66
1.3.2.1. Selective positive ion chemical ionization.	66
1.3.2.2. Selective negative ion chemical ionization.	68
 2. EXPERIMENTAL	
2.1 <u>Materials</u>	
2.1.1. Reagent gases	
2.1.1.1. Cylinder gases.	70
2.1.1.2. Reagent gases which are liquids at standard temperatures and pressures.	70
2.1.2. Mass spectrometry standards	70
2.1.3. Preparation of esters	
2.1.3.1. Esters of dibasic acids.	71
2.1.3.2. Esters of 2,2-bis(hydroxymethyl)propane-1,3-diol and 2-ethyl-hydroxymethylpropane-1,3 diol.	71
2.1.4. Other chemicals.	73
2.2 <u>The V.G. Micromass 12F spectrometer</u>	76
2.2.1. Modifications to the reagent gas inlet system to facilitate the introduction of ammonia, nitric oxide and reagent gases which are liquids at S.T.P.	83
2.3 <u>Measurement of pressures of gases in the ion-source</u>	88
2.3.1. The pressure gauge.	88
2.3.2. Connection of the pressure gauge to the ion-source.	88
2.3.3. Evaluation of the pressure gauge when coupled to the ion-source.	92
2.3.4. Measurement of reagent gas pressures in the ion-source.	93
2.3.5. Measurement of pressures in the ion-source due to samples introduced through the septum-inlet system.	94

CONTENTS (continued) -	<u>Page</u>
<u>2.4 Kinetic Studies</u>	
2.4.1. Measurement of ion-abundances: The ion-molecule reactions consequent upon the electron impact of pure reagent gases.	95
2.4.1.1. Methane.	95
2.4.1.2. Iso-butane.	96
2.4.1.3. Methylcycloalkanes.	97
2.4.1.4. Ammonia.	97
2.4.1.5. Fluorinated benzenes.	98
2.4.2. Measurement of ion-abundances in the ion-molecule reactions which give rise to the chemical ionization mass spectra of hydrocarbons when fluoro-benzene is the reagent gas.	98
<u>2.5 Lubricant base oil analysis</u>	100
2.5.1. Ester fluids.	101
2.5.2. Synthetic hydrocarbon fluids.	
2.5.2.1. Hydrogenated polyalphaolefins.	101
2.5.2.2. Synthetic aromatic hydrocarbon fluids.	102
2.5.3. Mineral oil fractions.	102
3. RESULTS	
<u>3.1. Kinetic Studies</u>	
3.1.1. Determination of a rate coefficient to assess interfacing of pressure gauge to ion-source.	104
3.1.2. Ion molecule reactions in reagent gas plasmas of:-	
3.1.2.1. Iso-butane.	111
3.1.2.2. Methylcyclopentane.	118
3.1.2.3. Methylcyclohexane.	127
3.1.2.4. Ammonia.	135
3.1.3. Fluorinated reagent gases.	141
3.1.3.1. Fluorobenzene.	141
3.1.3.2. Difluorobenzenes.	146
3.1.4. The chemical ionization mass spectra of selected aromatic compounds; changes of relative ion-abundances with variation of sample pressure.	155
<u>3.2. Chemical ionization mass spectra of lubricant base oils.</u>	
3.2.1. Ester base oils.	161
3.2.1.1. Dibasic acid esters.	161
3.2.1.2. Synthetic blends of dibasic acid esters.	164



CONTENTS (continued) -	Page
3.2.1.3. Esters of neopentyl polyols.	168
3.2.1.4. Lubricants. Ester lubricant blending component 'A'.	168
3.2.2. Hydrogenated polyalpha-olefin base oils.	172
3.2.2.1. Methane chemical ionization (CI) of hydrogenated polyalpha-olefine base oils.	172
3.2.2.2. Nitric oxide chemical ionization of hydrogenated polyalpha-olefin base oils.	181
3.2.2.3. Nitrogen/nitric oxide mixture chemical ionization of hydrogenated polyalpha-olefin base oils.	181
3.2.3. Synthetic aromatic hydrocarbon lubricants.	186
3.2.4. Fluorobenzene chemical ionization mass spectrometry of mineral oil lubricant base oils.	189
4. DISCUSSION	
4.1. <u>Reactions in hydrocarbon reagent gases.</u>	
4.1.1. Iso-butane.	196
4.1.2. Dependence of rate coefficients on ion stability and structure of neutrals.	197
4.1.3. A method of estimation of ion-source pressures for methylcycloalkane reagent gases.	203
4.2. <u>Mechanisms and evaluation of disappearance rate coefficients for reactions of ions in the ammonia reagent gas plasma.</u>	205
4.2.1. Reaction of primary ions from ammonia with ammonia.	205
4.2.2. Reaction of $\text{NH}_4^+$ with ammonia.	218
4.2.3. A simple method for estimation of ion-source pressures of ammonia for CIMS.	
4.2.3.1. For ammonia pressures less than 0.1 Torr.	227
4.2.3.2. For ammonia pressures greater than 0.1 Torr.	229
4.3. <u>Mechanisms of the reaction of ions in fluorinated benzene reagent gas plasmas.</u>	
4.3.1. Fluorobenzene.	231
4.3.2. Difluorobenzene.	240
4.4. <u>Significance of relative rates of reaction of the fluorobenzene reagent gas molecular ion (<math>\text{C}_6\text{H}_5\text{F}^+</math>) with aromatic compounds.</u>	245

CONTENTS (continued) -	<u>Page</u>
4.5. <u>Chemical ionization mass spectrometric analysis of lubricant base oils.</u>	
4.5.1. Ester base oils.	260
4.5.2. Hydrogenated polyalpha-olefin base oils.	269
4.5.3. Synthetic aromatic hydrocarbon lubricants.	279
4.5.4. Mineral oil analysis.	283
APPENDIX	
I. <u>Polarizabilities and dipole moments of organic molecules.</u>	288
II. <u>The computer data acquisition system.</u>	291
III. <u>Chemical and spectroscopic data of esters prepared as standards for ammonia CIMS.</u>	295
REFERENCES	300

<u>LIST OF TABLES</u>	<u>Page</u>
1.1 Composition of a typical multigrade automotive lubricant.	23
1.2 Composition of a typical jet aviation engine lubricant.	25
1.3 Synthetic lubricant base oils.	27
2.1 Esters of dibasic acids.	72
2.2 Tri-esters of 2-ethyl-2-hydroxymethylpropane-1,3-diol.	74
2.3 Tetra-esters of 2,2-bis(hydroxymethyl)propane-1,3-diol.	75
2.4 Conditions used in the chemical ionization mass spectrometry of the base oils.	103
3.1 Rates of reaction of $\text{CH}_4^+$ with methane at various ion-source field strengths.	110
3.2 Rate coefficients for the reaction of primary ions from iso-butane with iso-butane.	117
3.3. Rate coefficients for the reaction of primary ions for methylcyclopentane with methylcyclopentane.	126
3.4 Rate coefficients for the reaction of primary ions from methylcyclohexane with methylcyclohexane.	134
3.5 Rate coefficients for the reaction of primary ions from fluorobenzene with fluorobenzene.	147
3.6 Rate coefficients for the reaction of primary ions from difluorobenzenes with difluorobenzenes.	150
3.7 Relative abundances of ions in p-difluorobenzene at various pressures.	152
3.8 Relative abundances of ions in m-difluorobenzene at various pressures.	153

<u>LIST OF TABLES</u> (continued) -	<u>Page</u>
3.9 Relative abundances of ions in o-difluorobenzene at various pressures.	154
3.10 Ion abundances in fluorobenzene chemical ionization of alkylbenzenes.	159
3.11 Ion abundances in fluorobenzene chemical ionization of aromatics.	160
3.12 Relative abundances of ions resulting from ammonia CI of dibasic acid esters.	162
3.13 Fragmentation of protonated $(M + H)^+$ and ammoniated $(M + NH_4)^+$ ions of dibasic esters. ( $P_{NH_3} = 0.2$ Torr).	165
3.14 Blends of synthetic ester standards.	167
3.15 Proportion of sample ion current associated with the ammoniated $(M + NH_4)^+$ ion in the ammonia chemical ionization spectra of esters (M) of neopentyl polyols.	169
3.16 Relative abundances of principal ions observed in the ammonia chemical ionization mass spectra of esters lubricating blending component 'A'.	171
3.17 Identities assigned to components observed in blending component 'A'.	171
3.18 Principal $(M + 1)^+$ ions from methane CI of synthetic hydrocarbon lubricant base oils.	175-177
3.19 Variation in relative abundances of fragment ions in the methane chemical ionization mass spectra of various hydrogenated polyalpha-olefin base oils.	179-181
3.20 Mass to charge ratios (m/z) of the principal ions observed in the fluorobenzene and NO/N <sub>2</sub> CI mass spectra of the synthetic base oils SAH1.	187

<u>LIST OF TABLES</u> (continued) -	<u>Page</u>
3.21 Mass to charge ratios (m/z) of the principal ions observed in the fluorobenzene CI of the synthetic base oils.	188
3.22 Weight percents of aromatic components in MIN.1.	192
3.23 Weight percents of aromatic components in MIN.1.	193
3.24 Percent weight aromatic carbon in MIN.1.	195
4.1 Comparison of the rates of reaction of primary ions of same mass to charge ratios with reagent gases iso-butane, methylcyclopentane, and methylcyclohexane.	200
4.2 Reaction of $\text{NH}_3^+$ with ammonia.	208
4.3 Reaction of $\text{NH}_2^+$ with ammonia.	209
4.4 Reaction of $\text{NH}^+$ with ammonia.	210
4.5 Variation of $k'_{17} + k'_{-17}$ with ion-source field strength.	216
4.6 Variation of $(k'_{16} + k'_{-16})$ with ion-source field strength.	216
4.7 Third and second order rate coefficients for the reaction of $\text{NH}_4^+$ with $\text{NH}_3$ at various ion-source field strengths.	226
4.8 Rate coefficients for reaction of $\text{C}_6\text{H}_5\text{F}^+$ with alkyl benzenes.	250
4.9 Rate coefficients for reaction of $\text{C}_6\text{H}_5\text{F}^+$ with other aromatic compounds.	251
4.10 Structural information gained from methane chemical ionization mass spectrometry of hydrogenated polyalpha-olefins base oils.	274-276

## APPENDIX I

Polarizabilities and dipole moments of organic molecules. 289-291

## APPENDIX III Synthetic esters.

III.1 Compound identity and elemental analysis. 296-297

III.2 60 MHz NMR Data. 298-299

<u>LIST OF DIAGRAMS</u>	<u>Page</u>
1.1 Schematic diagram of mass spectrometer. Schematic potential energy diagrams.	42
1.2 Fast ion-molecule reactions.	53
1.3 Slow ion-molecule reactions.	53
1.4 Ionization potentials of some hydrocarbons.	67
1.5 Zinc dialkyldithiophosphate.	69
2.1.a Schematic drawing of ion-source.	77
2.1.b Connections to ion-source.	77
2.2 Schematic diagram of septum-inlet system.	79
2.3 Probe used to connect pressure gauge to ion-source.	79
2.4 V.G. Reagent gas inlet system.	84
2.5 Modified reagent gas inlet system.	86
2.6 Vapour line.	87
2.7 Baratron capacitance manometer pressure measurement system.	89
2.8 Probe assembly used to couple Baratron head to the ion-source.	91
3.1 Kinetic plot for the reaction $\text{CH}_4^+ + \text{CH}_4 \xrightarrow{k} \text{CH}_3 + \text{CH}_5^+$ .	107
3.2 Variation of ion abundance with ion-source pressure for iso-butane gas.	112
3.3 Kinetic plot for reaction of ions from iso-butane with iso-butane.	115
3.4 Fragmentation of iso-butane consequent upon electron impact ionization.	116

<u>LIST OF DIAGRAMS</u> (continued) -	<u>Page</u>
3.5 Postulated pathways to formation of primary ions from methylcyclopentane commensurate upon electron impact.	119
3.6 Variations in abundances, with ion-source pressure, of the principal ions in methylcyclopentane.	120
3.7 Variation in abundances of minor ions in methylcyclopentane as a function of ion-source pressure.	121
3.8 Kinetic plot for reaction of some primary ions from methylcyclopentane with methylcyclopentane.	124
3.9 Kinetic plots for reaction of other primary ions from methylcyclopentane with methylcyclopentane.	125
3.10 Possible pathways of fragmentation of methylcyclohexane consequent upon electron impact.	128
3.11 Variation in ion-abundances of ions, in methylcyclohexane reagent gas as a function of ion-source pressure (Part 1).	129
3.12 Variation in ion-abundances of ions, in methylcyclohexane reagent gas as a function of ion-source pressure (Part 2).	130
3.13 Kinetic plot for reaction of primary ions from methylcyclohexane with methylcyclohexane. (Part 1).	132
3.14 Kinetic plot for reaction of primary ions from methylcyclohexane with methylcyclohexane. (Part 2).	133
3.15 Variation in ion-abundance in ammonia reagent gas with ion-source pressure.	136
3.16 Kinetic plots for reaction of primary ions from ammonia with ammonia; Ion-source field strength $7.5 \text{ V cm}^{-1}$ .	138
3.17 Kinetic plot for reaction of $\text{NH}_4^+$ with ammonia at various ion-source field strengths.	140



<u>LIST OF DIAGRAMS</u> (continued) -	<u>Page</u>
3.18 Postulated fragmentation of fluorobenzene consequent upon electron-impact ionization.	142
3.19 Variation in ion-abundances in the fluorobenzene reagent gas as a function of ion-source pressure; Part 1 non cluster ions.	144
3.20 Variation in ion-abundances in the fluorobenzene reagent gas as a function of ion-source pressure; Part 2 cluster ions.	145
3.21 Postulated fragmentation of o-difluorobenzene consequent upon electron impact ionization.	148
3.22 Increase in abundance of the cluster ion $m/z = 189$ commensurate with the decrease in abundance of primary ion $m/z = 75$ in difluorobenzene.	151
3.23 Variation in reactant and product ion abundances for reaction of fluorobenzene molecular ions ( $m/z = 96,97$ ) with methylbenzene as a function of methylbenzene ion-source pressure.	157
3.24 Methane chemical ionization spectra of synthetic hydrocarbon base oil SHC-7	174
3.25 Nitric oxide chemical ionization mass spectra of SHC-22.	183
3.26 Comparison of chemical ionization spectra of SHC-11 recorded using $N_2$ /nitric oxide reagent gas or methane reagent gas.	184
3.27 Nitric oxide/nitrogen chemical ionization mass spectrometric analysis of SHC-30.	185
3.28 Fluorobenzene chemical ionization mass spectra of mineral oils.	190

<u>LIST OF DIAGRAMS</u> (continued) -	<u>Page</u>
4.1 Energy profile for hydride transfer reaction of primary ions in alkyl and cycloalkyl reagent gases.	202
4.2 Variation in rates of reaction of primary ions from ammonia with ammonia as a function of ion-source field strength.	212
4.3 Semi-equilibrium plot for reaction of primary ion $\text{NH}_3^+$ with ammonia.	215
4.4 Variation of abundance of primary ion $m/z = 75$ and cluster ion $m/z = 171$ , with ion-source fluorobenzene pressure.	233
4.6 Kinetic plot for reaction of two species with the same mass to charge ratio but different rates of reaction.	242
4.5 Tailing of ion abundance profile of peak $m/z = 96$ resulting from collision dissociation of cluster ions in the vicinity of the ion-source exit slit.	238
4.7 Kinetic plot for reaction of fluorobenzene molecular-ion with methylbenzene.	249
4.8 Variation in rate coefficient for reaction of fluorobenzene molecular-ion with various aromatic compounds as a function of difference in ionization energy.	255
4.9 Variation in collision efficiency as a function of difference in ionization energy, for reaction of fluorobenzene molecular ion with aromatic compounds.	256
5.11.1 Computer data system: Hardware.	292

<u>LIST OF SCHEMES</u>	<u>Page</u>
1.1 Thermal degradation of esters with beta hydrogens.	31
1.2 Production of lubricant fractions from crude oil.	32
3.1 Ammonolysis of dibasic acid esters.	116
4.1 Mechanism of reaction of primary ions with fluorobenzene.	232
4.2 Formation of cluster ions in fluorobenzene reagent gas.	235
4.3 Cluster ions containing two fluorbenzene molecules.	239
4.4 Fragmentation of poly-7-methyl-non-1-ene.	271
4.5 Fragmentation of poly-2-methyl-prop-1-ene.	273
4.6 Chemical structures of synthetic aromatic lubricant components.	280

## 1.1 INDUSTRIAL INTRODUCTION

### 1.1.1 Lubrication and the composition of lubricating oils.

A lubricant, derived from lubricare - meaning to make slippery, is a substance that reduces friction and resulting wear, between two sliding surfaces. It can be solid, liquid (studied in this work) or gas.

Examples of lubricants are to be found in nature, e.g. the synovial fluids in the joints of mammals. Pre-historic man used mud and reeds to lubricate sledges used for dragging game or timbers and rock for building. Animal fats were the first lubricants used on the axles of carts and continued in wide use until the petroleum industry arose in the late nineteenth century. Thereafter the majority of lubricants have been based on cheaper and more readily available mineral oil products with superior lubricating properties. However esters based on naturally occurring fats including mono-, di-, and triglycerides derived from transesterification or glycerolysis of lauric, tallow and vegetable oils are still used extensively in the lubrication of food-processing machinery<sup>1</sup> where the possibility of contact between food and lubricant prevents the use of many petroleum based materials. More recently, with the advent of the jet engine, resulting in the need for greater thermal and oxidative stability, there is a trend toward the use of synthetic lubricants. However these are more expensive than mineral oils and are used where higher performance is

required, e.g. modern turbo-fan jet engines.

During the lubrication process a pressure is developed within the lubricant. This pressure balances that applied to the two sliding surfaces maintaining the lubricant film and lowering the friction between them. The pressure being generated either externally by pumps, "hydrostatic lubrication" or by virtue of the shape of the two surfaces, "hydrodynamic lubrication"\*. The ability of an oil to lubricate when the applied pressure is high is defined as its "load carrying capacity". In order to function well the viscosity of liquid lubricants should not vary greatly with temperature; the variation of viscosity with temperature is defined by the "viscosity index" (VI). (A large value of VI corresponds to a small change in viscosity with temperature). As well as retaining a desirable viscosity under normal operating conditions the temperature at which a lubricant ceases to flow, the "pour point", should be as low as possible in order that difficulty is not encountered when starting cold machinery. (e.g. Canadian winter temperatures are often below  $-20^{\circ}\text{C}$  requiring automobile crankcase lubricants with low pour points in order that initial engine turn-over may be achieved by the starter motor and that good lubrication is achieved well before the engine has reached its normal operating temperature). In addition to lowering friction between two surfaces lubricants should have good resistance to thermal or

---

\* A more full description of lubrication theory may be found in "Lubrication and friction", see Ref.2.

oxidative degradation and aid in the prevention of corrosion. The need to enhance these properties and simultaneously protect the oil against adverse working environments led to the use of additives. Additives to reduce oxidation, to inhibit corrosion of metal surfaces, to improve the viscosity index and load carrying capacity, and to aid the dispersion of solid materials in total now account for 15% of the weight of a typical automotive lubricating oil. (See tables (1.1)).

The base oils that are the subject of this study find principal uses in (i) automotive and (ii) aviation lubricants. These applications are now discussed separately.

Until recently automotive oils were based almost entirely on mineral oils. However present engines, designed to enhance fuel economy requiring higher operating temperatures, demand an improved performance of their lubricants. Many manufacturers of lubricating oils are now partly or totally replacing mineral oils by synthetic materials (principally hydrogenated polyalphaolefins, see(1.1.2) and esters of dibasic acids, See(1.1.2)) to give higher thermal and oxidative stability, improve viscosity index and lower pour point.<sup>3</sup> Additives are still required, in the same concentrations, to reduce corrosion, wear and oxidation but lower concentrations of viscosity index improver and pour point depressant are required with synthetic oils. The composition of a typical multigrade automotive oil is given in table (1.1).

**TABLE 1.1** Composition of a typical multigrade automotive lubricant.

Component	Weight %	Chemical composition
Detergent/ dispersants ) a	10-15	Ca, Mg, Ba Phenates/sulphonates
Viscosity index Improver	10 <sup>b</sup>	Various polymers
Antioxidant/ antiwear	~ 1	Zinc dialkyl/diaryl-dithiophosphates
Other antioxidants	- Various	not necessarily present
Extreme pressure additives	0.1	Sulphur and phosphorus compounds
Base oil	to >80%	(i) Mineral oil (ii) Synthetic hydrocarbons/esters or mixtures with mineral oil

(a) Gasoline and diesel engine lubricants differ in the ratio quantity and type of dispersant/detergent.

(b) Less if synthetic base oil used.

The main requirement of aviation engine lubricants is good thermal stability at the high operating temperatures at which the oil must function. (Hot spots up to 300°C). This has been achieved through the use of highly stable (thermally stable to 340°C)<sup>4</sup> synthetic esters of neopentyl polyols (see 1.1.2). As weight is an important factor in aero-engine design, gear surfaces are minimised and thus high load carrying capacities are required. Jet engine oils are unlike their automotive counterparts being drained far less frequently and continuously vented to the atmosphere, the lubricant tanks being topped up after each flight. It is important therefore to minimise the formation of sludge and other deposits, which would build up in the oil circulation piping, as this leads to the need for costly engine overhauls. Modern airlines, travelling between areas of markedly differing climates require oils for their aircraft with similar viscosities at starting temperatures varying between -20 and +35°C whilst retaining suitably high viscosities at normal operating temperatures. Although esters of neopentyl polyols have high thermal stability and exhibit high viscosity indices, additives are still needed as illustrated by the typical aviation oil formulation shown in table (1.2).



TABLE 1.2

Composition of a typical jet aviation engine lubricant

Component	Weight %	Chemical composition
Antioxidant (two types)	~1% of each	(i) Hindered phenols 2,6-ditertiary butyl-4- methyl phenol  (ii) Aromatic amines e.g. phenyl- $\alpha$ -naphthylamine
Anti-wear/ extreme pressure	2 - 3	Complex additive mixtures e.g. substituted phosphate esters
Corrosion inhibitor  (may also have anti- wear properties)	0.2 or less	
Anti-foam agent	~25 ppm	Polysiloxane
Base oil	to >90%	(i) Dibasic acid ester ("Type I lubricants")  (ii) Esters of neopentyl polyols ("Type II lubricants")

1.1.2 Composition and physical properties of fluids used as lubricant base oils.

Two types of synthetic hydrocarbon find application as fluids for lubricant base oils (a) hydrogenated polyalphaolefins and (b) synthetic aromatic hydrocarbons. Polyalphaolefins are prepared by the controlled oligomerization of alphaolefins (typically of carbon number 8,10 or 12) using cationic or Ziegler type catalysts<sup>5</sup> resulting in fluids which are mixtures of products up to a degree of polymerisation, ca 5. Mixtures of alphaolefin of differing carbon chain length may be used to increase the number of components in the resulting fluid and thus reduce the pour point of the final lubricant base oil. Hydrogenation, and distillation to obtain fluids of desired viscosities results in lubricants (see table 1.3) which show greater thermal and oxidation stability, higher viscosity index and lower pour point than refined mineral oils. The thermal stability is ascribed to the inertness of saturated aliphatic hydrocarbons and the enhanced viscosity properties to the ability of long alkyl chains to uncoil and recoil as the temperature is raised and lowered. Synthetic aromatic hydrocarbons are normally prepared by Friedel Crafts condensations of benzene or toluene with alkyl chlorides or chlorinated alkyl aromatics (e.g. 2-Chloroethyl- benzene) to multi-substituted alkyl or alkyl-aryl aromatics as shown in table (1.3). Although these have better low temperature properties than refined

TABLE 1.3 Synthetic lubricant base oils

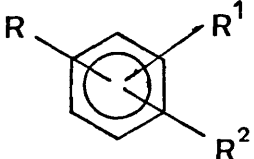
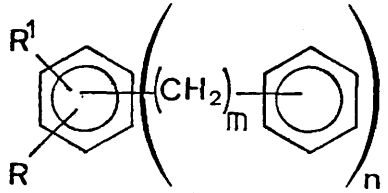
Type of fluid	Structure
Hydrogenated polyalpha olefins	$  \begin{array}{c}  R - C - (CH_2 - C)_n - R^2 \\    \qquad \qquad   \\  CH_3 \qquad \qquad R^1  \end{array}  $ <p> <math>n = 1, 5</math>  <math>R, R^1, R^2</math> various saturated alkyl chains         </p>
Alkyl aromatics	 <p> <math>R, R^1, R^2</math> may be saturated alkyl chains or alkyl aromatics         </p>
Aryl and alkylaryl aromatics	 <p> <math>m = 0-2, \quad n = 1-4</math>  <math>R</math> and <math>R^1</math> normally H or <math>CH_3</math> </p>
Dibasic acid esters	$R - O - \overset{O}{\parallel} C - (CH_2)_n - \overset{O}{\parallel} C - O - R^1$ <p> <math>R</math> and <math>R^1</math> are saturated groups  <math>R^1 = R^2</math> or <math>R^1 \neq R^2</math>  <math>n = 4 - 7</math> </p>

TABLE 1.3 Synthetic lubricant base oils (continued)

Type of fluid	Structure
Esters of neopentyl polyols	$  \begin{array}{c}  \text{CH}_2 \text{---} \text{O} \text{---} \overset{\text{O}}{\parallel} \text{C} \text{---} \text{R}^1 \\    \\  \text{R} \text{---} \text{C} \text{---} \text{CH}_2 \text{---} \text{O} \text{---} \overset{\text{O}}{\parallel} \text{C} \text{---} \text{R}^2 \\    \\  \text{CH}_2 \text{---} \text{O} \text{---} \overset{\text{O}}{\parallel} \text{C} \text{---} \text{R}^3  \end{array}  $
	<p>R may be <math>\text{CH}_3</math>, <math>\text{C}_2\text{H}_5</math></p>
	<p>or <math>\text{R}^4 \text{---} \overset{\text{O}}{\parallel} \text{C} \text{---} \text{O} \text{---} \text{CH}_2 \text{---}</math></p>
	<p><math>\text{R}^1, \text{R}^2, \text{R}^3, \text{R}^4</math> are saturated alkyl groups and may be the same or different.</p>

mineral oils they are not widely used in synthetic lubricants.

Synthetic ester fluids include (a) esters of dibasic acids and (b) esters of the polyols 2-ethyl-2-hydroxymethylpropane-1,3-diol and 2,2-bis(hydroxymethyl)propane-1,3-diol. Dibasic acid esters are prepared from either normal or branched-chain alcohols (Carbon number 8-13) and acids of carbon number 6 to 9. Several different alcohols may be used concurrently for esterification resulting in a lubricant which is a complex mixture of Nd different esters. Nd is given by equation (1.1.1) for  $n > 1$

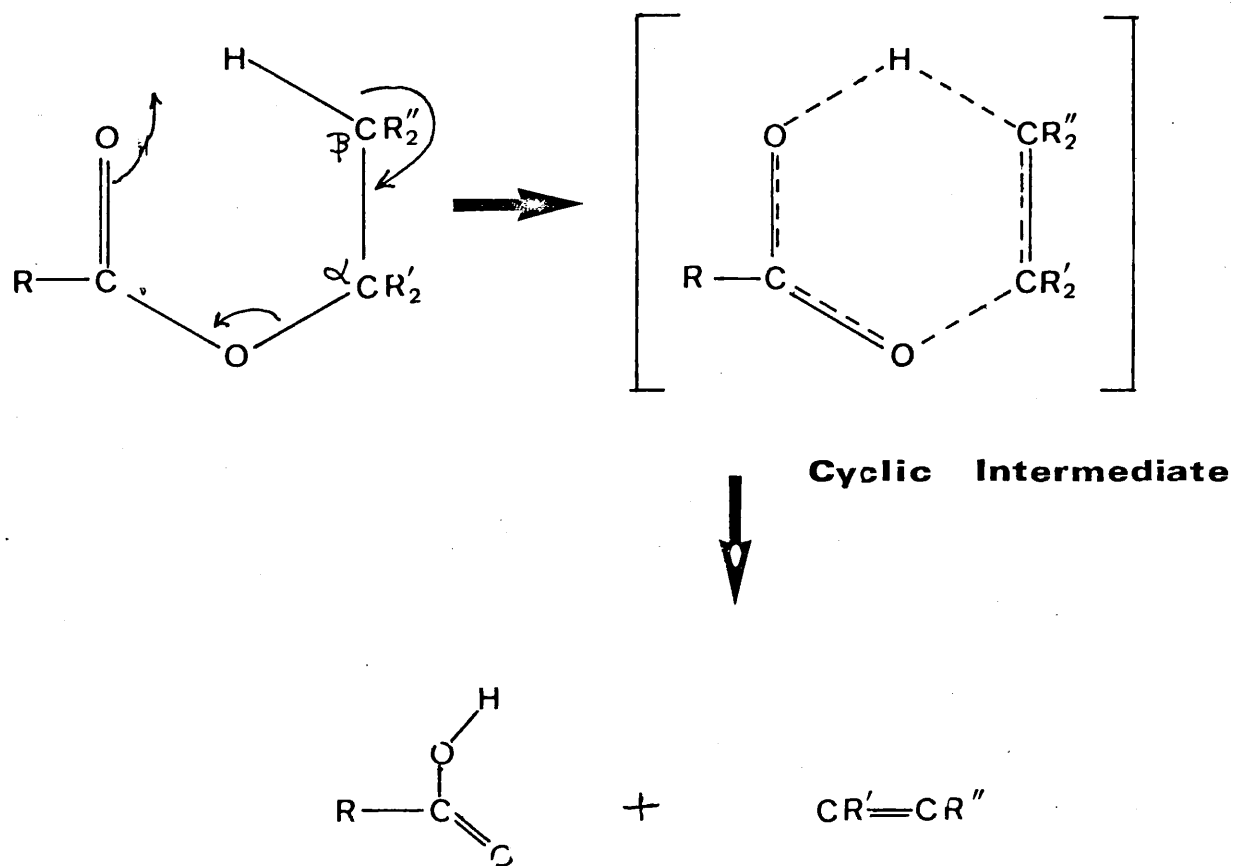
$$N_d = \frac{(n + 1)!}{2! (n - 1)!} \quad \text{--- (1.1.1)}$$

where n is the number of different alcohols. Dibasic acid esters are characterised by good thermal stability up to 250°C<sup>5</sup> Polyol esters may be prepared from saturated normal or branched-chain aliphatic monocarboxylic acids with the neopentyl polyols, 2-ethyl-2-hydroxymethylpropane-1,3-diol and 2,2-bis(hydroxymethyl)propane-1,3-diol. The use of more than one acid (n) or polyol in the esterification gives a base oil containing several (N) esters which results in a low pour point.<sup>6</sup> N is the sum of the number of different esters (Nr) resulting from each polyol having r hydroxyl groups, esterified by n different monobasic acids.

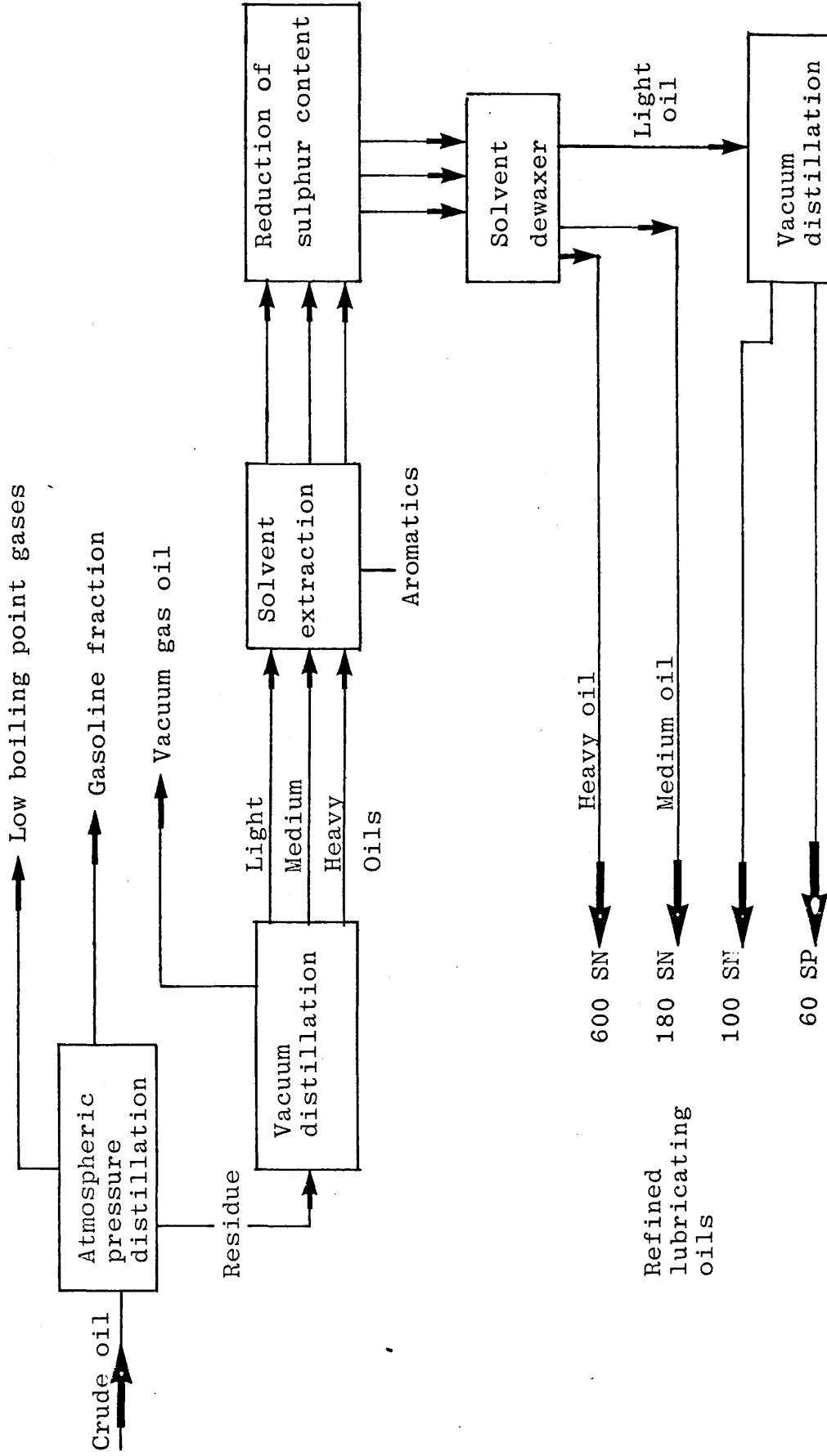
$$N_r = \frac{(n + r - 1)!}{r! (n - 1)!} \quad \text{--- (1.1.2)}$$

The alcoholic portions of these esters have no hydrogens on their beta carbons and as a result, cannot undergo degradations by the mechanism<sup>5</sup> shown in scheme (1.1). This explains their high thermal stability (stable up to 340°C).

Refined mineral oils used as lubricants are obtained by the methods illustrated in scheme (1.2). They are complex mixtures of typically aliphatic (20-45%) alicyclic (20 - 45%) and aromatic (10 - 40%) hydrocarbons. Compounds containing sulphur, oxygen and nitrogen are not believed to be present in appreciable quantities (~ 1%). Most sulphur containing compounds are deliberately removed during refining otherwise undesirable corrosive compounds would be formed, from their degradation, during the lifetime of the lubricant. The aliphatic components consist of branched-chain alkanes; much of the straight chain wax type materials present in unrefined oil are removed to lower the pour point and improve the viscosity index of the fluid. Little is known about the alicyclic portion of the refined oil but it is believed to consist mainly of multi-alkylated cyclo- and dicycloalkanes. The aromatic compounds are predominantly alkyl and cyclo-alkyl, benzenes and naphthalenes. (See section (4.5.4) for a more detailed discussion of the aromatic components in refined mineral oil lubricants).

SCHEME 1.1 THERMAL DEGRADATION OF ESTERS WITH BETA HYDROGENS

SCHEME 1.2      PRODUCTION OF LUBRICANT FRACTIONS FROM CRUDE OIL



Note : SN = Solvent Neutral (applies to the method of solvent purification)  
 SP = Spindle Oil.



1.1.3 Methods currently used in the analysis of lubricant base oils.

The importance of analytical methods to the oil industry for characterisation of lubricant base fluids cannot be overstated. To maintain quality control it is necessary for the refiner to be able to make comparisons of fluids derived from differing sources prior to formulation into lubricants. On the other hand base oils are analysed following extraction from fully formulated oils during the course of evaluation of a new lubricant. Analytical method development is an active area of research and reviews appear regularly on new methodology.<sup>7</sup> The need for compatibility between different laboratories requires the publication<sup>8</sup> of standard methods, many of which are in regular use.

Methods of analysis of base oils may be subdivided into, (a) those providing physical data of the bulk fluid, viz volatility, viscosity, density, flash point, pour point, thermal and oxidative stability and (b) those that lead to the elucidation of chemical composition. As certain physical properties are necessary for a particular lubricant (see section (1.1.1)) information gained from physical analyses indicate both the suitability of a base fluid and the various additives which will be required to generate the desired lubricant performance. The Physical properties which are usually specified in the description of a base fluid are determined by standard methods,<sup>8</sup> but these will not be

discussed here.

Performance characteristics of lubricant base fluids do depend on their chemical composition. In mineral oil fractions the proportion of aromatic to aliphatic hydrocarbon effects the thermal and oxidative stability, while the degree of branching of aliphatic chains effects the viscosity index. In the case of synthetic fluids hydrogenated polyalphaolefins impart excellent viscosity index properties, while  $\beta$ -hindered esters (see section (1.1.2)) find application where high thermal stability is required. The association of beneficial properties with particular chemical structures aids the development of new synthetic fluids.

Chemical compositions are typically presented in one of two ways, (a) as the relative proportion of each component or homologous series and (b) in terms of a hypothetical average molecule.<sup>9</sup> The latter is useful for making comparisons between oils and for monitoring processes such as hydrogenation of a complex mixture of unsaturated precursors when there are a large number of components and identification of each component would be very time consuming. Thus it is not surprising that many of the methods reported in the literature are for the determination of petroleum fractions.<sup>9,10</sup>  $^{13}\text{C}$  and  $^1\text{H}$  n.m.r. are particularly suited for the determination of average parameters as the observations depend upon the environment of atoms and on summation but do not distinguish between molecular components in

mixtures. The percentage of aromatic and aliphatic carbons in petroleum fractions is often determined using the Brands<sup>11</sup> infrared (IR) method based upon the intensities of bands at  $1600\text{ cm}^{-1}$  (aromatic ring breathing mode) and  $720\text{ cm}^{-1}$  (aliphatic  $\text{CH}_2$  rocking). This method is normally used for samples with "aromatic contents" lower than 20% by weight. Similarly the weight percentage of alkenyl, benzyl,<sup>12</sup> naphthyl<sup>13</sup> and polycyclic aromatic carbons are determined by ultraviolet (UV) spectrometry. Although average molecule data obtained using the methods is not as comprehensive or precise as that obtained using a combination of  $^{13}\text{C}$  and  $^1\text{H}$  NMR spectroscopy, estimates can be obtained more quickly and using less expensive instrumentation. The application to continuous monitoring of refinery products makes the IR and UV methods very suitable for quality control. However since the actual constituent molecules may be very different from the average molecule it is only possible to make limited correlations of the physical properties and performance to the relative properties of functional groups derived by the above methods.

When knowledge of the actual molecular composition, rather than a chemical characterisation, is required methods which analyse molecules rather than atomic environments have to be used. These "molecular" analyses may be subdivided into (a) those requiring separation prior to determination and (b) those where analysis is conducted on the total sample. Obviously

the latter method is more desirable, less time being required than for the separation methods.

#### 1.1.3.1 Mass spectrometric methods excluding GCMS

Standard methods for total hydrocarbon type analysis of mineral oils by 70 eV electron impact (EI) mass spectrometry have been published<sup>14</sup> and are routinely used for characterisation. Quantitation in these methods is achieved by summing the intensities of fragments believed to be derived from a particular type of hydrocarbon (e.g. the cycloalkanes) the sum then being multiplied by a suitable calibration (interference) factor.<sup>15</sup> Consequently only a measure of the relative concentrations of homologous series (e.g. cycloalkanes, n-alkanes) may be obtained. No information regarding the relative concentrations of constituent members is available. These methods are limited to fluids having narrow boiling-point range (different interference factors being required for different boiling ranges) and low heteroatom content (less than 10%). In an effort to obtain information concerning the molecular composition of mineral oil fractions, low energy (8-10 eV) electron impact high resolution mass spectrometry has been utilised.<sup>16</sup> Here it is assumed that the energy of the impacting electron is sufficient to ionize a hydrocarbon molecule, and that this is accompanied by little excess energy being imparted to the ion. Consequently little fragmentation should occur provided this excess energy is less than the appearance energy of any fragments. Thus only the

molecular ion of each component, of a mixture, should be observed. High resolution mass analysis facilitates the differentiation of ions of the same nominal mass but different molecular formulae. Hence qualitative and quantitative analysis may be conducted knowing mass to charge ratios and relative abundances of the molecular ions. As the ionization efficiency (number of ions produced for a given electron current) varies with both hydrocarbon type and molecular mass, suitable calibration factors have to be applied. In practice only the molecular formulae may be obtained using the analysis and prior separation of aromatic from saturated hydrocarbons is normally required as the higher electron energies required to ionize the saturate (ionization potentials are 1 - 3 eV greater than aromatics) lead to fragmentation of the aromatics. Additionally, the method suffers from several drawbacks viz: (a) the degree of substitution of an aromatic hydrocarbon considerably effects its ionization potential (e.g. n-butylbenzene 8.68 eV and 1,2,3,4-tetramethylbenzene 8.18 eV)<sup>17</sup> and ionization efficiency, leading to a change in sensitivity with degree of substitution, (b) the low appearance potentials (0 - 1 eV) of fragment ions of ions from saturated hydrocarbons, give rise to considerable fragmentation and poor analysis of fractions with high proportions of saturated hydrocarbons, and (c) the change in ionization efficiency with impacting electron energy is large when this is close to the compound's ionization potential.

Hence small changes in electron energy cause considerable change in observed relative intensities hindering the compatibility of data from different laboratories and instruments. Nevertheless remarkably good data appears to be obtainable by this method but another method for its verification is highly desirable.

Recently there has been interest in the use of chemical ionization mass spectrometry for the qualitative analysis of aromatic components in hydrocarbon mixtures.<sup>18,19</sup> Although the possibility for quantitation has been indicated<sup>18,20</sup> as yet no method has been published. The use of chemical ionization mass spectrometry (CIMS) for the analysis of lubricating fluids will be discussed in section (1.2).

#### 1.1.3.2 Methods requiring prior separation -

In order to obtain the most complete chemical description of a lubricating fluid it is still necessary to resort to separation and characterisation of the separated components. Gas liquid chromatography (GLC) using various detectors, but principally the flame ionization detector, is one of the main separation techniques. The advent of capillary columns and resulting high resolution has considerably increased both quality and quantity of data obtained. Standard GLC methods are used for "fingerprinting" and calculation of boiling point distributions<sup>21</sup> requiring less time and sample compared with previously employed molecular distillation.<sup>22</sup>

Dual detector systems, one being a selective detector, have been used to gain further information on the distribution of a particular functional group within the lubricant. The selective detection of sulphur containing compounds is of particular interest in lubricant analysis owing to their corrosive nature. Direct GLC of synthetic ester lubricants yields little information and it is particularly difficult to distinguish dibasic acid esters and those of neopentyl polyols. This problem is normally surmounted by hydrolysis of the ester fluid, separation of acidic and alcoholic portions and subsequent methylation of the acids followed by GC or GCMS of the resulting alcohols and methyl esters. However this is time consuming and the composition of the ester fluid must be deduced from the fragments rather than being directly observed. More recently a combination of GC for separation and quantitation and ammonia chemical ionization mass spectrometry for identification has been successfully applied to the characterisation of neopentyl polyol ester lubricants.<sup>23</sup> Similarly hydrogenated poly ( $\alpha$ -olefins) have been characterised using a combination of gas chromatography and methane chemical ionization mass spectrometry.<sup>24,25</sup> Blends of different types of synthetic fluids, i.e. mixtures of synthetic and mineral oils are increasing in popularity but are particularly difficult to analyse. Subsequent development of preparative high performance liquid chromatography (HPLC) using gradient elution with silica columns<sup>26</sup> has alleviated some of the

problems by facilitating the separation of blends of esters with either hydrogenated poly( $\alpha$ -olefins) or mineral oils. Further analysis may then be conducted on the separated fractions. Equally, separation of aromatic material in mineral oils may be conducted by analogous methods prior to low energy electron impact high resolution mass spectrometry. Molecular weight distribution information complementary to that determined by GC may be evaluated by gel permeation chromatography (GPC).<sup>26</sup> However since molecular geometry influences the molecular size to weight relationship, true molecular weights are only obtainable from analytical GPC if calibration curves are evaluated using compounds of the same type as the sample. Consequently in the case of complex lubricating oils, one is restricted to expressing a molecular weight as "equivalent molecular weight" to the series of compounds used in the calibration.

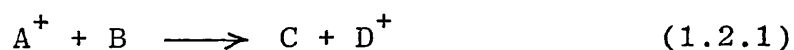
In summation the analysis of a lubricant, particularly a full formulated one, i.e. additives added, will require the use of many if not all of the methods described above. A useful guide to the order of use of such methods has recently been published.<sup>26</sup> Further discussion of lubricant analysis will be given in section (4.5).



## 1.2 GENERAL ASPECTS OF ION-MOLECULE INTERACTIONS

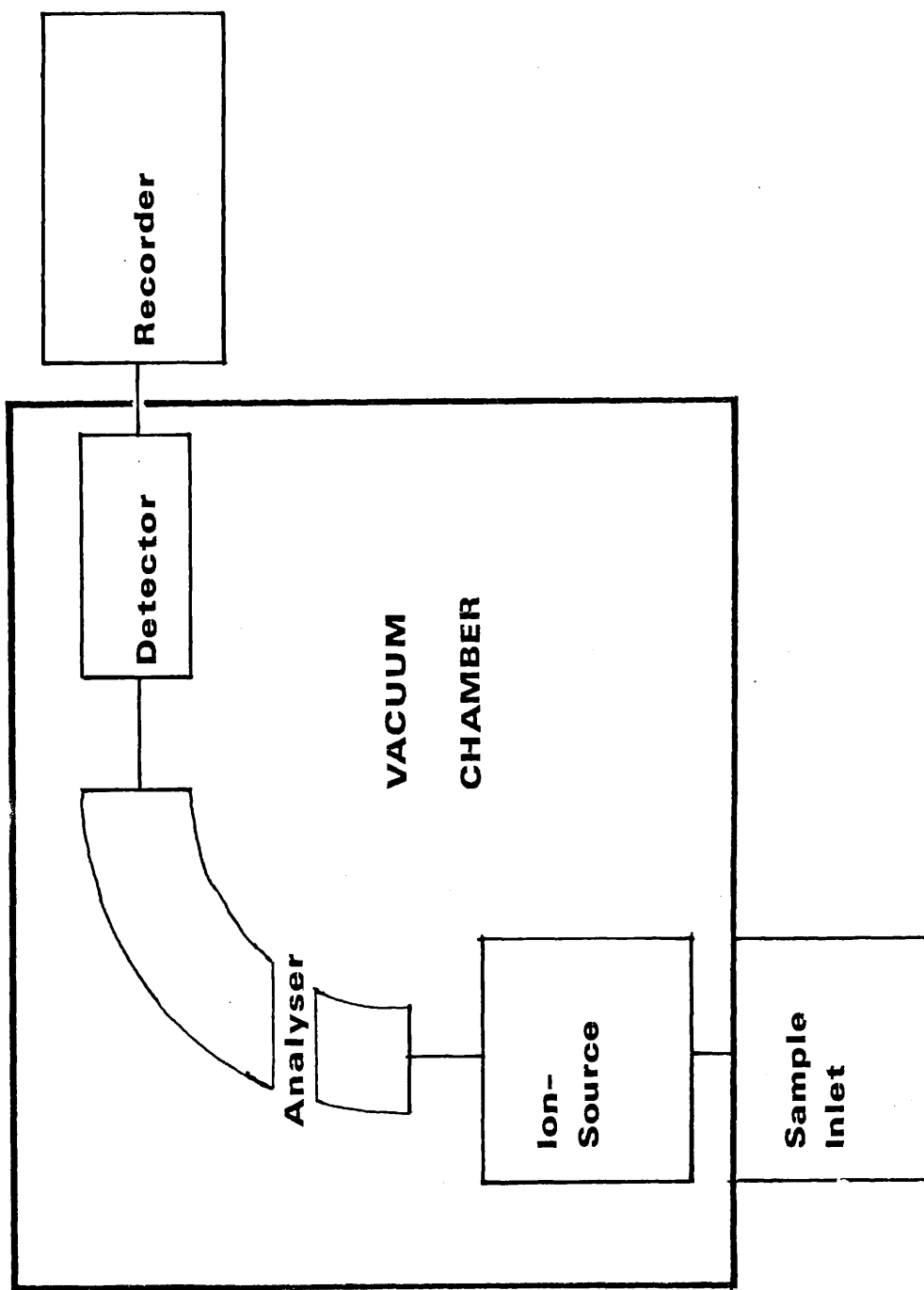
### 1.2.1 The use of mass spectrometers in the generation, analysis and detection of ions.

Ionization of sample molecules may be effected by various methods. Three such methods entail the passage of a beam of photons (photoionization),  $\alpha$ -particles (Radiolysis), or as in the current study, electrons (electron impact ionization) through the vapourised sample. A fourth makes use of the effect of a strong electric field (field ionization) to effect sample ionization. Ionization of organic molecules by the above methods leads to the formation of so called "molecular ions" which are often unstable and fragment to form smaller ions referred to as "primary ions". Additionally any of these ions may effect ionization of a substance, since a collision between an ion and molecule often results in an ion-molecule reaction:



A mass spectrometer is an instrument which utilizes ionization and subsequent fragmentation processes for chemical analysis. A schematic diagram of such an instrument is given in figure (1.1). In this study the ionization of gases and vapours, introduced through various inlet systems (see section (2.2)), was effected by electron impact in the ion-source, which is described in detail in section (2.2). When sample pressures are low ( $<10^{-5}$  Torr), ion-molecule reactions are unlikely to occur and the ions pass out of the source and are accelerated by means of

FIG(1,1) Schematic Diagram of Mass Spectrometer



an electric field maintained between the ion-source exit slit and a slit some 2-3mm removed from it. The latter slit is also used to focus the ion-beam and the sign of the potential applied to it determines whether positive or negative ions are extracted from the source. The ions next pass into the analyser where they are separated according to their mass to charge ratio ( $m/z$ ). The focused ion-beam then passes through a second slit, ("the collector slit") which may be adjusted to increase or decrease resolution, and finally impinges on the detector. The signals generated, are amplified and recorded. A good vacuum, ca.  $10^{-6}$  Torr, is maintained in: the region surrounding the ion-source, the analyser, and the detector in order that ions do not undergo reactions with neutral molecules after exit from the ion-source.

A number of different types of mass analysers and ion detectors are employed in mass spectrometer systems. Details of these may be found in books by Beynon<sup>27</sup> and McFadden.<sup>28</sup> The system employed in this work consists of a magnetic-sector analyser and electron-multiplier tube detector.

It may be shown that an ion of mass,  $m$ , charge  $z$ , accelerated through a potential difference of  $V$  volts and deflected by a magnetic field of strength  $B$ , applied perpendicularly to the plane of acceleration, will prescribe an arc of radius  $r$  in accordance with equation (1.2.2).

$$m/z = eB^2 r^2 / 2V \quad \text{--- (1.2.2)}$$

Mass spectrometers employing magnetic-sector analysers are generally constructed with a fixed radius-of-curvature so that for given values of B and V ion-beams with m/z given by equation (1.2.2) will pass through the collector slit and be detected. Thus systematic variation (scanning) of either the magnetic field or accelerating voltage, results in systematic variation in the mass-to-charge ratio of ions reaching the detector.

Generally ionization and subsequent fragmentation of sample molecular ions occurs in the ion-source. However some ions are metastable, remain intact upon withdrawal from the ion-source but fragment during acceleration. When this happens a diffuse peak appears in the spectrum, often at a non integral mass. In spectra obtained using mass spectrometers with magnetic-sector analysers the positions of peaks arising from fragmentation of metastable ions ( $m^*$ ) are given by equation (1.2.3)

$$m^* = \frac{m_2^2}{m_1} \quad \text{--- (1.2.3)}$$

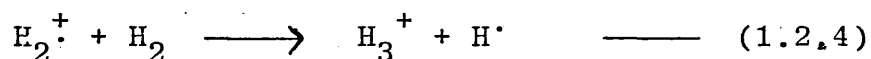
where  $m_1$  is the metastable ion mass and  $m_2$  the mass of the resulting fragment. Observation of diffuse peaks resulting from fragmentation of metastable ions is useful in suggesting pathways from molecular ions to primary ions and examples of such will be discussed later.

Descriptions of the construction of electron multipliers and their mode of operation may be found

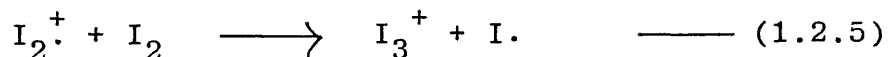
elsewhere.<sup>100</sup> However, the possible mass discrimination which may result from their use will be discussed in section (2.2).

1.2.2. Reaction between ions and molecules in the gas phase.

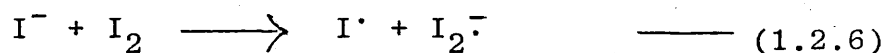
If ion-source pressures are increased greatly above that mentioned above (to ca. 0.01 Torr) collisions between ions and molecules will result, and ion-molecule reactions may take place. In 1916 Dempster<sup>29</sup> observed an ion of  $m/z = 3$  in the mass spectrum of hydrogen and suggested that this might be  $H_3^+$ . Later observations by Hogness and Lum,<sup>30</sup> and Smyth<sup>31</sup> that the intensity of the ion-beam  $m/z = 3$ , resulting from the ionization, of hydrogen varied with pressure led to the suggestion by Smyth<sup>32</sup> that  $H_3^+$  was formed by the ion-molecule reaction.



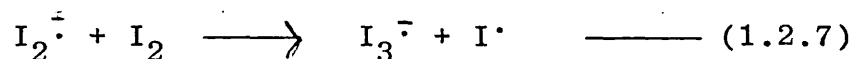
In 1928, Hogness and Harkness<sup>33</sup> reported reactions of both positive and negative ions in iodine showing that  $I_2^+$  was formed both by electron impact and by charge transfer from  $I^+$  and that  $I_3^+$  arose by reaction of  $I_2^+$  with neutral iodine.



The only primary negative ion observed was  $I^-$ , which underwent charge exchange with  $I_2$  to form  $I_2^-$

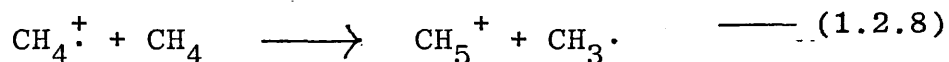


Further  $I_3^-$  was formed by the reaction



Reaction (1.2.4) was studied theoretically by Eyring, Hirschfelder and Taylor<sup>34</sup> in 1936 and they predicted a value for the collision coefficient. Excellent agreement was observed between this and an experimental result obtained subsequently.<sup>35</sup>

However it was not until the observation by Stevenson and Schissler,<sup>36</sup> and Field, Franklin and Lampe<sup>37</sup> in the United States, and Tal'roze and Lyubimova,<sup>38</sup> in the U.S.S.R. of the formation of  $CH_5^+$  by reaction (1.2.8), in the 1950's, that the study of ion-molecule reactions as now recognised began.



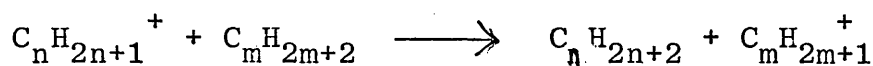
Later in 1965 while studying reaction (1.2.8) and others in methane at high pressures (ca. 1 Torr), Field and Munson noted that small concentrations (ca.1%) of impurities, e.g. ethane<sup>39</sup> or water<sup>40</sup>, had dramatic effects on the spectra of ions obtained. The subsequent explanation that the observed spectra resulted from reactions of  $CH_5^+$  and  $C_2H_5^+$  derived from methane, with neutral species led to the first description of chemical ionization mass spectrometry<sup>41</sup> by these researchers in 1966. This method of ionization is now used extensively and the current state of the technique is discussed in section (1.3).

The principal types of reaction known to occur

between ions and molecules in the gas phase are:

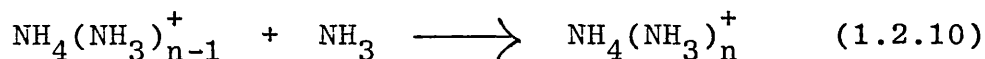
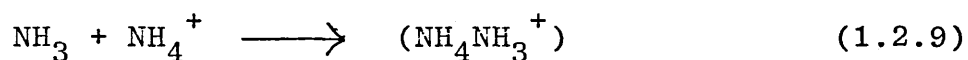
charge exchange reactions, exchange of protons, hydride ions or atoms and clustering processes. Examples of proton transfer, atom transfer and charge transfer were given in reactions (1.2.4) to (1.2.6) respectively.

Examples of hydride transfer are found in the reactions of carbenium ions with alkanes

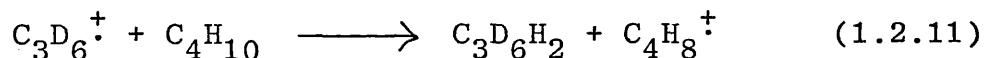


as first observed by Field and Lampe<sup>42</sup> in 1958. Clustering processes have been extensively studied by Kebarle.<sup>43</sup>

Examples of such reactions are



An example of two-atom-transfer reactions is the  $\text{H}_2^-$  transfer reaction<sup>44</sup>



As well as the large volume of kinetic data massed from experimental studies of ion-molecule reactions, considerable effort has been expended on theoretical treatment of ion-molecule reactions. Of particular relevance to the work described here is the Average Dipole Orientation theory (ADO) of Su and Bowers.<sup>45</sup> This theory uses statistical methods to calculate the

average orientation of polar molecules in the vicinity of an ion and then a Langevin procedure to calculate a collision capture rate constant. More recently the above authors have found it necessary to consider the conservation of angular momentum, during collisions between ions and polar molecules, to obtain theoretical rate constants and have developed the AADO<sup>46</sup> theory. Comparison of the capture rate constants with experimentally determined rate coefficients has considerably aided in development of reaction mechanisms (Vide infra).

### 1.2.3 Chemical ionization mass spectrometry

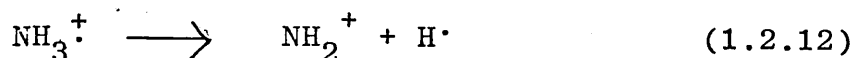
As already indicated in section (1.2.2) ions, formed by initial ionization of a gas, may effect ionization of other molecules by ion-molecule reactions. This forms the basis of chemical ionization mass spectrometry.<sup>47</sup>

In chemical ionization mass spectrometry a gas, the reagent gas, is present in the ion-source at relatively high pressures (ca. 0.1 - 2.0 Torr). Ionization is effected in the normal way, in the current study by electron impact. The 'primary ions' collide with the neutral gas and 'secondary ions' are formed in the resulting ion-molecule reaction. These secondary ions may now react with a second substance, i.e. the sample, introduced to the ion-source at a suitably low concentration (ca. <1%), to prevent possible ionization by the electron beam.

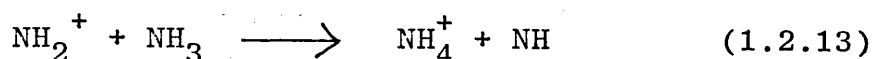
Chemical ionization may be illustrated by some reactions that occur when ammonia or nitric oxide is used as reagent gas. Electron impact of ammonia results



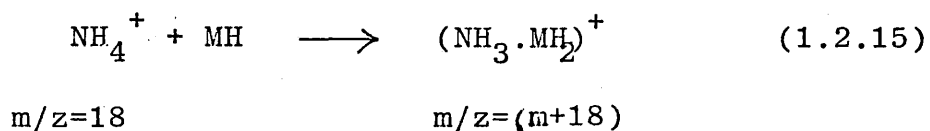
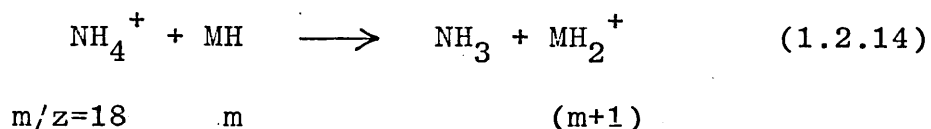
in the formation of the molecular ion-radical  $\text{NH}_3^{\cdot+}$  which then fragments to a variety of primary ions, e.g.  $\text{NH}_2^+$



The primary ions then separately react with ammonia, e.g.

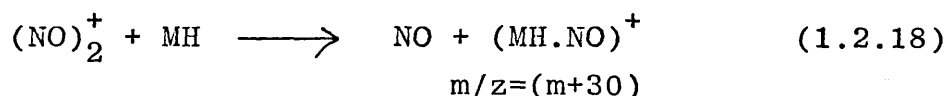
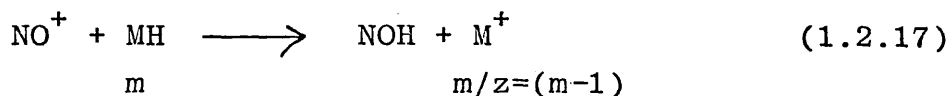
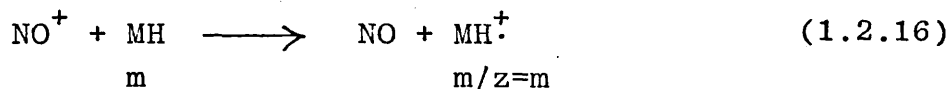


The ammonium ions so formed may then react with sample molecules (MH) in either a proton exchange (1.2.14) or an association (1.2.15) reaction.

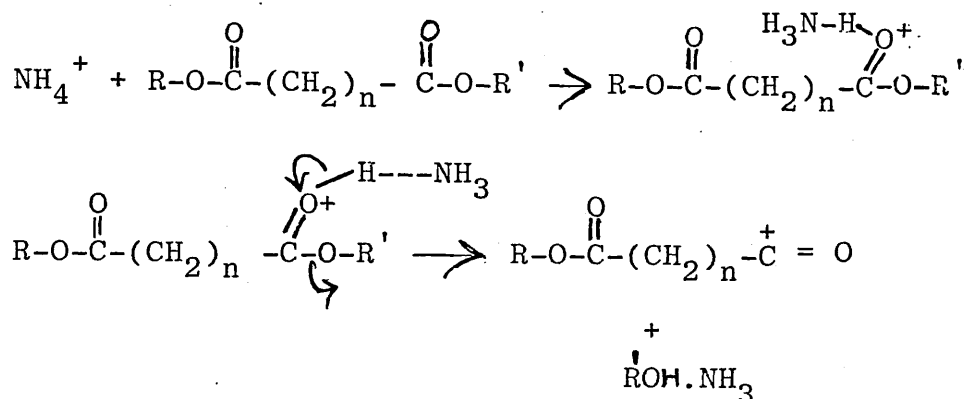


Proton exchange is the preferred reaction path only when the proton affinity of the sample is greater than that of ammonia.

When nitric oxide is the reagent gas  $\text{NO}^+$  and  $(\text{NO})_2^+$  result from initial ionization and subsequent ion-molecule reactions. The relative proportions of  $\text{NO}^+$  and dimer ion  $(\text{NO})_2^+$  will depend on the reagent gas pressure in the ion-source. Sample ionization is effected by  $\text{NO}^+$  via charge or hydride exchange reactions and by  $\text{NO}^+$  exchange from  $(\text{NO})_2^+$  as shown in reactions (1.2.16)-(1.2.18) respectively.



The ionic products of these reactions may decompose before leaving the ion-source, but such fragmentations are more easily rationalised than those resulting from electron impact ionization, e.g.



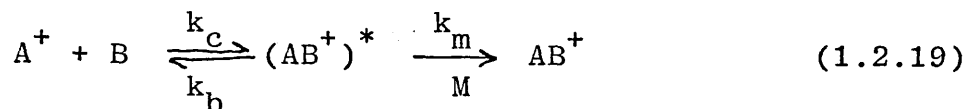
Since the quantity of energy imparted to the product ion is normally far less than in electron-impact ionization fragmentation is considerably reduced. Whereas the electron-impact mass spectrum of a sample may not show the presence of molecular ions, the corresponding chemical ionization mass spectrum usually does, aiding relative molecular mass determination. Often suitable choice of reagent gas and ion-source pressure can result in little or no fragmentation of product ions. Additionally since sample ionization results from a chemical reaction,

compounds with differing functional groups may be ionized by different reactant ions generated from the same or different reagent gases. (See section (1.3)).

A wide variety of reagent gases are now available for both positive and negative ion chemical ionization and several review articles on their use have been published.<sup>48,49,50</sup>

#### 1.2.4. Some current mechanisms of bimolecular ion-molecule reactions.

Bimolecular reactions may be conveniently divided into association reactions (e.g. (1.2.9) and (1.2.10)) and exchange reactions, e.g. ((1.2.4) - (1.2.7)). The latter may further be divided into fast exchange reactions which proceed at or near unit collision efficiency (rate coefficients  $\sim > 5 \times 10^{-10} \text{ cm}^3 \text{ molecule}^{-1} \text{ s}^{-1}$ ) and slow processes with collision efficiencies substantially below unity (rate coefficients  $\sim < 5 \times 10^{-10} \text{ cm}^3 \text{ molecule}^{-1} \text{ s}^{-1}$ ). Collision efficiency being defined as the number of capture collisions which result in reaction to products, all reactions are considered to pass through a collision complex  $(AB^+)^*$  formed in a capture collision. This activated complex may be (a) collision stabilised by a third body (M), resulting in a cluster ion (reaction (1.2.19)), (b) collision-dissociated to products (reaction (1.2.20)), or (c) proceed to products within one vibrational period of the complex (reaction (1.2.21)) as in fast exchange reactions or dissociate back to the reactants.



#### 1.2.4.1 Fast exchange reactions -

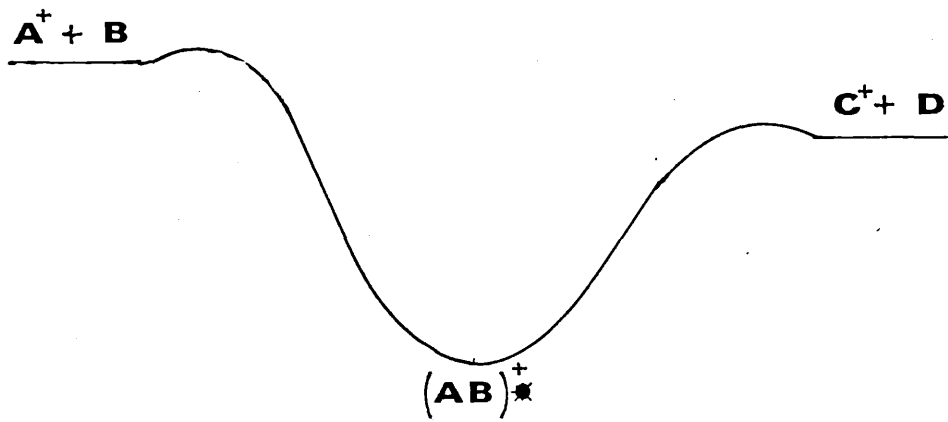
These are typified by exothermic charge exchange and some proton exchange reactions. Experimentally determined rate coefficients have been found to be comparable with collision capture rate constants estimated using ADO<sup>45</sup> and AADO<sup>46</sup> theory. Reactions are hence deduced to proceed at near unit collision efficiency. The energy profile for such reactions is given in figure (1.2).

#### 1.2.4.2 Slow exchange reactions -

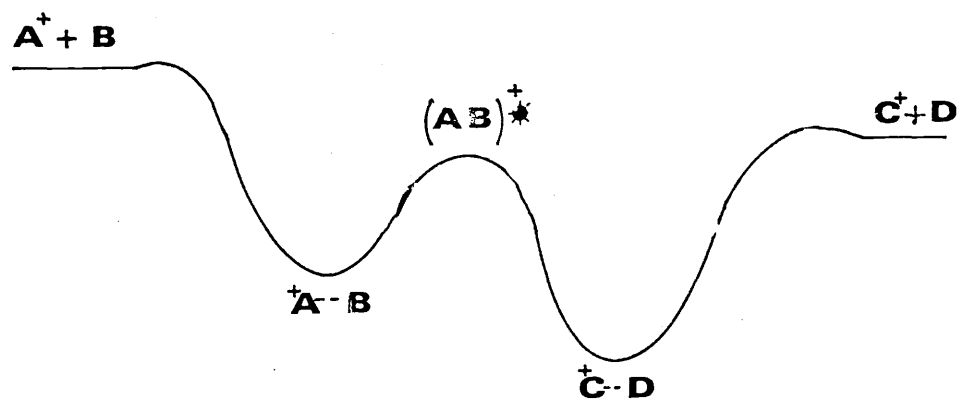
These reactions which proceed with collision efficiencies substantially below unity are typified by hydride exchange reactions of carbenium<sup>51</sup> ions and include many proton exchange reactions.<sup>52</sup> The low collision efficiencies may result from either an energy barrier higher than the energy of the separated reactants, or occurrence of a long lived collision complex which may require collision with a third body to give the products or dissociate unimolecularly either back to the reactant or to the products. These possibilities are

**SCHEMATIC POTENTIAL ENERGY DIAGRAMS**

FIG(1.2) Fast ion-molecule reactions.



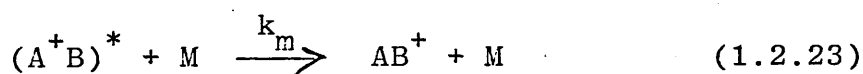
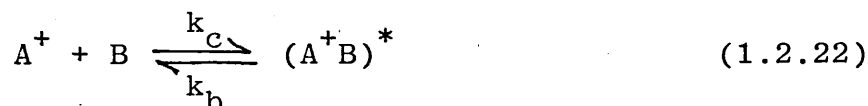
FIG(1.3) Slow ion-molecule reactions



discussed at length in section (4.1) and (4.2). A typical energy profile for such reactions is given in figure (1.3) for comparison with that given for fast exchange reactions.

#### 1.2.4.3 Association reactions -

These may be divided into clustering reactions, where the product ions are held together by weak bonding, and condensation reactions where new covalent bonds are formed. Only clustering reactions will be discussed here. The energy transfer mechanism first proposed by Rabinowitz<sup>53</sup> is considered to be applicable to ion-molecule reactions as demonstrated by researchers such as Bohme<sup>54</sup> and Meot-Ner and Field<sup>55</sup> (Reactions (1.2.22) and (1.2.23)).



By applying the steady state hypothesis to the collision complex  $(AB^+)^*$  the rate constant ( $k_f$ ) for forward reaction to  $AB^+$  may be written as

$$k_f = \frac{k_c k_m (M)}{k_b + k_m (M)} \quad (1.2.24)$$

At low pressure  $k_m(M) \ll k_b$

$$k_f = \frac{k_c k_m}{k_b} (M) \quad (1.2.25)$$

Thus the apparent second order rate coefficient  $k_f$  increases linearly with  $(M)$  at low pressure and the reaction exhibits

third-order kinetics.

Such clustering reactions are often characterised by a change from third order to second order kinetics as the gas pressure is increased. This mechanism will be shown to be applicable to explain the change in kinetic order observed in reactions of  $\text{NH}_4^+$  with ammonia (see section (4.2)).

For a more detailed discussion of the effects of temperature and pressure on reaction rates and mechanisms of ion-molecule reactions the reader is referred to the recent article by Meot-Ner.<sup>56</sup>

#### 1.2.5 Study of ion-molecule reactions and evaluation of rate coefficients.

##### 1.2.5.1 Reasons for the study of ion-molecule reactions -

Ion-molecule reactions are known to play an important part in the chemistry of flames,<sup>57</sup> the ionosphere<sup>58</sup> and interstellar clouds.<sup>59</sup> Clearly a greater understanding of ion-molecule reactions in the combustion of hydrocarbons is of prime importance to a society whose principal source of energy is the combustion of fossil fuels and should lead to more efficient combustion to gain the maximum possible energy return.

Recently much concern has been expressed regarding possible detrimental effects of aerosol solvents and other pollutants on ozone levels in the ionosphere. Ozone, which is known to restrict the quantity of ultraviolet radiation reaching the earth's surface, is itself formed in ion-molecule reactions. In fact changes in the

ionosphere are largely determined through ion-molecule interactions. It is hoped that through a greater understanding of the evolution of the ionosphere it may be possible to give long range forecasts of climatic change.

Additionally ion-molecule reactions are known to play important roles in Radiation chemistry<sup>60</sup> and processes occurring in the recently developed short wavelength molecular electronic transition gas lasers.<sup>61</sup>

However the particular reasons for the present study of ion-molecule reactions are associated with their use in chemical analysis, viz. the chemical ionization mass spectrometric analysis of lubricant fluids. These reasons are discussed later in section (1.3).

#### 1.2.5.2 Methods for the study of the kinetics of ion-molecule reactions -

Some of the more common methods used in the study of ion-molecule reactions are, continuous ion-extraction mass spectrometry,<sup>62</sup> ion/cyclotron/resonance spectrometry<sup>63</sup> drift-tube mass spectrometry<sup>64</sup>, flowing-afterglow mass spectrometry<sup>65</sup> and more recently selected-ion-flow-tube mass spectrometry.<sup>66</sup> Only the method used in the current study, namely continuous ion extraction, will be discussed here. For further details of the other methods the reader is referred to the references given above.

#### 1.2.5.3 The use of continuous ion-extraction mass spectrometry for the evaluation of rate coefficients of ion-molecule reactions -



A mass spectrometer permits rapid and accurate measurement of the intensities of ion-beams resulting from both reactants and products of reaction (1.2.1) and therefore provides a convenient means for the study of ion-molecule reactions. The concentrations of ions in the ion-source are much lower than that of neutral molecules and consequently the probability of a reaction between an ion  $A^+$  and neutral molecule B, following pseudo first order kinetics, is far greater than that for a reaction between an ion and any neutral fragment.

The rate equation for disappearance of  $A^+$  by reaction (1.2.1) is

$$-\frac{d[A^+]}{dt} = k[A^+][B]$$

integration gives

$$\dagger \log [A^+]/[A^+]_0 = -k[B]\tau \quad (1.2.26)$$

$k$  is the rate coefficient and  $\tau$  the mean residence time of the ion  $A^+$  in the ion-source,  $[A^+]$  the instantaneous concentration of  $A^+$  and  $[A^+]_0$  the concentration of  $A^+$  in the absence of reaction (1.2.1). Clearly measurement of the ion-source pressure of B and estimation of the mean residence time  $\tau$  are required in order that the rate constant may be determined. Pressure measurement used is described in section (2.3.1) and methods used for estimation of  $\tau$  are given in section (3.1.2).

---

<sup>†</sup> "log" will be used to indicate natural logarithms (ln) throughout this discussion.

Provided that equal intervals of time are spent collecting ions of different  $m/z$ , the magnitude of the signals generated by the detector will truly reflect the ion-beam currents, which in turn will truly reflect the concentration of ions in the source. So by arranging that mass spectral peak widths do not vary with  $m/z$  the relative concentrations of ions,  $N^+$ ,  $m/z = n$ , will be given by  $I_n/\Sigma I$  where  $I_n$  is the area of the relevant peak and  $\Sigma I$  the sum of the areas of all peaks in the spectrum, (i.e. the total ion-current). The quantity  $I_n/\Sigma I$  will be referred to as the relative ion-current and equation (1.2.26) becomes

$$\log \frac{I_n}{I_n^0} = -k [B]\tau \quad (1.2.27)$$

None of the above stated conditions for equation (1.2.27) to be valid are strictly adhered to in continuous ion extraction mass spectrometers since collimation slits, electron multiplier tubes and extraction of ions from the source are all known to lead to mass discrimination. However some effort has been made to minimize these as described in section (2.2).

The rate coefficients determined are at best time-averaged rate constants

$$k_{\text{exp}} = \frac{1}{\tau} \int_0^{\tau} k(t) dt \quad (1.2.28)$$

In order for the value of  $k_{\text{exp}}$  to be independent of the conditions under which it was determined the following

assumptions must be true: (i) any electric field must be uniform within the ion-source, (ii) the reactant ions initially should have thermal energies, (iii) the electron beam should be narrow in order that the position of ion-formation may be well defined. If these assumptions are valid then

$$t = v\tau/V_e \quad (1.2.29)$$

where  $v$  is the instantaneous velocity of the ion and  $V_e$  the ion-velocity at the ion-source exit. Then equation (1.2.28) becomes

$$k_{\text{exp}} = \frac{1}{V_e} \int_0^{V_e} k(v)dv \quad (1.2.30)$$

and  $k_{\text{exp}}$  is equated with a velocity averaged rate constant. Rate constants from continuous ion-extraction mass spectrometers can only be compared to those obtained from another method if the above assumptions are true and then only if the exit velocity of the ions are the same in both cases. The above assumptions may be tested by some experiments described by Henchman.<sup>64</sup>

Another difficulty is that a reaction may occur with an ion having a range of energies,  $0 \leq E \leq E_e$ , where  $E_e$  is its ion-exit energy. Additionally the energy distribution varies as a function of pressure owing to differences in attenuation of ions along the reaction path. However these effects can be minimized by reducing the

range over which pressure is varied and maintaining the same conditions of temperature, electric field strength and electron energy.

When reaction rates are determined by chemical ionization mass spectrometry reagent gas pressure, electric field strength, ion-source temperature and electron energy are held constant. Sample pressures are much lower than reagent gas pressures and provided sample pressure is only varied over a small range, the reactant ion energy distribution should be independent of the nature of the sample. Thus although the rate constants obtained may be in error by a factor of two<sup>64</sup> as a consequence of the lack of validity of assumption (i) - (iii) relative rates should be accurate and may therefore be compared.

### 1.3 CHEMICAL IONIZATION MASS SPECTROMETRY IN THE ANALYSIS OF COMPLEX MIXTURES WITHOUT THE NEED FOR PRIOR SEPARATION

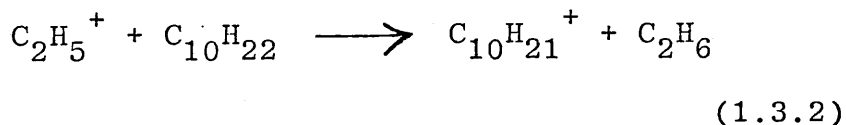
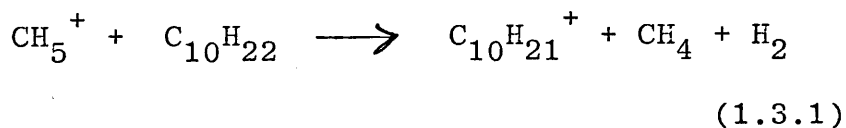
The basis of chemical ionization mass spectrometry has already been discussed. Attention was drawn to the fact that suitable choice of reagent gas can result in little fragmentation of the ionic species produced. Additionally through a correct choice of reactant ion, preferential ionization of chemically different compounds may be achieved. In this study chemical ionization methods have been developed for the analysis of lubricating base fluids (see(1.1.1)) without the need for prior separation of the many components in these fluids.

#### 1.3.1 Mixtures containing compounds of the same chemical type.

In this study such mixtures were typified by synthetic lubricants, namely hydrogenated polyalpha-olefins and ester fluids (see (1.1.2)). The reagent gases methane, nitric oxide and mixtures of nitric oxide and nitrogen were used in the analysis of hydrogenated poly-alphaolefins. Ammonia was found to be a suitable reagent for the study of ester fluids. A brief discussion of the use of these reagent gases by other workers now follows.

1.3.1.1 The use of Methane, Nitric oxide, and Nitric oxide/nitrogen mixtures as reagent gases in the chemical ionization of hydrocarbons -

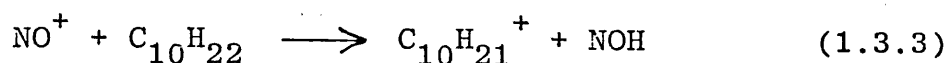
Shortly after chemical ionization (CI) mass spectrometry was first used<sup>41</sup>, Field and Munson published a series of papers dealing with methane CI of paraffins<sup>67</sup> olefins and acetylenes<sup>68</sup>, cycloalkanes,<sup>69</sup> and aromatics.<sup>70</sup> Bombarding methane with electrons at ion-source pressures of ~1 Torr produced a reagent gas plasma composed primarily of  $\text{CH}_5^+$  and  $\text{C}_2\text{H}_5^+$ . The principal mode of reaction of these ions was dissociative and non-dissociative hydride exchange (reactions (1.3.1), (1.3.2)), resulting in production of ions of mass (M-1) where M is the sample relative molecular mass. Additionally a series of alkyl fragments of formula  $\text{C}_n\text{H}_{2n+1}^+$  were formed which accounted for >32% of the ion current.



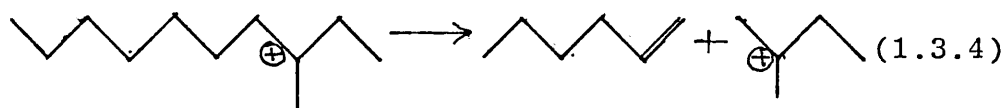
This represented a dramatic improvement over electron impact mass spectra in which the sample ion-current is typically divided between  $C_2-C_5$  fragments (80%), higher mass alkyl fragments (11%) and the molecular ion ( $M^+$ ) (0-4%). More recently Howard, McDaniel, Nelson and Blomquist<sup>25</sup> have obtained spectra of long chain alkanes, derived from insects, using methane reagent gas at an ion-source pressure of 0.5 Torr. They suggested that differences in the distribution of alkyl fragments in spectra of different alkanes can be related to position and length of branch chains.

Electron impact of nitric oxide at an ion-source pressure of 1 Torr results in the formation of  $NO^+$  and  $(NO)_2^+$ . Hunt and Harvey<sup>71</sup> showed that reaction of these ions with saturated hydrocarbons resulted in chemical ionization spectra where more than 90% of the sample ion-current arises from ions corresponding to  $M-1$ ,  $M-3$  and  $((M+30)-2)^+$ . However owing to the short filament life when using pure nitric oxide (~ 6 hrs) it was found necessary to use a mixture of ~20/1 nitrogen to nitric oxide as reagent gas. Here the  $N_2^+$  ion produced in the initial electron impact ionization reacts by a charge

exchange reaction with nitric oxide to produce the having after multiple collisions nitrosonium ion  $\wedge$  low internal energy. Subsequent reaction of this ion, primarily by hydride exchange, with saturated hydrocarbon (reaction (1.3.3)) results



in chemical ionization spectra in which more than 75% of the sample ion-current is carried by ions corresponding to (M-1). Hunt and Harvey<sup>71</sup> suggest that the reduction in fragmentation observed when using nitric oxide/nitrogen mixtures can be attributed to formation of sample ions with insufficient internal energy to surmount the energy barrier, of some  $88 \text{ kJ mol}^{-1}$ , for fragmentation by loss of olefins (e.g. reaction (1.3.4)).



#### 1.3.1.2 Ammonia chemical ionization reagent gas -

Upon electron impact ionization the ammonium ion,  $\text{NH}_4^+$ , results from ion-molecule reactions of primary ions. Both the kinetics<sup>72,73</sup> and the thermodynamics<sup>43,74</sup> of subsequent cluster formation  $(\text{NH}_3)_n\text{NH}_4^+$  have been extensively studied and the magnitude of n found to increase with decrease in gas temperature, and increase in ion-source pressure. Under normal chemical ionization the reagent gas spectra is dominated by  $\text{NH}_4^+$  (m/z=18) and  $\text{NH}_3\text{NH}_4^+$  (m/z=35) ions.

As already mentioned  $\text{NH}_4^+$  reacts by proton



exchange with compounds having a proton affinity (PA) greater than that of ammonia ( $845 \text{ kJ mol}^{-1}$ ) and by association with polar compounds. Little reaction with  $\text{NH}_4^+$  is observed for compounds of  $\text{PA} < 790 \text{ kJ mol}^{-1}$ .<sup>75</sup> Thus ammonia has been found particularly useful in ionization of organic compounds containing oxygen and/or nitrogen, namely, alcohols,<sup>76</sup> ketones,<sup>77,78</sup> carboxylic acids, dicarboxylic acids,<sup>79</sup> esters,<sup>80</sup> amines,<sup>81</sup> nitro-compounds, and many natural products.<sup>82,83,84</sup>

Deuterated ammonia ( $\text{ND}_3$ ) CI of compounds containing active hydrogens results in ionic species with masses of  $M+m$  where  $M$  is the mass of the corresponding ion when using ammonia CI and  $m$  the number of replaceable hydrogens. Using this phenomena Buchanan<sup>81</sup> was able to distinguish primary, secondary and tertiary amines.

More recently much attention has been directed to studies of ammonia CI of monosubstituted benzenes ( $\text{C}_6\text{H}_5\text{X}$ ) where  $\text{X} = \text{Cl}, \text{Br}, \text{I}, \text{and } \text{NO}_2$ . It has been suggested<sup>85</sup> that the ion formed corresponding to  $[\text{C}_6\text{H}_5\text{NH}_2]^+$  results from electrophilic aromatic ipso substitution.

Ammonia is also finding use as a reagent gas for negative ion chemical ionization and recent publications have included CI of phenothiazines<sup>86</sup> and selective ionization of sulphur compounds in gas oils.<sup>87</sup>

Finally, since little energy is transferred to sample molecules during their ionization by  $\text{NH}_4^+$ , molecular mass information may be obtained for molecules containing particularly labile bonds. (e.g. in explosives<sup>88</sup>).

1.3.2 Mixtures containing compounds of more than one chemical type.

Mass spectroscopic analysis of all the compounds having a particular functional group in a mixture containing compounds of several different functionalities is often required to obviate the need for prior separation; this is often time consuming and may not give perfect resolution of the compounds of interest. Recently there has been great interest in this use of chemical ionization mass spectrometry, particularly in fossil fuel analysis where the many components inhibit full chemical type separations.

Several general reviews have been published<sup>89,20</sup> on application of positive and negative ion CIMS which are now discussed separately.

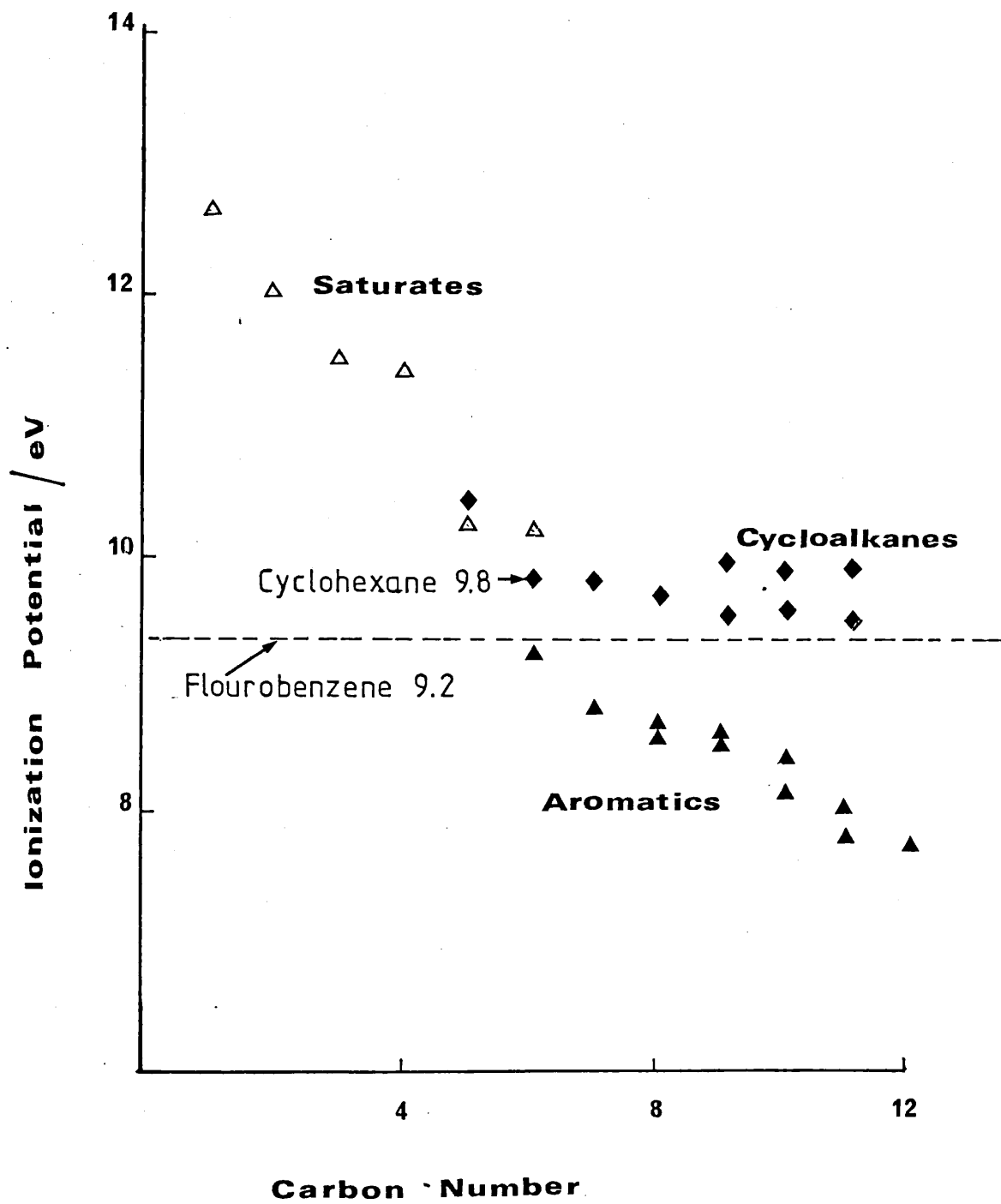
1.3.2.1 Selective positive ion chemical ionization -

Discriminatory ionization relies on generation of a mono-ionic plasma of an ion which reacts via a single channel with compounds of a given functional group.

Additionally for mixture analysis little energy should be imparted during sample ionization to minimize fragmentation. To date reagent gas ions reacting by charge or proton exchange have proved useful.

Wayne Sieck has used the  $C_6H_{12}^+$  ion, generated by photo-ionization of cyclohexane, for preferential ionization of aromatic components in gasoline and light fuel oils.<sup>18</sup> Discrimination is achieved since compounds of ionization potential greater than cyclohexane (IP = 9.83 eV)<sup>17</sup> (viz saturated hydrocarbons (see fig.(1.4))).

FIG(1.4) Ionization Potentials of some Hydrocarbons.

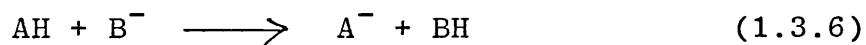


are not ionized, as charge exchange from  $C_6H_{12}^+$  would be endothermic. The method was primarily used for fingerprinting gasolines derived from different sources but possibilities for quantification of the results were indicated.

Ammonia CI has been used to effect preferential ionization of basic polar compounds, with proton affinities  $> 790 \text{ kJ mol}^{-1}$ , in non-polar matrices. (e.g. the selective ionization of nitrogen compounds in coal liquids.<sup>90</sup>)

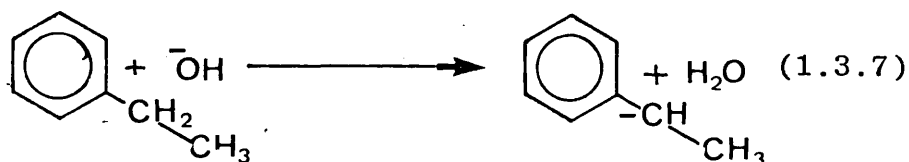
#### 1.3.2.2 Selective negative ion chemical ionization -

Selectivity is normally achieved by either the capture of thermal electrons (1.3.5) or through proton exchange reactions (1.3.6).



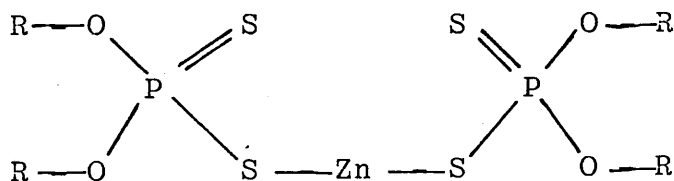
Methane and ammonia reagent gases act mainly as moderators, in negative ion chemical ionization (NICI), producing copious quantities of thermal electrons which ionize samples with high electron affinities as reaction (1.3.5). Preferential ionization of aromatic compounds, containing  $\alpha$  acidic hydrogens, using  $OH^-$  ions generated from  $N_2O$ /hexane mixtures has facilitated fingerprinting of fossil fuels<sup>20</sup> and crude oils.<sup>91</sup> Ionization resulting from proton abstraction (reaction (1.3.7)) gives abundant (M-1) ions. Unfortunately the rate of reaction (1.3.7) is

dependent on the ease of removal of  $H^+$ , (i.e. the relative acidity of the  $\alpha$ -hydrogen). Thus rates of reaction and hence CI sensitivities for different isomers, having the same nominal mass, are markedly different, and the technique not readily applicable to quantitation.



Recently  $\text{Cl}^-$  generated from carbon tetrachloride has been used for the preferential ionization of organo-metallic compounds <sup>92</sup> used as anti oxidant additives in lubricating oils. (e.g. zinc dialkyldithiophosphates (ZDDP's), fig (1.5) ). Provided a suitable ion-source pressure of  $\text{CCl}_4$  is used ionization of a sample  $\text{ML}_2$ , where M represents the metal ion and L the ligand, results in formation of two species  $[\text{ML}_2\text{Cl}]^-$  and  $\text{L}^-$ .

Fig. (1.5)



Zinc dialkyldithiophosphate

EXPERIMENTAL

## 2.1 MATERIALS

2.1.1 Reagent gases

## 2.1.1.1 Cylinder gases -

The reagent gases methane (B.D.H.; 99.0%) and isobutane (B.O.C.; 99.5%) were passed over molecular sieve and activated charcoal before admission to the mass spectrometer. Ammonia (Matheson 99.96%) and nitric oxide (Matheson 99.0%) were used without further purification.

## 2.1.1.2. Reagent gases which are liquids at standard temperatures and pressures -

Methylcyclopentane (Aldrich Chemical Co.; 98%) was dried over molecular sieve, type 4A and distilled prior to use. Methylcyclohexane (Aldrich Chemical Co.; 99%) was washed with concentrated sulphuric acid to remove aromatic hydrocarbons, dried over calcium chloride and distilled. All fluorinated benzenes (Fluorochem Ltd.) were purified by preparative g.l.c.<sup>†</sup> (stationary phase 10% SP100 on chromosorb W) to better than 99.9 + %, e.g. Fluorobenzene 99.99% by capillary g.l.c.\*

2.1.2. Mass spectrometry standards

Tris(pentafluoroethyl)-s-triazine (Lancaster Synthesis Ltd.) was used without purification.

---

\* Fluorobenzene of suitable purity may be obtained from Hoescht Ltd.

<sup>†</sup> The author wishes to thank Professor V. Gold of King's College for the use of the prep instrument.

### 2.1.3. Preparation of esters

#### 2.1.3.1 Esters of dibasic acids -

The dibasic acid esters, table (2.1) were prepared by the method described below for the preparation of bis(2-ethylhexyl) hexanedioate. The esters were characterised by NMR, IR and mass spectrometry.

To a mixture of hexanedioic acid (10 g, 0.069 mole), 2-ethylhexanol (28.6 g, 0.22 mole) was added conc. sulphuric acid (4 g) dropwise with warming. After refluxing for 6 hr with continual removal of water, the mixture was poured into water (100 cm<sup>3</sup>) and the organic layer separated. The aqueous layer was extracted with diethyl ether (2 x 25 cm<sup>3</sup>). The combined organic phases were washed with saturated sodium hydro<sup>gen</sup>carbonate, water and then dried over anhydrous sodium sulphate. After removal of solvent the residue was distilled under nitrogen at 0.1 mm Hg pressure. Other di-esters were prepared by analogous methods and solid products recrystallised from acetone following their distillation.

#### 2.1.3.2 Esters of 2,2 bis(hydroxymethyl)propane-1,3-diol and 2-ethyl-hydroxymethylpropane-1,3-diol. -

Esters of the polyols 2-ethyl-2-hydroxymethylpropane-1,3-diol (table (2.2)) and 2,2 bis(hydroxymethyl)propane-1,3-diol (table (2.3)) were prepared by the method described below for the preparation of 1,3-propanediol-2-ethyl-2-butylcarbonyloxymethyl-dipentanoate. The esters were characterised by NMR, IR, and mass spectrometry.

To a mixture of pentanoic acid (25.5 g, 0.25 mole),

TABLE 2.1 Esters of dibasic acids

Name	Boiling point °C	Melting point °C	Refractive index $n_{D20}$	Density $\rho_{20}$	Yield %
Bis(2-ethylhexyl)- hexanedioate	160 0.1mm Hg (190-200 @ 1) ‡		1.4480 (1.4471)† (1.4450)‡	0.9096	89.44
Bis(1-methyloctyl)- hexanedioate	190 @ 0.5 mm Hg		1.4432	0.8859	45
Bis(decyl)hexane- dioate	180 @ 0.1 mm Hg	25-26.5 (27.4)*			8.9
Bis(undecyl)hexane dioate		35.5-36 (34.7)*			24
Bis(dodecyl)hexane dioate	210 @ 0.1 mm Hg	39.5-40 (39.3)*			32
Bis(2-ethylhexyl) heptanedioate	180 @ 0.2mm Hg		1.4484 (1.4490)†	0.9018	70
Bis(2-ethylhexyl) octanedioate	200 @ 0.2mm Hg		1.4490 (1.4508)†	0.8982	69
Bis(2-ethylhexyl) nonanedioate	210 @ 0.2mm Hg (202-5 @ 0.5)‡		1.4494 (1.4463)‡	0.8880	66.8

Literature values of physical constants:

\* See Ref.93

‡ See Ref.95

† See Ref.94



2-ethyl-2-hydroxymethylpropane-1,3-diol (6.7 g, 0.05 mole) and toluene (30 cm<sup>3</sup>) was added sulphuric acid (98%, 0.3 g) dropwise with warming. After continuous removal of water during refluxing for 4 hrs, the mixture was poured into water (100 cm<sup>3</sup>) and the organic layer separated. The aqueous layer was extracted with diethyl ether (2 x 25 cm<sup>3</sup>) and the combined organic phase treated as described for the esters of dibasic acids (see above). The product was purified by fractional distillation under nitrogen at 0.1 mm Hg pressure.

#### 2.1.4 Other chemicals

All other liquids used in kinetic studies were dried over molecular sieve, type 4A, prior to use. Those having manufacturers' stated purities less than 99% were distilled after drying.

**TABLE 2.2** Tri-esters of 2-ethyl-2-hydroxymethyl-  
propane-1,3-diol

Acid used in preparation (see 2.1.3.2)	Boiling point °C	Refractive index $n_{D_{20}}$	Density $\rho$ g cm <sup>-3</sup>	Yield %
n-Pentanoic acid	170 @ 0.2 mm Hg (188-92 @ 2 mm Hg) †	1.4468 (1.4482) †	0.9704	41.5
n-Hexanoic acid	186 @ 0.1 mm Hg (230-5 @ 2 mm Hg) †	1.4480 (1.4490) †	0.9365	44
n-Heptanoic acid	210 @ 0.2 mm Hg (240-5 @ 2 mm Hg) †	1.4498 (1.4510) †	0.9407	17
n-Octanoic acid	230 - 234 @ 0.2 mm Hg (250-5 @ 2 mm Hg) †	1.4518 (1.4535) †	0.9275	55.0
n-Nonanoic acid	250 @ 0.2 mm Hg (270-8 @ 2 mm Hg) †	1.4538 (1.4550) †	0.9319	47

† Literature values see Ref. 96.

TABLE 2.3 Tetra-esters of 2,2 Bis(hydroxymethyl)propane-1,3 diol.

Acid used in preparation (see 2.1.3.2)	Boiling Point °C	Refractive index		Density $\rho$ g cm <sup>-3</sup>	Yield %
		$n_{D70}$	$n_{D20}$		
n-Pentanoic acid*		1.4313 (1.4310)†	1.4478	0.9808	30
n-Hexanoic acid	220 @ 0.2mm	1.4342 (1.4325)†	1.4508	0.9261	40
n-Heptanoic acid	250 @ 0.5mm	1.4370 (1.4350)†	1.4526	0.9526	29
n-Octanoic acid *		1.4379 (1.4370)†	1.4542	0.9260	20
n-Nonanoic acid *		1.4398 (1.4558)†	1.4558	0.9106	20

\*. Compound charred on boiling. Therefore no boiling point obtained. Purified on alumina column.

† Literature values see Ref.97.

## 2.2 THE V.G. MICROMASS 12F SPECTROMETER

The V.G. Micromass 12F mass spectrometer<sup>98</sup> is a 60°, 12.7 cm radius, magnetic sector instrument in which mass analysis is achieved by varying either the strength of the magnetic field (magnet scanning) or the accelerating voltage (voltage scanning).

Spectra reported in this work were produced by scanning the magnetic field, the accelerating voltage being maintained constant at 4000V for the kinetic studies and 3000V when recording spectra of lubricant base oils.

A schematic diagram of the ion-source of the mass spectrometer is given in figures (2.1a, 2.1b). The ion-source chamber consists of a cavity (C) milled out of a stainless-steel block (B). An electron-beam is produced by an emission-regulated filament (F) mounted outside the ion-source block. The beam enters the ion-source through a cylindrical aperture (A) of length 2mm and internal diameter 0.5mm. Ions formed in C leave the ion-source through the ion-exit slit, E. The drift of positive ions towards the exit slit is often assisted by maintaining the potential on the repeller plate (R) positive with respect to the exit-slit, E. The ion-exit slit, which is cut in the thin stainless steel plate, has dimensions of 0.05 mm x 5.0 mm. The temperature of the heated ion-source block was monitored by means of a chromel-alumel thermocouple (T) connected to an electronic thermometer.<sup>99</sup> During kinetic studies the

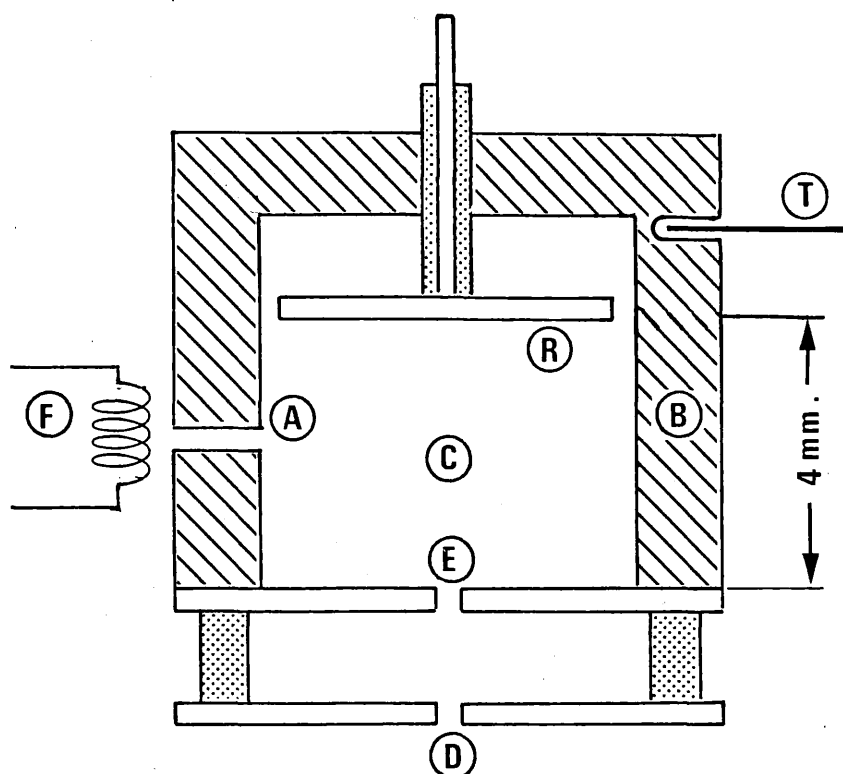


Fig. ( 2.1.a ) Schematic Drawing of Ion-Source

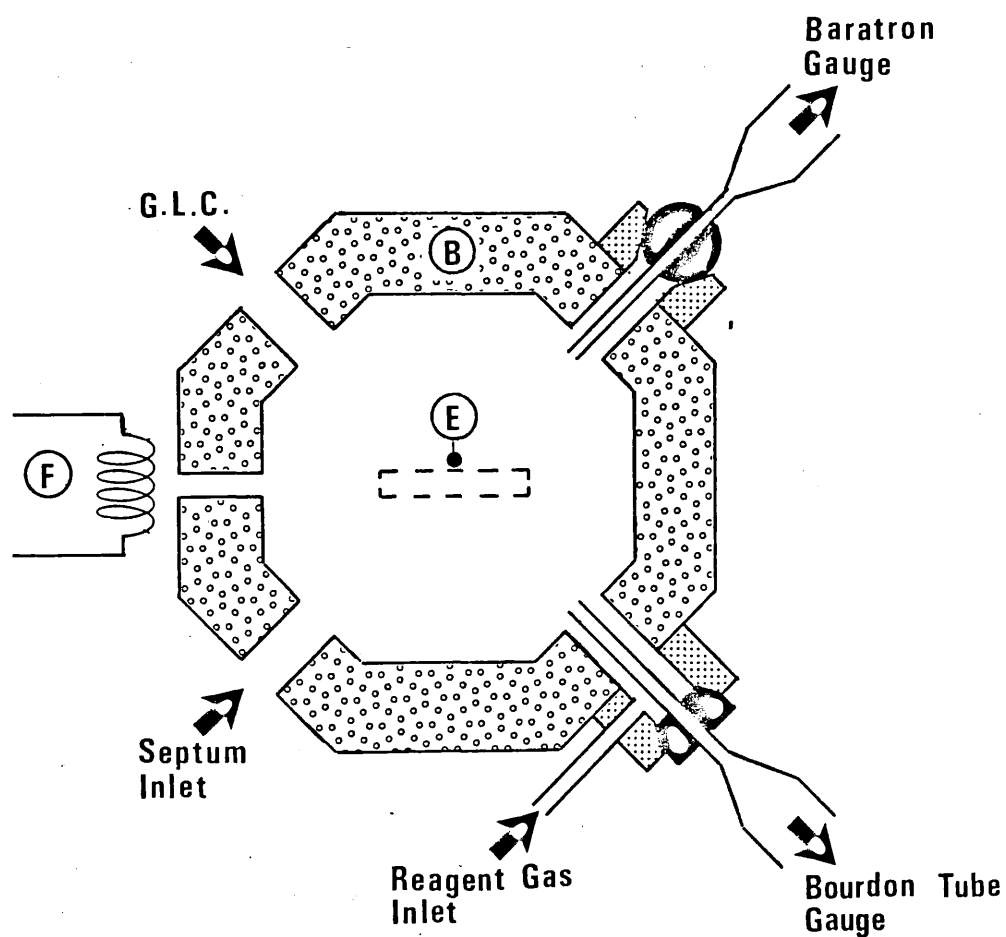


Fig. ( 2.1.b ) Connections to Ion - Source

electron-beam collimating magnets, normally fitted to the ion-source, were removed since the presence of magnetic fields in the ion-source is known to give rise to mass discrimination effects (see section 1.2).

The pressure in the housing surrounding the ion-source was generally lower than  $5 \times 10^{-5}$  Torr. Reagent gases and vapourized samples were introduced into the ion-source via ports bored through the ion-source block. (Fig.(2.1b)). These ports are omitted from figure (2.1a) for clarity. The reagent-gas-inlet (see section (2.2.1)) and sample-inlet systems are designed to form gas-tight seals with the ion-source block. The Micromass 12F spectrometer has three sample-inlet systems, viz. from a g.l.c. column, by way of a jet separator, a direct-insertion probe, and a septum-inlet system.

Liquid samples used in the kinetic studies were introduced through the septum-inlet system, a schematic diagram of which is given in figure (2.2). Known volumes of volatile liquid samples were injected into the heated reservoir (R) and vapourized. The vapour flows through the heated narrow-bore delivery tube (T) into the ion-source. The flow-rate is sufficiently slow that there is little (less than 1%) change in the pressure of sample in the ion-source (see section (2.3.5)), over a period of 10 min following injection of the sample into the reservoir.

Solutions of lubricant base oils were introduced via the direct insertion probe (see section

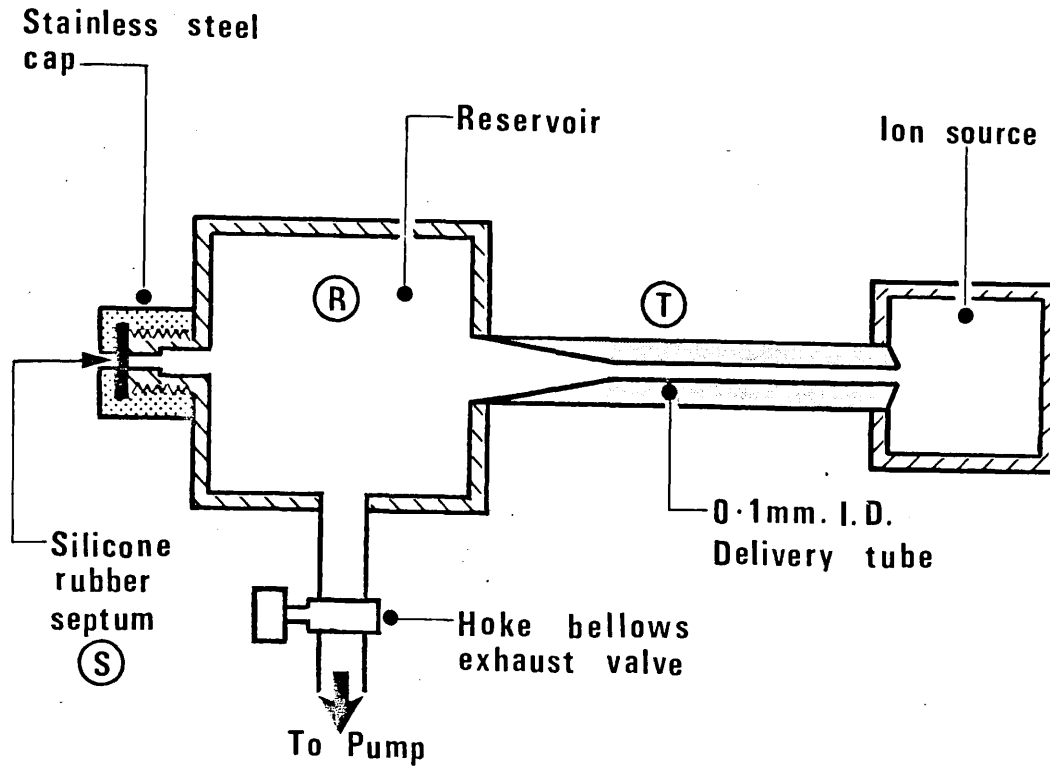


Fig. ( 2.2 ) Schematic Diagram of Septum - Inlet System

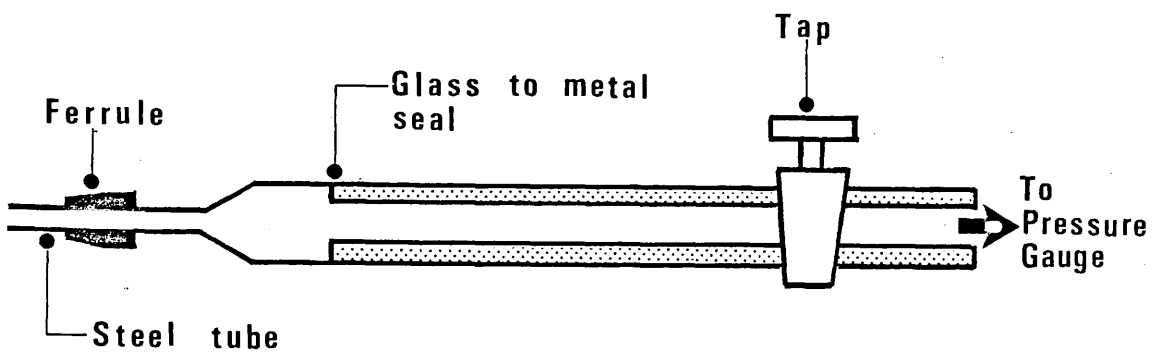


Fig. ( 2.3 ) Probe Used to Connect Pressure Gauge to Ion - Source

(2.5.1)).

Positive ions formed in the ion-source are accelerated by a potential difference (4000 V in kinetic studies, 3000 V in lubricant base oil analysis) applied between plates E and D (see figure (2.1a)), and the resulting ion-beam analysed by the magnetic field. The focussed ion-beams, separated according to their differing momenta pass through a collector slit and strike the first dynode of a 17-stage electron-multiplier tube. During the lubricant oil analysis the collector slit was adjusted such that a resolution of 900 (at 10% valley) was obtained. Both the collector slit and the electron-multiplier are known to introduce mass discrimination effects into the mass spectrum. The samples used in the kinetic studies did not produce ions of  $m/z > 250$  a.m.u. and it was found that spectra were not seriously affected by adjusting the collector slit to its maximum width (ca. 1mm). Hence the mass discrimination effect of the collector slit was minimized for kinetic experiments. By comparison, it is difficult to make corrections for mass discrimination effects arising from the use of an electron-multiplier as a detector. The gain of multiplier tubes is known to depend on not only the mass but also the kinetic energy, and the elemental composition of the ions striking their first dynode.<sup>100</sup> Insufficient data is presently available to allow general corrections for discrimination effects to be made.



The output from the multiplier was amplified then recorded either using a computer data system (see appendix II, lubricant oil analysis) or using an oscillograph 3005 recorder<sup>101</sup> (kinetic studies). In the oscillograph recorder three galvanometer mirrors reflect U.V. light onto photo-sensitive paper. The traces produced correspond to three attenuations, X0.01, X0.1, and X1.0, of the amplified ion-currents. For convenience the galvanometers will be numbered (1), (2) and (3), corresponding to attenuation factors of X0.01, X0.1 and X1.0 respectively.

For the kinetic studies it was assumed (a) that heights of peaks recorded by the u.v. recorder corresponded to ion-currents, and (b) that these truly reflect the relative abundances of ions in the ion-source realising that in the continuous extraction mass spectrometer not all the ions produced in the source are extracted. For the limited mass range (i.e. 0-250 amu) used in the kinetic studies, the variation in width of the bases of peaks was so small that the error introduced by assumption (a) is negligible. Errors due to assumption (b) were minimized by using normalized ion-currents in all kinetic calculations. Peak heights were measured to the nearest 0.5mm using a transparent ruler. The maximum relative errors incurred in the measurement of heights of peaks recorded by galvanometers (1) and (2) were ~ 1%, but those by galvanometer (3) were as high as 10%. However the absolute errors in normalised ion-currents of the principal ions (measured

from galvo's (1) and (2)) were probably less than 1%.

It was previously found<sup>52</sup> that for a given amplifier current, the peak heights recorded by the galvanometers were not exactly in the expected ratio 1:10:100. A calibration experiment<sup>52</sup> enabled the peak heights of ( $h_1$ ,  $h_2$ ) recorded by galvanometers (1) and (2) to be corrected to the value ( $h_3$ ) which would have been recorded by galvanometer (3).

$$h_3 = 10 \times ((1.071 \pm 0.018) h_2 - (0.040 \pm 0.007)) - (2.2.1)$$

$$h_3 = 100 \times ((0.971 \pm 0.025) h_1 - (0.438 \pm 0.008)) - (2.2.2)$$

All spectra reported in this work were obtained by scanning the magnetic field exponentially from high to low field, i.e. such that

$$m = m_0 \exp(-t/T) \quad (2.2.3)$$

where  $m$  is the mass of the ions collected at time,  $t$ ,  $m_0$  the mass of the ions collected initially, and  $T$  the time constant of the scan (i.e. the time required to scan one decade of mass units). Differentiation of equation (2.2.3) gives

$$dm = -m_0 \exp(-t/T) dt/T \quad (2.2.4)$$

or

$$dt = -T dm/m \quad (2.2.5)$$

Thus the time spent collecting ions of mass  $m$ ,  $\delta t$  is dependent upon the reciprocal of the resolution, ( $m/\delta m$ ) of the instrument and the time constant  $T$ . Since  $dt$  is independent of  $m$ , the heights of the various peaks in a

given spectrum may be compared with one another, to compare ion abundances, provided mass discrimination effects are small. Spectra reported for the kinetic studies were recorded using a time constant, T, of 30 sec/decade since the slow scan-rate results in better reproducibility of spectra. The only apparent disadvantage of this slow scanning was that occasionally the sensitivity of the instrument changed during the recording of a spectrum thus distorting the ratios of peak heights. Observation of any such effect was made by duplicating spectra.

2.2.1 Modifications to the reagent gas inlet system to facilitate the introduction of ammonia, nitric oxide and reagent gases which are liquids at S.T.P.

The reagent gas inlet system as supplied by the manufacturer is shown in figure (2.4). The precision diaphragm regulator (A) maintains a constant pressure of reagent gas in the ion-source (B) by varying the flow rate through the connecting tubes C,D and E. The narrow-bore tube (C) provides preliminary heating of the reagent gas and acts as a pressure restrictor maintaining a sufficiently high down stream pressure at regulator (A) for it to function correctly.

Although reagent gases ammonia and nitric oxide could be introduced to the ion-source by using corrosive resistant regulators and by-passing regulator (A), it was not possible to generate sufficiently high ion-source

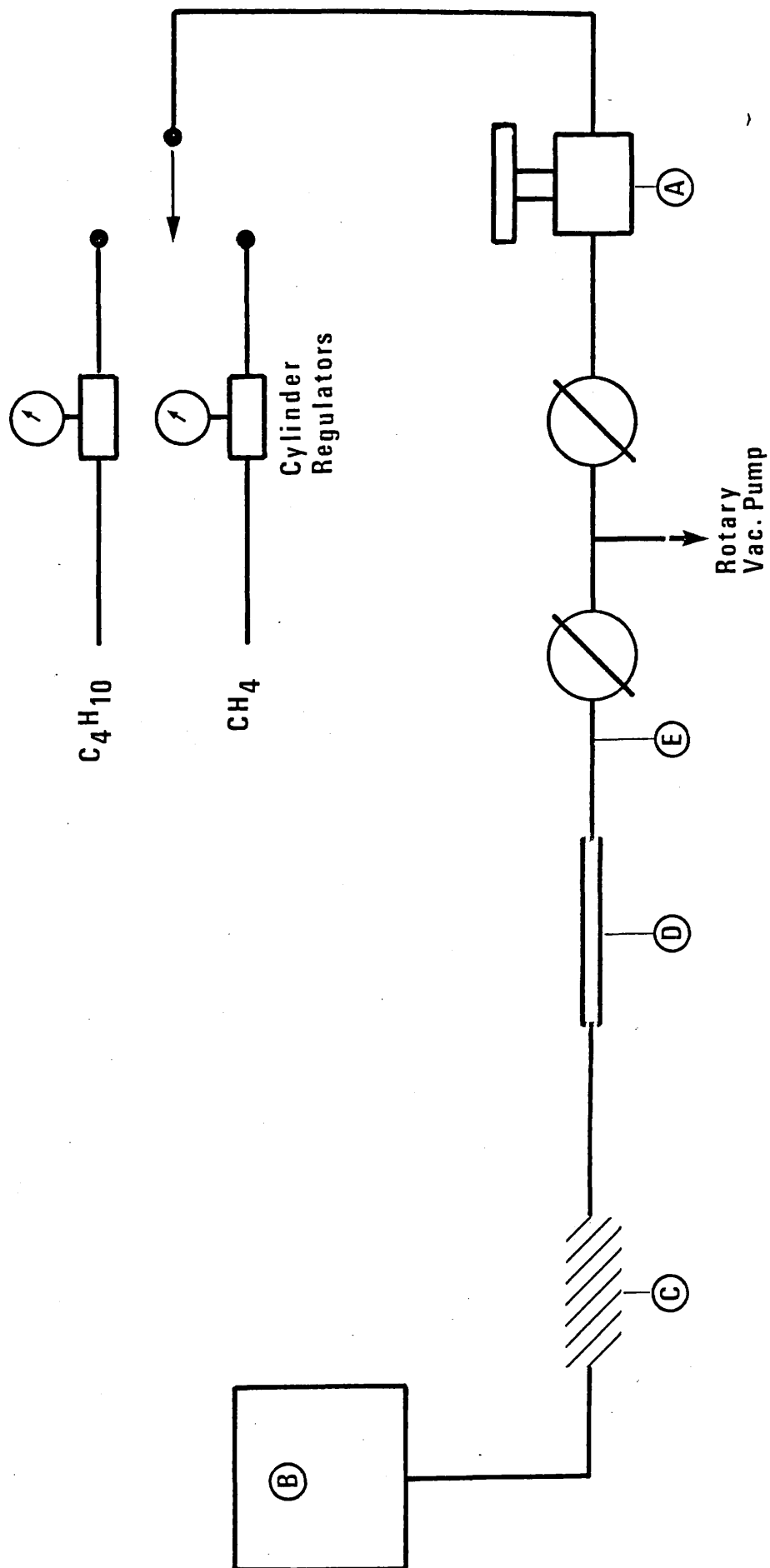


Fig. ( 2.4 ) V. G. Reagent Gas Inlet System

pressures, with reagent gases having vapour pressures as low as 150 Torr at 25°C.

The modified reagent gas inlet system used for all reagent gases studied is shown in figures (2.5) and (2.6). The narrow bore tubing originally ((C) figure (2.4)) connected to the ion-source was replaced by tubing of higher conductance to allow higher ion-source pressures to be generated. The two stage needle valve (F) provides accurate control of the ion-source pressure (viz.  $\pm$  0.05 m Torr) for both (a) high inlet pressures (viz. 1500-3000 Torr) from gas cylinders and (b) low inlet gas pressures (viz. 60-150 Torr) generated from a vapour line (G) (see figure (2.6)). The needle valve (F) being made of stainless steel was therefore resistant to corrosion by nitric oxide and ammonia. Compounds which are liquids at S.T.P. were introduced via the vapour line shown in figure (2.6). The liquids were freed from volatile impurities such as air by a series of freeze-pump-thaw cycles. The liquid reservoir was maintained at 15°C  $\pm$  0.2°C in order to give a stable pressure in the ballast volume and hence on the inlet side to the needle valve (F) in figure (2.5).

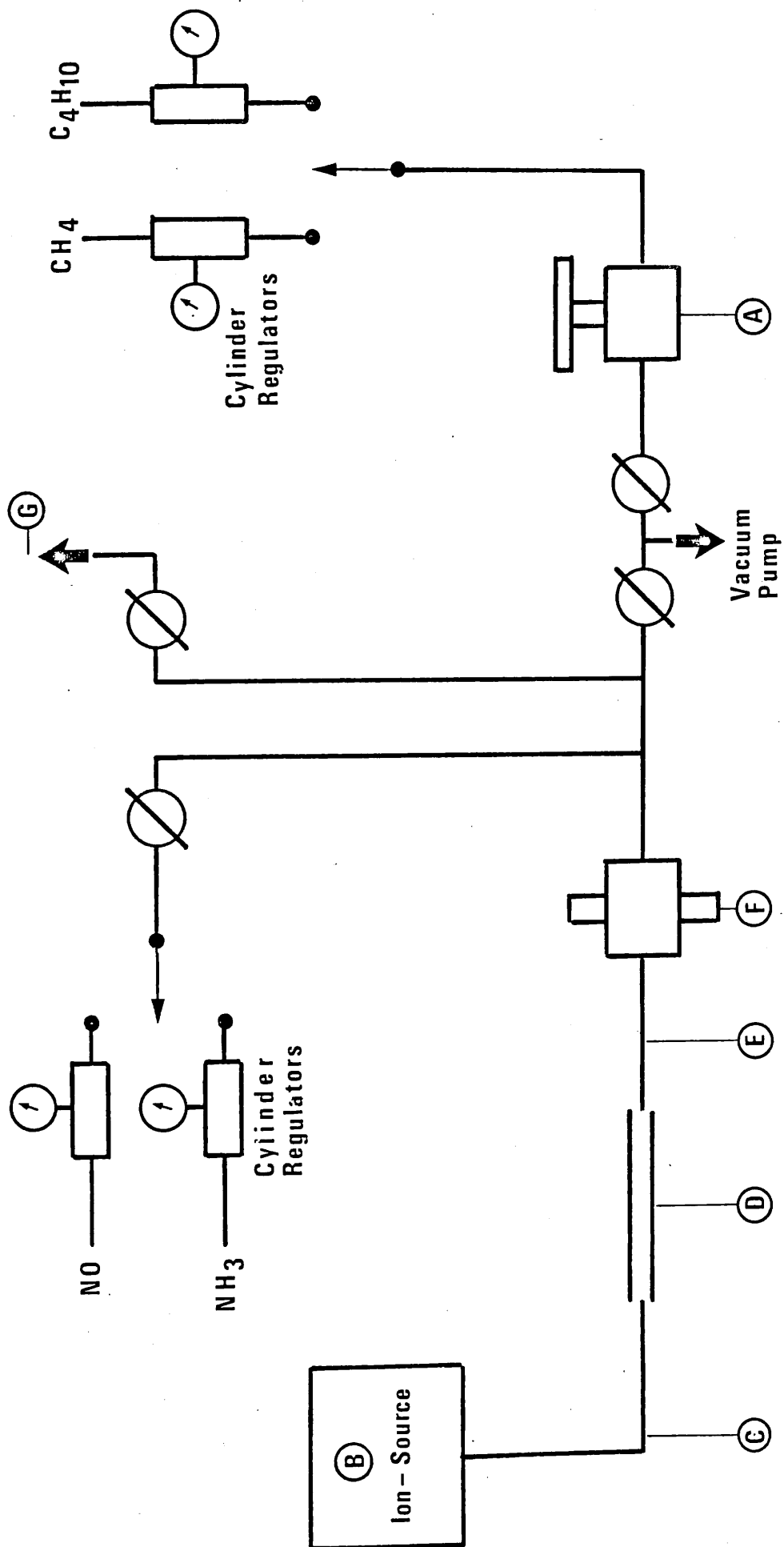


Fig- ( 2.5 ) Modified Reagent Gas Inlet System

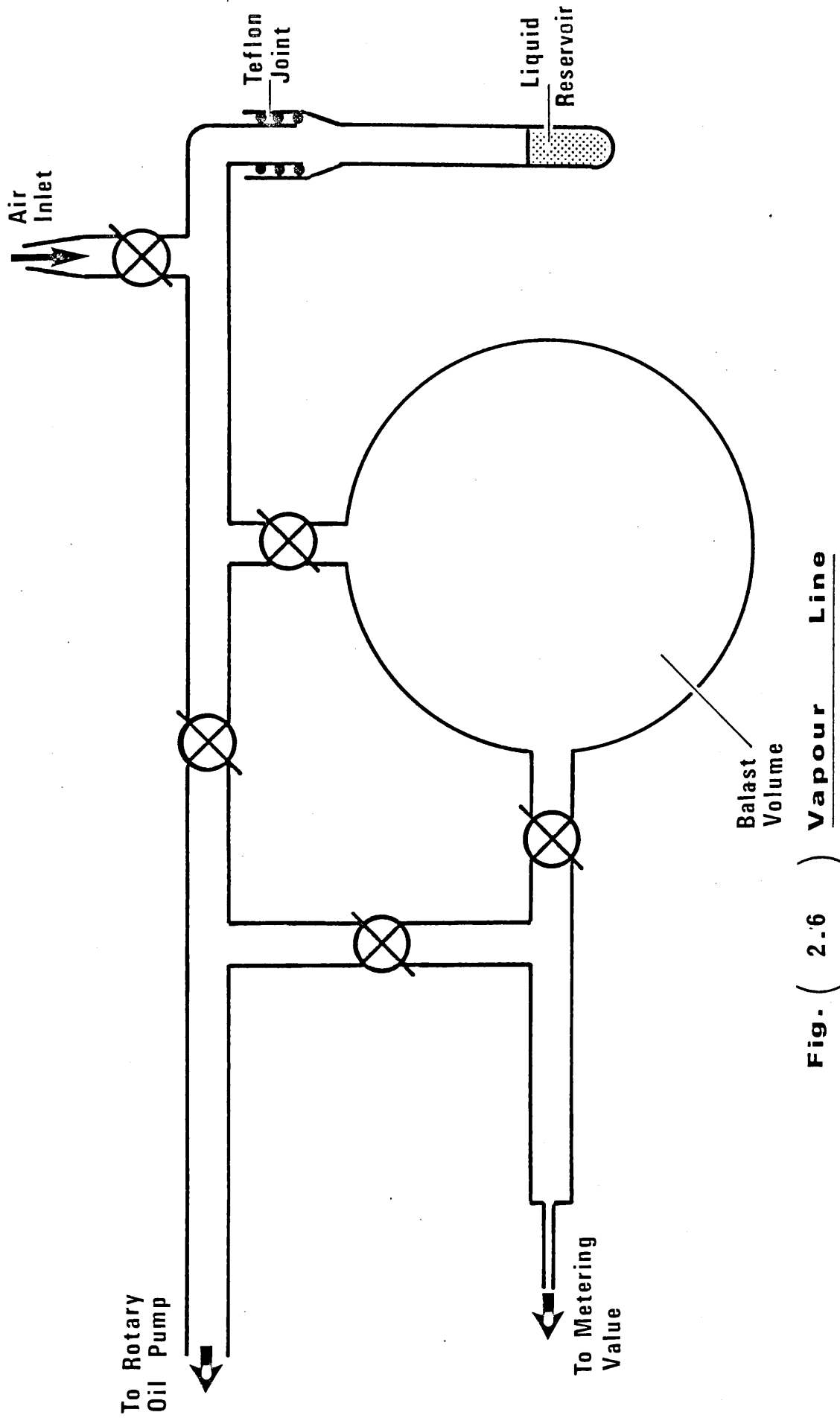


Fig. ( 2.6 ) Vapour Line

## 2.3 MEASUREMENT OF PRESSURES OF GASES IN THE ION-SOURCE.

### 2.3.1 The pressure gauge

Gas pressures in the ion-source were measured by means of a Baratron capacitance manometer pressure measurement system (MKS Instruments series 179)<sup>102</sup> shown in figure (2.7). The high accuracy sensor head (H) consists of a diaphragm type variable capacitance pressure transducer and preamplifier maintained at 35°C by a temperature controller within the electronic unit (E). As the pressure in the sensor head varies, the diaphragm moves causing a change in capacitance leading to a linear variation of the DC output voltage by the electronic control unit (E). This DC voltage is converted to an analogue pressure (Torr) display, (A), and read (BCD code), via a suitable interface, to a Dec PDP 11/34 mini computer.<sup>103</sup> The sensor head had been calibrated against NBS Traceable Factory Standards by the manufacturer. A digital offset facility (D) permitted small changes in pressure to be measured to a higher precision. Pressures were measured in the range  $5 \times 10^{-4}$  to 0.7 Torr with gauge errors varying from  $10^{-6}$  to  $10^{-4}$  Torr respectively.

### 2.3.2 Connection of the pressure gauge to the ion-source.

The pressure gauge was coupled to the mass spectrometer ion-source by means of a glass and metal probe assembly inserted through the ion-source housing port normally used for a capillary g.l.c. interface.



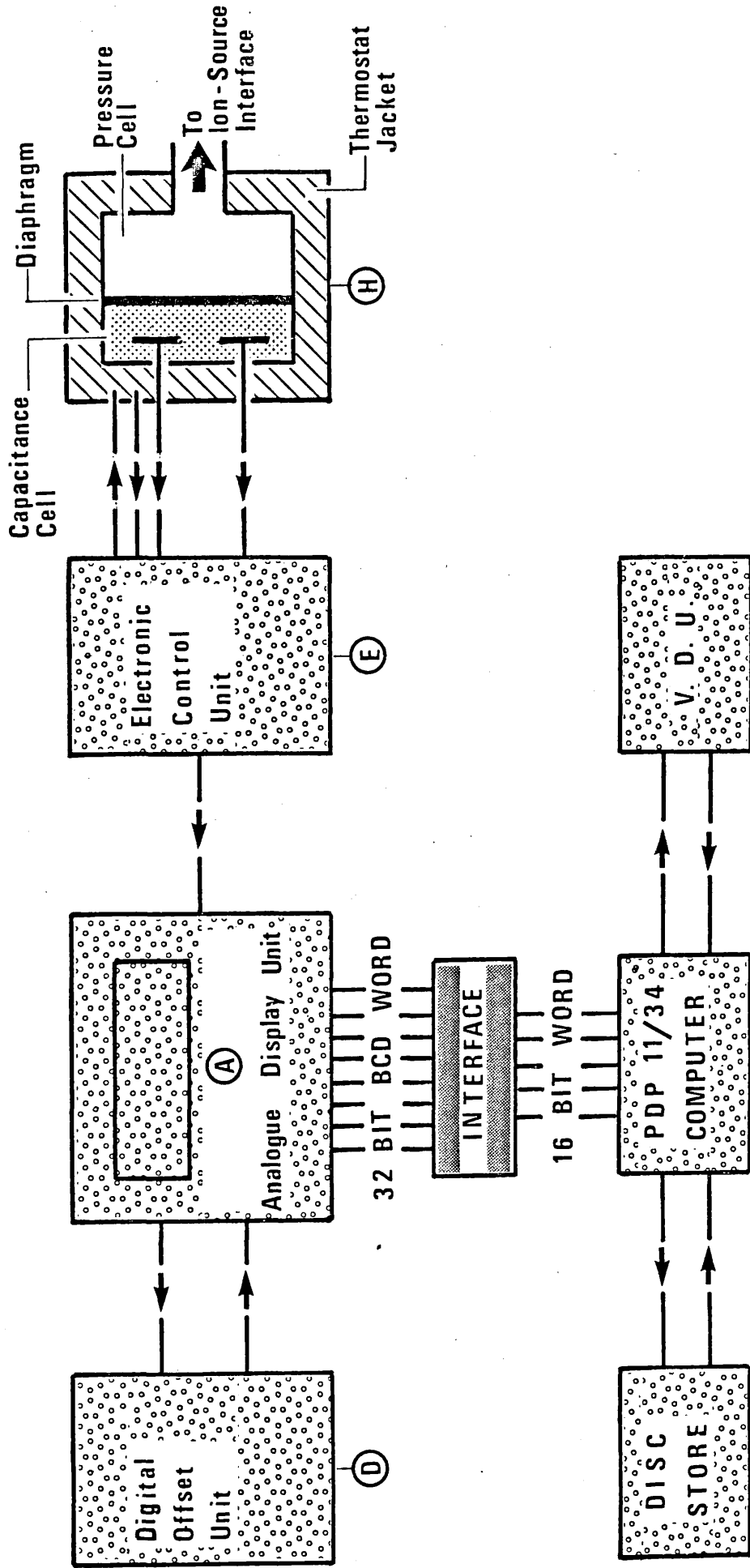


Fig. ( 2.7 ) Baratron Capacitance Manometer Pressure Measurement System

A schematic diagram of this assembly is given in figure (2.8). The stainless steel sleeves (SS) provided protection and support for the thick walled ground glass probe (P). The metal bellow (B1) and (B2) allowed the probe to be withdrawn from the ion-source to permit the source assembly to be removed from the mass spectrometer.

Bellows (B2) also served to isolate the Baratron pressure sensor, mounted on foam rubber, from vibrations. The glass probe contained a chain of twelve 2M ohm pyrofilm<sup>104</sup> resistors (R) interspaced with springs (S) and thermionic valve screen (V) to provide a high impedance electrical path<sup>105</sup> from the high potential ion-source to the ground potential Baratron sensor. No discharging from the ion-source was observed when operating with an accelerating voltage of 4K volts and ion-source pressures up to 0.7 Torr. The probe tip which made a gas tight seal with the ion-source consisted of a wide bore narrow metal tube on which was brazed a steel ball bearing (C). The metal tube was sufficiently long to penetrate into the ion-source cavity. The whole assembly was able to be removed easily and the ion-source plugged when samples of very low volatility were studied, since otherwise they might have been deposited in the probe. Since construction of the probe a simpler design for discharge suppression has appeared in the literature.<sup>106</sup> However the design, which involves packing the probe with glass wool, results in a higher resistance to gas flow and thus the need to correct Baratron pressure readings for thermal transpiration.<sup>107</sup>

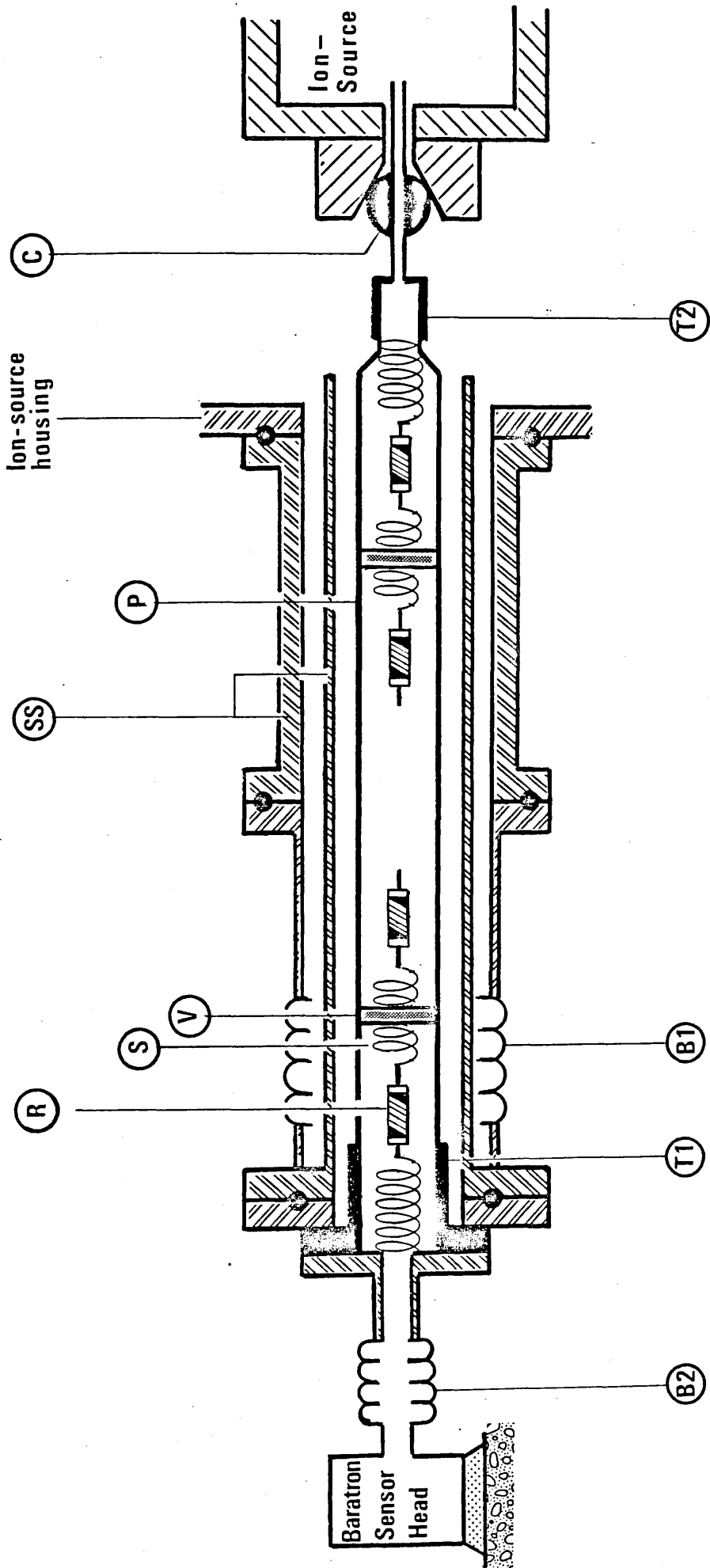


FIG-( 2.8 ) PROBE ASSEMBLY USED TO COUPLE BARATRON HEAD TO THE ION - SOURCE

### 2.3.3 Evaluation of the pressure gauge when coupled to the ion-source.

Prior to purchase of the Baratron gauge ion-source pressures were measured<sup>52</sup> using a Bourdon-tube gauge.<sup>108</sup> This gauge was coupled to the ion-source by means of a glass probe (fig.2.3) inserted into the mass spectrometer through the port normally used for the direct-insertion probe. In order to verify that ion-source pressures measured by the Baratron gauge were comparable with those obtained using the Bourdon-tube gauge, both gauges were temporarily coupled to the ion-source (see fig. 2.1b). Helium, methane and isobutane were separately introduced into the ion-source via the reagent gas inlet system (see section 2.2.1) generating pressures in the range 0.01 - 0.3 Torr which were simultaneously read using both gauges. During these experiments the accelerating voltage was maintained at 4K volts. Least squares analysis of the data resulted in the equations (2.3.1), (2.3.2) and (2.3.3) respectively,

$$\text{Helium } P_B = (0.932 \pm 0.004) P_T + (0.002 \pm 0.002) \quad (2.3.1)$$

$$\text{Methane } P_B = (0.963 \pm 0.013) P_T + (0.002 \pm 0.002) \quad (2.3.2)$$

$$\text{Isobutane } P_B = (0.968 \pm 0.012) P_T + (0.003 \pm 0.001) \quad (2.3.3)$$

where  $P_B$  and  $P_T$  were the pressures recorded by the Baratron and the Bourdon-tube gauges. In order to ascertain that there were no measurable pressure gradients across the source, resulting from the positioning of the reagent gas inlet, helium was alternatively introduced via the g.l.c.

inlet (see fig. 2.1b) located on the opposite side of the source. No variation in the relationship given by equation (2.3.1) was observed. The dead space between the Baratron sensor head and the ion-source was far smaller than that in the Bourdon-tube gauge system and it was concluded that pressures recorded by the factory calibrated Baratron truly reflected ion-source pressures. After these experiments the Texas gauge was disconnected from the ion-source.

#### 2.3.4 Measurement of reagent gas pressures in the ion-source.

Reagent gases were introduced into the ion-source by an inlet system (see fig. (2.5)) and the desired pressure set by a two stage needle valve (F). Coarse pressure variations of methane and isobutane were made using pressure regulator (A). The pressure recorded by the Baratron was monitored using a computer (see fig. (2.7)). Pressure stability was judged to be obtained when the variation was  $<0.007$  Torr over a period of 1.5 minutes.

2.3.5 Measurement of pressures in the ion-source  
due to samples introduced through the septum-  
inlet system.

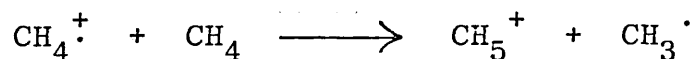
A description of the septum-inlet was given in section (2.2). The sample pressure generated in the ion-source when a few microlitres ( $< 25$ ) of sample was injected into the inlet-system reservoir was typically in the range 0.5-10 m Torr. For the kinetic experiments it was necessary to measure this pressure with the ion-source containing reagent gas (0.2 - 0.3 Torr). The reagent gas pressure was allowed to become stable and the Baratron reading offset to zero. The ion-source pressure generated by the sample, introduced via the septum-inlet, was measured to 0.01m Torr and monitored by the computer during the recording of mass spectra. The standard deviation in the pressure reading was typically 0.04 m Torr, leading to a maximum error in sample pressure of 8% at 0.5 m Torr and minimum error of 0.4% at 10 m Torr.

## 2.4 KINETIC STUDIES

### 2.4.1 Measurement of ion-abundances: The ion-molecule reactions consequent upon the electron impact of pure reagent gases.

#### 2.4.1.1 Methane -

The study of the kinetics of the reaction



was carried out using identical conditions to those used by R. Walder<sup>52</sup> in a previous study when a Bourdon-tube gauge was used to measure ion-source pressures. The ion-source block was maintained at  $177 \pm 2^\circ\text{C}$  and the mass spectrometer operated at an ion-source electric field strength of  $12.5 \text{ V cm}^{-1}$  (5 V repeller), emission current of  $10 \mu\text{A}$ , and electron energy of 500 eV. Methane was introduced to the ion-source via the reagent gas inlet system (2.2.1) and the pressure measured using the Baratron gauge as described in section (2.3.4). When the ion-source pressure was stable ( $\pm 0.02\text{m Torr}$ ) the mass spectrum was recorded as described in section (2.2). The pressure of methane in the ion-source was then changed

and after stabilisation the pressure and another spectrum recorded. In this way spectra of methane were acquired at various ion-source pressures in the range 0.01 - 0.25 Torr. Heights of peaks in the spectra were measured as described in section (2.2), and corrected for the different responses of the galvanometers by use of equations (2.2.1) and (2.2.2) to give the abundance ( $I_n$ ) of ions having mass to charge ratio ( $m/z$ )  $n$ .

#### 2.4.1.2 Isobutane -

Experiments to study the ion-molecule reactions consequent upon the electron-impact ionization of isobutane were carried out at an ion-source field strength of  $5 \text{ V cm}^{-1}$  (2 V repeller), emission current of  $50 \mu\text{A}$ , electron energy of 50 eV and ion-source block temperature of  $177 \pm 2^\circ\text{C}$ . Isobutane gas was introduced to the ion-source via the reagent gas inlet system (section 2.2.1) and the pressure measured using the Baratron gauge. Spectra were recorded when the Baratron gauge readings were constant. The isobutane pressures could be stabilized to  $\pm 0.07 \text{ m Torr}$  in the range 0.01 - 0.4 Torr. Heights of peaks in the spectra were measured as described in section (2.2) and corrected for differing galvanometer responses using equations (2.2.1) and (2.2.2). The relative abundance of ion  $m/z = n$  for each isobutane pressure was obtained by dividing the height of the appropriate peak by the sum of the height of all the peaks in the spectrum. The results of these experiments will



be discussed in section (3.1.2.1).

#### 2.4.1.3 Methylcycloalkanes -

Ion molecule reactions consequent upon the electron impact of the methylcycloalkanes; methylcyclopentane and methylcyclohexane were studied at an ion-source block temperature of  $177 \pm 2^{\circ}\text{C}$  and an ion-source field strength of  $5 \text{ V cm}^{-1}$  (2 V repeller). The electron energy was maintained at 50 eV and emission currents of 50 and 20  $\mu\text{A}$  were used for methylcyclopentane and methylcyclohexane respectively. The cycloalkanes were introduced via the reagent gas inlet system as described in section (2.2.1) with the liquid reservoir (fig. (2.6) page 87 ) maintained at  $14.5 \pm 0.2^{\circ}\text{C}$ . Spectra were obtained, in the same way as described for isobutane (2.4.1.2), in the pressure ranges 0.01 - 0.35 Torr for methylcyclopentane and 0.01 - 0.25 Torr for methylcyclohexane. Relative abundances ( $I_n$ ) at a given pressure were determined as before and these results are discussed in sections (3.1.2.2), (3.1.2.3) and (4.1).

#### 2.4.1.4 Ammonia -

Ion-molecule reactions consequent upon the electron impact of ammonia have been studied at an ion-source temperature of  $177 \pm 2^{\circ}\text{C}$  and electric field strength of 2.5, 5.0, 7.5, 10.0 and  $12.5 \text{ V cm}^{-1}$ . The electron energy was maintained at 50 eV and the emission current at 20  $\mu\text{A}$ . Ammonia was introduced via the reagent gas inlet system (see section (2.2.1)) and the pressure set

by means of the micrometering valve (see fig. (2.5)). Spectra were recorded as described previously (section (2.4.1.2)) at various pressures within the range 0.01 - 0.6 Torr and relative abundances calculated. These results are recorded in section (3.1.2.4) and discussed in sections (4.2.1.) and (4.2.2).

#### 2.4.1.5 Fluorinated benzenes-

Ion-molecule reactions consequent upon the electron impact of the fluorinated benzenes: fluorobenzene, o-, m-, and p- difluorobenzene have been studied at an ion-source block temperature of  $177 \pm 2^{\circ}\text{C}$  and ion-source field strength of  $5 \text{ V cm}^{-1}$ . The electron energy was maintained at 50 eV and the emission current at 50  $\mu\text{A}$ . The fluorinated benzenes were introduced from a vapour line (fig (2.6)) via the reagent gas inlet system (fig. (2.5)) and the ion-source pressure set by a micrometering valve. The liquid reservoir of the vapour line was maintained at  $15.5 \pm 0.2^{\circ}\text{C}$ . Spectra were recorded as described in section 2.2 at various pressures in the range 0.01 - 0.26 Torr. The relative abundances were calculated (see (2.4.1.2)) and the results recorded in sections (3.1.3.1) and (3.1.3.2) and discussed in section (4.3).

#### 2.4.2 Measurement of ion-abundances in the ion-molecule reactions which give rise to the chemical ionization mass spectra of hydrocarbons when fluorobenzene is the reagent gas.

The ion-molecule reactions which give rise to the

chemical ionization mass spectra of hydrocarbons were studied by following changes in the abundances of reactant ions with variation of sample pressure. Prior to commencement of any experiment the septum in the liquid sample inlet was renewed. All experiments were carried out with the ion-source at  $177 \pm 2^{\circ}\text{C}$ , an emission current of  $50 \mu\text{A}$ , an electron energy of 50 eV and an ion-source field strength of  $5 \text{ V cm}^{-1}$  (2 V repeller). Fluorobenzene was introduced into the ion-source at such a rate to give a fixed pressure of 0.2 Torr. The temperature of the inlet delivery tube was maintained at  $130^{\circ}\text{C}$  and that of the sample reservoir set between 170 and  $250^{\circ}\text{C}$  depending on sample volatility. When the fluorobenzene pressure and ion-source temperature were constant the Baratron reading was offset to zero. A known volume of sample was injected into the inlet reservoir and the pressure monitored during spectra acquisition as described in section (2.3.5). The sample was then pumped from the reservoir and a different volume injected. This process was repeated and spectra recorded for sample pressures in the range 0.5 - 10.0 m Torr.

The heights of peaks in the spectra were measured and normalised with respect to the total ion current as described in section (2.2). Suitable plots of normalised ion-currents (relative abundances) against pressure were used to determine the kinetics of reaction (see (3.1.4)).

## 2.5 LUBRICATING BASE OIL ANALYSIS

The base oils studied had kinematic viscosities in the range  $0.035 - 0.2 \text{ cm}^2 \text{ s}^{-1}$  (3.5 - 20.0 c Stokes at  $100^\circ\text{C}$ ) and could not be introduced via the liquid sample inlet. 2  $\mu\text{l}$  of solutions of the oil (4% W/W), in a suitable solvent, (see Table 2.4) were placed in pyrex probe sample tubes and after removal of solvent introduced via the direct-insertion probe. In the case of mineral oil fractions, analysed by fluorobenzene chemical ionization, an internal standard (0.01 W/W) (triphenyl benzene) was added to the oil sample prior to its dissolution in fluorobenzene (4% W/W). The heating of the probe ( $25^\circ\text{C}/\text{min}$ ) was controlled by a seven step temperature programmer (Eurotherm type 211)<sup>109</sup>. The programmer allowed fast, and accurate control of the temperature of the probe giving reproduceable volatilisation profiles of the oil sample from the sample tube. Spectra were recorded with an accelerating voltage of 3 k volts (which permits the collection of ions of 0-600 a m u) with a resolution of 900 at 10% valley. Throughout sample volatilisation, a suitable liquid (mass = M), hereinafter referred to as a "Sensitivity standard", was introduced at a constant rate, via the liquid inlet and the intensity of the ion current due to ion  $(M + m)^+$  (where  $m = +18, +1, -1$  or 0) recorded to monitor variations in sensitivity of the detector system. Spectra were recorded (a) using a data system (see Appendix II) at a rate of 9 spectra a minute or (b) at given probe

temperatures (Table 2.4) according to the method described in section (2.2). Conditions specific to the analysis of each type of lubricating fluid are now discussed in turn.

### 2.5.1 Ester fluids

Chemical ionization mass spectra of pure esters standards (see (2.1.3.1-2)), mixtures of these and industrial ester samples were obtained using ammonia reagent gas. The results obtained are recorded in section (3.2.1) and discussed in section (4.5.1).

### 2.5.2 Synthetic hydrocarbon fluids

#### 2.5.2.1 Hydrogenated polyalphaolefins -

Chemical ionization spectra have been obtained using methane, nitric oxide and mixtures of nitrogen and nitric oxide as reagent gases (see Table 2.4 for mass spectrometer operating conditions, sensitivity standard, and solvent in which samples were dissolved). When nitrogen/nitric oxide mixtures were used nitrogen was introduced via the g.l.c. interface to generate an ion-source pressure of ~0.15 Torr, and at the same time sufficient nitric oxide introduced via the reagent gas inlet system (see fig. (2.5) page 86 ) so that 99% of the reagent gas plasma ion-current was due to  $\text{NO}^+$  ( $m/z = 30$ ). The results gained from these analyses are recorded in section (3.3.2.1 - 3) and discussed in section (4.5.2).

### 2.5.2.2 Synthetic aromatic hydrocarbon fluids -

Chemical ionization mass spectra of synthetic aromatic hydrocarbons were obtained using (a) fluorobenzene reagent gas and (b) nitrogen/nitric oxide mixture reagent gas (see 2.5.2.1). Conditions used in the analysis are given in Table (2.4). The results obtained are recorded in section (3.2.3 ) and discussed in section (4.5.3).

### 2.5.3 Mineral oil fractions

These were analysed by fluorobenzene chemical ionization mass spectrometry; the results are recorded in section (3.2.4) and discussed in (4.5.4).

TABLE 2.4 Conditions used in the chemical ionization mass spectrometry of base oils

Base oil	Reagent gas	Ion-source pressure	Sample solvent	Mass spectrometer operating conditions		Sensitivity standard	Spectra acquisition	
				Repeller	Emission Electron energy		Data system	Oscillographic recorder at temps
Ester fluids	Ammonia	0.6 Torr <sup>*</sup>	Diethyl ether	2V	200 $\mu$ A	50 eV	Bis(methyl) hexanedioate	9 spec/min Probe 50-250 $^{\circ}$ C
Hydrogenated polyalpha olefins	Methane	0.2 Torr <sup>†</sup>	n-pentane	1V	200 $\mu$ A	100 eV		50, 100, 150, 200, 250 $^{\circ}$ C
"	Nitric oxide	0.2 Torr <sup>‡</sup>	n-pentane	2V	100 $\mu$ A	50 eV		100, 150, 200, 250 $^{\circ}$ C
"	Nitrogen/nitric oxide mixtures	0.2 Torr <sup>‡</sup>	n-pentane	1V	100 $\mu$ A	50 eV	1-Phenyl nonane	9 spec/min Probe 50-250 $^{\circ}$ C
Synthetic aromatic hydrocarbons	Fluoro-benzene	0.2 Torr <sup>‡</sup>	Fluoro-benzene	2V	20 $\mu$ A	50 eV		50, 100, 150, 200, 250 $^{\circ}$ C
"	Nitrogen/nitric oxide mixtures	0.2 Torr <sup>‡</sup>	n-pentane	2V	100 $\mu$ A	50 eV		50, 100, 150, 200, 250 $^{\circ}$ C
Mineral oil fractions	Fluoro-benzene	0.2 Torr <sup>‡</sup>	Fluoro-benzene	2V	20 $\mu$ A	50 eV	Ion m/z=191 see(4.5.3)	9 spec/min Probe 50-250 $^{\circ}$ C

\* Estimated by method discussed in section (4.2.3.2)

† Estimated by method of Hancock and Walder

$$* \log ([\text{CH}_4^+]_0 / [\text{CH}_4^+]) = k[\text{CH}_4]\tau$$

where  $[\text{CH}_4^+]$  is the abundance of  $\text{CH}_4^+$  ions,  $[\text{CH}_4^+]_0$  is the initial abundance of  $\text{CH}_4^+$  ions (i.e. in the absence of reaction (3.1.1)),  $[\text{CH}_4]$  is the number density (molec  $\text{cm}^{-3}$ ) of methane molecules in the ion-source, and  $\tau$  is the residence time (seconds) of  $\text{CH}_4^+$  ion. If the heights of peaks ( $I_n$ ), having  $m/z = n$ , measured in the spectrum may be assumed to accurately reflect the relative abundances of the ions in the ion-source (see 1.3.3) then

$$\log (I_{16}^0 / I_{16}) = k[\text{CH}_4]\tau$$

If further it can be assumed that (3.1.1) is the only reaction undergone by  $\text{CH}_4^+$  over the pressure range studied (0.01 - 0.25 Torr) then

$$[\text{CH}_4^+]_0 = [\text{CH}_4^+] + [\text{CH}_5^+]$$

hence

$$\log ((I_{16} + I_{17}) / I_{16}) = k[\text{CH}_4]\tau \quad (3.1.2)$$

where  $I_{17}$  is the abundance of the  $\text{CH}_5^+$  ion. The quantity  $[\text{CH}_4]$ , the number density of methane molecules in the ion-source, may be calculated from the equation of state of an ideal gas:

$$[\text{CH}_4] = P_{\text{CH}_4} / k_B T = P_{\text{CH}_4} N \quad (3.1.3)$$

where  $k_B$  is Boltzman's constant ( $1.3806 \times 10^{-23} \text{ JK}^{-1}$ ),  $T$  the absolute temperature (K) and  $P_{\text{CH}_4}$  the pressure ( $\text{Nm}^{-2}$ ). However it is usual to report rate coefficients of ion-molecule reactions in units of  $\text{cm}^3 \text{ molecule}^{-1} \text{ s}^{-1}$  although

---

\* 'log' refers to Napierian Logarithms throughout.



pressure measurements are made in units of Torr, (this work) or m Bar. The necessary conversion factors are taken in the value of  $N$  viz.  $2.146 \times 10^{16}$  for the ion-source temperature (450K) used in this study.

Hence (3.1.2) becomes

$$\log \left( \frac{I_{16} + I_{17}}{I_{16}} \right) = kNP_{\text{CH}_4} \tau \quad (3.1.4)$$

A plot of the data obtained in the experiment is given in Figure (3.1), and from the slope of the line,  $kN\tau$ ,  $k$  can be estimated provided the ion-source residence time,  $\tau$ , of  $\text{CH}_4^+$  is known.

There are two methods for the estimation of ion residence times. In the first it is assumed that under the conditions of the experiment (pressure  $<0.3$  Torr, electric field strength  $12.5 \text{ Vcm}^{-1}$ ), each ion experiences only a few collisions with methane molecules before exiting the ion-source, and that these collisions do not change the velocity of the ion significantly. If these assumptions are valid then the free-fall formula<sup>64</sup>, (3.1.5), for an ion drifting in an electric field may be used for residence time estimation.

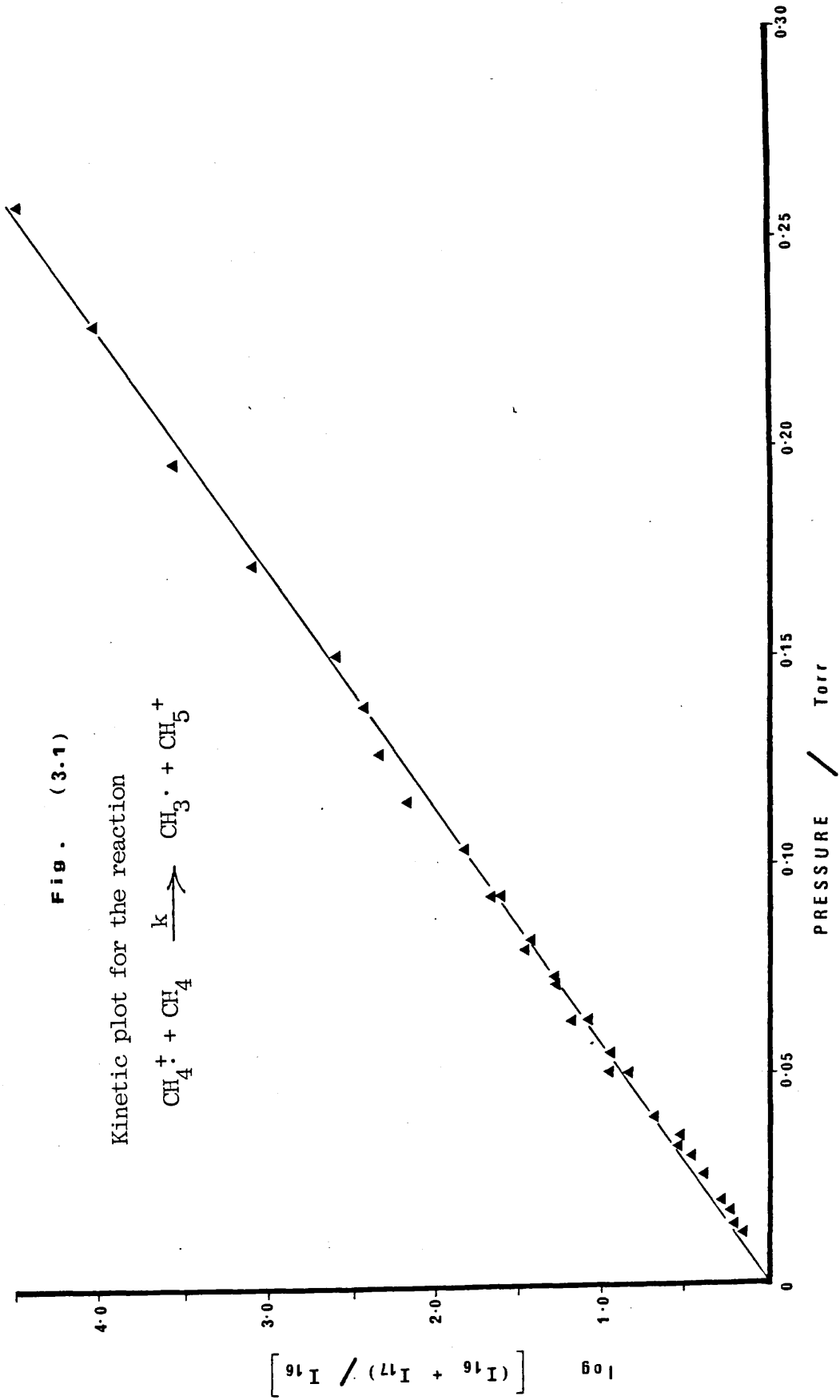
The free-fall formula is

$$\tau = \left( \frac{2md}{zE} \right)^{\frac{1}{2}} \quad (3.1.5)$$

where  $d$  is the mean distance travelled by the ion (cm),  $m$  and  $z$  are the mass (kg) and charge (C) of the ion, and  $E$  is the electric field strength ( $\text{Vm}^{-1}$ ).

Fig. (3.1)

Kinetic plot for the reaction



In the second method the effects of collisions are taken into account for invoking ion-mobility considerations. The drift velocity of an ion may be obtained from equation (3.1.6) where  $K$  is the ion-mobility and  $E$  is as defined above. If

$$V = KE \quad (3.1.6)$$

an experimental value of  $K$  is not available then the reduced mobility  $K_0$ , related to  $K$  by equation (3.1.7) may be estimated using equation (3.1.8)

$$K = K_0 (760/P) (T/273) \quad (3.1.7)$$

$$K_0 = 13.876/(\alpha\mu)^{\frac{1}{2}} \quad (3.1.8)$$

where the pressure ( $P$ ) is measured in Torr,  $T$  is the absolute temperature (K),  $\mu$  the reduced mass of the ion and neutral (in a.m.u.) and  $\alpha$  the angle-averaged polarizability (in  $\text{\AA}^3$ )\* of the neutral. Since  $\tau = d/v$  it can be seen that the residence time is given by

$$\tau = 273(\alpha\mu)^{\frac{1}{2}} dP / (10546ET) \quad (3.1.9)$$

If collisions are important the residence time is directly proportional to the pressure and consequently the apparent kinetic order of the reaction with respect to methane will appear greater by one order.

The data in Figure (3.1) clearly shows this not to be so. Thus it is assumed that  $\tau$  may be estimated from equation (3.1.5) as previously noted.<sup>52</sup> The mean distance

---

\*See Appendix I for polarizabilities and dipole moments of neutrals studied in this work.

travelled by the ion (d) is taken as half the distance between the ion-exit slit and the repeller plate (0.2 cm), as the  $\text{CH}_4^+$  ions are assumed to be evenly distributed throughout the ion-source at these pressures<sup>110</sup>. The mean residence time was calculated to be  $7.3 \times 10^{-7}$  sec. Least squares analysis of the data gave a gradient of  $18.78 \pm 0.24$  leading to a value of  $(11.6 \pm 0.2) \times 10^{-10} \text{ cm}^3 \text{ molecule}^{-1} \text{ s}^{-1}$  for the rate coefficient for reaction of  $\text{CH}_4^+$  with methane. This is in excellent agreement with both literature values and with previous work in this department. The result when combined with the good agreement in pressure readings by the Texas and Baratron gauges (see 2.3.3), when simultaneously connected to the ion-source, showed that a suitable coupling of the Baratron gauge to the ion-source had been achieved.

Subsequently values of  $k_{16}$  have been evaluated at various field strengths between 2.5 and 12.5  $\text{V cm}^{-1}$ , see table (3.1), and found to be invariant. Since these values were obtained using a mean ion-drift distance of 0.2 cm, the distance between the electron beam and ion exit slit, it is assumed that the mean distance travelled by an ion in the source is independent of field strength at pressure 0.01 - 0.2 Torr.

TABLE 3.1 Rates of reaction of  $\text{CH}_4^+$  with methane at various ion source field strengths.

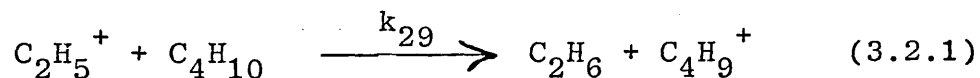
Field Strength $/\text{V cm}^{-1}$	Rate coefficient $\times 10^{10}/\text{cm}^3 \text{ molecule}^{-1} \text{ s}^{-1}$
12.5	(11.6 $\pm$ 0.2)
11.25	(12.06 $\pm$ 0.5)
8.75	(12.19 $\pm$ 0.2)
6.25	(12.11 $\pm$ 0.4)
4.0	(12.12 $\pm$ 0.3)

### 3.1.2 Ion molecule reactions in reagent gas plasmas of:-

#### 3.1.2.1. Iso-butane

The experimental method employed for the study of reactions of primary ions derived from iso-butane with iso-butane was the same as used by R. Walder in a previous study using the 12F spectrometer,<sup>52</sup> and is described elsewhere (see 2.4.1.2).

Electron impact ionization of iso-butane results in formation of  $C_4H_{10}^+$  which fragments to produce various primary ions <sup>figure (3.4)</sup>. Variation of the relative ion-currents ( $I_n/\Sigma I$ ) of these ions ( $m/z=n$ ) with ion-source pressure is shown in figure (3.2). The relative ion-currents of the primary ions decrease, whereas that of  $C_4H_9^+$  increases in the pressure range 0 - 0.4 Torr, and thereafter remains essentially constant. It is assumed that all the primary ions react with iso-butane to form  $C_4H_9^+$ , e.g.



Provided the ion-source residence times can be estimated rates of reactions of this type may be obtained by observing the decrease in the relative ion-currents of the primary ions. By use of equations (3.1.5) and (3.1.9) (taking  $d = 0.2 \text{ cm}^*$ ) it can be shown that for iso-butane pressures greater than 0.05 Torr the residence time estimated by consideration of ion-mobilities is greater than that suggested by the free fall method. Therefore unlike the methane system collisions

---

\* as determined for methane (see 3.1.1).

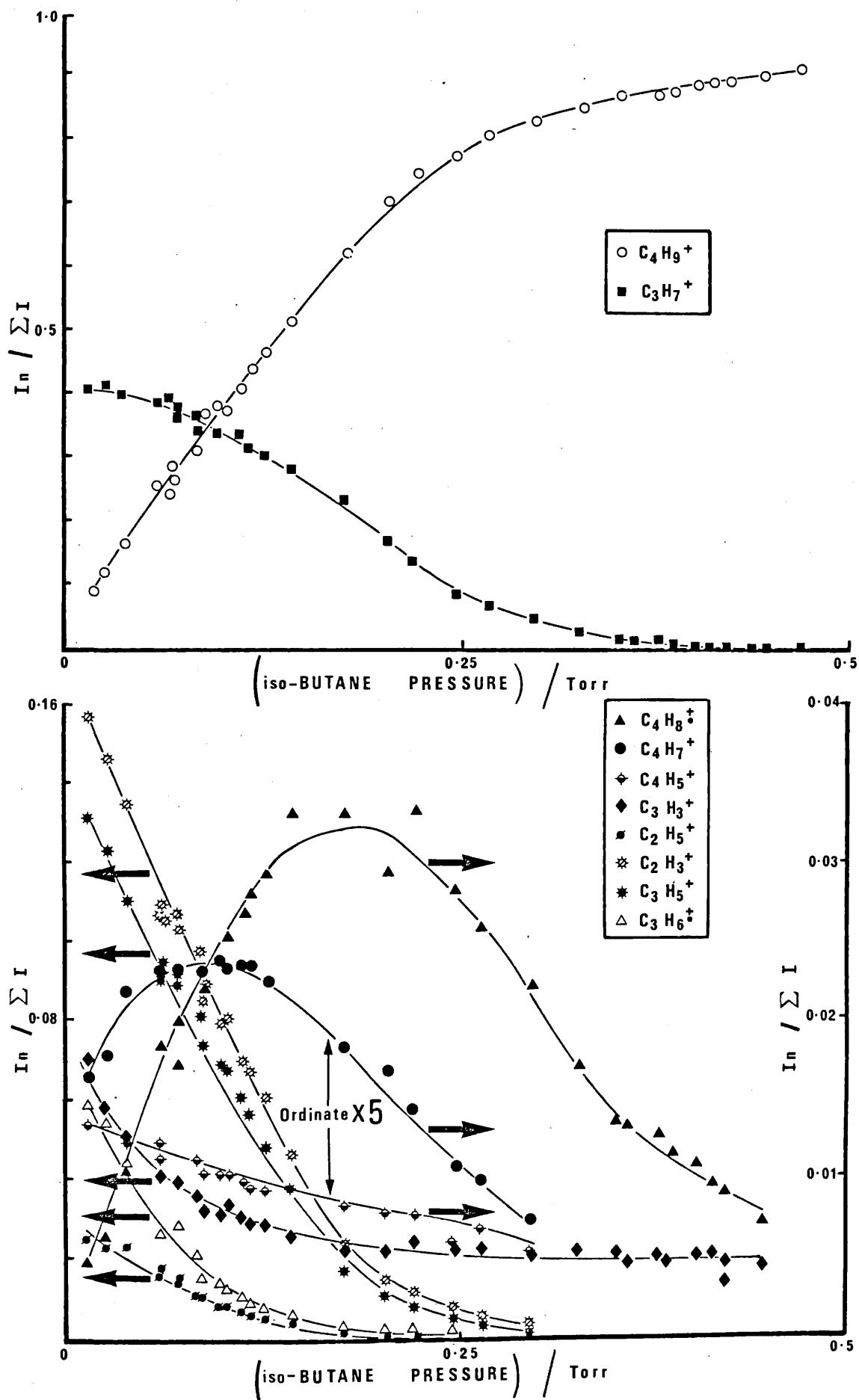


Fig. [ 3.2 ]

Variation of ion abundance with ion-source pressure for iso-butane reagent gas.

are important and better estimates of residence times will be obtained by taking account of ion-mobilities. This is as expected since a collision of an ion with the larger iso-butane molecule would result in a greater change in momentum than a collision of the same ion with methane. In addition the number of these collisions increases with further increases in ion-source pressure (0.05 to 0.4 Torr). From equation (3.2.1)

$$-d \frac{[C_2H_5^+]}{dt} = k_{29} [C_2H_5^+] [C_4H_{10}]$$

and the integrated rate-equation for the reaction of  $C_2H_5^+$  is

$$- \log ( [C_2H_5^+] / [C_2H_5^+]_0 ) = k_{29} [C_4H_{10}] \tau \quad (3.2.2)$$

where  $[C_4H_{10}]$  is the number density of iso-butane molecules in the ion-source. This is obtained from the ion-source pressure,  $P$ , using equation (3.2.3) where  $N$  is as previously defined (see (3.1.1) equation (3.1.3)).

$$[C_4H_{10}] = P_{C_4H_{10}} N \quad (3.2.3)$$

The residence time,  $\tau$ , as given by equation (3.1.9) is directly proportional to the ion-source pressure. So provided the heights ( $I_n$ ) of the peaks, having  $m/z=n$ , in the recorded spectrum accurately reflects the relative abundances of ions in the ion-source, equation (3.2.2) may be written as

$$- \log ( I_{29} / I_{29}^0 ) = k_{29} \beta_{29} N P^2_{C_4H_{10}} \quad (3.2.4)$$



where

$$\beta_{29} = 273(\alpha\mu_{29})^{\frac{1}{2}} d/(10546 ET) \quad (3.2.5)$$

$I_{29}^0$ , the abundance of  $C_2H_5^+$  in the absence of reaction with iso-butane, is not readily accessible. To reduce the effect of loss of reactant ions through collisions with the ion-source chamber walls the extraction of the rate coefficient is made using relative ion-currents ( $I_n/\Sigma I$ ) where  $\Sigma I$  is the total ion-current). Thus equation (3.2.4) becomes

$$\log (I_{29}/\Sigma I) - \log(I_{29}^0/\Sigma I^0) = -k_{29}\beta_{29}NP^2 C_4H_{10} \quad (3.2.6)$$

hence a plot of  $\log (I_{29}/\Sigma I)$  against the square of the iso-butane pressure should give a straight line of gradient  $k_{29}\beta_{29}N$  and intersect  $\log (I_{29}^0/\Sigma I^0)$  corresponding to the relative abundance of  $C_2H_5^+$  in the electron impact spectrum of iso-butane.

Equations similar to (3.2.6) can be derived for bimolecular reactions of all the primary ions from iso-butane with iso-butane and kinetic plots for the processes are given in figure (3.3). Rate coefficients evaluated from gradients, determined by least squares analysis of these lines, are given in table (3.2) and are in reasonable agreement with previous measurements in this laboratory.<sup>52</sup> The reactions of some primary ions were observed not to obey second order kinetics throughout the entire pressure range studied and thus the pressure range over which they adhered is appended.

iso-BUTANE REAGENT GAS

$$\left( P_{i-C_4H_{10}} \right)^2 / \text{Torr}^2$$

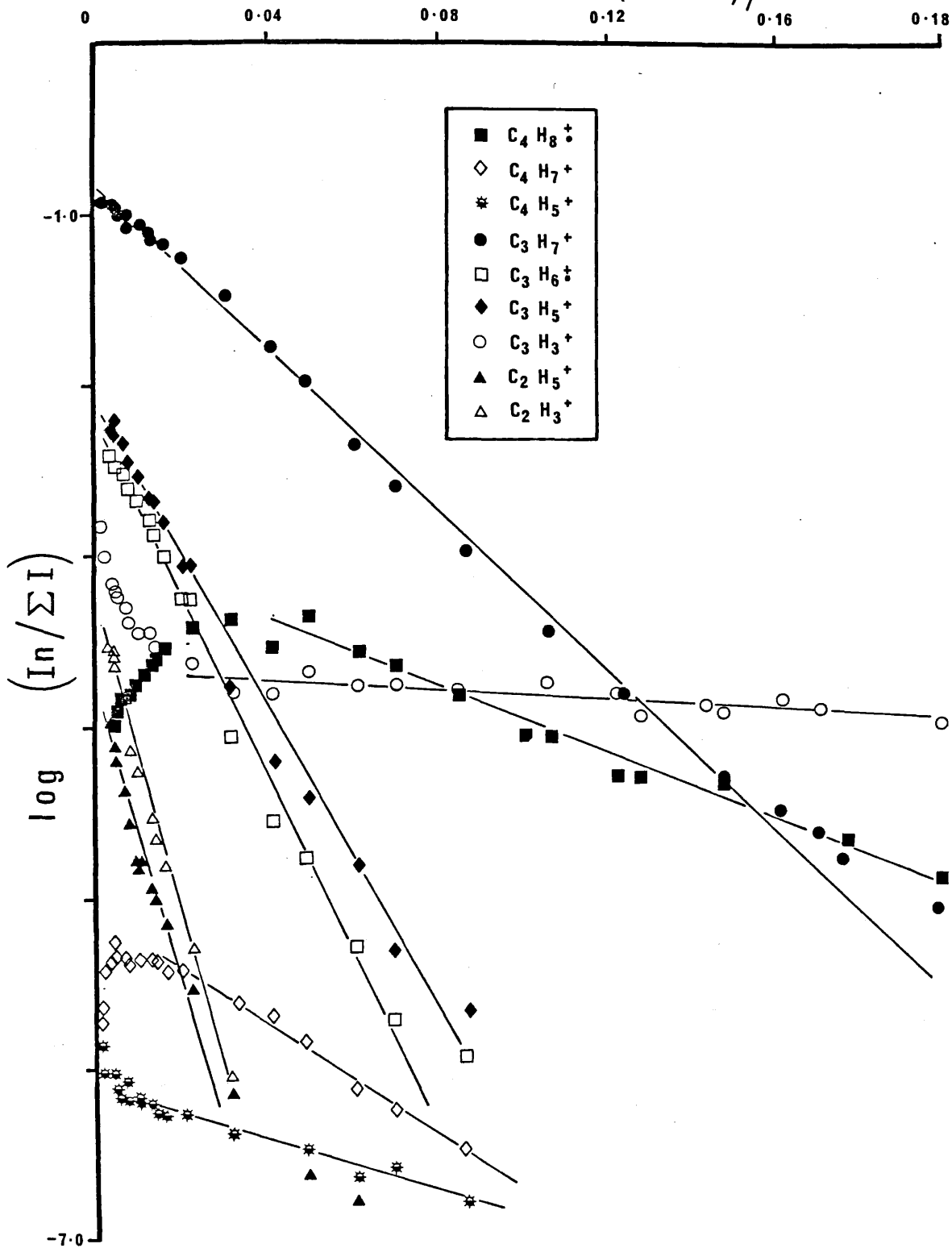
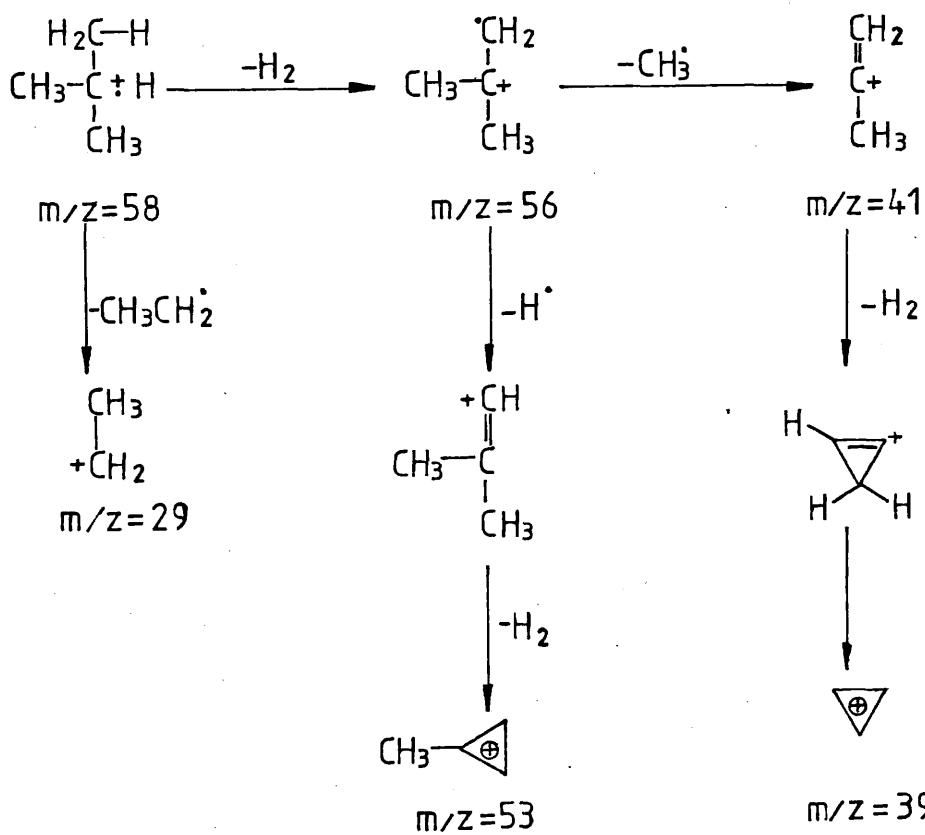
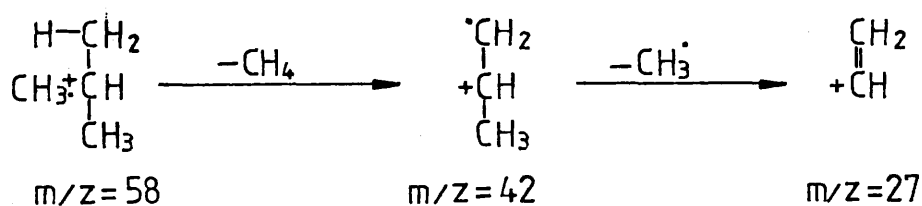
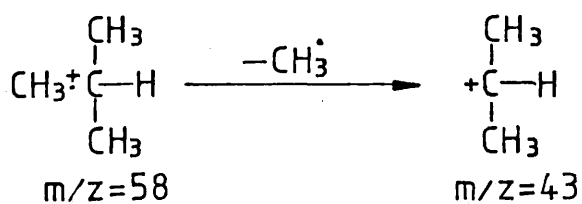


Fig. [ 3.3 ]

Kinetic plot for reaction of ions from iso-butane with iso-butane.

Fig(3.4) Fragmentation of iso-butane consequent upon electron impact ionization. See Ref 52.



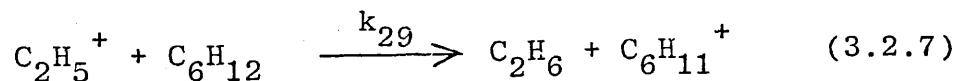
**TABLE 3.2** Rate coefficients for the reaction of primary ions from isobutane with iso-butane

Ion	m/z	Rate coefficient $\times 10^{11}/\text{cm}^3 \text{ molec}^{-1}$ $\text{s}^{-1}$	$\text{Log} (I_n^0/\Sigma I)$	Pressure range over which second order kinetics hold /Torr
$\text{C}_2\text{H}_3^+$	27	$16.0 \pm 0.8$	$-(3.23 \pm 0.07)$	0.03 - 0.18
$\text{C}_2\text{H}_5^+$	29	$13.0 \pm 0.4$	$-(3.84 \pm 0.06)$	0.03 - 0.18
$\text{C}_3\text{H}_3^+$	39	$0.20 \pm 0.04$	$-(3.68 \pm 0.03)$	0.18 - 0.46
$\text{C}_3\text{H}_5^+$	41	$6.88 \pm 0.16$	$-(2.06 \pm 0.03)$	0.03 - 0.26
$\text{C}_3\text{H}_6^+$	42	$7.43 \pm 0.18$	$-(2.19 \pm 0.04)$	0.03 - 0.26
$\text{C}_3\text{H}_7^+$	43	$3.16 \pm 0.04$	$-(0.90 \pm 0.03)$	0.03 - 0.46
$\text{C}_4\text{H}_5^+$	53	$1.12 \pm 0.06$	$-(6.11 \pm 0.03)$	0.11 - 0.30
$\text{C}_4\text{H}_7^+$	55	$2.08 \pm 0.08$	$-(5.14 \pm 0.03)$	0.11 - 0.30
$\text{C}_4\text{H}_8^+$	56	$1.28 \pm 0.04$	$-(2.99 \pm 0.04)$	0.22 - 0.46

## 3.1.2.2. Methylcyclopentane

Spectra were obtained at various ion-source pressures in the range 0.01 - 0.35 Torr and relative ion-currents for the ions observed calculated, at each pressure, as already described. (See 2.4.1.2 and 2.4.1.3).

The molecular ion  $C_6H_{12}^+$  formed upon electron impact ionization of methylcyclopentane readily fragments to produce primary ions. Possible fragmentation pathways are illustrated in figure (3.5), where a \* denotes the observation of fragmentation of a metastable ion (see 1.2.3) in support of a fragmentation pathway. Variations of relative ion-currents of these primary ions with ion-source pressure are given in figures (3.6) and (3.7). As the pressure of methylcyclopentane is increased the relative ion-currents of the primary ions decrease. This is attributable to their reacting with methylcyclopentane in a similar way to that already described for iso-butane. However unlike iso-butane there are three product ions namely  $C_6H_{12}^+$ ,  $C_6H_{11}^+$  and  $C_6H_{10}^+$ . The  $C_6H_{11}^+$  ion is likely to be produced by similar reactions to those which result in the formation of  $C_4H_9^+$  in isobutane, typified by the hydride transfer reaction of  $C_2H_5^+$  with methylcyclopentane (equation 3.2.7)



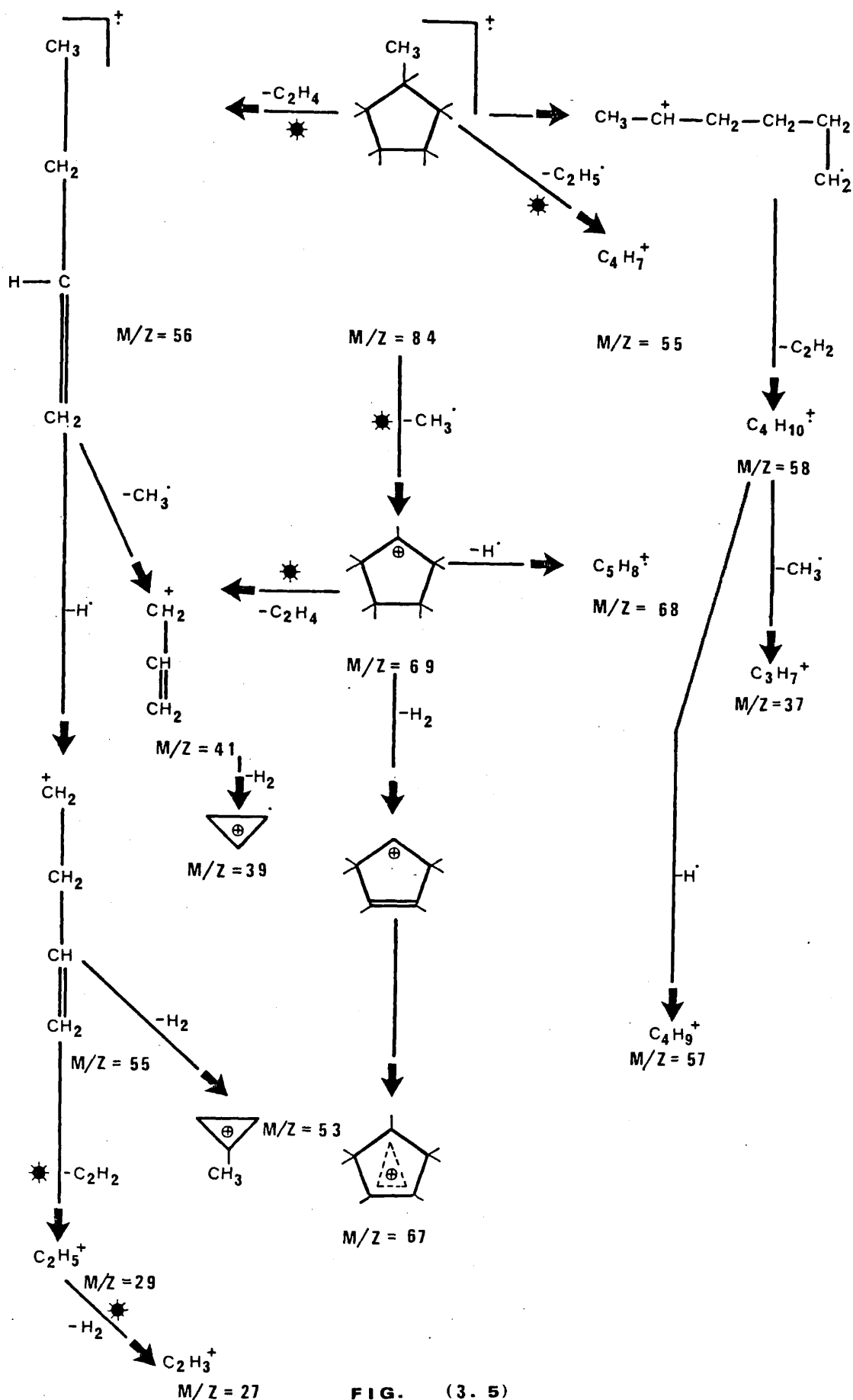


FIG. (3.5)

Postulated pathways to formation of primary ions from methylcyclopentane commensurate upon electron impact.

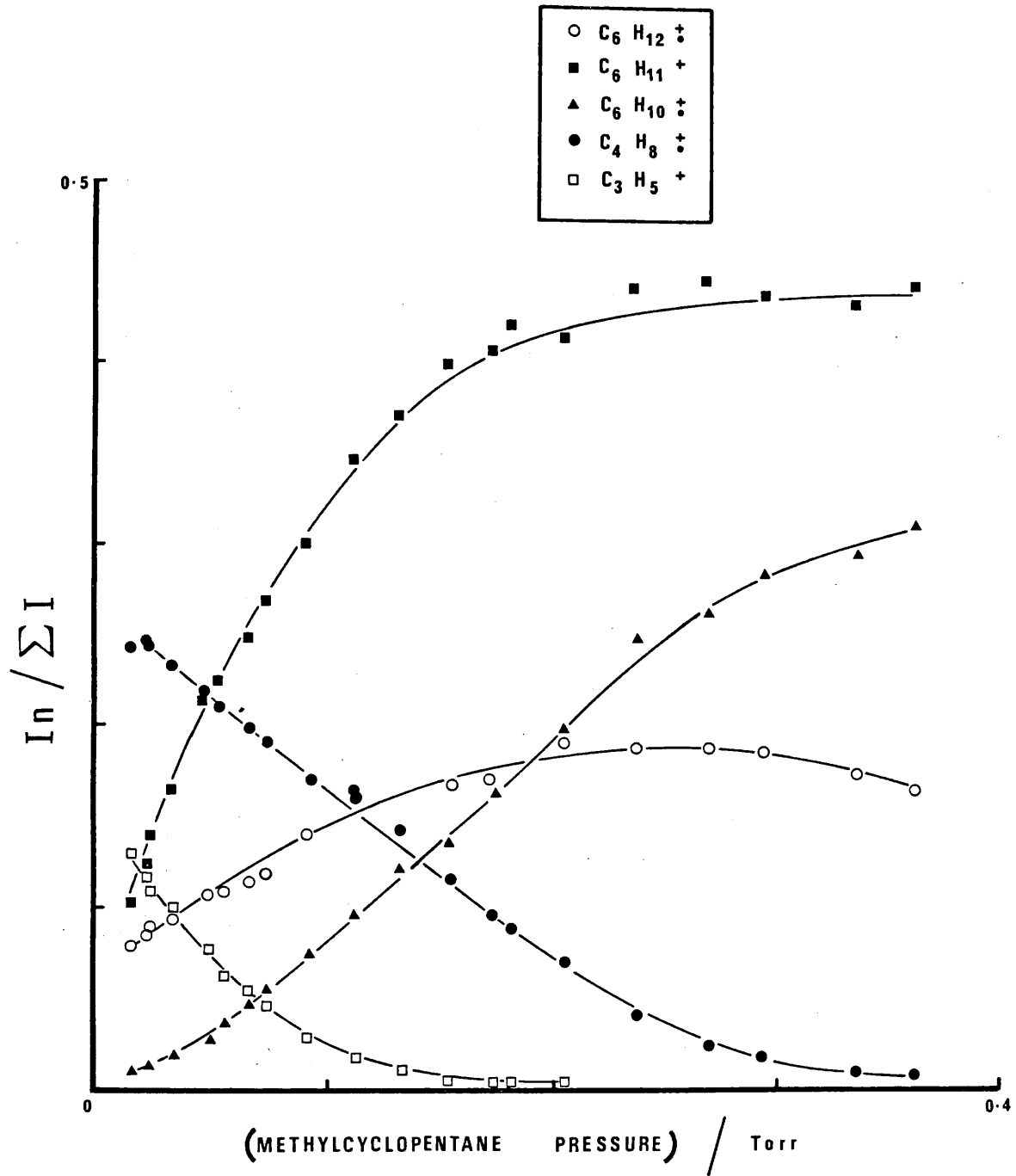


Fig. (3.6)

Variations in abundances, with ion-source pressure, of the principal ions in methylcyclopentane.

121  
Fig. (3.7)

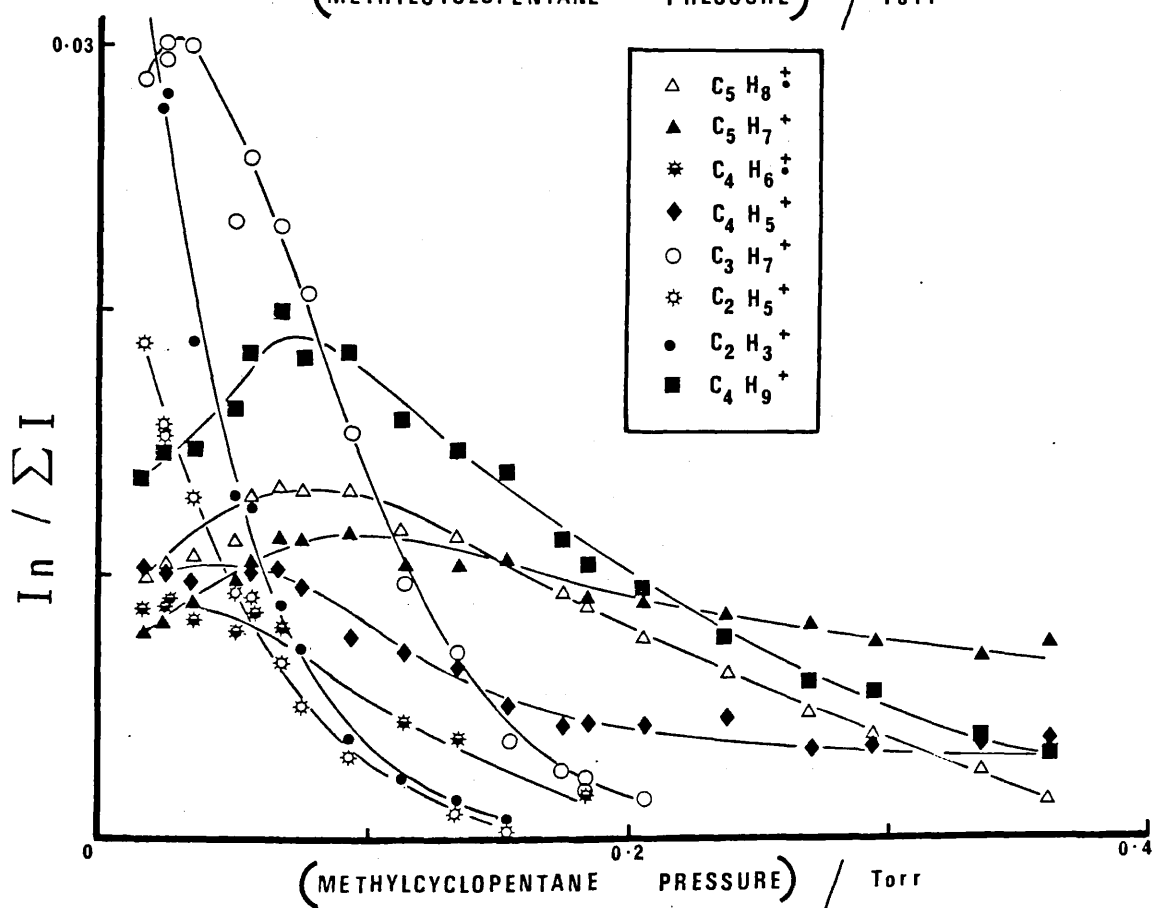
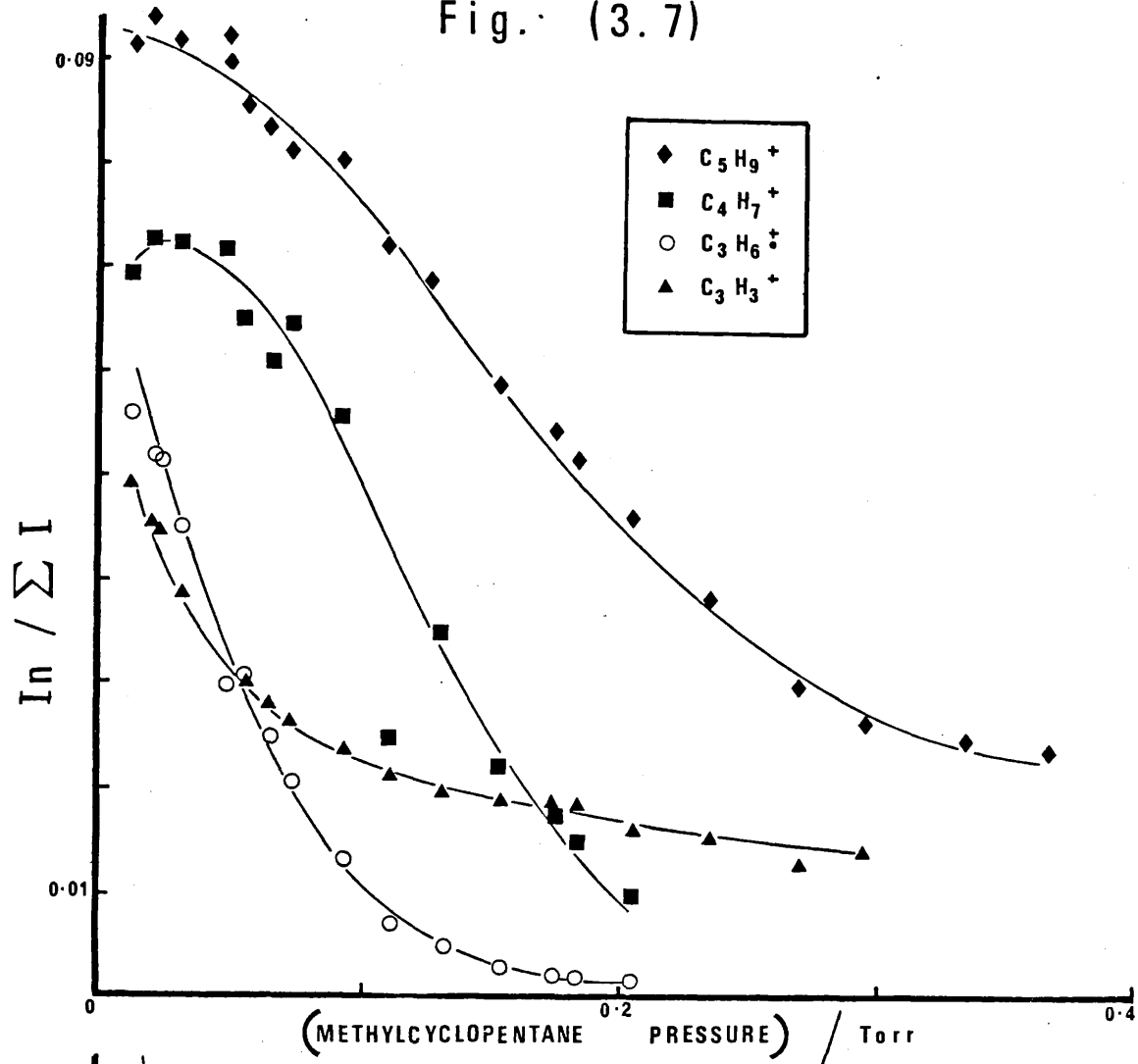
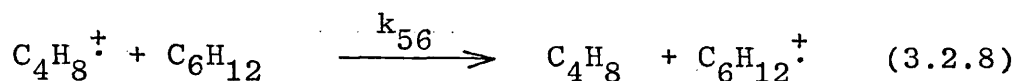


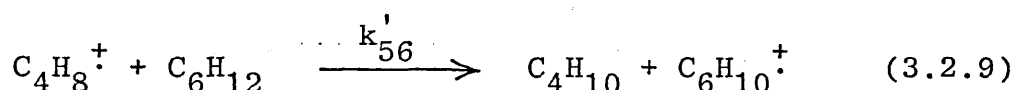
Fig.(3.7) Variation in abundances of minor ions in methylcyclopentane as a function of ion-source pressure.



A relatively high abundance of the molecular ion  $C_6H_{12}^+$  is observed at methylcyclopentane pressures of 0.01–0.4 Torr compared to the apparent absence of the molecular ion  $C_4H_{10}^+$  in iso-butane at >0.1 Torr. The lower ionization potential of methylcyclopentane (10.3eV)<sup>111</sup> compared to iso-butane (11.4 eV)<sup>111</sup> makes charge transfer reactions e.g. (3.2.8) more energetically favourable than similar reactions in iso-butane.



Formation of the ion,  $C_6H_{10}^+$  ( $m/z=82$ ), which accounts for 30% of the total ion-current at 0.35 Torr, is visualised to be by the two atom transfer reaction (3.2.9).



If a primary ion reacts with methylcyclopentane to give more than one product ion the rate-coefficient determined from consideration of its disappearance will be a composite rate coefficient for the reaction channels. Further considerations will be given to this in section (4.1.2).

Equations similar to (3.2.5) can be derived for reaction of the primary ions of  $m/z=n$  with methylcyclopentane, as illustrated by equation (3.2.10)

$$\log (I_n/\Sigma I) - \log (I_n^0/\Sigma I^0) = -k_n \beta_n NP^2 C_6H_{12} \quad (3.2.10)$$

where  $\beta_n$  is evaluated from equation (3.2.11)

$$\beta_n = 273 (\alpha \mu_n)^{\frac{1}{2}} d / (10546 \text{ ET}) \quad (3.2.11)$$

in which  $\alpha$  is the angle averaged polarizability of methylcyclopentane ( $11.03 \text{ \AA}^3$ )<sup>112</sup>,  $\mu_n$  the reduced mass of the reactant ion and methylcyclopentane and the other terms are as defined in section (3.1.1). Provided reactions of the primary ions obey second order kinetics and the measured relative ion-currents truly represent the relative abundances of ions in the source, rate coefficients may be obtained from the gradients of semilogarithmic plots of the relative ion-currents against the square of the pressure. Such plots are given in figures (3.8) and (3.9) and the rate coefficients, calculated from the gradients of the lines, obtained by the least squares method, are given in table (3.3). Since the reactions of these primary ions appear not to obey second order kinetics throughout the entire pressure range studied, the range of pressure for which a linear kinetic plot was obtained is also given.

The significance of the relative magnitude of the rate coefficients is discussed in section (4.1.2) and compared to those obtained for primary ions of the same mass reacting with iso-butane and methylcyclohexane.

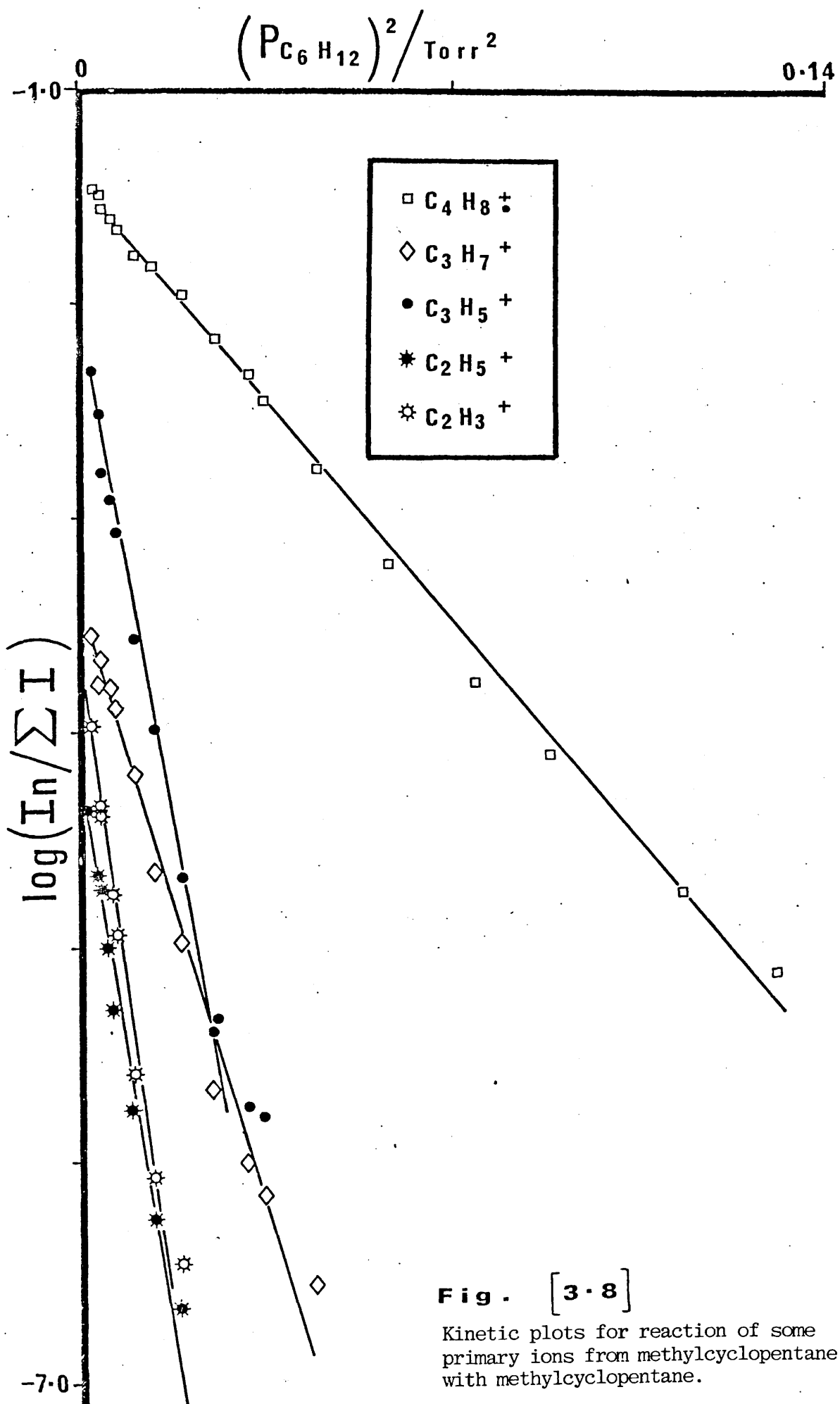


Fig. [3.8]

Kinetic plots for reaction of some primary ions from methylcyclopentane with methylcyclopentane.

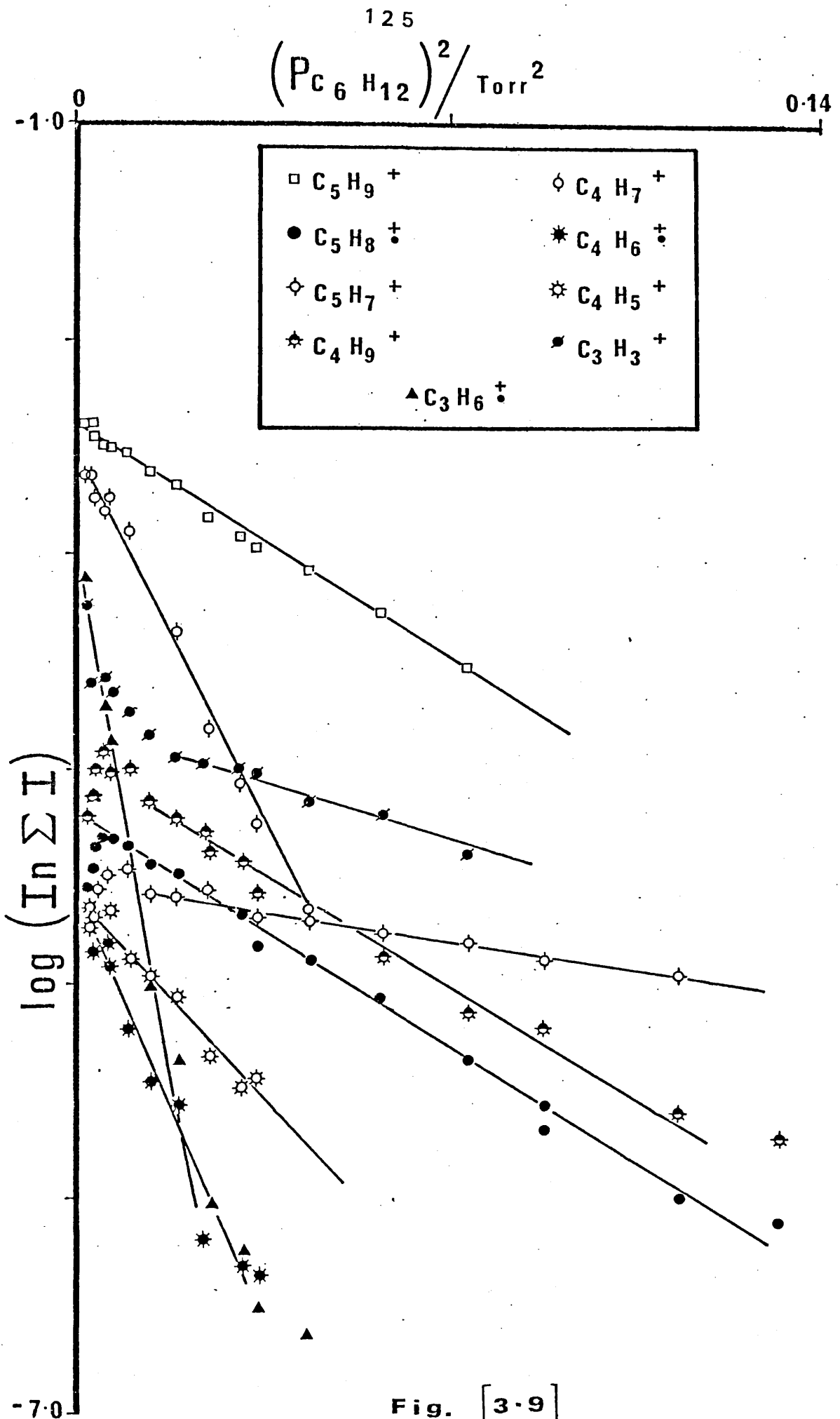


Fig. [3.9]

Kinetic plots for reaction of other primary ions from methylcyclopentane with methylcyclopentane

TABLE 3.3 Rate coefficients for the reaction of primary ions from methylcyclopentane with methylcyclopentane

Ion	m/z	Rate coefficient $\times 10^{11}/\text{cm}^3 \text{ molec}^{-1} \text{ s}^{-1}$	$\text{Log} (I_n^0 / \Sigma I^0)$	Pressure range over which second order kinetics hold. /Torr.
$\text{C}_2\text{H}_3^+$	27	$24.2 \pm 1.3$	$-(3.86 \pm 0.06)$	0.03 - 0.11
$\text{C}_2\text{H}_5^+$	29	$21.3 \pm 1.1$	$-(4.24 \pm 0.06)$	0.03 - 0.11
$\text{C}_3\text{H}_3^+$	39	$0.99 \pm 0.08$	$-(3.78 \pm 0.03)$	0.13 - 0.27
$\text{C}_3\text{H}_5^+$	41	$14.9 \pm 0.5$	$-(2.30 \pm 0.05)$	0.03 - 0.15
$\text{C}_3\text{H}_6^+$	42	$15.5 \pm 0.9$	$-(3.09 \pm 0.07)$	0.03 - 0.13
$\text{C}_3\text{H}_7^+$	43	$9.63 \pm 0.29$	$-(3.45 \pm 0.04)$	0.03 - 0.18
$\text{C}_4\text{H}_5^+$	53	$3.39 \pm 0.27$	$-(4.49 \pm 0.05)$	0.05 - 0.18
$\text{C}_4\text{H}_6^+$	54	$5.78 \pm 0.32$	$-(4.66 \pm 0.05)$	0.03 - 0.18
$\text{C}_4\text{H}_7^+$	55	$5.43 \pm 0.18$	$-(2.52 \pm 0.03)$	0.03 - 0.18
$\text{C}_4\text{H}_8^+$	56	$3.14 \pm 0.04$	$-(1.46 \pm 0.02)$	0.03 - 0.34
$\text{C}_4\text{H}_9^+$	57	$1.55 \pm 0.07$	$-(4.00 \pm 0.04)$	0.11 - 0.34
$\text{C}_5\text{H}_7^+$	67	$0.37 \pm 0.02$	$-(4.57 \pm 0.07)$	0.17 - 0.34
$\text{C}_5\text{H}_8^+$	68	$1.57 \pm 0.02$	$-(4.22 \pm 0.01)$	0.07 - 0.34
$\text{C}_5\text{H}_9^+$	69	$1.56 \pm 0.04$	$-(2.41 \pm 0.01)$	0.03 - 0.27

## 3.1.2.3 Methylcyclohexane

Similar primary ions to those already discussed for methylcyclopentane reagent gas were observed in the electron impact ionization spectrum of methylcyclohexane and some possible pathways leading to their formation from the molecular ion,  $C_7H_{14}^+$ , are given in figure (3.10); a \* again denotes the observation of a supportive metastable ion decomposition.

Plots of variation in relative ion-currents with ion-source pressure of the principal ions observed are given in figures (3.11) and (3.12). Only ions of mass: charge ratio less than 82 show decreases in their relative ion-currents with increase of methylcyclohexane pressure and therefore only these are considered to participate in ion-molecule reactions resulting in the formation of the product ions  $C_7H_{14}^+$ ,  $C_7H_{13}^+$  and  $C_7H_{12}^+$  ( $m/z=98, 97$  and  $96$  respectively). Formation of these ions is considered to be by charge exchange, hydride and two atom transfer respectively as with methylcyclopentane. (c.f. equations (3.2.8 - 9)). The rate coefficients were obtained from gradients of the kinetic plots given in figure (3.13) and (3.14) using equations (3.2.10) and (3.2.5) where  $\alpha$  is the angle averaged polarizability of methylcyclohexane ( $12.90 \text{ \AA}^3$ )<sup>112</sup> and  $\mu$  the reduced mass of a reactant ion and methylcyclohexane.

The ion-currents for the ions  $C_6H_{11}^+$  and  $C_6H_{10}^+$  were found to be independent of ion-source pressure,

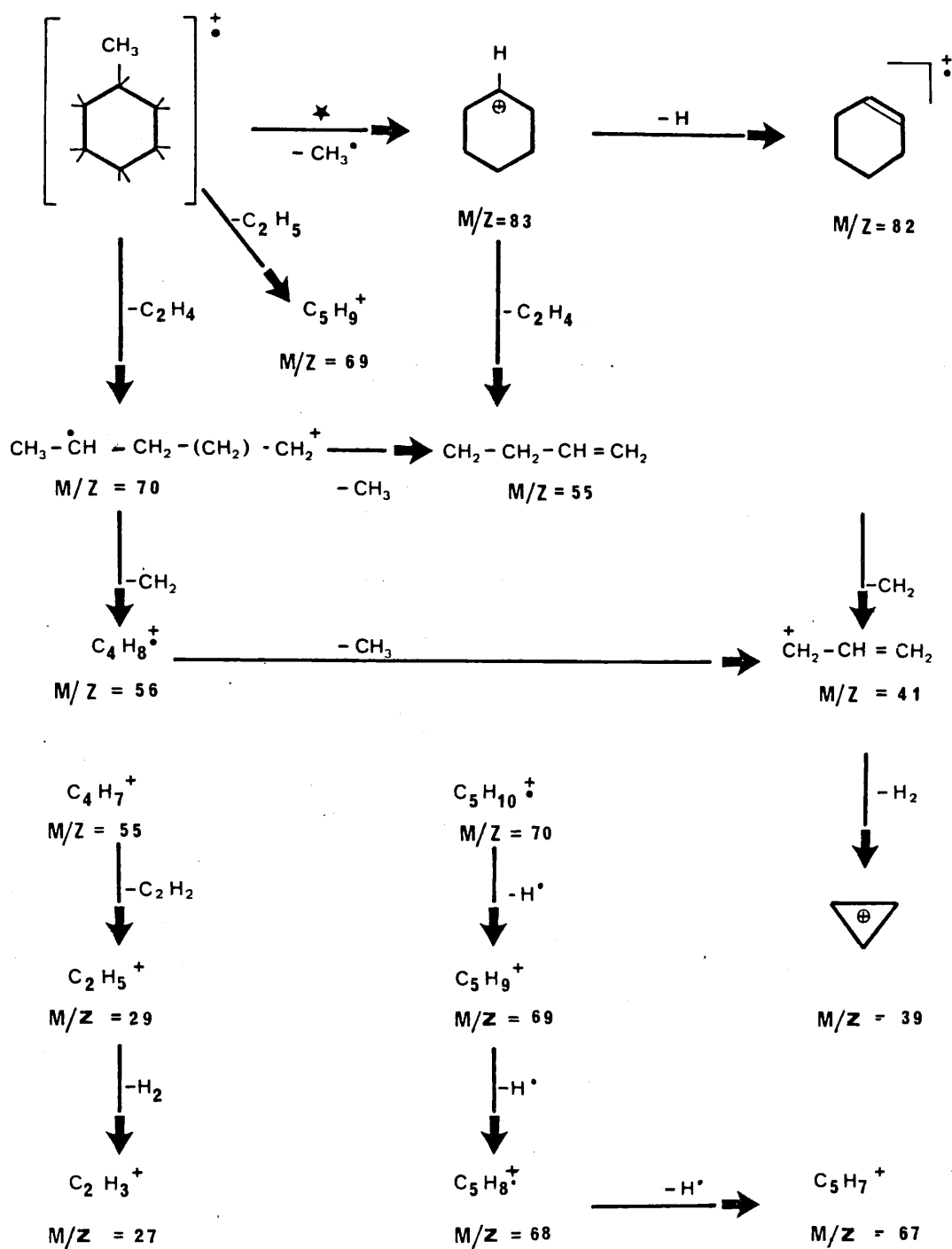


FIG. (3. 10)

Possible pathways of fragmentation of methylcyclohexane consequent upon electron impact.

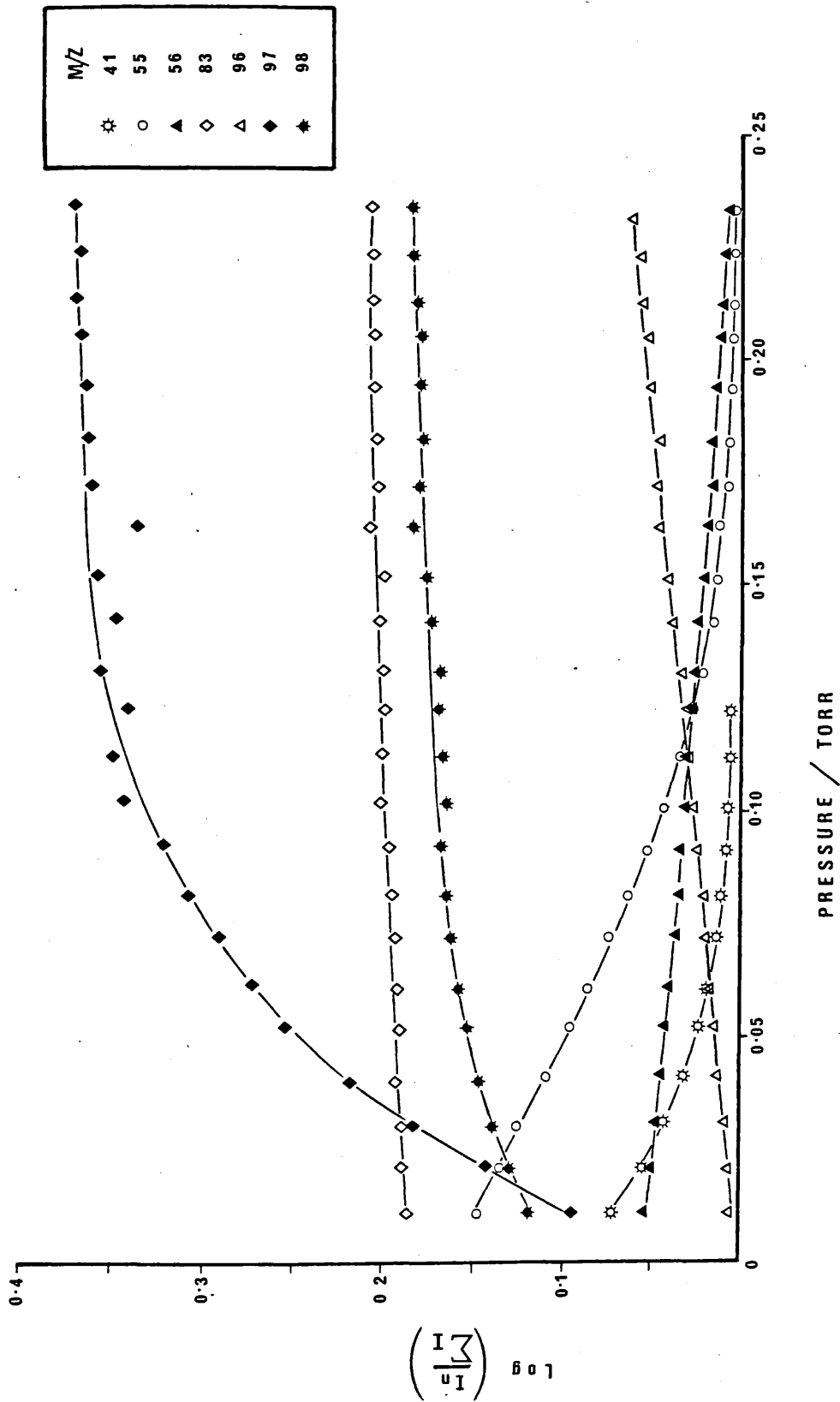


FIG. (3.11)

Variation in ion-abundances of ions, in methylcyclohexane reagent gas as a function of ion-source pressure. (Part 1).



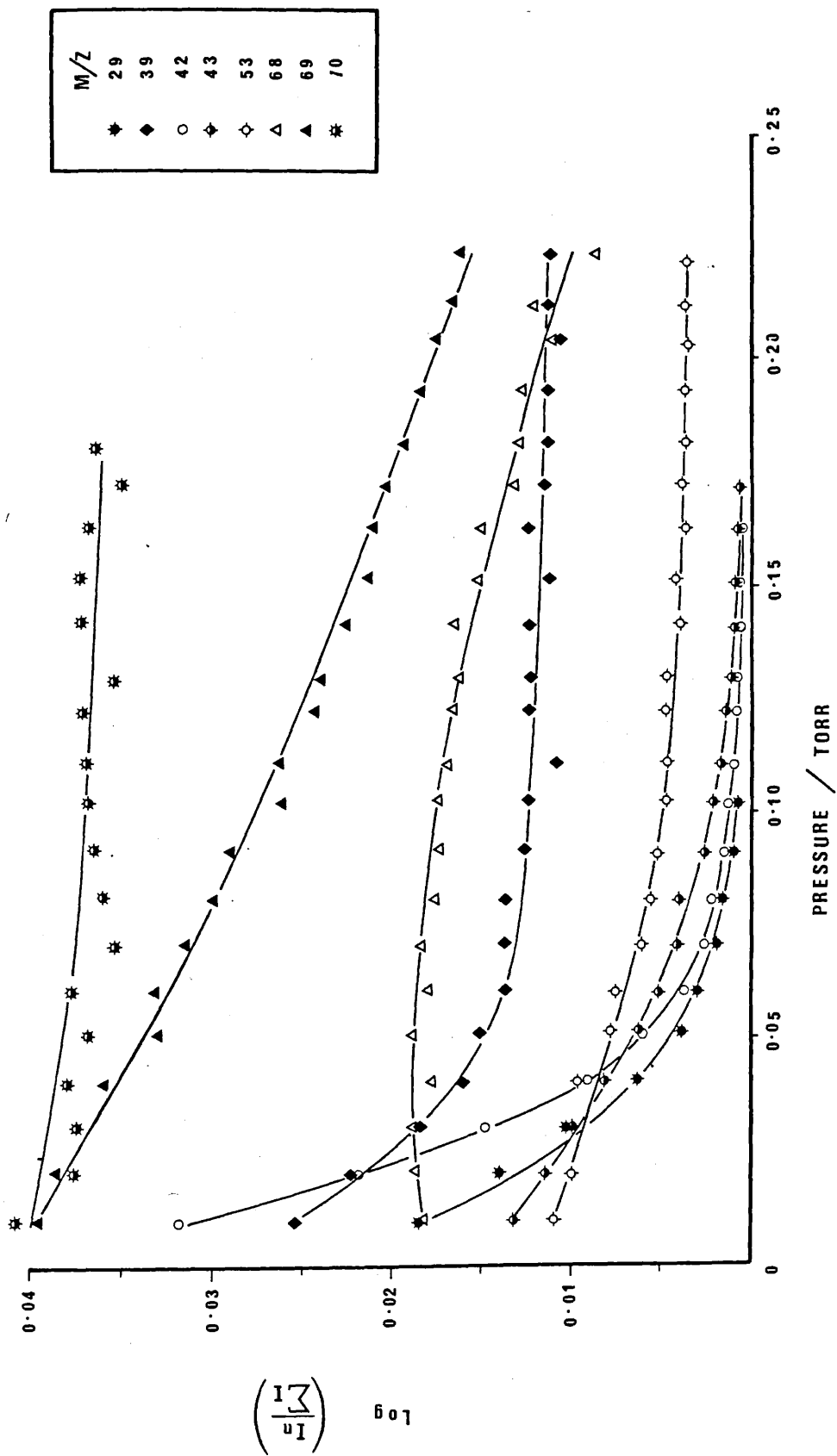


FIG. (3. 12)

Variation in ion-abundances of ions in methylcyclohexane reagent gas as a function of ion-source pressure. (Part 2).

possibly this was a consequence of their high stability resulting from low hydride and electron affinities respectively. Alternatively these ions could have arisen from chemical ionisation of small quantities ca (<0.1)% of methylcyclopentane impurity. Such CI formed ions would not be as reactive as methylcyclohexane ions. If formation of these two ions was by fragmentation of product ions, their ion-currents would have been expected to increase with that of the product ion. This was not observed. If they arose through chemical ionization of methylcyclopentane then a considerable ion-current due to  $C_6H_{12}^+$  (M/z=84) should have been observed. (c.f. methylcyclopentane reagent gas (3.1.2.2)). However its absence suggests the methylcyclohexane used in this study was free from methylcyclopentane. The constancy of ion-currents due to  $C_6H_{11}^+$  and  $C_6H_{10}^+$  has to be attributed to their relative high stability. This will receive further discussion in section (4.1.2) together with the relative magnitudes of rate coefficients obtained for the other primary ions in Table (3.4).

$$\left( \frac{P_{C_7H_{14}}}{0.03 \text{ Torr}} \right)^2$$

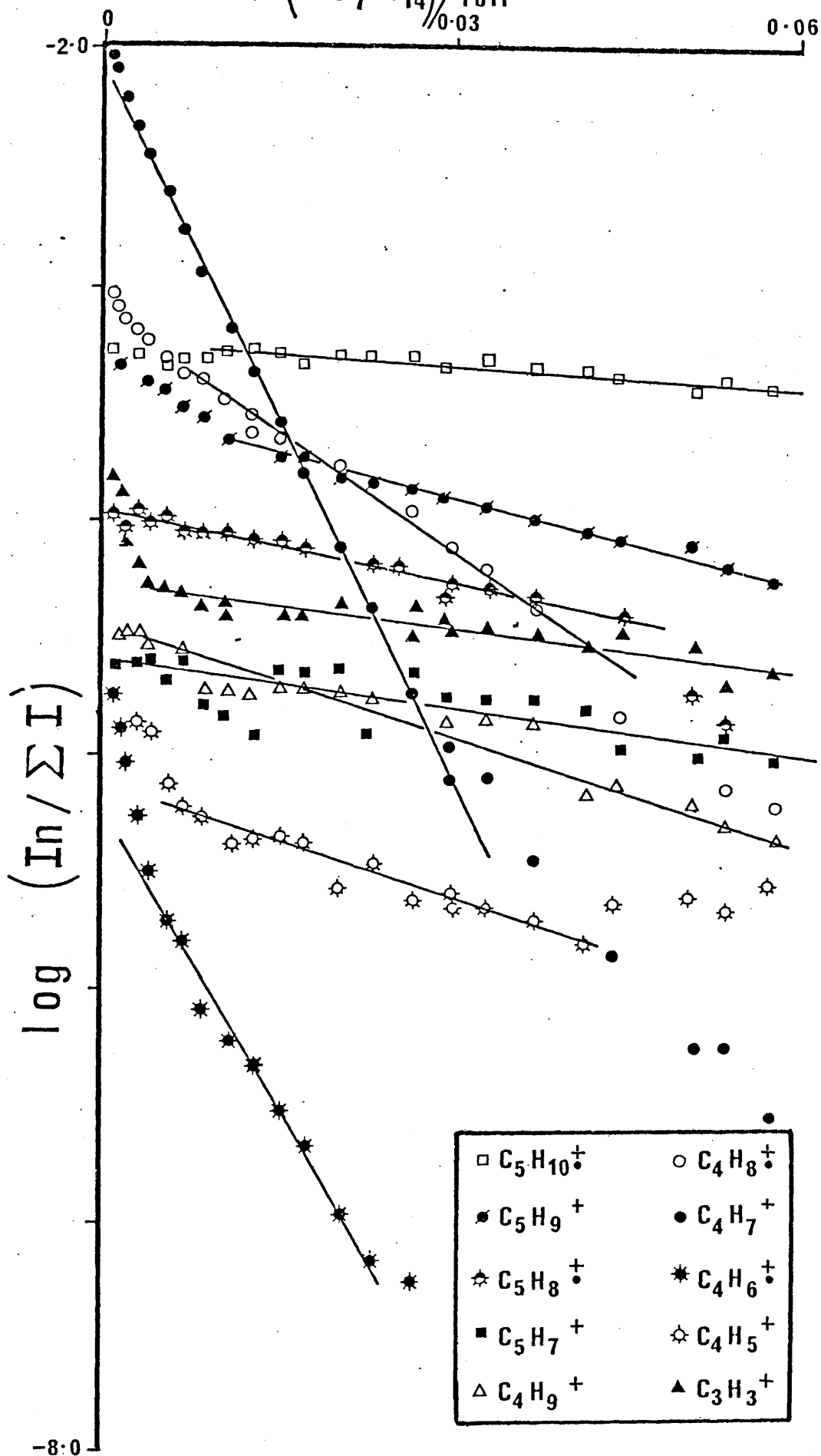


Fig. [3-13] Kinetic plot for reaction of primary ions from methylcyclohexane with methylcyclohexane (Part 1).

$$\left( P_{C_7 H_{14}} \right)^2 / \text{Torr}^2$$

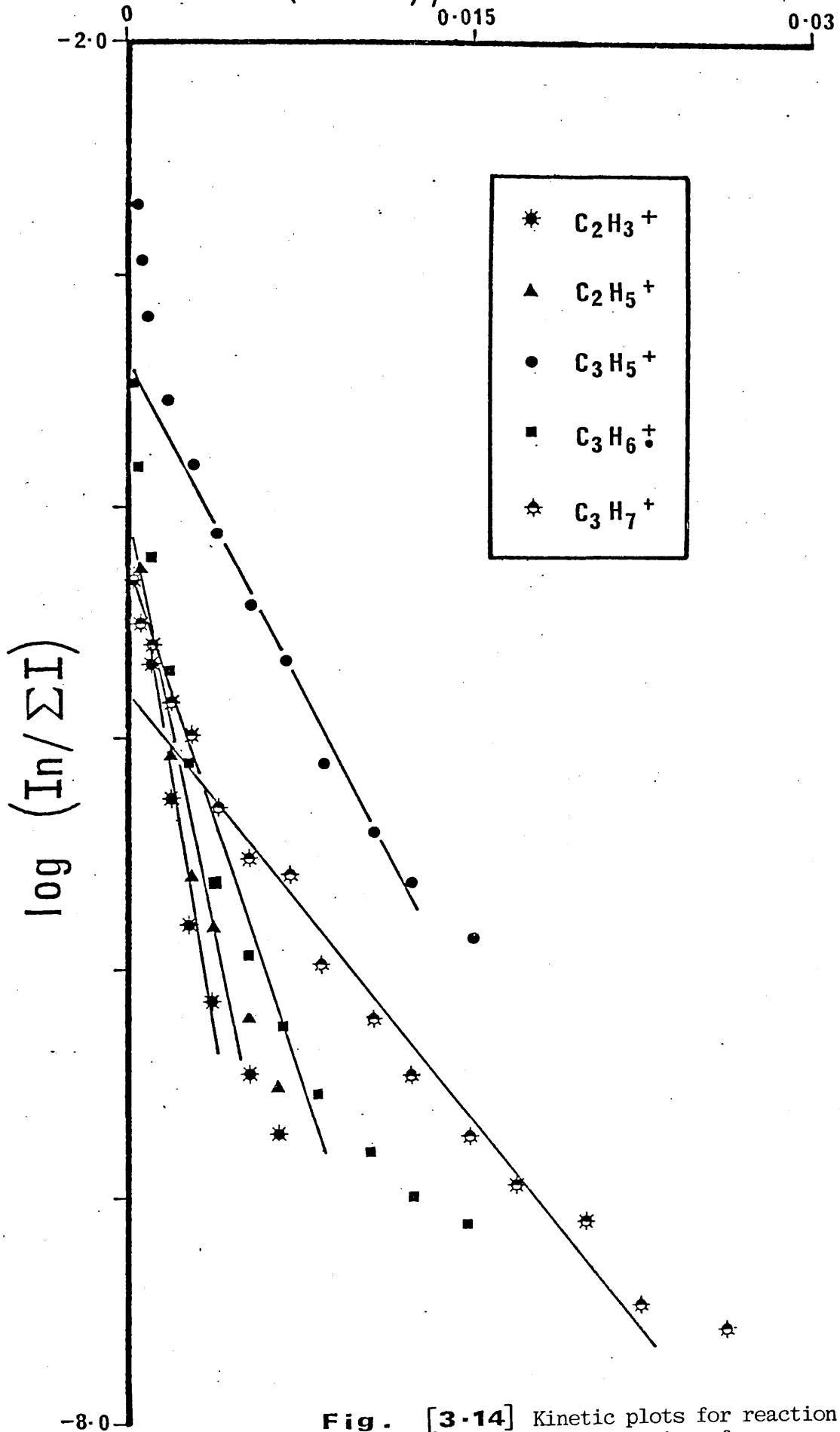


Fig. [3-14] Kinetic plots for reaction of primary ions from methylcyclohexane with methylcyclohexane. (Part 2).

**TABLE 3.4** Rate coefficients for the reaction of primary ions from methylcyclohexane with methylcyclohexane

Ion	m/z	Rate coefficient $\times 10^{11}/\text{cm}^3 \text{ molec}^{-1}$ $\text{s}^{-1}$	$\text{Log} (I_n^0/\Sigma I^0)$	Pressure range over which second order kinetics hold. /Torr.
$\text{C}_2\text{H}_3^+$	27	$61.1 \pm 6.5$	$-(4.21 \pm 0.14)$	0.01 - 0.07
$\text{C}_2\text{H}_5^+$	29	$52.5 \pm 5.3$	$-(4.16 \pm 0.12)$	0.01 - 0.07
$\text{C}_3\text{H}_3^+$	39	$0.43 \pm 0.10$	$-(4.34 \pm 0.02)$	0.07 - 0.23
$\text{C}_3\text{H}_5^+$	41	$22.2 \pm 1.0$	$-(3.27 \pm 0.06)$	0.04 - 0.10
$\text{C}_3\text{H}_6^+$	42	$21.4 \pm 2.4$	$-(4.69 \pm 0.17)$	0.04 - 0.11
$\text{C}_3\text{H}_7^+$	43	$11.7 \pm 0.5$	$-(4.96 \pm 0.65)$	0.06 - 0.15
$\text{C}_4\text{H}_6^+$	54	$7.90 \pm 0.24$	$-(5.30 \pm 0.04)$	0.07 - 0.15
$\text{C}_4\text{H}_7^+$	55	$9.43 \pm 0.22$	$-(2.11 \pm 0.04)$	0.04 - 0.17
$\text{C}_4\text{H}_8^+$	56	$3.16 \pm 0.06$	$-(3.14 \pm 0.01)$	0.07 - 0.20
$\text{C}_4\text{H}_9^+$	57	$1.19 \pm 0.10$	$-(4.49 \pm 0.03)$	0.04 - 0.24
$\text{C}_5\text{H}_7^+$	67	$0.61 \pm 0.08$	$-(4.58 \pm 0.03)$	0.04 - 0.24
$\text{C}_5\text{H}_8^+$	68	$1.00 \pm 0.04$	$-(3.95 \pm 0.02)$	0.04 - 0.20
$\text{C}_5\text{H}_9^+$	69	$1.15 \pm 0.04$	$-(3.52 \pm 0.02)$	0.12 - 0.24
$\text{C}_5\text{H}_{10}^+$	70	$0.29 \pm 0.04$	$-(3.25 \pm 0.01)$	0.10 - 0.24

## 3.1.2.4 Ammonia

The  $\text{NH}_3^+$  ion ( $m/z=17$ ) consequent upon the electron-impact ionization of ammonia fragments by loss of hydrogen atom or molecule, resulting in the formation of  $\text{NH}_2^+$  ( $m/z=16$ ) and  $\text{NH}^+$  ( $m/z=15$ ) primary ions respectively. Variations in the relative abundances of these and higher molecular weight cluster ions, in ammonia, have been studied as a function of ammonia pressure (0.01 - 0.6 Torr) and ion source field strength, (2.5 - 12.5 V  $\text{cm}^{-1}$ ), to facilitate direct estimation of ion-source pressure from reagent gas spectra.

From a plot of relative ion-currents, recorded while maintaining an ion-source field strength of 7.5 V  $\text{cm}^{-1}$ , against pressure (figure (3.15)) the relative abundances of ions  $\text{NH}_3^+$  are seen to decrease initially with increased pressure but to remain essentially constant at pressures greater than 0.1 Torr, while that of  $\text{NH}_4^+$  increases to a maximum at ~0.1 Torr. As with hydrocarbon reagent gases this is attributed to reactions of the primary ions  $\text{NH}_3^+$ ,  $\text{NH}_2^+$  and  $\text{NH}^+$ , in this case by proton transfer, with neutral ammonia to produce  $\text{NH}_4^+$ .

In section (4.2.1) it will be shown that information concerning the kinetics of these reactions may be obtained from the gradients of plots of  $\log I_n/\Sigma I$  corresponding to the log of the relative ion current for ion of  $m/z=n$ , against the pressure. Accordingly such plots for the reactions of  $\text{NH}_3^+$ ,  $\text{NH}_2^+$  and  $\text{NH}^+$ , at an

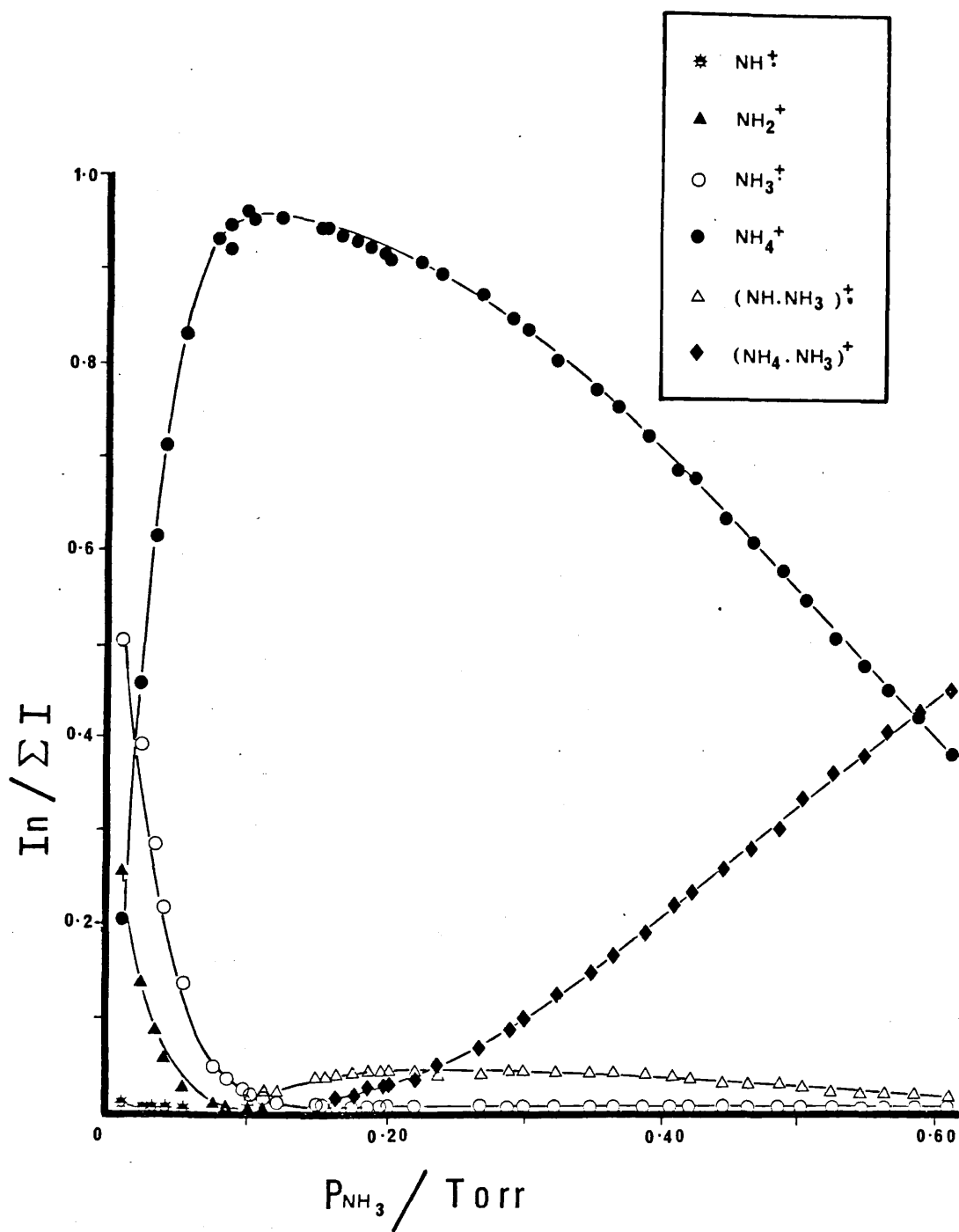


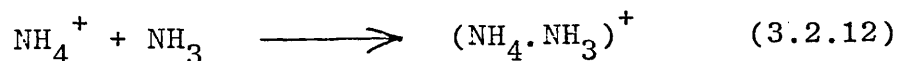
FIG. (3.15)

Variation in ion-abundance in ammonia reagent gas with ion-source pressure.

ion-source field strength of  $7.5 \text{ V cm}^{-1}$  are given in figure (3.16) respectively. A linear dependence of  $\log(I_n/\Sigma I)$  on pressure is observed below an ion source pressure  $P_a$ . Values of  $P_a$  for each ion at various ion-source field strengths are given in tables (4.2), (4.3) and (4.4) in section (4.2.1). However above this pressure a departure from linearity is seen until a pressure  $P_e$  above which  $\log(I_n/\Sigma I)$  remains essentially constant with further pressure increases. A possible explanation for this behaviour is given in section (4.2.1).

Reproducibility and the large magnitude of the variations in  $\log(I_n/\Sigma I)$  for ions  $\text{NH}_3^+$  and  $\text{NH}_2^+$  with ion-source pressure 0.01 - 0.15 Torr and field strengths of  $2.5 - 12.5 \text{ V cm}^{-1}$  prompted development of a method for determination of pressure from reagent gas spectra at  $<0.15$  Torr. This method is described in section (4.2.3.1).

In the pressure range 0.15 - 0.6 Torr the decrease in relative abundance of  $\text{NH}_4^+$  is commensurate with the increase of  $\text{NH}_4\text{NH}_3^+$  (figure (3.15)). Such behaviour is assumed to reflect solvation of  $\text{NH}_4^+$  by neutral ammonia, the overall reaction written as



However the mechanism of the reaction is more complicated than suggested by equation (3.2.12). It will be shown in section (4.2.2) that information on the kinetics of reaction (3.2.12) is obtained if  $\log(I_{18}/\Sigma I)$  (log of



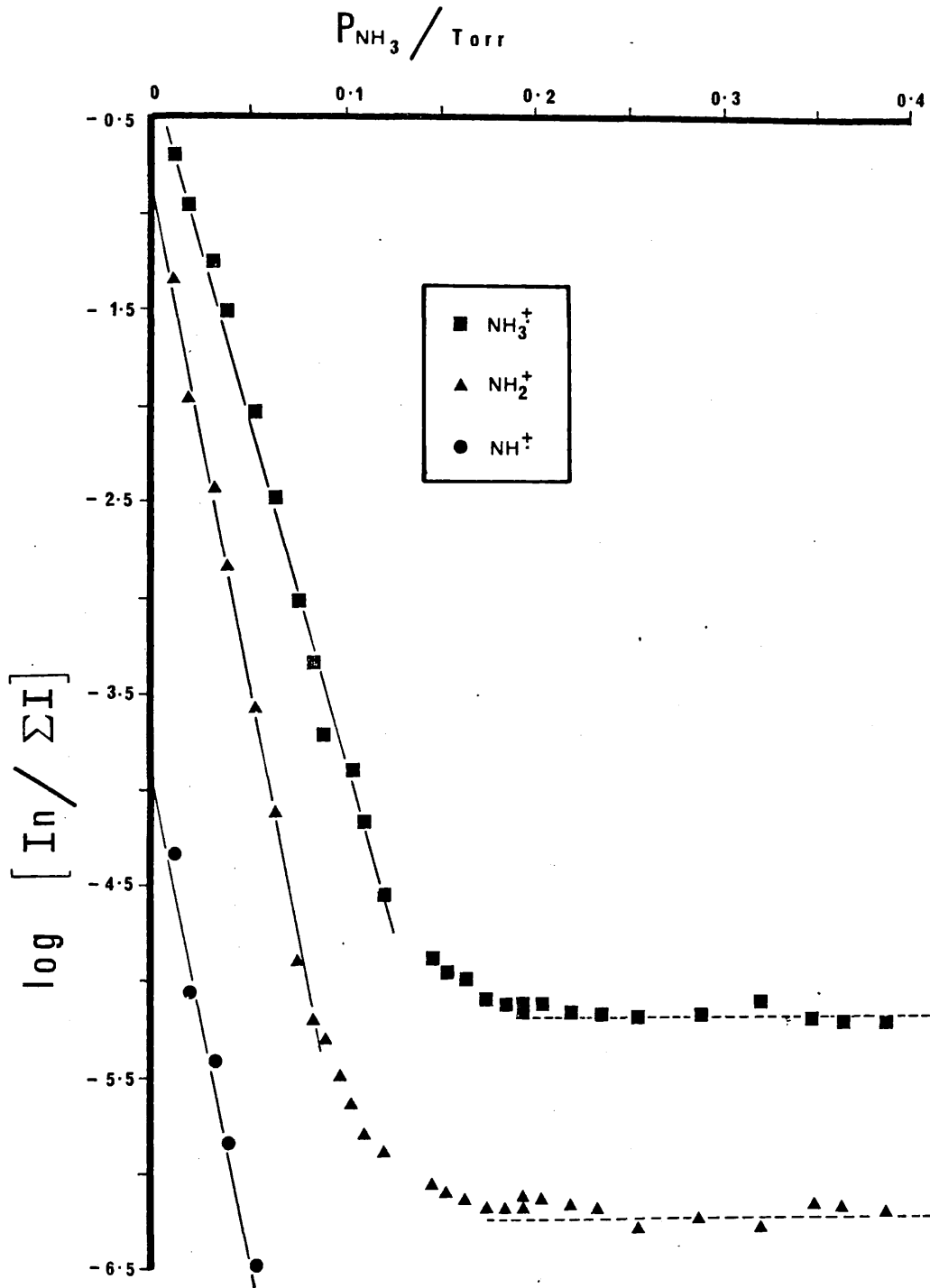


Fig. (3.16)

Kinetic plots for reaction of primary ions from ammonia with ammonia; Ion-source field strength  $7.5 \text{ V cm}^{-1}$ .

relative ion-current of  $\text{NH}_4^+$ ) is plotted against the square of ion-source ammonia pressure. Accordingly the graphs in figure (3.17) show variations in  $\log (I_{18}/\Sigma I)$  at various ion-source field strengths. It is apparent that a departure from linearity, in these plots, occurs at low ion-source pressures and large field strengths. Further it will be shown in section (4.2.3.2) that, from measurement of relative ion-currents of  $\text{NH}_4^+$  in reagent gas spectra and use of a suitable equation containing constants evaluated in section (4.2.2), ion-source pressures of ammonia in excess of 0.15 Torr may be estimated.

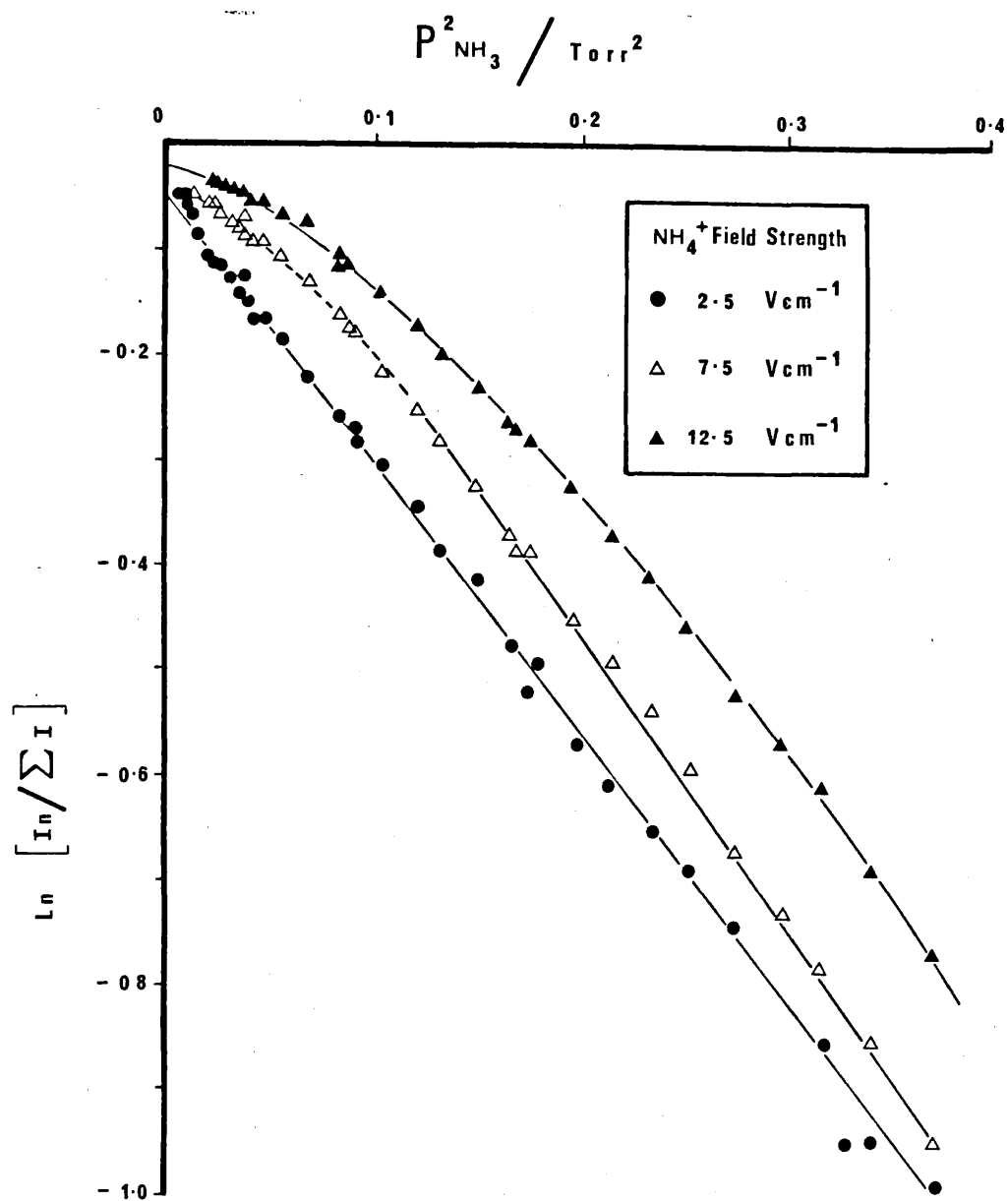


FIG. (3.17)  
Kinetic plot for reaction of  $\text{NH}_4^+$  with ammonia at various ion-source field strengths.

### 3.1.3 Fluorinated reagent gases.

Fluorobenzene reagent gas was found to only ionize aromatic components in hydrocarbon mixtures. A study of the variation of relative abundance of primary ions in the reagent plasma was conducted to ascertain (a) the most suitable operating pressure, (b) whether ion-source gas pressure could be determined from the reagent gas spectra and (c) the degree of variation in abundances of "undesirable" adduct ions with pressure. Difluorobenzenes were also studied to investigate whether these might prove to be more suitable reagent gases. The results obtained for mono- and difluorobenzenes are discussed separately.

#### 3.1.3.1 Fluorobenzene

The electron impact spectra of fluorinated benzenes have been reported in the literature,<sup>113</sup> and are characterised by particularly large ion-currents for their molecular ions. However little indication is given regarding fragmentation pathways. Plausible fragmentations leading to the principal primary ions are given in figure (3.18), where a '\*' denotes the observation of a broad peak, resulting from fragmentation of a metastable ion, in support of the transition. Additionally the mass differences between primary ions in the spectra of fluorobenzene and per-deuterofluorobenzene were used to determine the number of hydrogen atoms in some of the fragment ions.

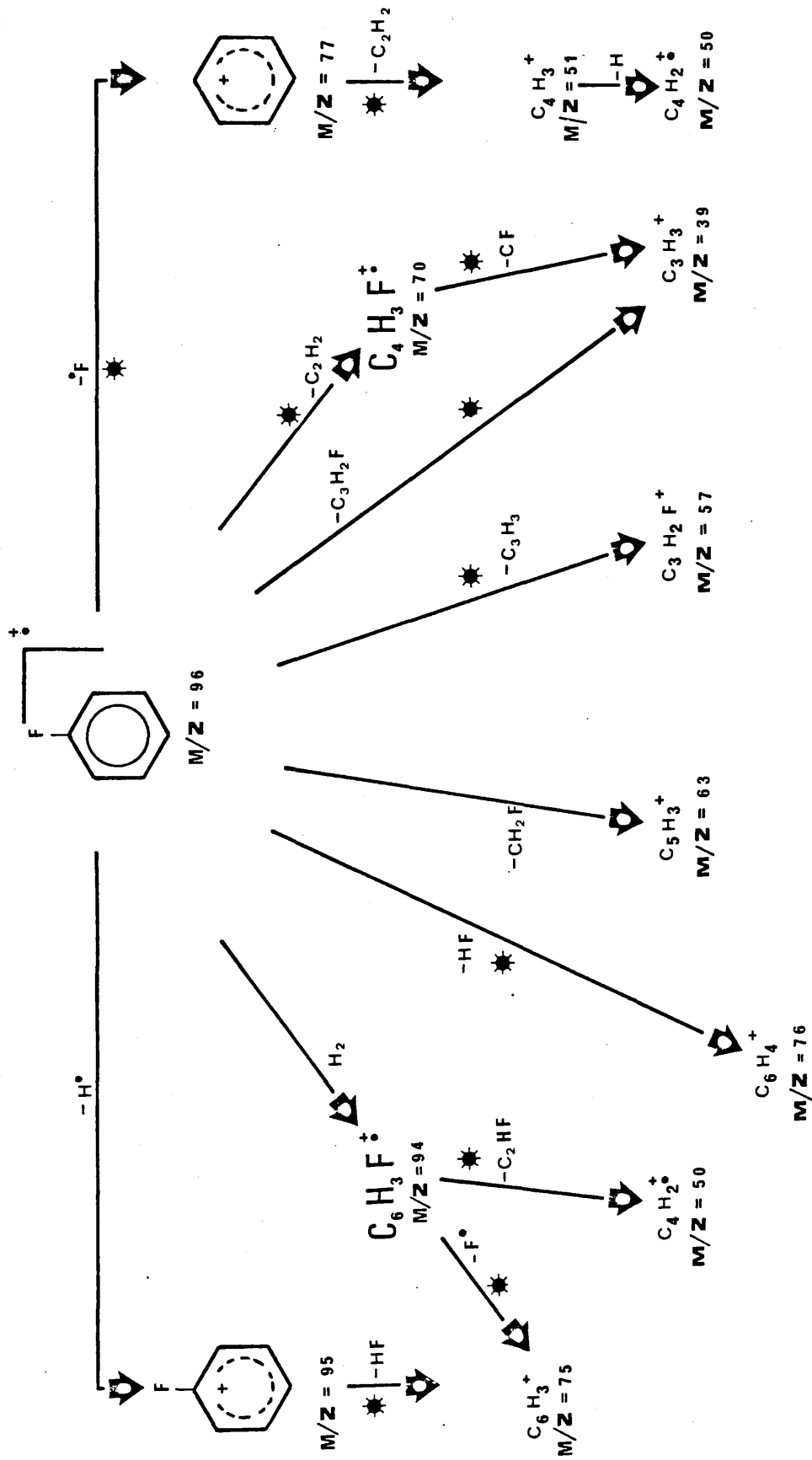
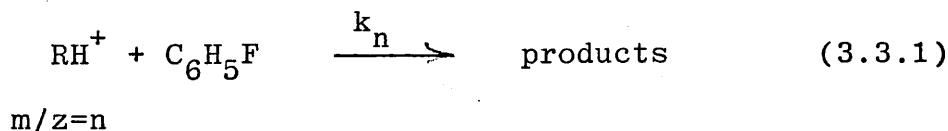


FIG. (3.18)

Postulated fragmentation of fluorobenzene consequent upon electron-impact ionization.

Upon increase of ion-source pressure the relative abundance of the molecular ion  $C_6H_5F^+$  ( $m/z = 96$ ) and its  $^{13}C$ -analogue,  $m/z = 97$ , increases until the two ions account for ~80% of the total ion-current at 0.05 Torr. Above this pressure, although the relative abundances of the primary ions continued to decrease, no further increase in that of the molecular ion was observed. (See Figure (3.19)). However, ions having  $m/z$  values  $> 96$  are observed and their relative abundances increase with ion-source pressure (Figure (3.20)). It is suggested that these ions are formed by association reactions of primary ions with fluorobenzene. (See Section 4.3.1).

For the reaction of a primary ion ( $RH^+$ ,  $m/z = n$ ) with fluorobenzene, as given in equation (3.3.1).



provided the reaction is bimolecular, the rate of disappearance of  $RH^+$  is given by:

$$-\frac{d[RH^+]}{dt} = k_n [RH^+] C_6H_5F \quad (3.3.2)$$

The integrated rate equation is then

$$\log \frac{I_n}{\Sigma I} = -k_n N \beta_n P_{C_6H_5F}^2 + \log \frac{I_n^0}{\Sigma I^0} \quad (3.3.3)$$

where  $\beta_n$  and  $N$  are as previously described, (see Section (3.1.2)),  $\log (I_n/\Sigma I)$  and  $\log (I_n^0/\Sigma I^0)$  are the relative ion-currents of  $RH^+$  at ion-source pressures  $P_{C_6H_5F}$  and say  $<10^{-5}$  Torr respectively.

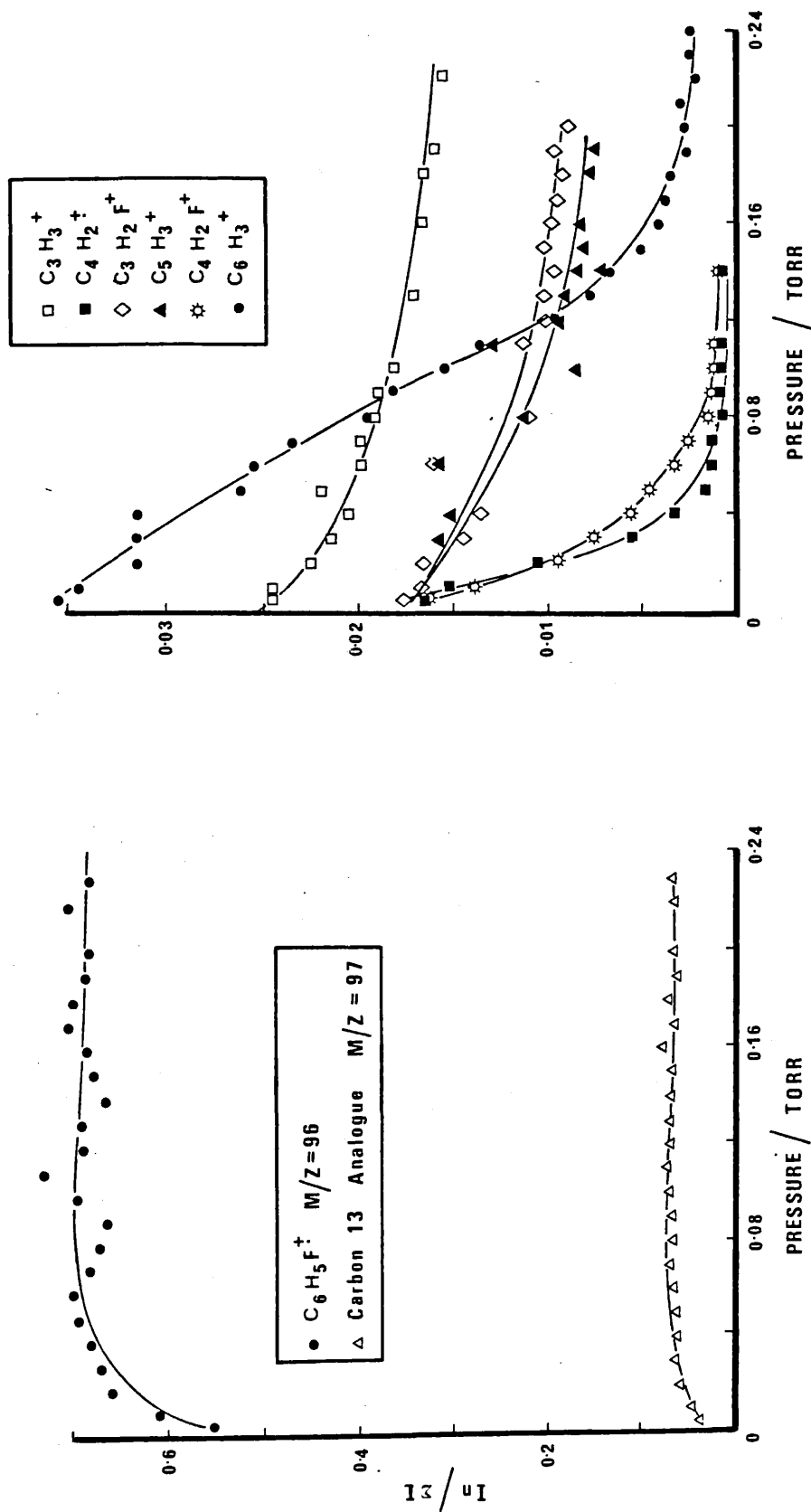


FIG (3.19)

Variation in ion-abundances in the fluorobenzene reagent gas as a function of ion-source pressure;  
 Part 1 non cluster ions.

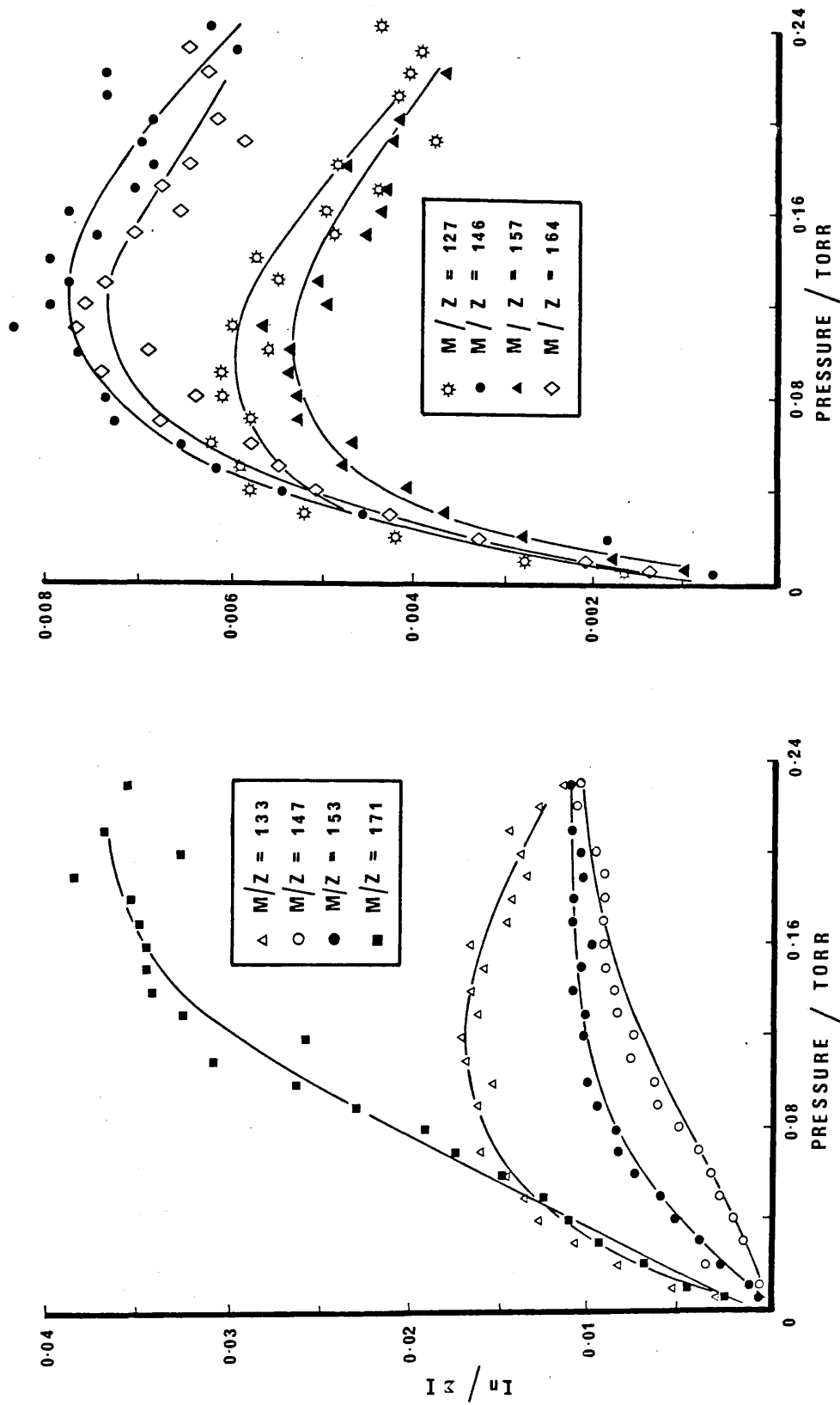


FIG. (3. 20)

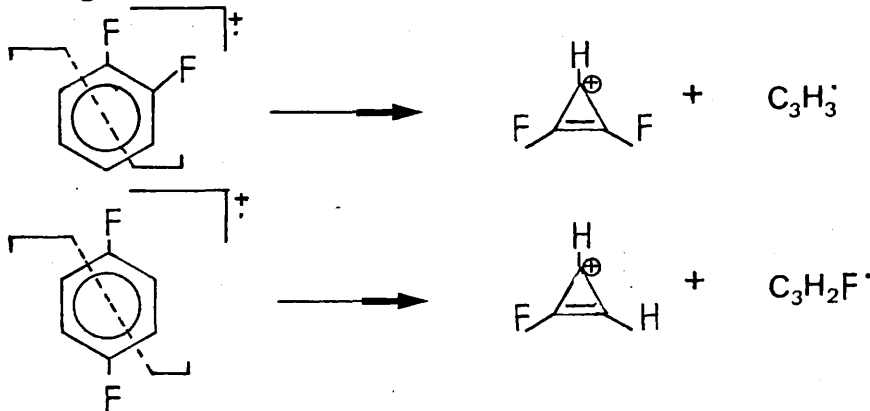
Variation in ion-abundances in the fluorobenzene reagent gas as a function of ion-source pressure; Part 2 cluster ions.



Values of the rate coefficient  $k_n$ , are given in Table (3.5) with the pressure range over which a linear plot of  $(I_n/\Sigma I)$  against  $P_{C_6H_5F}^2$  was maintained. The significance of the values is discussed in Section (4.3.1).

### 3.1.3.2 Difluorobenzenes -

Plausible pathways to the formation of primary ions observed in the electron impact spectra of difluorobenzenes are given in figure (3.21). In the case of o-difluorobenzene it is likely that the ion-current observed corresponding to  $m/z = 75$  results from two ions with different atomic compositions, namely  $C_6H_3^+$  and  $C_3HF_2^+$ . This may also be the case in m-difluorobenzene. However the formation of  $C_3HF_2^+$  from p-difluorobenzene is unlikely since this would require fluorine migration prior to fragmentation as illustrated below.



The relative abundance of molecular ions varied little above 0.05 Torr, while the relative abundances of primary ions continued to decrease with increased pressure throughout the range studied. Cluster ions were observed and the mechanism of their formation is discussed in Section (4.3.2). Rate coefficients for

TABLE 3.5 Rate coefficients for the reaction of primary ions from fluorobenzene with fluorobenzene.

Ion	m/z	Rate coefficient $\times 10^{11} / \text{cm}^3 \text{ molec}^{-1} \text{ s}^{-1}$	Pressure range over which second order kinetics hold/Torr.
$\text{C}_6\text{H}_5^+$	77	$7.71 \pm 0.80$	0.01 - 0.12
$\text{C}_6\text{H}_4^+$	76	$4.08 \pm 0.62$	0.01 - 0.14
$\text{C}_6\text{H}_3^+$	75	$8.36 \pm 0.27$	0.01 - 0.16
$\text{C}_4\text{H}_3\text{F}^+$	70	$1.71 \pm 0.30$	0.1 - 0.2
$\text{C}_4\text{H}_2\text{F}^+$	69	$3.04 \pm 0.95$	0.09 - 0.21
$\text{C}_5\text{H}_3^+$	63	$1.02 \pm 0.27$	0.1 - 0.2
$\text{C}_5\text{H}_2^+$	62	$23.0 \pm 3.16$	0.01 - 0.1
$\text{C}_3\text{H}_2\text{F}^+$	57	$8.33 \pm 0.48$	0.1 - 0.2
$\text{C}_4\text{H}_2^+$	50	$47.85 \pm 15.3$	0.02 - 0.08
$\text{C}_3\text{H}_3^+$	39	$0.29 \pm 0.21$	0.01 - 0.24

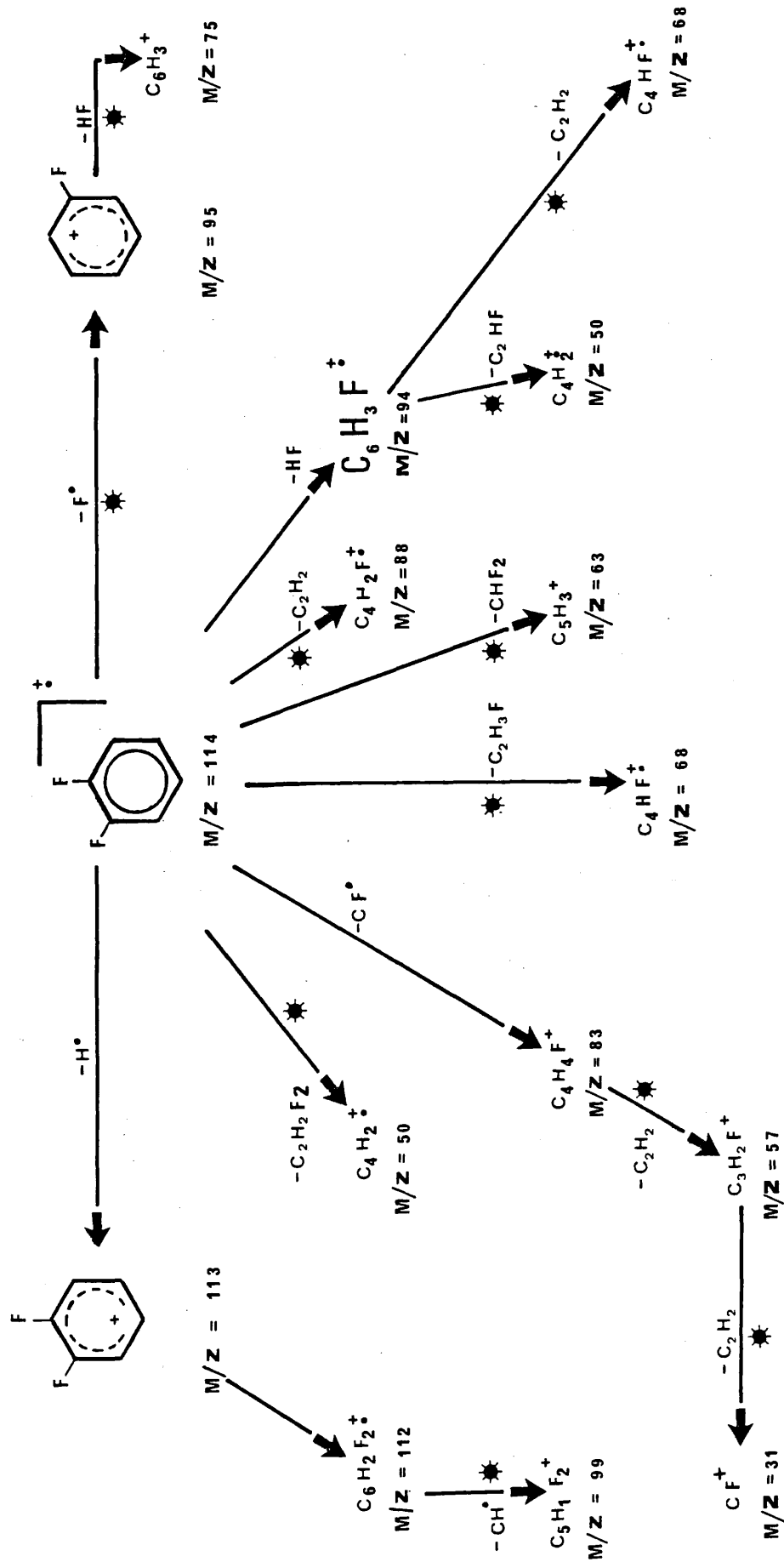


FIG. (3.21)

Postulated fragmentation of o-difluorobenzene consequent upon electron impact ionization.

the disappearance of principal primary ions have been evaluated and are given in Table (3.6)).

The observed relative abundance of the molecular ions, at 0.2 Torr, of 85% and 83% for o- and p-fluorobenzene were greater than in fluorobenzene. In all the difluoro reagents cluster ions with  $m/z = 145$ , 151, 171, 175, 177, 182, 189 and 207 were observed. The ion with  $m/z = 177$  resulting from reaction of the primary ion  $m/z = 63$  is the most abundant cluster ion. As with fluorobenzene increase in cluster ion abundance is commensurate with decrease in a particular primary ion, e.g. ion  $m/z = 189$  and ion  $m/z = 75$  in o-difluorobenzene, Figure (3.22). Relative abundances of principal primary and cluster ions recorded at 0.05, 0.1, 0.15 and 0.2 Torr are given in Tables (3.7 - 9). Plausible reaction pathways to the cluster ion are discussed in Section (4.3.2).

TABLE (3.6) Rate coefficients for the reaction of primary ions from difluorobenzenes with difluorobenzenes

Ion	m/z	Rate coefficients $\times 10^{11}/\text{cm}^3 \text{ molec}^{-1} \text{ s}^{-1}$		
		o-difluoro	m-difluoro	p-difluoro
$\text{C}_6\text{H}_3\text{F}_2^+$	113		$1.02 \pm 0.16$	$1.14 \pm 0.24$
$\text{C}_6\text{H}_4\text{F}^+$	95	$0.83 \pm 0.18$	$2.28 \pm 0.33$	$0.55 \pm 0.05$
$\text{C}_6\text{H}_3\text{F}^+$	94	$0.82 \pm 0.11$	$1.36 \pm 0.15$	$0.35 \pm 0.10$
$\text{C}_6\text{H}_2\text{F}^+$	93	$14.79 \pm 1.05$	$3.96 \pm 0.20$	$6.75 \pm 1.10$
$\text{C}_4\text{H}_2\text{F}_2^+$	88	$1.36 \pm 0.28$	$1.84 \pm 0.25$	$0.63 \pm 1.02$
$\text{C}_5\text{H}_2\text{F}^+$	81		$3.85 \pm 0.31$	$2.06 \pm 0.15$
$\text{C}_6\text{H}_3^+$	† 75	$14.8 \pm 0.3$	$4.32 \pm 0.28$	$4.37 \pm 0.14$
$\text{C}_3\text{HF}_2^+$	† 75	$1.39 \pm 0.31$		
$\text{C}_4\text{H}_3\text{F}^+$	70	$3.05 \pm 0.65$	$1.23 \pm 0.26$	
$\text{C}_4\text{H}_2\text{F}^+$	69	$33.0 \pm 2.3$	$6.44 \pm 0.80$	
$\text{C}_5\text{H}_4^+$	64	$2.77 \pm 0.54$	$2.18 \pm 0.21$	$0.78 \pm 0.15$
$\text{C}_5\text{H}_3^+$	63	$1.00 \pm 0.50$	$2.96 \pm 0.15$	$0.70 \pm 0.07$
$\text{C}_5\text{H}_2^+$	62	$53.0 \pm 3.0$	$10.1 \pm 1.1$	$40.5 \pm 7.4$
$\text{C}_3\text{H}_2\text{F}^+$	57	$0.27 \pm 0.11$	$2.95 \pm 0.28$	$5.45 \pm 0.26$
$\text{C}_4\text{H}_3^+$	51	$32.8 \pm 1.8$	$6.46 \pm 0.88$	$23.4 \pm 2.3$
$\text{C}_4\text{H}_2^+$	50	$95.3 \pm 1.4$	$95.7 \pm 19.4$	
$\text{C}_3\text{H}_3^+$	39		$1.34 \pm 0.30$	$0.18 \pm 0.14$
$\text{C}_3\text{H}_2^+$	38	$71.0 \pm 5.9$	$56.6 \pm 8.7$	
$\text{C}_3\text{H}^+$	37	$131.9 \pm 27.0$	$102.3 \pm 22.6$	
$\text{CF}^+$	31	$74.1 \pm 7.0$	$17.6 \pm 3.9$	

† Two ions with same nominal m/z. See text.

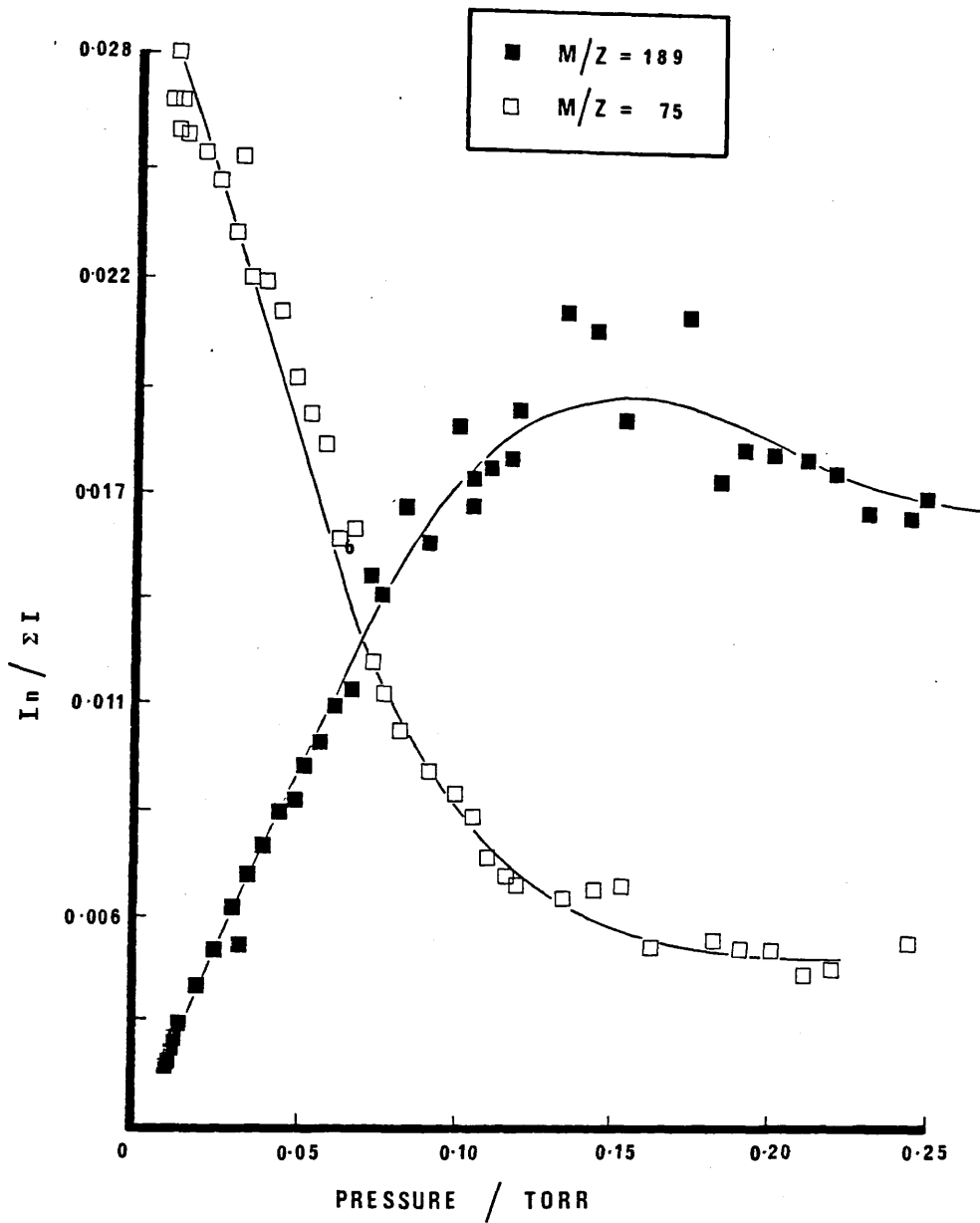


FIG. (3.22)

Increase in abundance of the cluster ion  $m/z = 189$  commensurate with the decrease in abundance of primary ion  $m/z = 75$  in difluorobenzene.

TABLE 3.7 Relative abundances of ions in p-difluorobenzene at various pressures.

Ion	m/z	Relative abundance at pressure x/Torr				
		0.01	0.05	0.1	0.15	0.2
$C_3H_3^+$	39	0.007	0.005	0.005	0.005	0.004
$C_4H_2^+$	50	0.013	-	-	-	-
$C_4H_3^+$	51	0.006	0.003	-	-	-
$C_3H_2F^+$	57	0.033	0.019	0.013	0.014	0.012
$C_5H_3^+$	63	0.009	0.064	0.045	0.039	0.034
$C_5H_4^+$	64	0.009	0.005	0.004	0.004	0.003
$C_6H_3^+$	75	0.020	0.014	0.010	0.006	0.003
$C_4H_2F_2^+$	88	0.032	0.007	0.005	0.005	0.004
$C_6H_3F^+$	94	0.012	0.005	0.004	0.003	0.003
$C_6H_4F_2^+$	114	0.608	0.733	0.745	0.718	0.735
† $C_6H_4F_2^+$	115	0.040	0.048	0.051	0.053	0.054
$C_7H_4F_3^+$	145	0.003	0.007	0.008	0.008	0.008
$C_9H_5F_2^+$	151	0.004	0.009	0.011	0.012	0.010
$C_9H_8F_3^+$	171	-	0.003	0.007	0.011	0.010
$C_{11}H_5F_3^+$	175	0.002	0.005	0.006	0.006	0.006
$C_{11}H_7F_2^+$	177	-	0.008	0.020	0.030	0.031
$C_{10}H_5F_3^+$	182	-	0.002	0.002	0.003	0.003
$C_{12}H_7F_2^+$	189	0.002	0.007	0.012	0.019	0.020
$C_{12}H_6F_3^+$	207	-	0.003	0.004	0.005	0.006

† Carbon thirteen analogue of  $C_6H_4F_2^+$

TABLE 3.8 Relative abundances of ions in m-difluorobenzene at various pressures.

Ion	m/z	Relative abundance at pressure x/Torr				
		0.01	0.05	0.1	0.15	0.2
$C_3H_3^+$	39	0.012	0.009	0.009	0.008	0.005
$C_4H_2^+$	50	0.028	0.001	-	-	-
$C_4H_3^+$	51	0.008	0.005	0.003	0.002	-
$C_3H_2F^+$	57	0.036	0.025	0.018	0.013	0.013
$C_5H_3^+$	63	0.105	0.095	0.074	0.053	0.037
$C_5H_4^+$	64	0.012	0.008	0.006	0.005	0.004
$C_6H_3^+$	75	0.026	0.027	0.022	0.012	0.005
$C_4H_2F_2^+$	88	0.046	0.016	0.012	0.010	0.006
$C_6H_3F^+$	94	0.020	0.014	0.012	0.009	0.008
$C_6H_4F_2^+$	114	0.491	0.560	0.540	0.561	0.608
† $C_6H_4F_2^+$	115	0.035	0.047	0.045	0.045	0.050
$C_7H_4F_3^+$	145	0.002	0.013	0.016	0.015	0.010
$C_9H_5F_2^+$	151	0.003	0.017	0.022	0.021	0.014
$C_9H_8F_3^+$	171	-	0.003	0.008	0.009	0.009
$C_{11}H_5F_2^+$	175	-	0.009	0.012	0.011	0.007
$C_{11}H_7F_2^+$	177	-	0.008	0.029	0.038	0.034
$C_{10}H_5F_3^+$	182	-	0.003	0.004	0.004	0.004
$C_{12}H_7F_2^+$	189	-	0.008	0.018	0.022	0.017
$C_{12}H_6F_3^+$	207	-	0.005	0.010	0.012	0.010

† Carbon thirteen analogue of  $C_6H_4F_2^+$



Table 3.9. Relative abundances of ions in o-difluorobenzene at various pressures.

Ion	m/z	Relative abundance at pressure x/Torr				
		0.01	0.05	0.1	0.15	0.2
$C_3H_3^+$	39	0.011	0.008	0.007	0.006	0.006
$C_4H_2^+$	50	0.014	-	-	-	-
$C_4H_3^+$	51	0.008	0.004	-	-	-
$C_3H_2F^+$	57	0.028	0.017	0.011	0.011	0.010
$C_5H_3^+$	63	0.097	0.065	0.041	0.029	0.033
$C_5H_4^+$	64	0.012	0.006	0.005	0.003	0.003
$\ddagger C_6H_3^+$	75	0.027	0.020	0.009	0.006	0.005
$C_4H_2F_2^+$	88	0.040	0.015	0.008	0.007	0.005
$C_6H_3F^+$	94	0.016	0.009	0.007	0.006	0.006
$C_6H_4F_2^+$	114	0.536	0.637	0.678	0.703	0.718
$\dagger C_6H_4F_2^+$	115	0.039	0.049	0.053	0.054	0.055
$C_7H_4F_3^+$	145	0.006	0.014	0.013	0.012	0.009
$C_9H_5F_2^+$	151	0.006	0.019	0.017	0.017	0.003
$C_9H_8F_3^+$	171	-	-	-	-	-
$C_{11}H_5F_2^+$	175	0.003	0.008	0.009	0.007	0.006
$C_{11}H_7F_2^+$	177	0.001	0.017	0.032	0.031	0.029
$C_{10}H_5F_3^+$	182	-	-	-	-	-
$C_{12}H_7F_2^+$	189	0.002	0.009	0.018	0.021	0.019
$C_{12}H_6F_3^+$	207	0.002	0.005	0.007	0.009	0.007

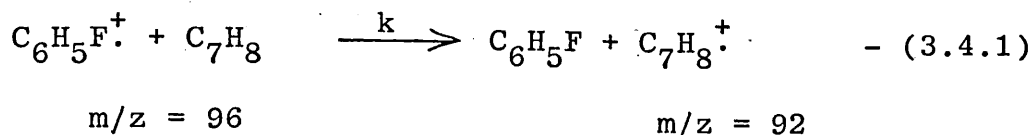
$\dagger$  Carbon thirteen analogue.

$\ddagger$  Also some  $C_3HF_2^+$

3.1.4 The chemical ionization mass spectra of selected aromatic compounds; changes of relative ion-abundance with variation of sample pressure.

If analysis of aromatic components in complex hydrocarbon mixtures, e.g. mineral oils, was to be accomplished using fluorobenzene reagent gas then ionization should produce ideally one ionic species per aromatic compound and fragmentation of this species should be minimal. Since quantitation of aromatic material was also desired the relative reactivities, towards the reactant ion, eq.(3.4.1), of typical aromatic compounds were required in order that any correction factors, resulting from differences in reactivity, could be applied. To these ends fluorobenzene chemical ionization of selected alkylbenzene, alkyl-naphthalenes, alkylthiophenes, alkyl-furans and some miscellaneous compounds was studied as a function of sample pressure. The results so obtained are now described.

Upon addition of methylbenzene to the ion-source giving a partial pressure of 0-4m Torr (see Section (2.4.2)), already containing fluorobenzene at 0.2 Torr, the relative abundance of the fluorobenzene molecular ion,  $m/z = 96$ , decreased while that of an ion,  $m/z = 92$ , the methylbenzene molecular ion, increased. This is attributed to ionization of methylbenzene in a charge exchange reaction with the fluorobenzene molecular ion.



Since the decrease in relative abundance of fluorobenzene molecular ion is essentially equally matched by an increase of methylbenzene molecular ion, Figure (3.23), any reactions of other ions in the fluorobenzene plasma are regarded as negligible, and may be neglected. The rate coefficient for reaction of  $\text{C}_6\text{H}_5\text{F}^+$  with methylbenzene acts as a suitable measure of reactivity. A discussion of the kinetics of reactions similar to (3.4.1), and their rate coefficients will be given in Section (4.4). The reaction of the various alkylbenzenes, alkyl naphthalenes, alkyl thiophenes and alkyl furans were found to be similar to that observed for methylbenzene. The relative abundances of  $\text{C}_6\text{H}_5\text{F}^+$  and those ions resulting from sample ionization at sample pressures ( $P_s$ ) of  $\sim 0.5$  mTorr and  $\sim 3.0$  mTorr are given in Tables (3.10) and (3.11). These tables clearly show that the reduction in fluorobenzene molecular ion abundance is matched by increases in sample ion abundances, indicating that for all the compounds studied only the reaction of  $\text{C}_6\text{H}_5\text{F}^+$  is of any significance. The relative abundances of other fluorobenzene ions were invariant with sample pressure. Additionally table (3.10) shows that ions with mass to charge ratio less than the sample molecular ion were observed, but having only small relative abundances. These ions result from fragmentation of the

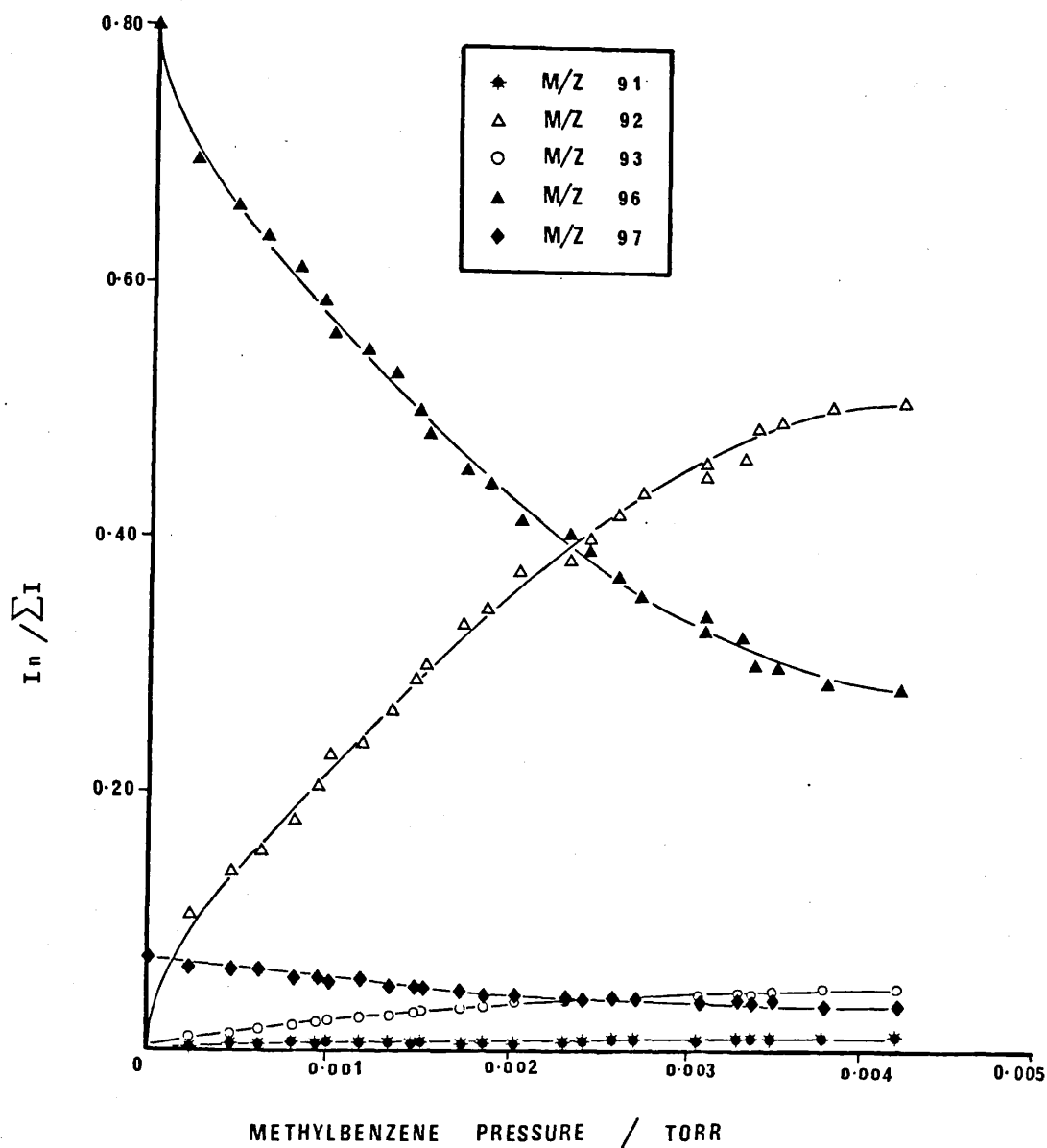
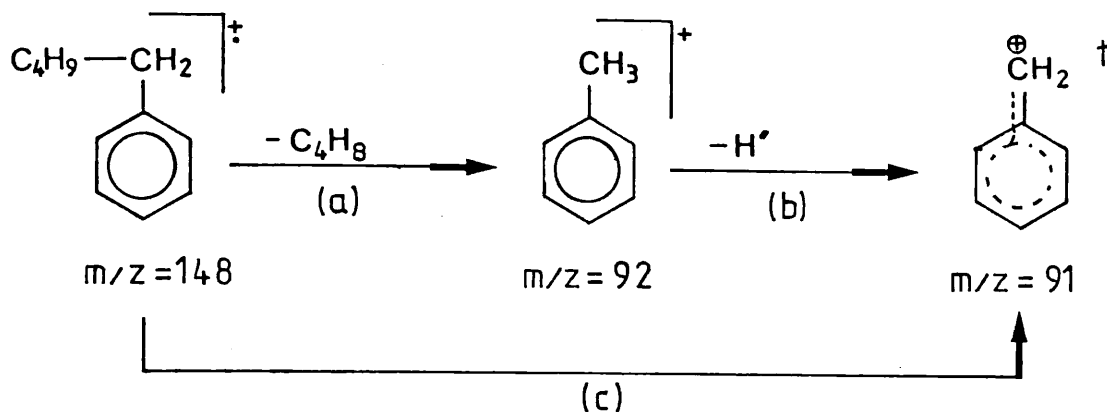


FIG. (3.23)

Variation in reactant and product ion abundances for reaction of fluorobenzene molecular ions ( $m/z = 96, 97$ ) with methylbenzene as a function of methylbenzene ion-source pressure.

molecular ions by processes similar to those illustrated below for n-pentylbenzene



In tables (3.10) and (3.11) 'a', 'b' or 'c' beside relative abundances indicate that a broad peak at  $m/z = m^*$ , as given by equation (1.2.3), support the appropriate pathway. The relative abundance of fragment ions observed for xylene, ethylbenzene, mesitylene resulting from loss of a methyl radical were very low, normally accounting for <1% of the total sample ion-current. Only isopropylbenzene shows a higher proportion of fragment ions ( $m/z = 105$ ), 3% of the sample ion current, formed by loss of methyl radical. No fragmentation was observed for the alkylfurans and alkylthiophenes studied. Thus since fragmentation ion abundances are typically less than 1% of sample molecular ion abundances they may be neglected when analysing complex hydrocarbon mixtures (see Section (3.2.4)).

---

<sup>†</sup> Believed to be the most likely structure formed for alkyl benzenes. See Ref. (114).

TABLE 3.10 Ion abundances in fluorobenzene chemical ionization of alkylbenzenes.

SAMPLE	P <sub>S</sub> /m Torr	C <sub>6</sub> H <sub>5</sub> F <sup>+</sup> M <sup>+</sup>	Sample M <sup>+</sup>	Relative abundances			
				Ion m/z=91	Ion m/z=92	(M-CH <sub>3</sub> ) <sup>+</sup> (M-C <sub>2</sub> H <sub>5</sub> ) <sup>+</sup> (M-C <sub>3</sub> H <sub>7</sub> ) <sup>+</sup> (M-C <sub>4</sub> H <sub>9</sub> ) <sup>+</sup>	
n-Pentylbenzene	0.5	0.62	0.15	0.001	0.001		0.001
	3.0	0.27	0.47	0.006 <sup>b</sup>	0.006 <sup>a</sup>		0.006 <sup>b</sup>
n-Butylbenzene	0.8	0.59	0.18	0.002	0.002	0.002	
	3.0	0.29	0.46	0.007 <sup>b</sup>	0.006 <sup>a</sup>	0.006 <sup>b</sup>	
n-Propylbenzene	0.4	0.55	0.18	0.002		0.002	
	2.9	0.25	0.47	0.008 <sup>c</sup>		0.008 <sup>c</sup>	
Isopropylbenzene	0.5	0.57	0.17			0.003	
	3.0	0.23	0.48			0.015	
1,3,5 Trimethylbenzene	0.7	0.58	0.19			0.001	
	3.1	0.28	0.49			0.006	
n-Ethylbenzene	0.5	0.63	0.14	0.002		0.002	
	3.0	0.30	0.46	0.010 <sup>c</sup>		0.010	
1,2 Dimethylbenzene	0.5	0.63	0.13	-		-	
	3.0	0.29	0.49	0.006		0.006	
1,3 Dimethylbenzene	0.6	0.54	0.20	-		-	
	2.9	0.23	0.56	0.005		0.005	
1,4 Dienthylbenzene	0.5	0.62	0.15	-		-	
	3.0	0.35	0.43	0.005		0.005	
Methylbenzene	0.5	0.63	0.13	-		-	
	3.0	0.33	0.43	0.005		0.005	

a,b,c - See text.

TABLE 3.11 Ion abundances in fluorobenzene chemical ionization of aromatics.

SAMPLE	Sample pressure /m Torr	Relative abundances			
		$C_6H_5F^+$	Sample $M^+$	$(M-H)^+$	$m/z=83$ $(M-CH_3)^+$
2,5-Dimethylthiophene	0.5	0.60	0.17		
	3.3	0.30	0.48		
2-Methylthiophene	0.6	0.58	0.21		
	3.0	0.36	0.43		
Thiophene	0.6	0.62	0.15		
	3.0	0.39	0.39		
2-Methylfuran	0.5	0.56	0.20	0.001	
	3.1	0.24	0.55	0.002	
Furan	0.5	0.62	0.14		
	3.0	0.39	0.38		
2-Ethyl-naphthalene	0.6	0.51	0.25		0.001
	3.0	0.21	0.54		0.006
1-Methylnaphthalene	0.5	0.60	0.14		
	3.0	0.26	0.49		
Cyclohexylbenzene	0.5	0.55	0.19	0.001	-
	2.8	0.30	0.42	0.005	0.006

## 3.2 CHEMICAL IONIZATION MASS SPECTRA OF LUBRICANT BASE OILS.

### 3.2.1 Ester base oils.

A series of compounds characteristic of those esters found in modern lubricants were prepared and purified by the methods given in Section (2.1.3). Physical properties and spectroscopic data determined on the pure compounds are to be found in Section (2.1.3) and Appendix III respectively. The ester fluids comprise two groups, namely those prepared from dibasic acids and long alkyl chain alcohols, type I lubricants, and those resulting from esterification of 2-ethyl-2(hydromethyl)-propane-1,3-diol, (Trimethylpropane), and 2,2-bis(hydromethyl)-propane-1,3-diol, (Pentaerythritol), with long alkyl chain monobasic acids, type II lubricants. Ammonia chemical ionization mass spectra of these and a representative lubricant blending component 'A' were recorded using the condition described in Section (2.5.1). Results pertaining to esters of dibasic acids, neopentyl polyols and lubricant blending component are recorded separately.

#### 3.2.1.1 Esters of dibasic acids.

The relative abundance of ions resulting from ammonia chemical ionization, at ion-source ammonia pressures of 0.2 and 0.7 Torr of a series of dibasic acid esters are given in Table (3.12). Examination of this table indicates that the spectra comprise primarily two ionic species with mass to charge ratios that can be



TABLE 3.12. Relative abundances of ions resulting from ammonia CI of dibasic acid esters.

ESTER (M)	Ammonia Pressure /Torr	Relative ion abundances <sup>13</sup> C containing ions included									
		(M+NH <sub>4</sub> ) <sup>+</sup>	(M+H) <sup>+</sup>	((M+NH <sub>4</sub> +H) -R) <sup>+</sup>	((M+NH <sub>4</sub> ) -R) <sup>+</sup>	((M+NH <sub>4</sub> ) -OR) <sup>+</sup>	((M+NH <sub>4</sub> ) -HOR) <sup>+</sup>	((M+NH <sub>4</sub> ) -R) <sup>+</sup>	((M+NH <sub>4</sub> ) -2R) <sup>+</sup>	((M+H) -2R) <sup>+</sup>	
bis(Dodecyl)hexandioate	0.7	0.881	0.027	0.018	0.003	0.002	0.004	0.004	0.004	0.005	
" (Undecyl)	0.7	0.875	0.028	0.016	0.003	0.001	0.006	0.004	0.005		
" (Decyl)	0.7	0.860	0.032	0.016	0.004	0.002	0.007	0.005	0.006		
" "	0.2	0.632	0.250	0.009	0.004	0.007	0.022	-	0.034		
" (1-Methyloctyl)	0.7	0.750	0.090	0.088	-	0.005	0.007	0.004	0.004		
" (2-Ethylhexyl)	0.7	0.863	0.057	0.016	0.004	0.002	0.004	0.003	0.003		
" "	0.2	0.543	0.332	0.023	0.003	0.008	0.009	0.002	0.019		
" (Methyl)	0.7	0.943	0.035	0.003	0.002	-	-	-	0.002		
" "	0.2	0.708	0.252	-	0.007	-	-	0.005	0.002		
" (2-Ethylhexyl)heptandioate	0.7	0.886	0.022	0.019	0.003	-	0.002	0.004	-		
" ( " )octandioate	0.7	0.894	0.019	0.023	0.002	0.001	0.002	0.003	0.004		
" ( " )nonandioate	0.7	0.938	0.020	0.018	0.002	-	-	-	0.004		

R = Alcoholic alkyl group.

attributed to addition of a proton ( $(M+H)^+$ ) or ammonium ion ( $(M+NH_4)^+$ ) to the sample ester (M), e.g. bis(dodecyl)-hexandioate for which  $(M+H)^+$  and  $(M+NH_4)^+$  ions account for ~91% of the total sample ion-current, when ions containing carbon thirteen isotope are included. However the ratio of ion-current carried by  $(M+H)^+$  and  $(M+NH_4)^+$  ions was observed to vary considerably with ammonia pressure. High ammonia pressures producing essentially monoionic sample spectra, e.g. at 0.7 Torr, 94% of the sample ion-current for bis(2-ethylhexyl)nonanedioate was due to  $(M+NH_4)^+$  ions. However at lower pressures considerable quantities of  $(M+H)^+$  ions were produced, e.g. 33% of the sample ion current for bis(2-ethylhexyl)hexandioate results from  $(M+H)^+$  at ammonia pressure of 0.2 Torr. Additionally some of  $(M+H)^+$  ions result from fragmentation by loss of  $NH_3$  from  $(M+NH_4)^+$  ions. Broad peaks at a mass  $m^*$  (see equation (1.2.3)) consistent with fragmentation of metastable ions in support of the above stated transition were observed. Other fragment ions were observed but their relative abundances were typically less than 2% of the sample ion-current. Bis(1-methyloctyl)hexanedioate was an exception, 9% of the sample ion-current resulted from an ion, with  $m/z=290$ , consistent with loss of  $C_9H_{18}$  from the  $(M+NH_4)^+$  cluster ion.

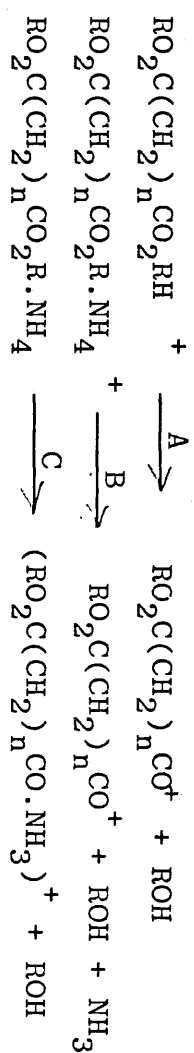
"Metastable peaks" were observed for fragmentation by loss of ROH from  $(M+H)^+$  ions, where R represents an ester alkyl group, and for loss of  $H_3N.HOR$

from  $(M+NH_4)^+$  ions. See Table (3.13). However only small quantities of the product ions  $((M+H)-ROH)^+$  were observed. At the high ammonia pressure used solvation of  $((M+H)-ROH)^+$  ions is likely to result in a reduction of these species. Noticeable ion-currents were detected at m/z's consistent with the solvated ions  $((M+H)-ROH).NH_3^+$ . Additionally "metastable peaks" were observed for formation of  $((M+NH_4)-HOR)^+$  by direct loss of ROH from  $(M+NH_4)^+$  ions, when the number of  $CH_2$  units separating the ester acyl groups (n) was greater than four, see Table (3.13). Weinkam and Gal<sup>115</sup> have proposed a mechanism for exchange of OR with  $NH_3$  in ammonia chemical ionization of dibasic acid methyl esters, Scheme (3.1) which requires  $n \geq 4$ . The data recorded in this study, suggests a similar mechanism to be operative for long alkyl chain esters.

### 3.2.1.2 Synthetic blends of dibasic acid esters.

The results obtained from ammonia CI analysis of three synthetic mixtures, Blend 1 - 3, are given in Table (3.14). Good agreement between the values obtained by ammonia CI and the true composition, percent weight, was obtained. Since the mixtures contained esters with different structures, viz. degree of alkyl chain branching and number of  $CH_2$  groups separating acidic functions, it is apparent that structure little affects sensitivity. From the data obtained it is apparent that quantitative data obtained by ammonia CI should have a mean accuracy of  $\pm 3\%$  absolute.

TABLE 3.13 Fragmentation of protonated (M+H)<sup>+</sup> and ammoniated (M+NH<sub>4</sub>)<sup>+</sup> ions of dibasic acid esters. (P<sub>NH<sub>3</sub></sub> = 0.2 Torr).



Metastable peaks for fragmentations

ESTER RO <sub>2</sub> C(CH <sub>2</sub> ) <sub>n</sub> CO <sub>2</sub> R	A		B		C	
	m/z Observed	Calculated	Observed	Calculated	Observed	Calculated
bis(Dodecyl)hexandioate	181.0	182.6	176.5	176.4	197.2	
" (Undecyl)	174.6	176.0	169.1	169.9	190.7	
" (Decyl)	168.5	169.5	163.2	163.0	184.2	
" (1-Methyloctyl)	162.5	163.0	156.0	156.3	177.9	
" (2-Ethylhexyl)	156.0	156.6	150.0	149.7	171.6	
" (2-Ethylhexyl)heptandioate	168.0	168.9	162.0	161.8	184.0	184.0
" (2-Ethylhexyl)octandioate	180.5	181.4	174.0	173.9	197.0	196.6
" (2-Ethylhexyl)nonandioate	193.0	193.9	187.0	186.3	209.5	209.3

SCHEME 3.1 Ammonolysis of dibasic acid esters.

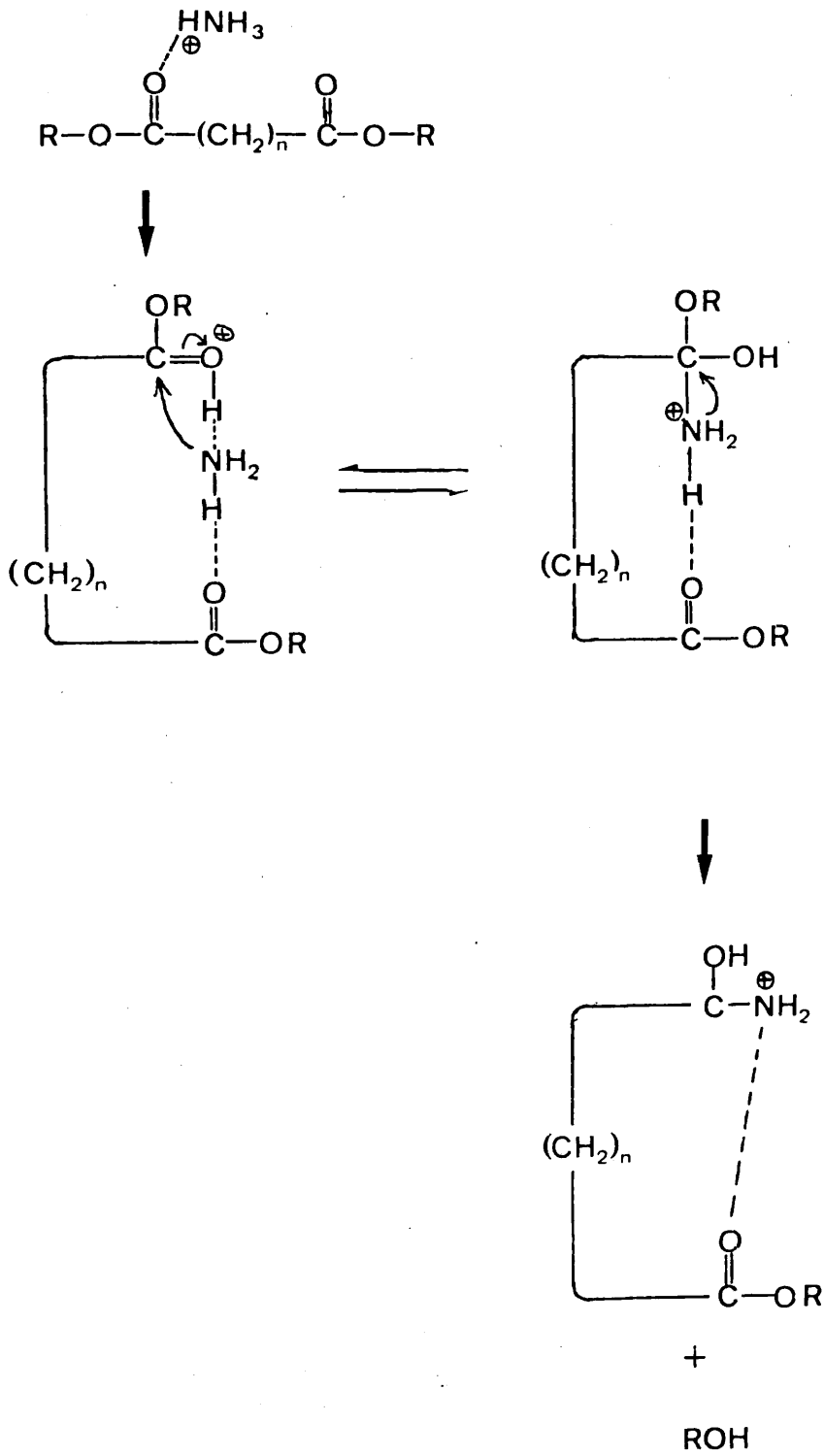


TABLE 3.14

Blends of synthetic ester standards.

COMPONENTS	<u>BLEND 1</u>		<u>BLEND 2</u>		<u>BLEND 3</u>	
	% Wt.	% Wt. Found	% Wt.	% Wt. Found	% Wt.	% Wt. Found
Bis(Dodecyl)hexanedioate	53	51	27	23	31	29
Bis(Undecyl)hexanedioate	47	49	74	77	27	25
Bis(2-Ethylhex yl)nonanedioate					42	46

### 3.2.1.3 Esters of the neopentylpolyols

2-ethyl-2(hydroxymethyl)-propane-1,3 diol  
and 2,2 bis(hydroxymethyl)-propane-1,3 diol.

Ammonia chemical ionization resulted in essentially monoionic sample spectra, at an ammonia pressure of 0.7 Torr, as shown in Table (3.15). E.g. 2-ethyl-2-pentylcarbonyloxymethyl-1,3 propane-dihexanoate (M) for which 99.6% of the sample ion-current was due  $(M+NH_4)^+$  ions. No "metastable peaks" were observed.

### 3.2.1.4 Ester lubricant blending component 'A'.

The results obtained from the normalization and subsequent summation of spectra recorded during volatilization of the blending component 'A' by the method recorded in Section (2.5) are given in Table (3.16). Two separate volatilizations were performed to assess reproducibility. The mass to charge ratios of the principal ions observed, excluding  $^{13}C$  analogues, are given in Table (3.16), and assuming these to be  $(M+NH_4)^+$  ions, the molecular mass of any component, equal to  $(m/z-18)$ , was readily obtained. The ion-currents obtained for the  $(M+18)^+$  ions, including  $^{13}C$  analogues were then summed and the relative proportion due to each ion, molar %, found. Using the molecular masses, deduced from the ion mass to charge ratios, the percentage weight of each component could be obtained and is appended in Table (3.16). Clearly reasonable reproducibility between the two evaluations was obtained, particularly since the results are the mean of ~60 spectra recorded over a

TABLE 3.15 Proportion of sample ion current associated with the ammoniated  $(M+NH_4)^+$  ion in the ammonia chemical ionization spectra of esters (M) of neopentyl polyols.

Acyl group RCO	Alcoholic group	
	2-Ethyl-2(hydroxymethyl) -1,3-propanediol	bis-2,2(hydroxymethyl) -1,3-propanediol
Pentaoyl -	99.4	97.3
Hexaoyl -	99.6	98.1
Heptaoyl -	98.6	) Mass spectra not ) recorded owing to ) low sample ) volatility.
Octaoyl -	96.9	
Nonaoyl -	97.1	



period of 6 minutes (see Section (2.5)). The observed ion mass to charge ratios are consistent with those expected for dibasic acid esters which differ in mass by one  $\text{CH}_2$ , (mw = 14), unit.

At the high ion-source pressure used, 0.7 Torr, no fragment ions were observed, and thus no information regarding the acid moiety of the ester could be obtained directly. However, as seen from Table (3.12), at lower ammonia pressures there is an increase in the relative abundances of  $(\text{M}+\text{H})-2\text{R})^+$  ions, for example bis(ethylhexyl)hexandioate and bis(decyl)hexandioate. Thus by obtaining spectra of blending component 'A' at lower pressures, ca. 0.2 Torr, it should be possible to observe ions which will indicate both their molecular mass and the carbon number of the remaining acidic moiety. Such an analysis was conducted on blending component 'A'. The only fragment ion observed with m/z consistent with a  $(\text{M}+\text{H})-2\text{R})^+$  structure was m/z=145. If this ion is assumed to be of  $(\text{M}+\text{H})-2\text{R})^+$  type, where M is the ester and R the alcoholic alkyl groups then the ion observed may be assigned the molecular formula  $\text{C}_6\text{H}_9\text{O}_4$ . This ion would arise from esters of hexandioic acid. Accordingly the carbon number of the acid and of the various alcohols used in preparing blending component 'A' may be deduced and the components named accordingly, Table (3.17).

**TABLE 3.16** Relative abundances of principal ions observed in the ammonia chemical ionization mass spectra of ester lubricant blending component 'A'.

Mass to charge ratio (m/z) of principal sample ions.	(m/z - 18)	Relative proportions				
		molar % †		% Wt.		
		Run 1	Run 2	Run 1	Run 2	Mean
500	482	5.0	3.9	4.8	3.7	4.3
514	496	24.7	24.5	24.2	24.0	24.1
528	510	65.0	67.8	65.5	68.3	66.9
542	524	5.3	3.8	5.5	3.9	4.7

† See text

**TABLE 3.17** Identities assigned to components observed in blending component 'A'

(M+18) <sup>+</sup> ion (m/z)	RMM	Adipates
500	482	bis(Dodecyl)
514	496	Tridecyl, dodecyl
528	510	bis(Tridecyl)
542	524	Tetradecyl, tridecyl

### 3.2.2 Hydrogenated polyalpha-olefin base oils.

Chemical ionization mass spectra of hydrogenated polyalpha-olefin (PAO) base oils were obtained using (i) methane, (ii) nitric oxide and (iii) mixtures of nitrogen and nitric oxide as reagent gases. Although spectra obtained with nitric oxide exhibited less fragmentation, little data was collected, because the ease of oxidation of the source filament resulted in failure after only 4-6 hours operation. However, as noted by Hunt and Harvey,<sup>71</sup> if nitric oxide is mixed with suitable quantities of nitrogen, (see Section (2.5)), oxidation is prevented and normal filament lifetimes are possible. Spectra of PAO's obtained using a mixture of nitrogen and nitric oxide as reagent gas showed little difference from those obtained with pure nitric oxide. For these reasons discussion is concentrated on data obtained using either methane or nitrogen/nitric oxide mixtures as reagent gases.

All the PAO's studied were industrial products and are referred to here only by a reference number. Viz SHC-1 to SHC-30.

#### 3.2.2.1 Methane chemical ionization (CI) of hydrogenated polyalpha-olefin base oils.

Samples were volatilized into the ion-source from the direct insertion probe and spectra recorded at probe temperatures of 50, 100, 150, 200 and 250°C as described in Section (2.5). Since the fluids normally contained more than one component volatilization occurred over a range of temperatures  $t_1 \rightarrow t_2$  specific to each base oil; spectra were

obtained within this temperature range.

A typical methane CI spectrum of the base oil, SHC-7, recorded at a probe temperature of 100°C, is given in Figure (3.24). The base peak in the spectrum has  $m/z = 337$ , and knowing that only carbon and hydrogen are present indicates it corresponds to  $C_{24}H_{49}^+$ . Another ion  $m/z = 449$ , of considerably lower relative abundance,  $C_{32}H_{65}^+$ , was similarly observed. Both these ions have relative abundances considerably in excess of all others having  $m/z > M-60$  and  $M+60$ . Therefore it is likely that  $C_{24}H_{49}^+$  and  $C_{32}H_{65}^+$  are  $(M-1)^+$  ions, where  $M$  is the mass of the PAO, resulting from hydride exchange between methane reagent gas ions and the synthetic hydrocarbon molecules. The parent molecules are the long chain alkanes  $C_{24}H_{50}$  and  $C_{32}H_{66}$ . The carbon number of  $(M-1)^+$  ions observed in spectra recorded throughout the volatilization of SHC-7, at probe temperatures of 100, 150 and 200°C, are recorded in Table (3.18) along with similar information obtained for the other base oils studied. From Table (3.18) the number of components, and the number of carbons in each, for each base oil is readily obtained, e.g. SHC-7 contains three components having 24, 32 and 40 carbons respectively.

From Figure (3.24) it is apparent that although the "pseudo molecular ions"  $(M-1)^+$  are clearly visible, considerable fragmentation occurs by successive loss of alkene units ie 14n daltons. In most of the methane

---

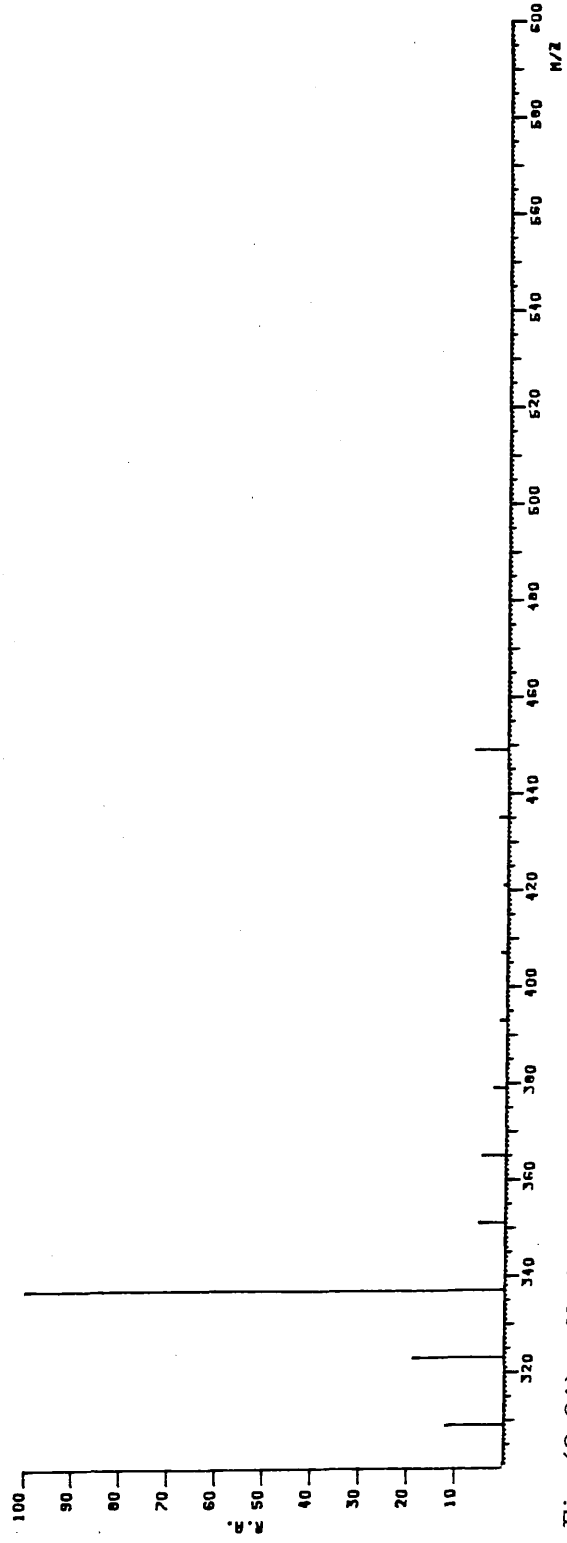
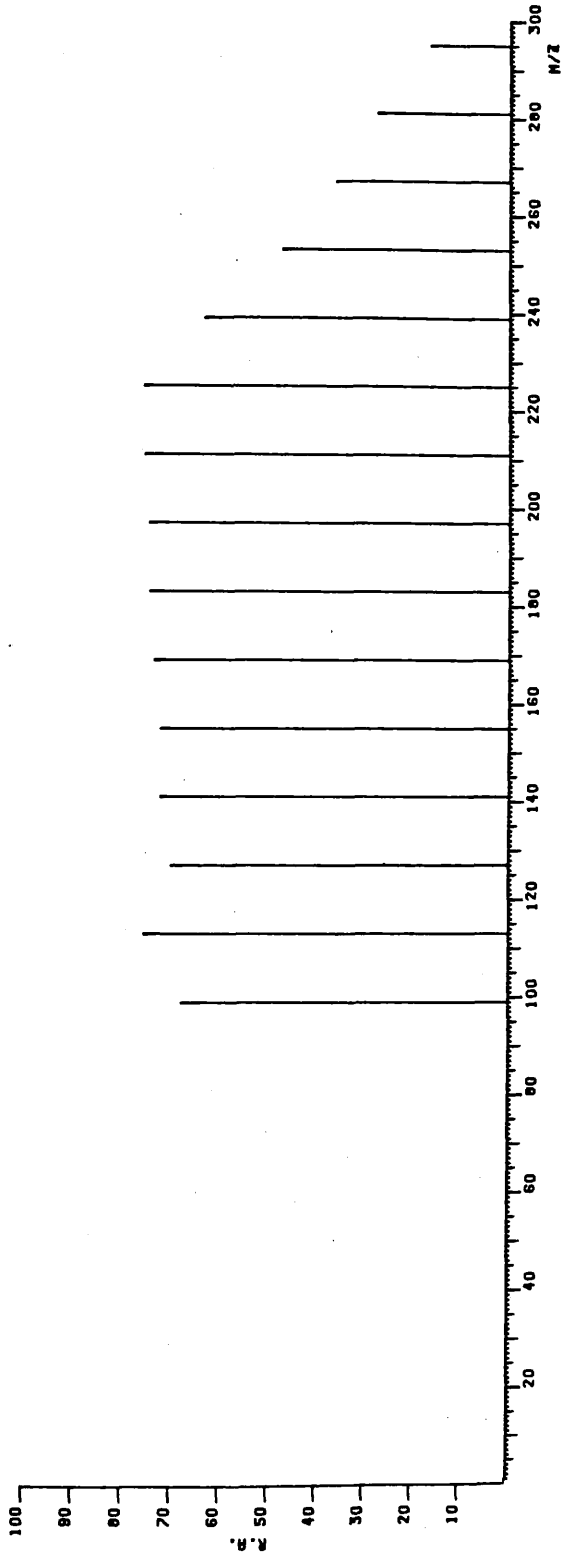


Fig. (3.24). Methane chemical ionization spectra of synthetic hydrocarbon base oil SHC-7.

TABLE 3.18A Principal (M-1)<sup>†</sup> ions from methane CI of synthetic hydrocarbon lubricant base oils.

Base oil	Solid probe Temperature /°C	Carbon number of principal (M-1) <sup>†</sup> ions <sup>†</sup>
SHC-1	50	<u>24</u> , <u>23</u> , 20, 19, 27, 28.
	100	27, 28, 32, 31
SHC-2	50	<u>30</u> , 20
	150	30
SHC-3	150	30
	200	<u>30</u> , 40
SHC-4	150	30
	200	<u>30</u> , 40
	250	40
SHC-5	150	<u>30</u> , <u>28</u> , <u>32</u> , 42, 44
	200	<u>42</u> , <u>44</u> , 46
	250	<u>44</u> , <u>42</u> , 46
SHC-6	250	<u>42</u> , <u>44</u> , 48
SHC-7	100	<u>24</u> , 32
	150	<u>24</u> , 32
	200	<u>32</u> , 40
SHC-8	100	<u>24</u> , 32
	150	<u>24</u> , 32
	200	<u>32</u> , 40
	250	<u>32</u> , 40
SHC-9	50	20
SHC-10	150	30
SHC-11	100	<u>30</u> , 40
	150	40
SHC-12	250	40
SHC-13	100	<u>24</u> , 32
	150	24, 32
	200	32

† (i) Ions in decreasing order of relative abundance from left to right.

(ii) Most abundant ions are underlined.

**TABLE 3.18B** Principal (M-1)<sup>†</sup> ions from methane CI of hydrogenated polyalpha-olefin lubricant base oils.

Base oil	Solid probe Temperature / °C	Carbon number of principal (M-1) <sup>†</sup> ions†
SHC-14	100	<u>26</u> , <u>24</u> , <u>28</u> , 36, 38
	150	<u>26</u> , <u>28</u> , 34, 36, 22
	200	<u>34</u> , <u>36</u> , 38
SHC-15	100	<u>26</u> , 24, 28
	150	<u>26</u> , 28, 24, 30
	200	<u>28</u> , 30, 34, 36
SHC-16	100	<u>24</u> , 22, 26, 28
	150	<u>26</u> , 28, 24, 30, 32
	200	<u>34</u> , 36, 32, 38, 40
SHC-17	150	<u>24</u> , 26, 28, 30
	200	<u>30</u> , <u>32</u> , 34, 36, 38
	250	<u>36</u> , 34, 38, 40
SHC-18	150	<u>26</u> , 28, 30, 32, 34
	200	<u>34</u> , 36, 32, 38, 40
SHC-19	150	<u>26</u> , 28, 30, 32
SHC-20	150	30
	200	30
SHC-21	150	30
	200	<u>30</u> , 40
	250	<u>30</u> , 40
SHC-22	150	30
	200	30, 40
	250	30, 40
SHC-23	150	30
	200	<u>30</u> , 40
	250	30, 40
SHC-24	- No clear (M-1) ions.	

† (i) Ions in decreasing order of relative abundance from left to right.

(ii) Most abundant ions are underlined.

TABLE 3.18C Principal (M-1)<sup>+</sup> ions from methane CI of hydrogenated polyalpha-olefin lubricant base oils.

Base oil	Solid probe Temperature /°C	Carbon number of principal (M-1) <sup>+</sup> ions <sup>†</sup>
SHC-25		) Series ending at C <sub>40</sub>
SHC-26		
SHC-27	100	<u>24</u> , 32
SHC-28	150	30
	200	30, 40
	250	40
SHC-29	150	30
	200	30, 40
	250	40

<sup>†</sup> (i) Ions in decreasing order of relative abundance from left to right.

(ii) Most abundant ions are underlined.



spectra less than 10% of the sample ion current was derived from the  $(M-1)^+$  ions. Such high fragment-ion abundances precluded the use of  $(M-1)^+$  ion abundances for quantitation of each component.

Howard, McDaniel, Nelson and Blomquist<sup>25</sup> have shown that the position of branching in long chain alkanes may be deduced from the relative abundance of fragmentations. Although the above authors observed less fragmentation, since they used higher reagent gas pressures, ca.0.5 Torr, the rules they proposed can still be applied to the data collected in the current study. In particular, by using the observation that fragment ion(s) resulting from  $\alpha$ -cleavage at a methyl branch point were more intense than adjacent ion fragments. Since synthetic hydrocarbons are normally prepared from  $\alpha$ -olefins only one such methyl branch per molecule is expected.

This being so, only the fragment ion resulting from loss of  $CH_3\cdot$  from the molecular ion should be considerably more abundant than its adjacent fragments. However this was not the case for several fluids which exhibited particularly abundant  $(M-29)^+$  fragments. To highlight these observations the relative abundance of  $(M-1)^+$ ,  $(M-15)^+$ ,  $(M-29)^+$  and  $(M-43)^+$  ions of the PAO component, in several base oils are given in Table (3.19). The significance of the ratios of  $(M-15)^+$ ;  $(M-29)^+$ ;  $(M-43)^+$  abundances will be discussed in Section (4.5.2).

TABLE 3.19A Variation in relative abundance of fragment ions in the methane chemical ionization mass spectra of various hydrogenated polyalpha-olefin base oils.

Base oil	Probe Temp °C	Peak height			(M-1) <sup>+</sup> m/z	(a) M-15	Relative abundance			Ratio a : b : c
		M-1	M-15	M-29			(b) M-29	(c) M-43		
SHC-1	50	1.75	1.60	0.65	337	91	37	34	10 : 4 : 4	
	100	0.80	0.80	0.31	393	100	38	47	10 : 4 : 5	
SHC-2	150	0.80	0.10	0.06	421	12	7	11	10 : 6 : 9	
SHC-3	150	0.90	0.18	0.12	421	19	13	18	10 : 7 : 9	
SHC-4	100	0.55	0.15	0.13	421	27	23	27	10 : 8 : 10	
SHC-7	50	9.0	1.25	0.8	337	14	9	12	10 : 6 : 8	
	100	0.33	0.08	0.04	337	24	11	17	10 : 4 : 7	
	150	1.0	0.20	0.14	449	20	14	15	10 : 7 : 7	
SHC-8	200	0.65	0.17	0.13	449	26	19	28	10 : 7 : 11	
SHC-9	50	0.44	0.11	0.07	281	24	15	31	10 : 8 : 15	
SHC-10	150	0.20	0.02	0.01	421	10	5	10	10 : 6 : 13	
SHC-11	150	0.18	0.03	0.02	421	14	8	14	10 : 6 : 10	
SHC-12	250	0.12	0.03	0.02	561	25	13	21	10 : 5 : 8	
SHC-13	150	0.41	0.05	0.04	337	12	10	12	10 : 8 : 10	
SHC-20	100	0.17	0.05	0.07	421	27	40	33	10 : 15 : 12	
SHC-21	150	0.24	0.07	0.09	421	29	38	35	10 : 13 : 12	

† Normalised to (M-1) ion intensity.

TABLE 3.19B Variation in relative abundance of fragment ions in the methane chemical ionization mass spectra of various hydrogenated polyalpha-olefin base oils.

Base oil	Probe Temp °C	Peak height			(M-1) <sup>+</sup> m/z	(a) M-15	Relative abundance †			Ratio a : b : c
		M-1	M-15	M-29			(b) M-29	(c) M-43		
SHC-22	150	0.1	0.03	0.05	421	25	45	10	10 : 18 : 16	
	200	0.15	0.04	0.06	421	27	40	30	10 : 15 : 11	
SHC-23	150	0.17	0.05	0.07	421	27	40	33	10 : 15 : 12	
	100	0.15	0.08	0.07	337	50	46	60	10 : 9 : 12	
SHC-27	100	0.15	0.08	0.07	337	50	46	60	10 : 9 : 12	

† Normalised to (M-1) ion intensity.

3.2.2.2 Nitric oxide chemical ionization of hydrogenated polyalpha-olefin base oils.

As noted above use of the reagent gas resulted in a reduction of both fragmentation, Figure (3.25), and filament life. The latter precludes regular use of this reagent. Unfortunately a "Townsend Discharge", which can operate in oxidising atmospheres, is not readily available for most mass spectrometers.

3.2.2.3 Nitrogen/nitric oxide mixture chemical ionization of hydrogenated polyalpha-olefin base oils.

The NO/N<sub>2</sub> and methane CI spectra of SHC-11 given in Figure (3.26) clearly show that the reduction in fragmentation obtained using nitric oxide only, (see Figure (3.25)) is maintained when nitrogen is added. It was found that by reducing the quantity of sample introduced into the ion source and using a linear temperature ramp for the probe heater, further reductions in fragmentation were obtained. See Figure (3.27). The spectrum of SHC-30 shown in Figure (3.27) was acquired using the data system, (see Appendix (2)), which facilitated spectra acquisition throughout the period of sample volatilization. The total ion-current chromatogram Figure (3.27) obtained during the volatilization of SHC-30 indicates two components to be present, the lower boiling component having an (M-1)<sup>+</sup> ion with m/z = 505 equivalent to C<sub>36</sub>H<sub>73</sub><sup>+</sup> and resulting from C<sub>36</sub>H<sub>74</sub>. The (M-1)<sup>+</sup> ion

for the higher boiling material was not observed since it had  $m/z > 600$ , i.e. above the limit of the calibration routine of the current data system.

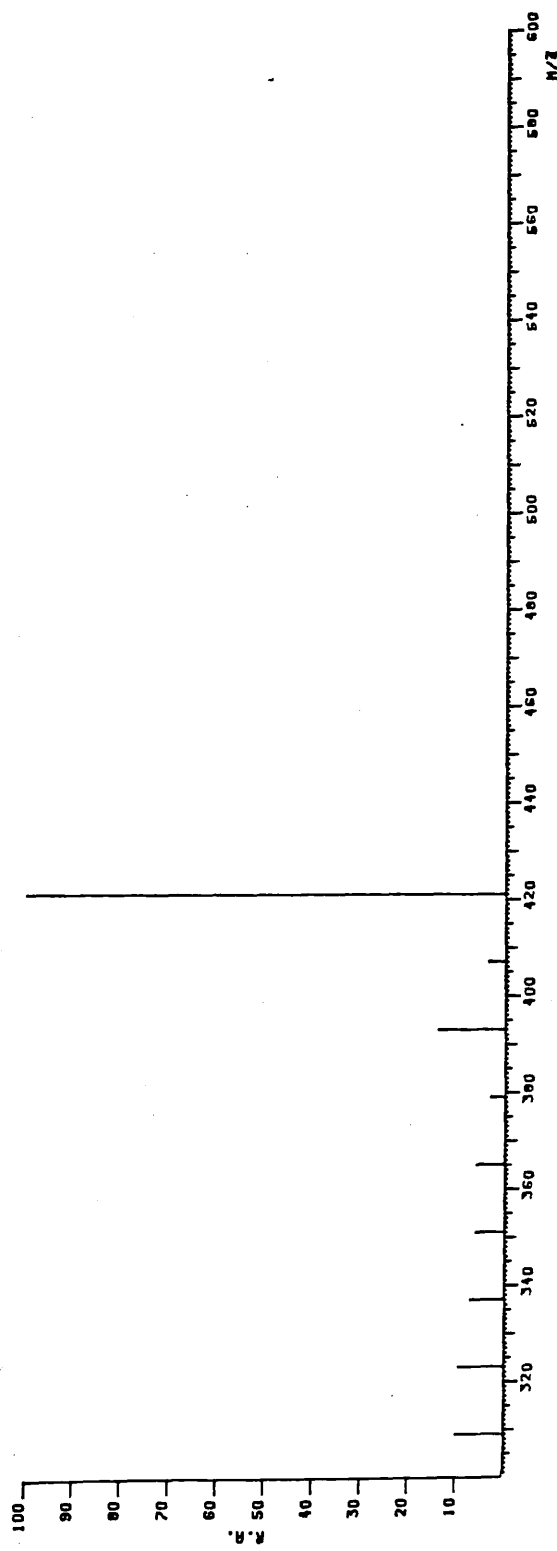
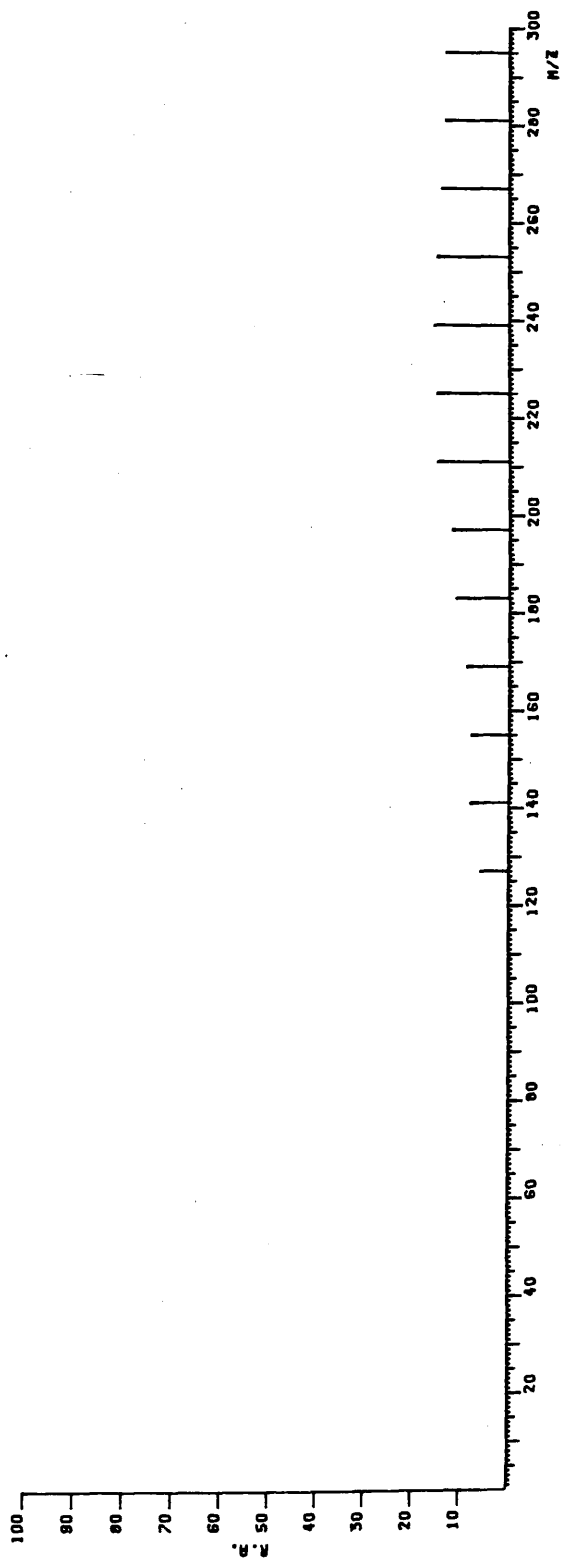


Fig. (3.25) Nitric oxide chemical ionization mass spectra of SHC-22.

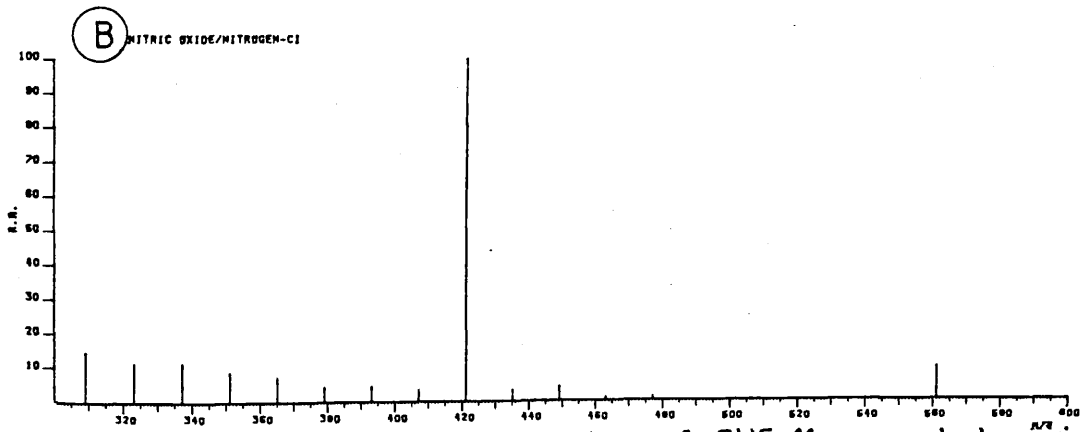
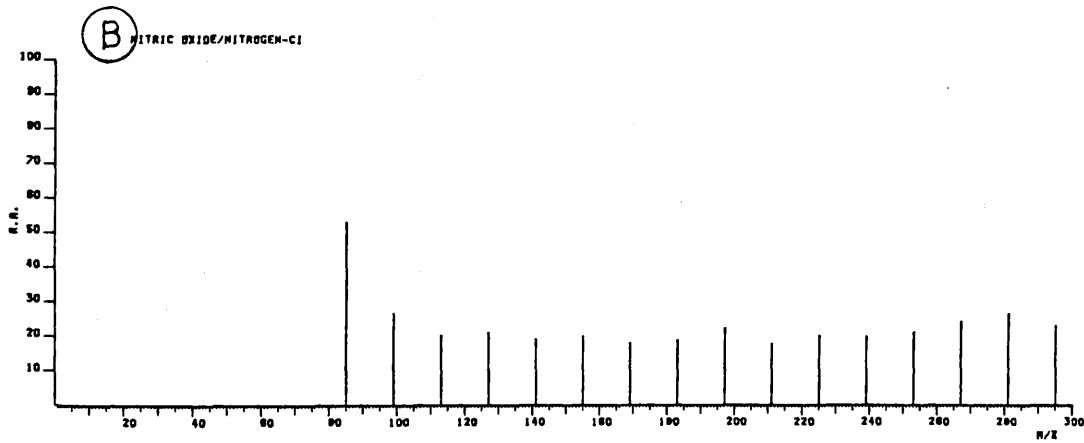
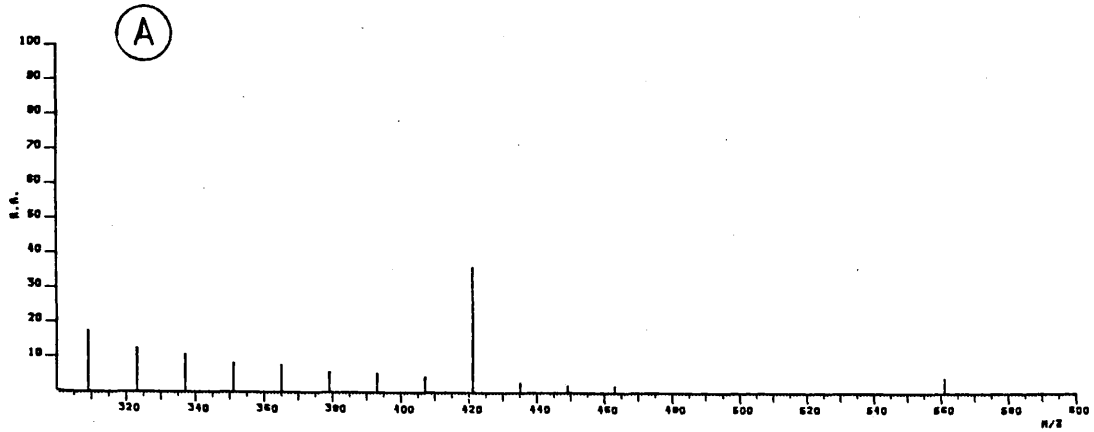
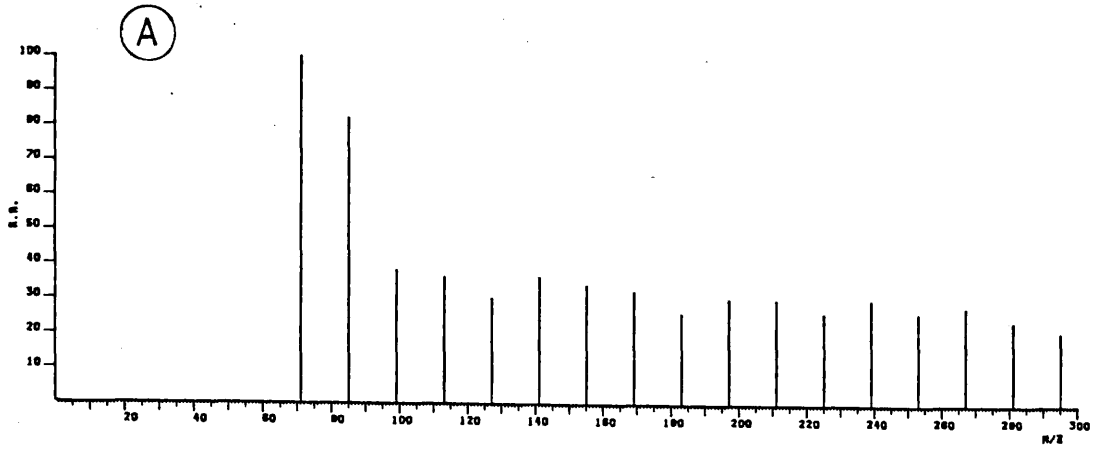


Fig (3.26) Comparison of CI spectra of SHC-11 recorded using (A)Methane reagent gas and (B) Nitrogen/Nitric oxide reagent gas.

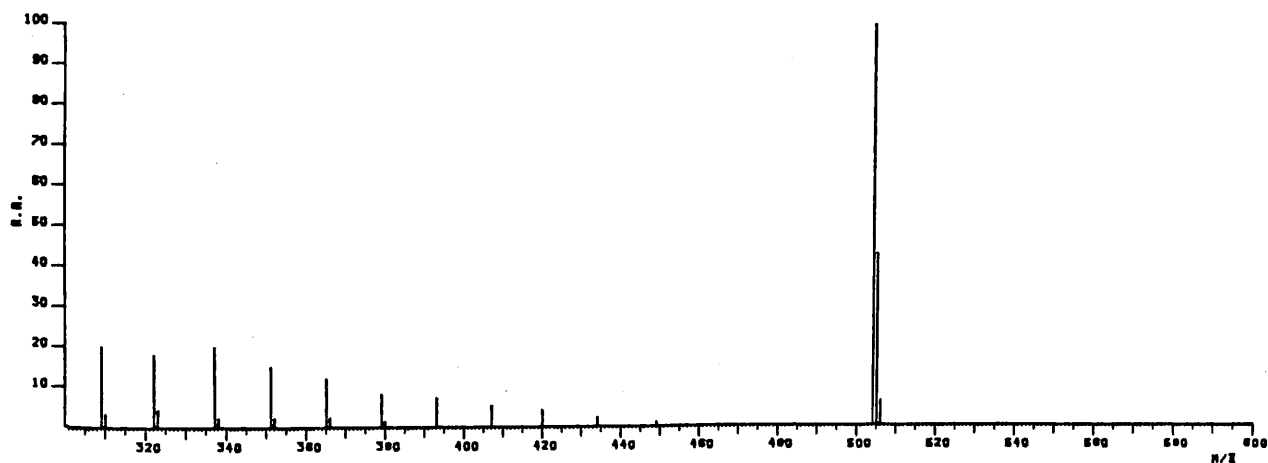
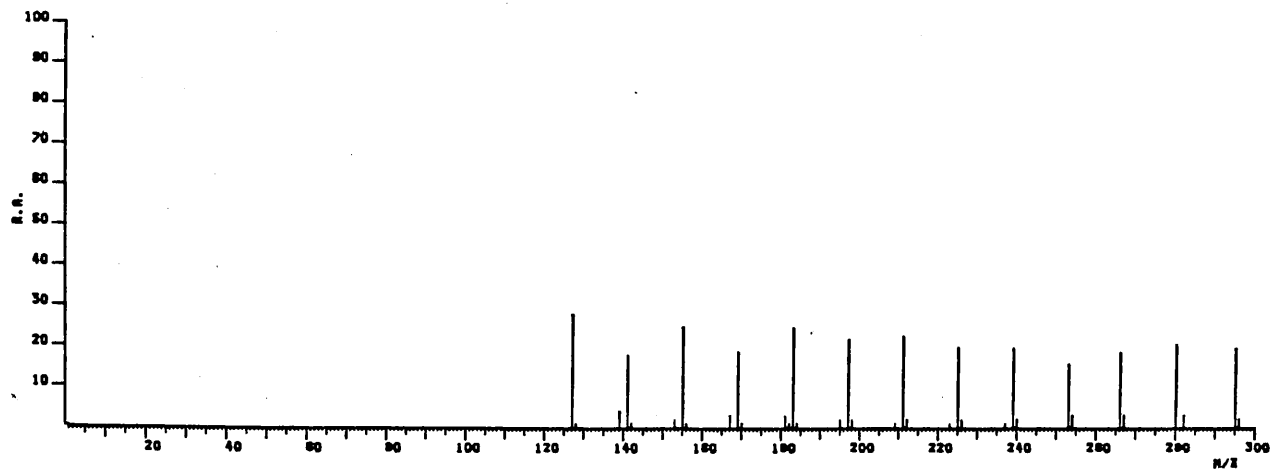
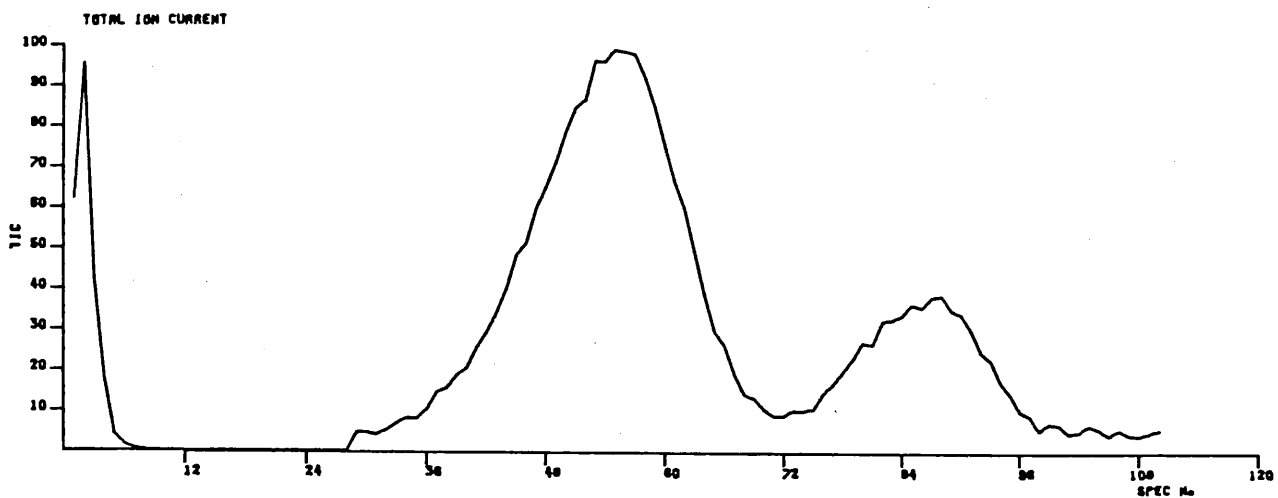


Fig. (3.27) Nitric oxide/nitrogen chemical ionization mass spectrometric analysis of SHC-30.



### 3.2.3 Synthetic aromatic hydrocarbon lubricants

Three representative synthetic aromatic hydrocarbon lubricating fluids, SAH1, SAH2 and SAH3 were initially analysed using fluorobenzene reagent gas. Since fluorobenzene only ionizes aromatic material NO/N<sub>2</sub> chemical ionization spectra were also recorded to detect any non-aromatics. Only SAH1 contained noticeable quantities of non-aromatic compounds, indicated by odd mass ions in the NO/N<sub>2</sub> spectra. The mass and relative abundance of the principal ions observed for each fluid are given in Tables (3.20) and (3.21). The ions are grouped according to the structural assignment described in Section (4.5.3).

**TABLE 3.20** Mass to charge ratios (m/z) of the principal ions observed in the fluorobenzene and NO/N<sub>2</sub> CI mass spectra of the synthetic base oil SAH1

Carbon number	m/z	Structural type *									
		A	R.A.	m/z	B	R.A.	m/z	C	R.A.	m/z	D
20										281 †	3
21										295 †	1
22										309 †	2
23				308		2					
24				322		3					
25				336		3					
26	358		Trace					356		Trace	
27	372		4					370		2	
28	386		12					384		4	
29	400		19					398		5	
30	414		17					412		5	421 4
31	428		6					426		2	
32	442		2								
Total R.A.			60			8				18	4

\* See Scheme (4.4) for structures.

† Only observed when using NO/N<sub>2</sub> reagent gas.

TABLE 3.21 Mass to charge ratios (m/z) of the principal ions observed in the fluorobenzene CI of the synthetic base oil:-

.1 - SAH2.

Carbon number	Structural type *					
	E		F		G	
	m/z	R.A.	m/z	R.A.	m/z	R.A.
18	230	4	236	81	242	5
19			250	Trace		
24	306	3	312	4	318	3
Total R.A.		7		85		8

.2 - SAH3

Structural type *	Carbon number						
	20	21	22	23	27	28	29
H (m/z)	258	272	286	300	348	362	376
Relative abundance R.A.	11	34	35	10	4	3	3

\* See Scheme (4.4) for structures.

3.2.4 Fluorobenzene chemical ionization mass spectrometry of mineral oil lubricant base oils.

Two representative mineral base oils, MIN.1 and MIN.2 were analysed by fluorobenzene chemical ionization mass spectrometry. Spectra were acquired during volatilization of samples by the method described in Section (2.5). It was found that the intensity of ion  $m/z=247$  in the fluorobenzene reagent gas plasma was invariant with the quantity of aromatic sample introduced into the ion source. Therefore the intensity of this ion was monitored, throughout mineral oil volatilization, and spectra normalised to it prior to the summation procedure described in Section (3.2.1.4). The "total mass spectrum" of the oil so obtained for MIN.1, viscosity 5.1 centi stokes at  $100^{\circ}\text{C}$ , is given in Figure (3.28), spectrum A. The height of each line representing the molal abundance of each ion. Since the fluorobenzene chemical ionization results in ionization of only aromatic hydrocarbons and without fragmentation, (see Section (4.4)) each ion, mass  $m$ , in spectrum A represents an aromatic compound of molecular mass  $m$ . Additionally, the relative abundance of each ion represents the relative concentration, (molar percent of total aromatic material), of each component, provided sensitivity towards ionization does not vary between compounds of different structure and molecular mass. See sections (4.4) and (4.5.4).

In order to determine the quantities of

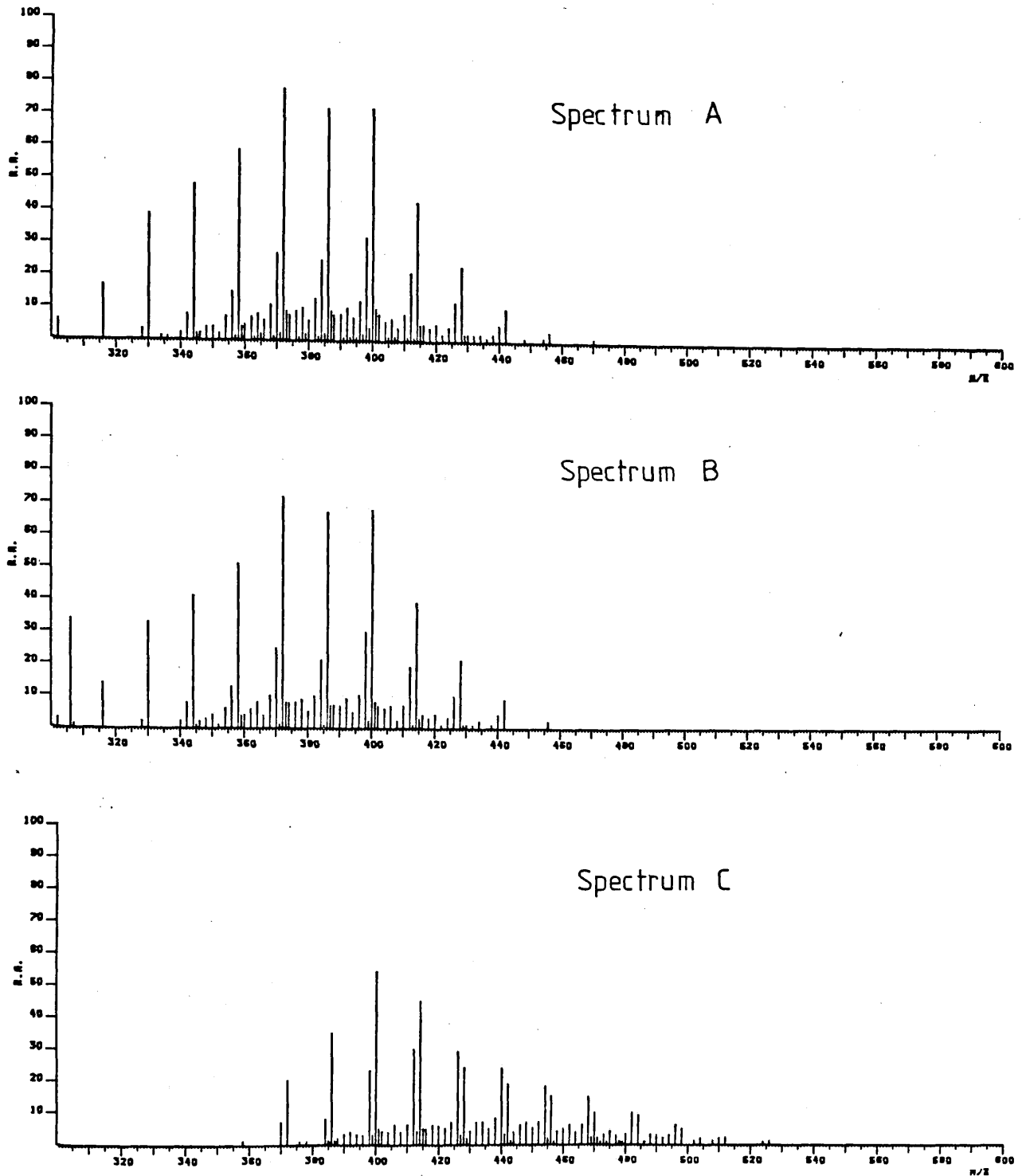


Fig. (3.28) Fluorobenzene chemical ionization mass spectra of mineral oils.

each aromatic component present a known quantity of an internal standard, viz. triphenylbenzene  $m/z=306$ , was added to MIN.1 and the "total mass spectrum" obtained, e.g. spectrum B figure (3.28). Examination of this spectra showed that an ion  $m/z=306$  is the only distinguishing feature from spectrum A, thus demonstrating the excellent reproducibility of successive analyses.

Knowing the quantity of standard added to MIN.1 prior to analysis, i.e. as percent weight (WS), and using equation (3.4.2) the quantity ( $\% \text{ Wt}_m$ ), of aromatic constituents giving an ion mass  $m$ , was readily obtained from its relative abundance ( $\text{R.A.}_m$ ).

$$\% \text{ Wt}_m = \frac{(\text{R.A.}_m/m)}{(\text{R.A.}_{306}/306)} \times \text{WS} \quad (3.4.2)$$

The quantities so obtained, grouped according to compound type, i.e. value of  $z$ , as defined in equation (3.4.3) where C=carbon and H=hydrogen, are recorded in Table (3.22).

$$m = C_n H_{(2n - z)} \quad (3.4.3)$$

Aromatic compounds containing only carbon and hydrogen with  $z = 6, 8, 10, 12, 14, 16$  and  $18$  may be taken to correspond to: alkylbenzenes, cycloalkylbenzenes, dicycloalkylbenzenes, alkylnaphthalenes, cycloalkyl-naphthalenes, dicycloalkylnaphthalenes and alkylanthracenes respectively.

The data obtained from a similar analysis of the higher boiling fluid, MIN2 of viscosity  $7.8$  centi stokes at  $100^\circ\text{C}$  is given in table (3.23) and spectrum C. ( Figure 3.28)). As expected

TABLE 3.22 Weight percent of aromatic components in MIN.1

Carbon number	6	8	10	12	14	16	18	Total
21								
22	0.110							0.110
23	0.450	0.040						0.490
24	1.070	0.085	0.004		0.001	0.002		1.162
25	1.350	0.277	0.074	0.009	0.027	0.030	0.014	1.781
26	1.755	0.450	0.221	0.064	0.149	0.131	0.094	2.864
27	2.597	0.910	0.372	0.150	0.279	0.235	0.142	4.685
28	2.493	0.804	0.400	0.204	0.333	0.308	0.291	4.833
29	2.619	1.143	0.396	0.191	0.347	0.289	0.294	5.279
30	1.564	0.755	0.277	0.112	0.280	0.237	0.314	3.539
31	0.882	0.430	0.150	0.056	0.177	0.154	0.194	2.043
32	0.390	0.176	0.049	0.015	0.089	0.072	0.081	0.872
33	0.103	0.034	0.007	0.002	0.030	0.016	0.012	0.204
34	0.007							0.007
35								
Total	15.390	5.104	1.950	0.803	1.712	1.474	1.436	27.869

TABLE 3.23 Weight percents of aromatic components in MIN.2

Carbon number	z										Total
	6	8	10	12	14	16	18	Total			
26	0.002										0.002
27	0.171	0.004									0.175
28	0.363	0.074			0.003	0.001					0.441
29	0.648	0.236	0.016	0.011	0.023	0.017	0.004				0.955
30	0.589	0.382	0.054	0.034	0.047	0.038	0.026				1.170
31	0.330	0.400	0.084	0.045	0.068	0.059	0.055				1.041
32	0.281	0.337	0.093	0.060	0.079	0.073	0.044				0.967
33	0.216	0.262	0.089	0.059	0.088	0.083	0.041				0.838
34	0.168*	0.207*	0.079	0.048	0.074	0.071	0.043				0.690
35	0.130	0.144	0.062	0.034	0.055	0.053	0.029				0.507
36	0.061	0.076	0.029	0.012	0.046	0.032	0.015				0.271
37	0.024	0.032	0.009	0.002	0.018	0.015	0.005				0.105
38	0.005	0.006	0.001		0.003	0.002					0.017
39											
Total	2.988	2.160	0.516	0.305	0.504	0.444	0.262				7.179

\* z assigned from accurate mass measurement.



the aromatic components in MIN.2 are of higher molecular mass than those in MIN.1. Additionally the chemical composition of the two fluids are markedly different. The major components of MIN.1, at all carbon numbers are the alkylbenzenes, ( $z=6$ ), whereas the cycloalkylbenzenes, ( $z=8$ ), are dominant for carbon number greater than 30 in MIN.2. Interestingly the quantities of cycloalkylnaphthalenes, ( $z=14$ ), are greater than those of alkyl naphthalenes, ( $z=12$ ) in both fluids.

The aromatic content of MIN.1 had previously been determined by the Brandes method,<sup>11</sup> which determines the total weight percent aromatic carbon in a fluid. For comparison weight percents aromatic carbon, present as each component were determined, and are recorded in Table (3.24). The value for total weight percent aromatic carbon of 5.9% so obtained is in good agreement with the value of  $7 \pm 2\%$  obtained by the Brandes method. A similar determination for MIN.2 gave a value of 2.0%, somewhat lower than that of 5% obtained by the Brandes method.

TABLE 3.24 Percent weight aromatic carbon in MIN:1

Carbon number	6	8	10	12 <sup>Z</sup>	14	16	18	Total
21								
22	0.0262							
23	0.1025	0.0092						
24	0.2335	0.0187	0.0009		0.0002	0.0005		
25	0.2826	0.0583	0.0157	0.0019	0.0058	0.0065	0.0030	
26	0.3530	0.0910	0.0449	0.0131	0.0307	0.0271	0.0196	
27	0.5026	0.1771	0.0728	0.0295	0.0552	0.0467	0.0284	
28	0.4650	0.1508	0.0754	0.0387	0.0634	0.0590	0.0560	
29	0.4714	0.2068	0.0720	0.0349	0.0637	0.0534	0.0546	
30	0.2720	0.1319	0.0464	0.0198	0.0497	0.0422	0.0562	
31	0.1484	0.0727	0.0255	0.0096	0.0303	0.0265	0.0336	
32	0.0635	0.0288	0.0081	0.0025	0.0148	0.0120	0.0136	
33	0.0163	0.0054	0.0011	0.0003	0.0026	0.0026	0.0019	
34	0.0011							
35								
Total	2.938	1.6048	0.3628	0.1503	0.3164	0.2765	0.2669	5.9157

#### 4.1 REACTIONS IN HYDROCARBON REAGENT GASES

##### 4.1.1. Iso-Butane

The values obtained for rate coefficients, for reaction of primary ions with iso-butane in this study were generally slightly lower than those obtained in a previous study.<sup>52</sup> Additionally, as indicated by the experiments with methane, the effective mean-ion drift distance is 0.2 cm and as such was used in estimation of residence time for iso-butane primary ions.

Some doubt must be cast on the pressure determination in either this or the previous examinations of the iso-butane plasma in this laboratory. It has already been shown that ion-source iso-butane pressures measured simultaneously by both the Baratron and Texas gauges gave essentially the same reading (see 2.3.3). However it should be noted that the original probe used to couple the Texas gauge to the ion-source was modified prior to the comparison of the two gauge systems. The modification ensured proper penetration of the ion-source cavity by the probe tip (see figure (2.1)) and increased the confidence in the measuring of ion-source pressures. The iso-butane used in this study was dried prior to its introduction to the ion-source to eliminate the possibility of water acting as a third body.<sup>52,116</sup> leading to enhanced rates of reaction. However it seems unlikely that the small quantity of water known to be present in iso-butane (~ 0.1%) would result in any

significant increase in rate coefficients for the reaction of its primary ions. Therefore it seems more plausible that during the earlier measurements there was either poor sealing between the Texas-probe and the ion-source or insufficient penetration of the ion-source cavity by the probe, with the result that the pressure readings consequently were lower than the true ion-source pressure.

Subsequent redetermination of rate coefficients for the reaction of the primary ion  $C_3H_7^+$  with iso-butane, over a period of 1½ years, have shown excellent agreement with the value of  $3.16 \times 10^{-11} \text{ cm}^3 \text{ molec}^{-1} \text{ s}^{-1}$  recorded in table (3.1) and lead to increased confidence in the values of rate coefficients for the other primary ions reported here. Confidence in the reproducibility of these rate coefficients has been used routinely to ascertain whether reconnection of the Baratron gauge to the ion-source had been successfully achieved after periods of removal for either cleaning or mass spectrometry of low volatility materials (see 2.3.2), e.g. lubricating fluids.

#### 4.1.2. Dependence of rate coefficients on ion stability and structure of neutrals.

Cyclohexane<sup>18</sup> has been used as a reagent gas, for preferential ionization of aromatic components in hydrocarbon mixtures, in a photo-ionization mass spectrometer. Initially it was hoped that methylcycloalkane reagent gases would be suitable for use in mass spectrometers where primary ionization is by electron-impact.

Provided the reagent gas plasma consisted of primarily molecular ions then the low ionization potential (IP) of alkylcycloalkanes (viz. methylcyclohexane IP = 9.76eV) would make reaction with alkanes unfavourable. Aromatic compounds whose ionization potentials are less than 9.8eV would be ionized by charge transfer. Thus preferential ionization would be achieved. However, at ion-source pressures of ~0.2 Torr the reagent gas plasmas of methylcyclopentane and methylcyclohexane are not mono-ionic; three ions contribute to ~80% of the total ion-current. Further, the principal ion in each case arises from hydrogen atom loss from the molecular ion. The main reaction channel of such an ion is hydride transfer and accordingly it can ionize both alkanes and cyclo-alkanes. Preferential ionization of aromatic hydrocarbons is thus unobtainable with these reagent gases.

The high abundance of (M-1) ions in the methylcycloalkane plasmas is similar to that observed for isobutane where, above 0.4 Torr,  $C_4H_9^+$  accounts for > 95% of the total ion-current. Additionally the mechanism of formation of these ions is the same, mainly hydride transfer. Since the methylcycloalkanes are more complex molecules it is interesting to compare the rates of reactions of primary ions with different neutral reagents. Such a comparison is given in Table (4.1), from which it is seen that rates of reaction increase with complexity of the neutral and, with a few exceptions (viz.  $C_3H_3^+$  and  $C_4H_5^+$ ), decreases

with the complexity of the reactant ion. The low reactivity of ions  $C_3H_3^+$  and  $C_4H_5^+$  may be ascribed to their possessing the particularly stable cyclopropenium and methylcyclopropenium structures. Such variations in rate coefficient with ion and neutral complexity are in broad agreement with the observations of Field and Meot-Ner<sup>117</sup> for slow ion-molecule reactions. Therefore one may conclude that a similar mechanism operates, viz. that an energy barrier, which is assumed to decrease with increasing exothermicity of reaction, exists between the collision complex  $\{R_1-H \dots R_2\}^+$  and the associated products  $\{R_1 \dots HR_2\}^+$  (see Fig.(4.1)). However it should be remembered that for a true comparison it is necessary to assume that primary ions of similar mass derived from cycloalkanes and iso-butane have similar excess energy. This is unlikely, since those ions generated from alkylcycloalkane precursors may well possess less excess energy since they are the product of more successive fragmentations.

In methylcyclopentane the rate of reaction of  $C_4H_8^+$  ( $m/z = 56$ ) is much larger than that expected from comparison with its rate with methylcyclohexane.

Since the ionization potentials of all  $C_4H_8$  molecules are lower (by  $\sim 0.4$  eV) than that of methylcyclopentane, charge transfer would be endothermic. If its reaction was only feasible by charge transfer, it would be necessary to postulate that  $C_4H_8^+$  was formed in an excited state, i.e. possessing considerable excess

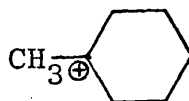
TABLE 4.1

Comparison of the rates of reaction of primary ions of same mass to charge ratio with reagent gases iso-butane, methylcyclopentane, and methylcyclohexane.

Ion	m/z	Rate coefficients $\times 10^{11}/\text{cm}^3 \text{ molec}^{-1} \text{ s}^{-1}$		
		Iso-butane	Methylcyclo- pentane	Methylcyclo- hexane
$\text{C}_2\text{H}_5^+$	27	$16.0 \pm 0.8$	$24.2 \pm 1.3$	$61.1 \pm 6.5$
$\text{C}_2\text{H}_5^+$	29	$13.0 \pm 0.4$	$21.3 \pm 1.1$	$52.5 \pm 5.3$
$\text{C}_3\text{H}_3^+$	39	$0.20 \pm 0.04$	$0.99 \pm 0.08$	$0.43 \pm 0.1$
$\text{C}_3\text{H}_5^+$	41	$6.88 \pm 0.16$	$14.9 \pm 0.5$	$22.2 \pm 1.0$
$\text{C}_3\text{H}_6^+$	42	$7.43 \pm 0.18$	$15.5 \pm 0.9$	$21.4 \pm 2.4$
$\text{C}_3\text{H}_7^+$	43	$3.16 \pm 0.04$	$9.63 \pm 0.29$	$11.7 \pm 0.5$
$\text{C}_4\text{H}_5^+$	53	$1.12 \pm 0.06$	$3.39 \pm 0.27$	not evaluated
$\text{C}_4\text{H}_6^+$	54	not evaluated	$5.78 \pm 0.32$	$7.90 \pm 0.24$
$\text{C}_4\text{H}_7^+$	55	$2.08 \pm 0.08$	$5.43 \pm 0.18$	$9.43 \pm 0.22$
$\text{C}_4\text{H}_8^+$	56	$1.28 \pm 0.04$	$3.14 \pm 0.04$	$3.16 \pm 0.06$

internal energy. However as shown in section (3.1.2.2)  $C_4H_8^{\cdot+}$  may react via a two atom transfer reaction with methylcyclopentane, forming  $C_6H_{10}^{\cdot+}$  ( $m/z = 82$ ). In figure (3.6) it is seen that the decrease in  $C_4H_8^{\cdot+}$  is commensurate with an equal increase in  $C_6H_{10}^{\cdot+}$ . Therefore it seems likely that  $C_4H_8^{\cdot+}$  reacts primarily by the two atom transfer route and that removal of hydrogen from methylcyclopentane is particularly facile.

In the methylcyclohexane plasma the relative abundances of ions  $m/z = 83$  and  $70$  attributed to  $C_6H_{11}^+$  and  $C_5H_{10}^{\cdot+}$  were observed to be invariant with pressure. This behaviour is attributed to their low reactivities. Since the ionization potentials of pentanes are considerably lower than methylcyclohexane, if  $C_5H_{10}^{\cdot+}$  has the pentenyl structure, charge exchange would not be energetically favoured. Whereas if it was cyclopentyl, since the ionization potential of cyclopentane ( $10.34 \text{ eV}$ )<sup>111</sup> is considerably greater than that of methylcyclohexane, charge exchange would be expected. Thus the observed low reactivity may indicate  $C_5H_{10}^{\cdot+}$  to be a pentenyl ion radical. Such a structure would be consistent with the fragmentation pathway postulated (figure (3.10)). If the  $C_6H_{11}^+$  ion exists primarily as a cyclic structure then its hydride affinity would be expected to be similar to that of

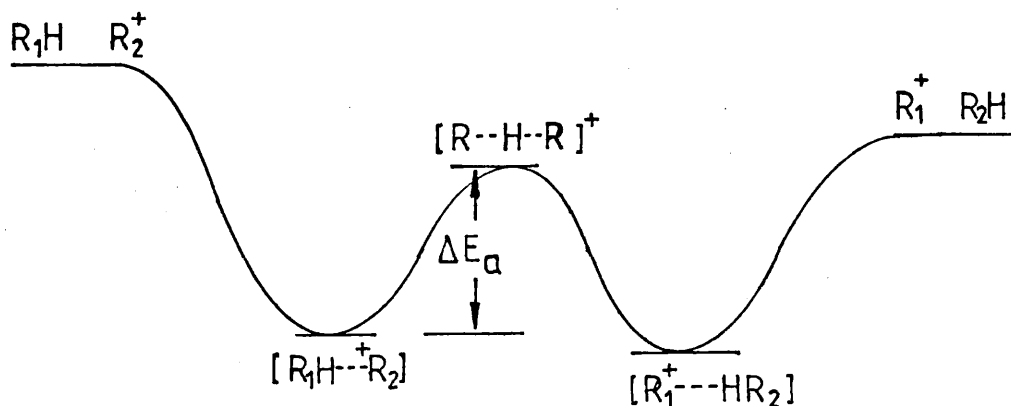




Thus the reaction of  $C_6H_{11}^+$  with methylcyclohexane would be very slow as observed. However if ring opening occurs earlier, then its reaction with methylcyclohexane might reasonably be expected to be faster. Therefore it seems likely that the ion  $m/z=83$  is  $cyclo-C_6H_{11}^+$ .

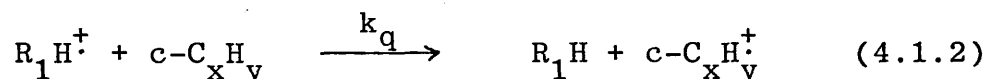
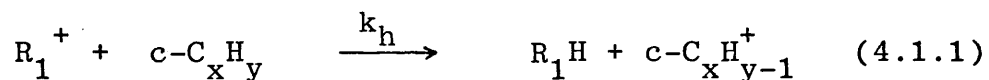
The considerable variation in the relative abundance of ions  $m/z=56$  in methylcyclopentane and  $m/z=55$  in methylcyclohexane prompted the development of a method for estimation of ion-source reagent pressures directly from reagent spectra. The method used was similar to that previously reported for iso-butane<sup>52</sup> and is given below.

FIGURE 4.1      ENERGY PROFILE FOR HYDRIDE TRANSFER  
REACTIONS OF PRIMARY IONS IN ALKYL AND  
CYCLOALKYL REAGENT GASES.



4.1.3 A method of estimation of ion-source pressures for methylcycloalkane reagent gases.

The reactions of primary ions from cycloalkane reagent gases with the neutral reagent may be represented by equations (4.1.1) for hydride transfer and (4.1.2) for charge exchange.



Since these reactions would be expected to obey pseudo first order kinetics the kinetic equations are:

$$\log \left[ \frac{I_{R_1}^o}{I_{R_1}} \right] = -Nk_h \tau_{R_1} P_{c-C_xH_y} \quad (4.1.3)$$

$$\log \left[ \frac{I_{R_1H}^o}{I_{R_1H}} \right] = -NK_q \tau_{R_1H} P_{c-C_xH_y} \quad (4.1.4)$$

where  $N$ ,  $\tau$ ,  $P_{c-C_xH_y}$  are described in Section (3.1.1).

$k_q$  and  $k_h$  are the rate coefficients for charge and hydride exchange as recorded in tables (3.3) and (3.4) for methylcyclopentane and methylcyclohexane. Rearrangement of (4.1.3) and (4.1.4) yields

$$P_{C-C_xH_y} = \log \left[ \frac{I_n^0}{I_n} \right] / N \tau_n k_n \quad (4.1.5)$$

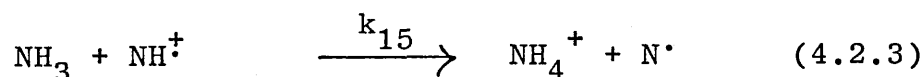
where  $I_n$  and  $I_n^0$  are the relative ion-currents of the reactant ion ( $m/z = n$ ) at pressure  $P$  and  $P < 10^{-5}$  Torr,  $N$  is as given in equation (4.2.29),  $\tau_n$  is the reactant ion residence time as evaluated from equation (3.1.9) and  $k_n$  is the rate coefficient. Thus from measurement of the relative ion-current of a reactant ion, a knowledge of the mean drift distance of ions (see section 3.1.1) and the ion-source temperature, and using values of  $k_n$  and  $I_n^0$  recorded in tables (3.3) and (3.4), the ion-source pressures of the two cycloalkane reagent gases studied may be estimated. For the best results it is recommended that a primary ion whose relative ion-current varies considerably with pressure be used, e.g.  $C_4H_8^+$   $m/z = 56$  for methylcyclopentane and  $C_4H_7^+$   $m/z = 55$  for methylcyclohexane.

4.2 MECHANISMS AND EVALUATION OF DISAPPEARANCE  
RATE COEFFICIENTS FOR REACTIONS OF IONS  
IN THE AMMONIA REAGENT GAS PLASMA.

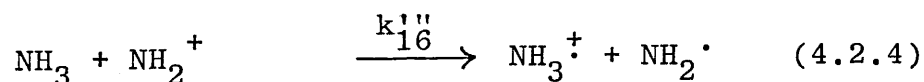
Reactions of primary ions resulting from electron impact ionization of ammonia, leading to the formation of  $\text{NH}_4^+$ , at ion-source pressures less than 0.15 Torr, are discussed in section (4.2.1). The solvation of  $\text{NH}_4^+$  by neutral ammonia observed at pressure in excess of 0.15 Torr is discussed in section (4.2.2).

4.2.1 Reaction of primary ions from ammonia with ammonia.

The primary ions  $\text{NH}_3^+$ ,  $\text{NH}_2^+$  and  $\text{NH}^+$  ( $m/z = 17$ , 16 and 15) react by proton transfer with ammonia to form  $\text{NH}_4^+$



Additionally some  $\text{NH}_2^+$  may react by charge transfer as shown in 4.2.4.



Provided the proportion of  $\text{NH}_4^+$  formed by reaction of the secondary  $\text{NH}_3^+$ , generated from reaction of  $\text{NH}_2^+$  with ammonia (reaction 4.2.4), is small compared to that produced from the molecular ion  $\text{NH}_3^+$  resulting from electron

impact of ammonia (viz. at low ion-source pressures and short ion-residence times) the rate equation for disappearance of  $\text{NH}_3^+$  is

$$-d \frac{[\text{NH}_3^+]}{dt} = k_{17}' [\text{NH}_3][\text{NH}_3^+] \quad (4.2.5)$$

Hence applying pseudo first order kinetics and taking the relative ion-current ( $I_{17}/\Sigma I$ ) recorded in the mass spectrum to truly reflect the ion abundance in the source

$$\log(I_{17}/\Sigma I) - \log(I_{17}^0/\Sigma I^0) = -k_{17}' N_{\text{NH}_3} \tau_{17} \quad (4.2.6)$$

and the rate coefficient  $k_{17}'$  may be evaluated provided the ion-source residence time of  $\text{NH}_3^+$ , ( $\tau_{17}$ ) can be estimated. Since the ion-source ammonia pressure is low and the ion and neutral are both small in size it is reasonable to assume that ion mobility will be little affected by collisions and hence the free fall formula (equation (3.1.5)) may be used for estimation of  $\tau_{17}$ . Accordingly  $\tau_{17}$  is then independent of pressure and a straight line should be obtained for a plot of logs of relative ion-current against pressure. A plot for data obtained at  $7.5 \text{ V cm}^{-1}$  ion-source field strength is given in figure (3.16). Disappearance rate coefficients calculated from the gradients of such lines are recorded in table (4.2). Additionally values of  $P_c^{17}$ , the ion-source pressure for which values of  $\tau_{17}$  estimated by both free fall and ion-mobility assumptions are equivalent,

$p_a^{17}$  the pressure above which plots of  $\log (I_{17}/\Sigma I)$  against pressure ceases to be linear, and  $p_e^{17}$  the pressure above which  $\log (I_{17}/\Sigma I)$  is essentially invariant are tabulated. Equations similar to (4.2.6) may be derived for reaction of  $\text{NH}_2^+$  and  $\text{NH}^+$ , and values of  $k_n^+$ ,  $p_a^n$  and  $p_e^n$ , for ions of  $m/z = n$ , are given in table (4.3) for  $n = 16$  and table (4.4) for  $n = 15$ .

The rate of disappearance of  $\text{NH}_2^+$  is the sum of the rates of reactions (4.2.2) and (4.2.4). Hence

$$-d \frac{[\text{NH}_2^+]}{dt} = k_{16}'' [\text{NH}_3] [\text{NH}_2^+] + k_{16}''' [\text{NH}_3] [\text{NH}_2^+]$$

or

$$-d \frac{[\text{NH}_2^+]}{dt} = k_{16}' [\text{NH}_3] [\text{NH}_2^+]$$

where

$$k_{16}' = k_{16}'' + k_{16}''' \quad (4.2.7)$$

The disappearance rate coefficient  $k_{16}'$  estimated from the gradient of the plot in figure (3.1.6) is a composite rate-coefficient, values of  $k_{16}''$  for reaction by proton transfer and  $k_{16}'''$  for reaction via charge transfer not being separately evaluated. Values of  $k_{16}''$  and  $k_{16}'''$  have been determined by ICR experiments and are recorded in the literature. Care must be exercised when comparing these values with those recorded for  $k_{16}'$ .

Examination of the values of  $k_{17}'$ ,  $k_{16}'$  and

TABLE 4.2  
Reaction of  $\text{NH}_3^+$  with ammonia

Ion-source field strength $/V \text{ cm}^{-1}$	Rate coefficient $k_{17}^1 \times 10^{+10}$ $/\text{cm}^3 \text{ molec}^{-1} \text{ s}^{-1}$	$P_{17}^R / \text{Torr}$	$P_C^{17} / \text{Torr}$	$P_a^{17} / \text{Torr}$	$P_e^{17} / \text{Torr}$
2.5	$15.8 \pm 1.8$	$0.01-0.05$	0.041	0.05	0.08
5.0	$17.2 \pm 1.0$	$0.01-0.07$	0.058	0.08	0.13
7.5	$17.9 \pm 1.0$	$0.01-0.09$	0.071	0.09	0.16
10.0	$19.4 \pm 0.2$	$0.01-0.1$	0.082	0.10	0.20
12.5	$19.4 \pm 0.4$	$0.01-0.10$	0.092	0.10	0.21

TABLE 4.3

Reaction of  $\text{NH}_2^+$  with ammonia

Ion-source field strength /V $\text{cm}^{-1}$	Rate coefficient $k_{16} \times 10^{10}$ /cm <sup>3</sup> molec <sup>-1</sup> s <sup>-1</sup>	$P_{16}^R$ /Torr	$P_c^{16}$ /Torr	$P_a^{16}$ /Torr	$P_e^{16}$ /Torr
2.5	20.3 ± 1.4	0.01-0.05	0.042	0.05	0.12
5.0	24.2 ± 1.0	0.01-0.09	0.059	0.09	0.15
7.5	26.3 ± 0.9	0.01-0.12	0.072	0.12	0.18
10.0	27.1 ± 1.1	0.01-0.11	0.083	0.11	0.22
12.5	28.6 ± 1.2	0.01-0.15	0.093	0.15	0.25



TABLE 4.4

Reaction with  $\text{NH}_4^+$  with ammonia

Ion-source field strength $/\text{V cm}^{-1}$	Rate coefficient $k_{15} \times 10^{10}$ $/\text{cm}^3 \text{ molec}^{-1} \text{ s}^{-1}$	$P_{15}^R/\text{Torr}$	$P_C^{15}/\text{Torr}$	$P_a^{15}/\text{Torr}$
2.5	$18.1 \pm 1.3$	0.01-0.041	0.041	0.04
5.0	$21.6 \pm 0.5$	0.01-0.06	0.057	0.06
7.5	$25.9 \pm 0.6$	0.01-0.06	0.070	0.06
10.0	$26.0 \pm 0.9$	0.01-0.07	0.081	0.07
12.5	$26.1 \pm 0.9$	0.01-0.07	0.091	0.07

$k'_n$  (tables (4.2), (4.3) and (4.4)) indicates a dependence of rate coefficient upon ion-source field strength. Larger values of  $k'_n$  are obtained with higher field strengths. Since rate coefficients of ion-molecule reactions should ideally be determined in the absence of electric fields (see section (1.2)) it is desirable to estimate values of  $k'_n$  at zero field strength. Fortunately, as seen in figure (4.2), variation of  $k'_{17}$  and  $k'_{16}$  with ion-source field strength (E) was essentially linear and values of  $k_{17}$  and  $k_{16}$ , the rate coefficient at zero field strength,<sup>†</sup> were obtained by curve fitting, using a weighted least squares method, to equations (4.2.8) and (4.2.9) respectively.

$$k'_{17} = k_{17} + f_{17}E \quad (4.2.8)$$

$$k'_{16} = k_{16} + f_{16}E \quad (4.2.9)$$

The values of  $(14.2 \pm 0.8) \times 10^{-10} \text{ cm}^3 \text{ molec}^{-1} \text{ s}^{-1}$  and  $(21.8 \pm 1.8) \times 10^{-10} \text{ cm}^3 \text{ molec}^{-1} \text{ s}^{-1}$  obtained for  $k_{17}$  and  $k_{16}$  respectively are in excellent agreement with those of  $(15.5 \pm 0.8) \times 10^{-10} \text{ cm}^3 \text{ molec}^{-1} \text{ s}^{-1}$  and  $(24.2 \pm 2.0) \times 10^{-10} \text{ cm}^3 \text{ molec}^{-1} \text{ s}^{-1}$  obtained by Huntress and Pirizzotto<sup>118</sup> in an ion cyclotron resonance (ICR) experiment. Such rate coefficients are determined almost in the absence of electric fields. It should be noted that in the current study no variation in  $\log(\ln/\Sigma I^0)$  was observed

---

<sup>†</sup> This statement is not absolutely true since many factors other than field strength affect values of rate coefficients. See section (1.2).

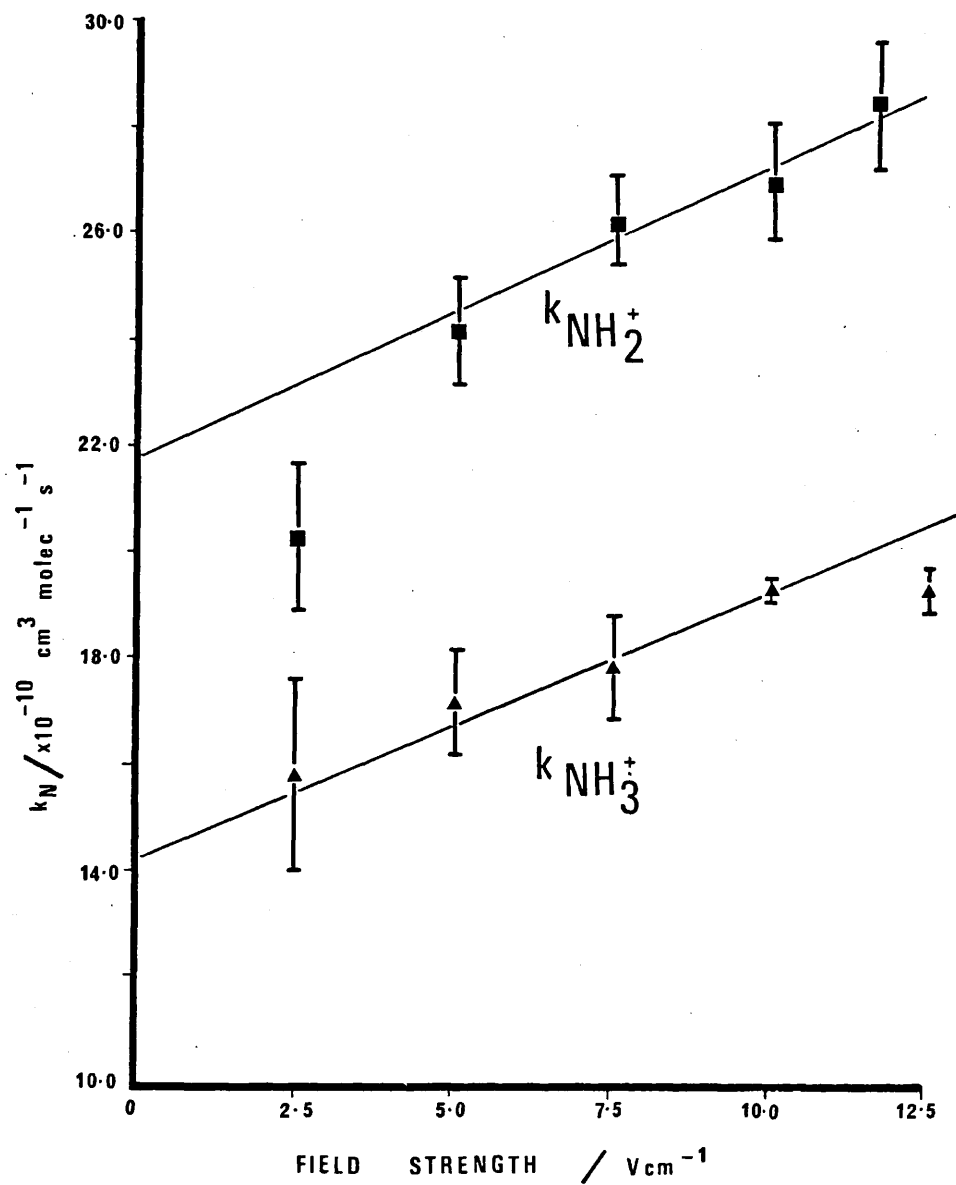
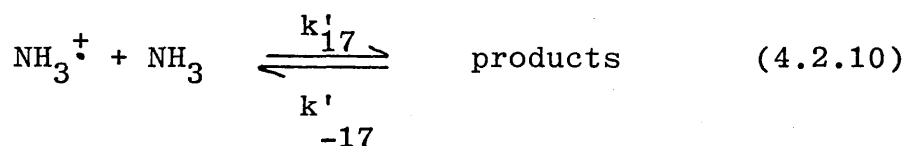


Fig. (4.2)

Variation in rates of reaction of primary ions from ammonia with ammonia as a function of ion-source field strength.

with changes in field strength. Values of  $(5.2 \pm 1.6) \times 10^{-11}$  and  $(5.6 \pm 2.0) \times 10^{-11} \text{ cm}^4 \text{ V}^{-1} \text{ molec}^{-1} \text{ s}^{-1}$  were obtained for  $f_{17}$  and  $f_{16}$  respectively.

It was observed (see section (3.1.2.4) that plots of  $\log (I_n/\Sigma I)$  against pressure, for ions  $\text{NH}_3^+$ ,  $m/z = 17$ , and  $\text{NH}_2^+$ ,  $m/z = 16$ , ceased to be linear at pressure greater than  $P_a$  Torr and that the relative ion-currents ( $I_n/\Sigma I$ ) remained essentially constant for pressures in excess of  $P_e$  Torr. If some back reaction were taking place then the constancy of  $I_n/\Sigma I$  at pressure above  $P_e$  Torr may be attributable to attainment of equilibrium, e.g.



The kinetics of the approach to equilibrium taking place in the pressure range  $0.01 - P_e^{17}$  Torr are described by equation (4.2.11) where  $a_e$ ,  $a$  and  $a_o$  are the equilibrium concentration, instantaneous concentration at time  $t$  and concentration in the absence of reaction of  $\text{NH}_3^+$ .

$$(k'_{17} + k'_{-17}) = \frac{1}{t[\text{NH}_3]} \ln \left[ \frac{(a_o - a_e)}{(a - a_e)} \right] \quad (4.2.11)$$

hence for  $a_o = I_{17}^o/\Sigma I^o$ ,  $a = I_{17}/\Sigma I$  and  $a_e = I_{17}^e/\Sigma I^e$ , the relative ion current at pressure  $P_e^{17}$ ,

$$\log \left[ \frac{I_{17}}{\Sigma I} - \frac{I_{17}^e}{\Sigma I^e} \right] = - (k'_{17} + k'_{-17}) N \tau_{17} P_{NH_3} - \log \frac{I_{17}^o}{\Sigma I^o} - \frac{I_{17}^e}{\Sigma I^e} \quad (4.2.12)$$

$(k'_{17} + k'_{-17})$  the composite rate coefficient for forward

and reverse reactions may be obtained from a plot of

$\log \left[ \frac{I_{17}}{\Sigma I} - \frac{I_{17}^e}{\Sigma I^e} \right]$  against pressure. Such a

plot for reaction of  $NH_3^+$  at an ion-source field strength of  $7.5 \text{ V cm}^{-1}$  is given in figure (4.3) and is linear

throughout the pressure range  $0.01 - P_e^{17}$ . A similar

equation to (4.2.12) may be derived for reaction of  $NH_2^+$ ,

$m/z = 16$ . Values of  $(k'_{17} + k'_{-17})$  and  $(k'_{16} + k'_{-16})$  are

given in tables (4.5) and (4.6). These composite rate coefficients show the same dependence upon field strength as previously observed for  $k'_{17}$  and  $k'_{16}$ . Hence values of  $1.6 \times 10^{-10} \text{ cm}^3 \text{ molec}^{-1} \text{ s}^{-1}$  and  $0.7 \times 10^{-10} \text{ cm}^3 \text{ molec}^{-1} \text{ s}^{-1}$  were obtained for  $k_{16}$  and  $k_{17}$  the rate coefficients for back reactions at zero field strength. The small values of rate coefficients of the back reaction, an order of magnitude less than those for forward reaction, implies that only at high product and low reactant concentrations will the reactant concentration be significantly affected by that formed in back reactions. This is in agreement with the observed departure from linearity in plots of  $\log (I_n/\Sigma I)$  slightly below  $P_e$ .

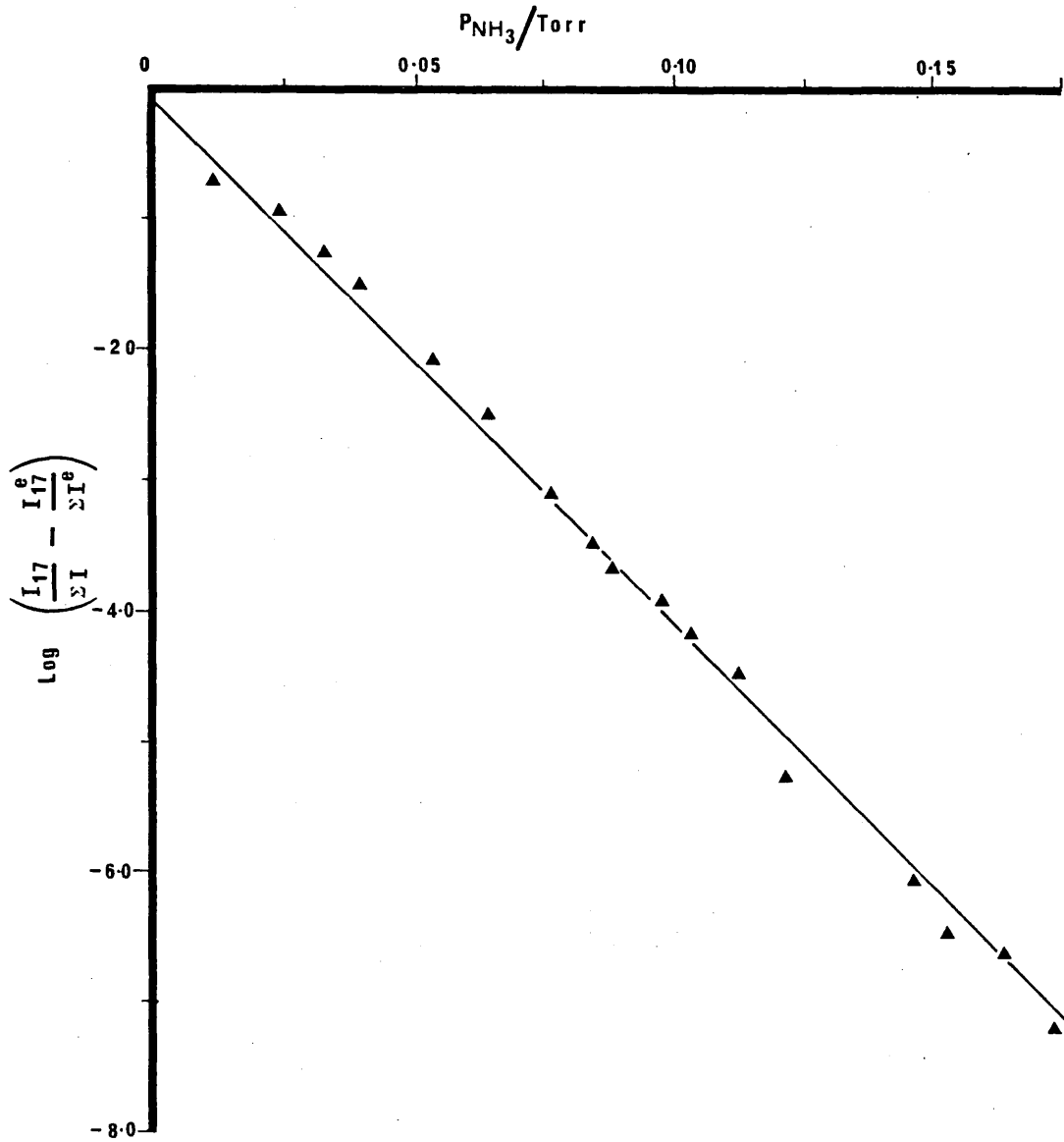


FIG. (4.3)

Semi-equilibrium plot for reaction of primary ion  $NH_3^+$  with ammonia.

TABLE 4.5

Variation of  $k'_{17} + k'_{-17}$  with ion-source field strength

Ion-source field strength /V cm <sup>-1</sup>	$10^{10}(k'_{17} + k'_{-17})$ /cm <sup>3</sup> molec <sup>-1</sup> s <sup>-1</sup>
2.5	16.5 ± 0.8
5.0	17.8 ± 0.7
7.5	19.9 ± 0.5
10.0	20.5 ± 0.3
12.5	21.9 ± 0.5

TABLE 4.6

Variation of  $(k'_{16} + k'_{-16})$  with ion-source field strength

Ion-source field strength /V cm <sup>-1</sup>	$10^{10}(k'_{16} + k'_{-16})$ /cm <sup>3</sup> molec <sup>-1</sup> s <sup>-1</sup>
2.5	24.0 ± 1.6
5.0	25.6 ± 0.9
7.5	26.8 ± 1.4
10.0	28.4 ± 1.1
12.5	30.0 ± 1.0

The proton and charge transfer reactions of  $\text{NH}_3^+$  and  $\text{NH}_2^+$  with ammonia may be designated as fast ion-molecule reactions since their rate coefficients are of the order  $10^{-9} \text{ cm}^3 \text{ molec}^{-1} \text{ s}^{-1}$ .<sup>56</sup> For such reactions the rate coefficient may be equated with the collision capture rate  $k_c$ . Since ammonia is polar, possessing a permanent dipole,  $k_c$  can be calculated from equation (4.2.13) which has been derived from the average dipole orientation (ADO) theory of Su and Bowers.<sup>45</sup>

$$k_c = \frac{2 \pi q}{\mu v} \left[ \frac{\alpha}{\mu v^2} + c \mu_D \frac{1}{\mu v} \right] \quad (4.2.13)$$

$q$  is the charge on the reactant ion,  $\mu$  the reduced mass of the ion and neutral,  $\alpha$  and  $\mu_D$  the polarizability and dipole moment of the neutral. The mean drift velocity,  $v$ , of the ion is estimated using the free fall formula equation (3.1.5) and  $c$  is a "locking constant"<sup>119</sup> which depends on the degree that the dipole is aligned with the ionic charge during collision. Equation (4.2.13) indicates that  $k_c$  should show little, but if any, negative ( $v^{-1}$ ) dependence on drift velocity. In equation (4.2.14),  $d$  is the mean distance travelled by the reactant ions prior to their collision with ammonia, and in equation (4.2.13) it is seen that little variation in collision capture and thus rate coefficient is expected with change in ion-source field strength ( $E$ ).



$$v = d \left( \frac{z E}{2md} \right)^{\frac{1}{2}} \quad (4.2.14)$$

The observed variations in  $k_{16}$  and  $k_{17}$  with ion-source field strength are therefore contrary to that predicted by theory.

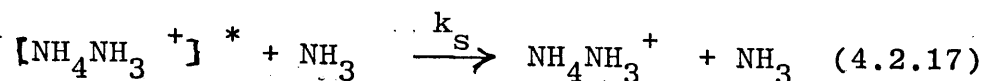
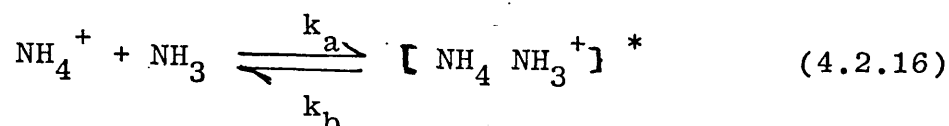
Meisels, Polley and Illies<sup>120</sup> have shown that ion-mobilities in ammonia are lower than expected from simple consideration of ion-dipole interactions. This reduction in mobility results in an increased residence time ( $\tau$ ) which can be accounted for by a change in the dependence of  $\tau$  upon field strength as shown in equation (4.2.15)

$$\tau = \left( \frac{2 md}{z} \right)^{\frac{1}{2}} E^{-r} \quad (4.2.15)$$

where  $r < \frac{1}{2}$ . It is not possible to evaluate  $r$  since  $d$ , the mean distance travelled by an ion before exiting from the source, may also vary with field strength. However it is sufficient to say that the "free-fall" equation (3.1.5) does not appear to be adequate in estimation of the residence times of the ions  $\text{NH}_3^+$  and  $\text{NH}_2^+$ .

#### 4.2.2 Reaction of $\text{NH}_4^+$ with ammonia.

The association reaction of  $\text{NH}_4^+$  with ammonia is assumed to proceed via the energy transfer mechanism (see section (1.2)) as given in equations (4.2.16) and (4.2.17)



where ammonia acts as the third body. Thus assuming the collision complex,  $[\text{NH}_4\text{NH}_3^+]^*$ , to be short lived and applying Bodenstein's steady state hypothesis the rate of disappearance of  $\text{NH}_4^+$  is given by

$$-d \frac{[\text{NH}_4^+]}{dt} = \frac{k_a k_s [\text{NH}_4^+] [\text{NH}_3]^2}{k_b + k_s [\text{NH}_3]} \quad (4.2.18)$$

Integration of this equation gives

$$-\log \frac{[\text{NH}_4^+]}{[\text{NH}_4^+]_0} = \frac{k_a k_s \tau [\text{NH}_3]^2}{k_b + k_s [\text{NH}_3]} \quad (4.2.19)$$

in which  $\tau$  is the ion-source residence time of  $\text{NH}_4^+$  and  $[\text{NH}_4^+]_0$ , the hypothetical abundance of  $\text{NH}_4^+$ , in the absence of reaction with  $\text{NH}_3$ . Since  $\text{NH}_4^+$  is continually produced from the reactions discussed in section (2.2.1),  $[\text{NH}_4^+]_0$  is inaccessible by experimental means. In order that the rate of disappearance of  $\text{NH}_4^+$  is not affected by rates of its formation, these should be at least an order of magnitude faster. As will be seen later this assumption was correct.

Equation (4.2.19) may be rewritten as

$$\log (I_{18}/\Sigma I) = -k_f \tau_{18} [\text{NH}_3] + \log (I_{18}^0/\Sigma I) \quad (4.2.20)$$

where  $k_f$  is the rate coefficient for the forward reaction to products. From equation (4.2.19) and (4.2.20)

$$k_f = \frac{k_a k_s [\text{NH}_3]}{k_b + k_s [\text{NH}_3]} \quad (4.2.21)$$

If the rate of dissociation of  $[\text{NH}_4^+ \text{NH}_3]^*$  is significantly greater than that of its stabilisation (i.e.  $k_b \gg k_s [\text{NH}_3]$ ) then  $k_f = k_a k_s [\text{NH}_3] / k_b$  and the reaction should display third order kinetics. Such behaviour was observed as curvature in the plots of  $\log(I_{18}/\Sigma I)$  against  $P_{\text{NH}_3}^2$ , (see figure (3.17), when the probability of a stabilising collision prior to dissociation was low, as a consequence of a low pressure and short ion-source residue times (i.e. high field strength)). Conversely when the probability of collisional stabilisation of  $[\text{NH}_4^+ \text{NH}_3]^*$  is high  $k_s [\text{NH}_3] \gg k_b$  (viz high pressures, and longer ion-residence times)  $k_f$  becomes equal to  $k_a$  and the overall kinetics are second order. Since the residence time of  $\text{NH}_4^+$  is dependent on ion-mobility,  $\tau_{18}$  will depend on pressure and equation (4.2.19) becomes

$$\log(I_{18}/\Sigma I) = - \frac{k_a k_s^\beta \tau_{18}^3 P_{\text{NH}_3}^3 N^2}{k_b + k_s P_{\text{NH}_3} N} + \log(I_{18}^0/\Sigma I) \quad (4.2.22)$$

where  $N$  is as previously described and

$$\beta_{18} = \frac{273 d}{K_o 760 ET} \quad (4.2.23)$$

If the energy transfer mechanism is obeyed for the reaction of  $\text{NH}_4^+$  with ammonia the plots of  $\log(I_{18}/\Sigma I)$  against  $P_{\text{NH}_3}^2$

should be curved at low pressure and high field strength and linear at high pressure and low field strength. The data obtained in the current study was in agreement with that expected. See figure (3.17).

In equation (4.2.23)  $d$ ,  $E$  and  $T$  are as previously defined and  $K_0$  is the reduced mobility of  $\text{NH}_4^+$  in ammonia ( $\text{cm}^2 \text{V}^{-1} \text{s}^{-1}$ ).  $K_0$  is readily obtained from ion drift theory and given by

$$K_0 = 13.876 / (\alpha \mu)^{\frac{1}{2}} \quad (4.2.24)$$

where  $\alpha$  is the angle averaged polarizability of ammonia ( $\text{\AA}^3$ ) and  $\mu$  the reduced mass of the ion-molecule pair in a.m.u. Using equation (4.2.24) a reduced mobility of  $K_0 = 3.12 \text{ cm}^2 \text{V}^{-1} \text{s}^{-1}$  is obtained for  $\text{NH}_4^+$  moving in  $\text{NH}_3$ , hereafter referred to as the reduced mobility at the "polarizability limit". However recent studies of ion-mobilities in a chemical ionization mass spectrometer ion-source by Polley, Illies and Meisels<sup>120</sup> yielded an experimental value of  $K_0 = (1.29 \pm 0.04) \text{ cm}^2 \text{V}^{-1} \text{s}^{-1}$ . Normally the "polarizability limit" value of  $K_0$  compares well with experimentally obtained values. Polley et al ascribed their lower experimental value to clustering reactions in ammonia reducing the ion-mobility. Since ion-residence times are not readily determined in the instrument used in the current studies, but are estimated from ion-mobilities, use of the correct value of  $K_0$  when

evaluating  $\beta_{18}$ , (equations (4.2.22) and (4.2.23)), and subsequently  $k_f$ , (equations (4.2.21) and (4.2.22)) is vital. The large differences in rate constant obtained using each value of  $K_0$  are illustrated in table (4.7). Since the experimental value of  $K_0$ , was determined in a chemical ionization mass spectrometer it is assumed to be the more correct so the rate coefficients were calculated using a value of  $1.29 \text{ cm}^2 \text{V}^{-1} \text{ s}^{-1}$ .

At high pressures and low field strengths when the reaction of  $\text{NH}_4^+$  with ammonia becomes second order, the second order rate coefficient,  ${}^2k_f$ , is readily obtained from a plot of  $\log(I_{18}/I)$  against  $P_{\text{NH}_3}^2$ . Values obtained for  ${}^2k_f$ , table (4.7), were observed to vary considerably with ion-source electric field strength. The variation is similar to that observed for rates of reaction of  $\text{NH}_3^+$  and  $\text{NH}_2^+$  with ammonia, namely a near linear increase in reaction rate with field strength. Since  ${}^2k_f$  may be equated with  $k_a$ , (the collision rate of  $\text{NH}_4^+$  with  $\text{NH}_3$ , which according to ADO theory is not expected to vary greatly with field strength, see section (4.2.1)), the observed variation is contrary to current theory. If the rate coefficient is indeed independent of field strength then the observed variation may result from the estimated values of ion-source residence times being too low. Clearly this indicates that the mobility of ions in ammonia under the influence of electric fields warrants further study, since the

theory currently available is inadequate.

At lower pressures and higher field strength third order kinetics are obeyed and plots of  $\log(I_{18}/\Sigma I)$  against  $P_{\text{NH}_3}^3$  were linear, facilitating determination of  ${}^3k_f$ , the third order rate coefficient for forward reaction. The values obtained are recorded in table (4.7) and clearly vary little with field strength. This probably results from more correct estimations of ion residence time being obtained at the lower pressures at which third order kinetics are observed. The mean value of  $7.9 \times 10^{-28} \text{ cm}^6 \text{ molecule}^{-2} \text{ s}^{-1}$  will be used in comparison with literature values.

Unfortunately few determinations of  ${}^2k_f$  and  ${}^3k_f$  are reported in the literature, most workers having measured only equilibrium constants. The two most complete studies are those by Meot-Ner and Field,<sup>55</sup> and Bowers et al.<sup>73</sup> In the earlier study Meot-Ner and Field noted that not only both  ${}^2k_f$  and  ${}^3k_f$  varied with temperature but also that the temperature coefficients of these rate coefficients vary with temperature. This makes comparison of the current data, obtained at 450K, with their results, obtained at 350K, difficult. However they have determined a temperature dependence of  $T^{-3.2}$  for their data at 375K. Using this, approximate values of  $1.3 \times 10^{-11} \text{ cm}^3 \text{ molecule}^{-1} \text{ s}^{-1}$  and  $5.7 \times 10^{-28} \text{ cm}^6 \text{ molecule}^{-2} \text{ s}^{-1}$  may be estimated for  ${}^2k_f$  and  ${}^3k_f$  respectively at 450K. The agreement with the value of

$7.9 \times 10^{-28} \text{ cm}^6 \text{ molecule}^{-2} \text{ s}^{-1}$  obtained for  ${}^3k_f$  in the current study is amazingly good, particularly considering that methane was used as the third body in the study by Meot-Ner and Field.<sup>55</sup> The value of  $6.4 \times 10^{-27} \text{ cm}^6 \text{ molecule}^{-2} \text{ s}^{-1}$  at 302K obtained in the more recent low pressure ( $1 \times 10^{-4} - 3 \times 10^{-3} \text{ Torr}$ ) ICR experiment by Bowers et al.<sup>73</sup> may be compared with a value of  $3 \times 10^{-27} \text{ cm}^6 \text{ molecule}^{-2} \text{ s}^{-1}$  at this temperature estimated from the data of Meot-Ner and Field.<sup>55</sup> Since the study by Bowers et al.<sup>73</sup> was carried out in pure ammonia where  $\text{NH}_3$  acts as the third body it could suggest that  $\text{NH}_3$  is a better third body than  $\text{CH}_4$ . The value of  ${}^3k_f$  obtained in the current study which is less than that obtained by Meot-Ner and Field<sup>55</sup> is thus not in general agreement with the result of Bowers et al.<sup>73</sup>

The values for  ${}^2k_f$  obtained at 450K and  $12.5 \text{ V cm}^{-1}$  and  $10 \text{ V cm}^{-1}$  in the current study are near to the value of  $1.3 \times 10^{-11} \text{ cm}^3 \text{ molecule}^{-1} \text{ s}^{-1}$  obtained by Meot-Ner and Field.<sup>55</sup> However the values obtained at low field strength which are probably nearer the true value are almost an order of magnitude slower, e.g.  ${}^2k_f = 2.43 \times 10^{-12} \text{ cm}^3 \text{ molecule}^{-1} \text{ s}^{-1}$  at  $2.5 \text{ V cm}^{-1}$ . This suggests that the reaction efficiency in the current study was lower, i.e. a larger proportion of  $[\text{NH}_4^+ \text{NH}_3]^*$  dissociated before stabilization could take place. The  $\text{NH}_4^+$  ion formed is expected to have energy imparted from the electric fields in excess of that resulting from the gas temperature. Therefore it is reasonable to expect the collision

complex,  $[\text{NH}_4^+ \cdot \text{NH}_3]^*$ , to possess greater excess energy than the same complex formed in the studies of Meot-Ner and Field, which were conducted under nearly field free conditions. It is therefore reasonable to suggest that the lifetime of  $[\text{NH}_4^+ \cdot \text{NH}_3]^*$  may be shorter. Hence a higher fraction of complex ions would dissociate before collision stabilization could take place, resulting in a reduction in the rate of formation of product.

Alternatively  $k_a$ , the rate of formation of the collision complex, may well be slower. Bowers<sup>73</sup> estimated this value from experimental data and found it to be considerably less than that predicted by ADO theory which Field and Meot-Ner<sup>55</sup> had used to evaluate  $^3k_f$ . However the certainty of their method to evaluate  $k_a$  is in considerable doubt and therefore it seems most plausible that the low value of  $^2k_f$  obtained in the current study results from the collision complex  $[\text{NH}_4^+ \cdot \text{NH}_3]^*$  having a shorter half life.

As will be shown in section (4.2.3.2) a direct observation of  $\log(I_{18}/\Sigma I)$  may be used in estimation of ion-source pressures on instruments not fitted with a Baratron or other similar pressure measuring gauge.



TABLE 4.7

Third and second order rate coefficients for the reaction of  $\text{NH}_4^+$  with  $\text{NH}_3$  at various ion-source field strengths.

Ion-source field strength. $/V \text{ cm}^{-1}$	Third order coefficient	Second order rate coefficient
	$3_k \times 10^{28} / \text{cm}^6 \text{ molec}^{-1} \text{ s}^{-1}$ †	$2k_f^+ \times 10^{12} / \text{cm}^3 \text{ molec}^{-1} \text{ s}^{-1}$
	$K_O = 1.29$	$K_O = 1.29$
	$K_O = 3.12$	$K_O = 3.12$
2.5	Not determined	$2.43 \pm 0.04$
5.0	$8.86 \pm 0.42$	$5.29 \pm 0.16$
7.5	$6.71 \pm 0.21$	$8.09 \pm 0.22$
10.0	$7.93 \pm 0.17$	$10.53 \pm 0.34$
12.5	$8.00 \pm 0.10$	$13.11 \pm 0.96$
		$5.88 \pm 0.10$
		$12.88 \pm 0.39$
		$19.10 \pm 0.52$
		$25.47 \pm 0.82$
		$31.7 \pm 2.32$

+ errors with 95% confidence

† errors  $\pm 1$  standard deviation.

4.2.3. A simple method forestimation of ion-source pressures of ammonia for CIMS.

4.2.3.1. For ammonia pressures less than 0.1 Torr.

As discussed previously, below 0.1 Torr, the reactions of primary ions  $\text{NH}_2^+$  and  $\text{NH}_3^+$  with ammonia obey pseudo first order kinetics. Rearranging the kinetic equation (4.2.6), for the reaction of  $\text{NH}_3^+$  with ammonia, the pressure,  $P_{\text{NH}_3}$ , is given by

$$P_{\text{NH}_3} = \log \left[ \frac{I_{17}^0}{I_{17}} \right] / N \tau_{17} k'_{17} \quad (4.2.25)$$

where  $I_{17}$  and  $I_{17}^0$  ( $\log(I_{17}^0) = (0.09 \pm 0.06)$ ) are the relative ion-currents of  $\text{NH}_3^+$  at an ion-source pressure,  $P$  and say  $P = 10^{-5}$  respectively,  $k'_{17}$  the rate coefficient at an ion-source field strength ( $E$ ,  $(\text{Vcm}^{-1})$ ),  $\tau_{17}$  the ion-source residence time of  $\text{NH}_3^+$  and  $N$  the usual factor for the conversion of pressure (Torr) to number density, ( $\text{molec.cm}^{-3}$ ).  $N$  is defined in equation (4.2.26)

$$N = \frac{1.3332 \times 10^{-4}}{k T} \quad (4.2.26)$$

where  $k$  is Boltzman's constant and  $T$  the absolute temperature. Values of  $k'_{17}$  were reported in table (4.2) and vary linearly with ion-source field strength in accordance with equation (4.2.8) where  $k_{17}$  is the rate coefficient at zero field strength.  $\log(I_{17}^0)$  does not vary with field strength and values of  $f_{17}$  and  $k_{17}$  have already been given in section (4.2.1).  $\tau_{17}$  may be determined from the "free fall" formula, equation (4.2.27),

knowing the repeller voltage (V), the distance (cm) between the repeller plate and the ion-source exit slit ( $2\ell$ ),  $m$  the mass of  $\text{NH}_3^+$  (kg) and  $e$  the proton charge (c).

$$\tau_{17} = 10^{-2} (2\ell m/eE)^{\frac{1}{2}} = 2\ell(m/eV)^{\frac{1}{2}} \times 10^{-2} \quad (4.2.27)$$

(The mean distance travelled by the ion is assumed to be  $\ell$ , see section (3.1.1)).

Combining equations (4.2.25), (4.2.26), (4.2.27) and rearranging equation (4.2.8), the ammonia pressure may be determined from equations (4.2.28) and (4.2.29).

$$P_{\text{NH}_3} = \{-1.229 \times 10^{-14} (\log I_{17} + 0.09) V^{\frac{1}{2}} T\} / k'_{17} \ell \quad (4.2.28)$$

$$k'_{17} = 10^{-11} (142 + 2.6 V/\ell) \quad (4.2.29)$$

By similar arguments the ammonia pressure may be determined using the relative ion-current of  $\text{NH}_2^+$  using equations (4.2.30) and (4.2.31) and was the subject of a recent publication.<sup>122</sup>

$$P_{\text{NH}_3} = \{-1.267 \times 10^{-14} (\log I_{16} + 0.75) V^{\frac{1}{2}} T\} / k'_{16} \ell \quad (4.2.30)$$

$$k'_{16} = 10^{-11} (218 + 2.8 V/\ell) \quad (4.2.31)$$

As already discussed  $k'_{16}$  and  $k'_{17}$  are not expected to vary greatly with temperature and this was observed to be true. The inclusion of temperature in equations (4.2.21) and (4.2.23) results from the dependence of  $N$  on temperature.

The version of equation (4.2.33) originally reported<sup>122</sup> was for pressure determination at 450K and may be obtained by replacing T by 450 in equation (4.2.30).

4.2.3.2. For ammonia pressures greater than 0.1 Torr.

In section (4.2.2) it was shown that the clustering of  $\text{NH}_4^+$  with neutral ammonia proceeds via the energy transfer mechanism. Application of such leads to the equation (4.2.22). If the stabilising collision rate of  $[\text{NH}_4 \cdot \text{NH}_3^+]^*$  is fast, i.e. at sufficiently high pressures,  $k_s \text{NP}_{\text{NH}_3} > k_b$ , equation (4.2.22) reduces to equation (4.2.32).

$$\log(I_{18}/I_{18}^0) = -2k_f \beta_{18} P_{\text{NH}_3}^2 N \quad (4.2.32)$$

$I_{18}^0$  ( $\log I_{18}^0 = -0.042 \pm 0.005$ ) the relative ion-current in the absence of reactions (4.2.16) and (4.2.17),

$\beta_{18} = 273 \times \ell / K_0 760 \text{ ET}$ , where  $K_0 = 1.29 \text{ cm}^2 \text{V}^{-1} \text{s}^{-1}$  is the reduced mobility of  $\text{NH}_4^+$  in ammonia,<sup>120</sup> and  $k_{18}$  the second order rate coefficient, at ion-source field strength  $E$  ( $\text{V cm}^{-1}$ ), as given in table (4.7).

Rearrangement of equation (4.2.32) to equation (4.2.33) shows how the ammonia pressure may be measured with the field strength set to  $2.5 \text{ V cm}^{-1}$ .

$$P_{\text{NH}_3}^\dagger = 5.9 \times 10^{-3} [-(\log I_{18} + 0.042)VT]^{1/2} / \ell \quad (4.2.33)$$

The pressure should be determined at low field strengths since ion residence times are greater and thus equation (4.2.32) holds over a larger range of pressure (see

---

<sup>†</sup>The constants in this equation are slightly different to those reported in a previous publication.<sup>122</sup> This is due to improved values of  $2k_f$  and the use of  $K_0 = 1.29$ .

figure 3.17). Additionally  $k_f^2$  is expected to vary considerably with temperature<sup>55</sup> and this was observed to be true in the current study, even though ion energies are expected to be much in excess of thermal energies. Therefore when using equation (4.2.33) for pressure estimation between 0.1 and 0.6 Torr, the ion-source block temperature should be near to 450K, i.e. that used in this study.

The use of the relative ion currents of  $\text{NH}_2^+$ ,  $\text{NH}_3^+$  or  $\text{NH}_4^+$  in ammonia reagent gas spectra, a dimension of the ion-source and recording the repeller voltage enables pressure determination for the ranges 0-0.1 and 0.1-0.6 Torr respectively, analogous to the methods already described for methylcycloalkanes.

4.3 MECHANISM OF THE REACTION OF IONS IN  
FLUORINATED BENZENE REAGENT GASES.

4.3.1 Fluorobenzene

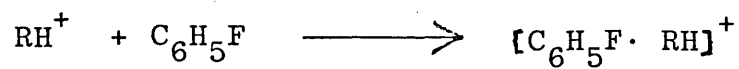
A possible mechanism for the reaction of primary ions from fluorobenzene with fluorobenzene is outlined in Scheme (4.1) and discussed below.

Initial collision of a primary ion,  $\text{RH}^+$ , ( $m/z = n$ ) with fluorobenzene is assumed to result in a short lived collision complex. The subsequent fate of this complex will depend to a large extent on whether or not it collides with another fluorobenzene molecule. At low pressure such a collision is unlikely and only fast ion-molecule reactions, e.g. charge exchange (equation (A) Scheme (4.1)), are likely to take place. Conversely at higher ion-source pressures, when collision stabilisation (B) of the complex is more likely, the formation of cluster ions is expected. These cluster ions may remain intact or undergo simple fragmentations to species of greater stability (C and D).

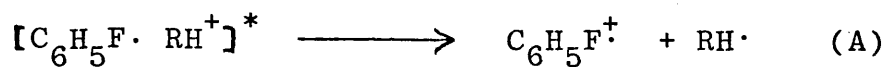
The observed constancy of molecular ion relative abundance and increase in cluster ion abundance above 0.05 Torr is in good agreement with the above proposed mechanism.

The principal cluster ion in the fluorobenzene plasma was observed to have  $m/z = 171$ . Additionally increase in the relative abundance of this ion was commensurate with a decrease in  $\text{C}_6\text{H}_3^+$ ,  $m/z = 75$ , Figure (4.4). Thus the ion  $m/z = 171$  is probably formed by electrophilic addition of  $\text{C}_6\text{H}_3^+$  to fluorobenzene.

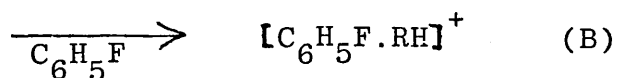
SCHEME 4.1 MECHANISM OF REACTION OF PRIMARY IONS WITH FLUOROBENZENE.



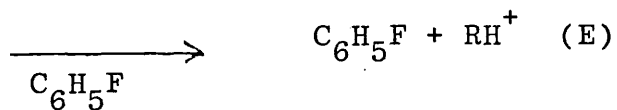
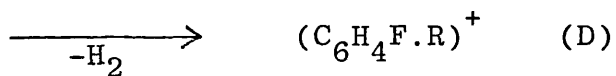
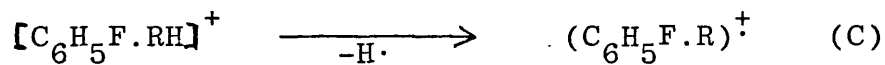
Collision complex



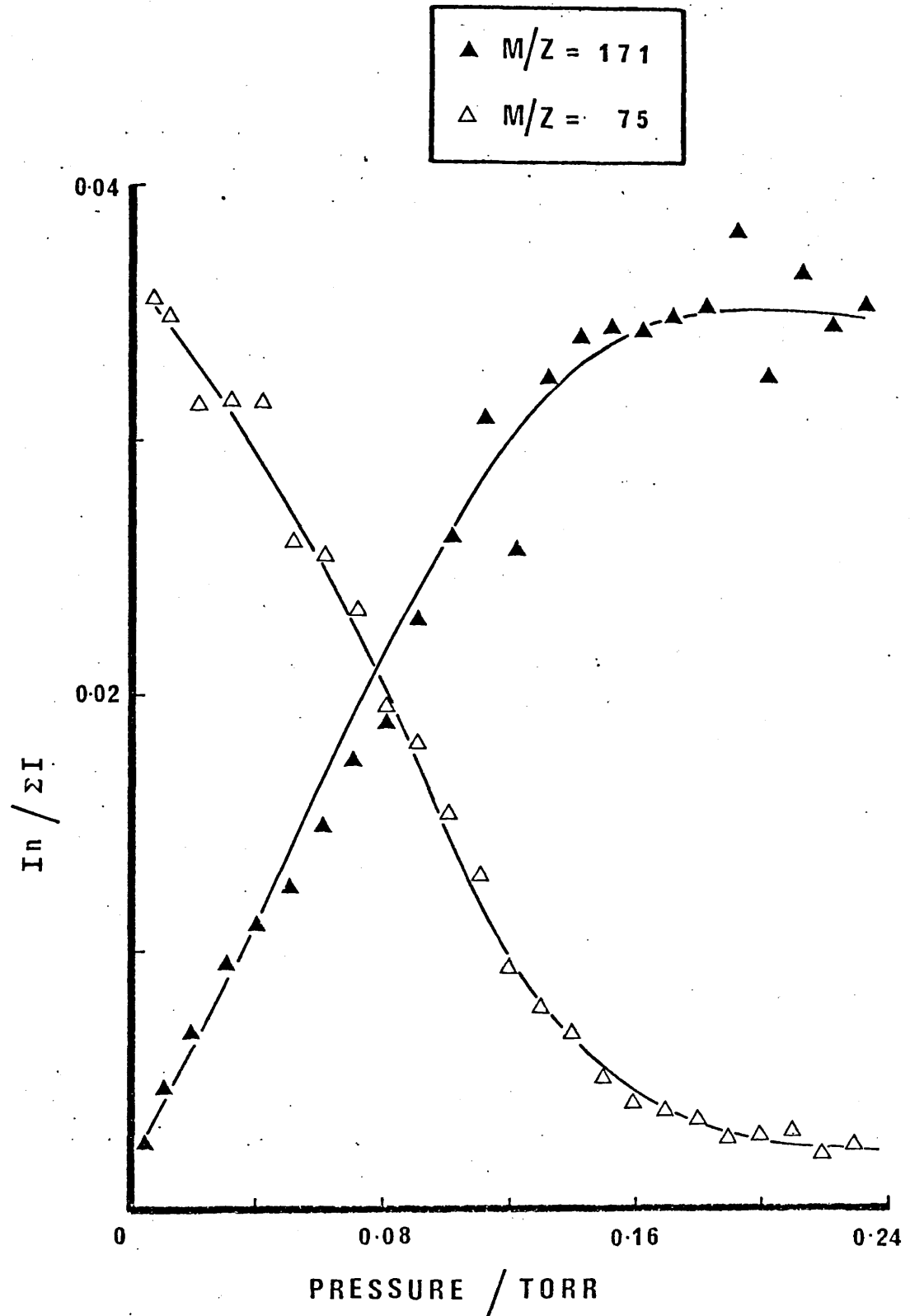
Charge exchange.



Collision stabilisation



Collision dissociation

**FIG. (4.4)**

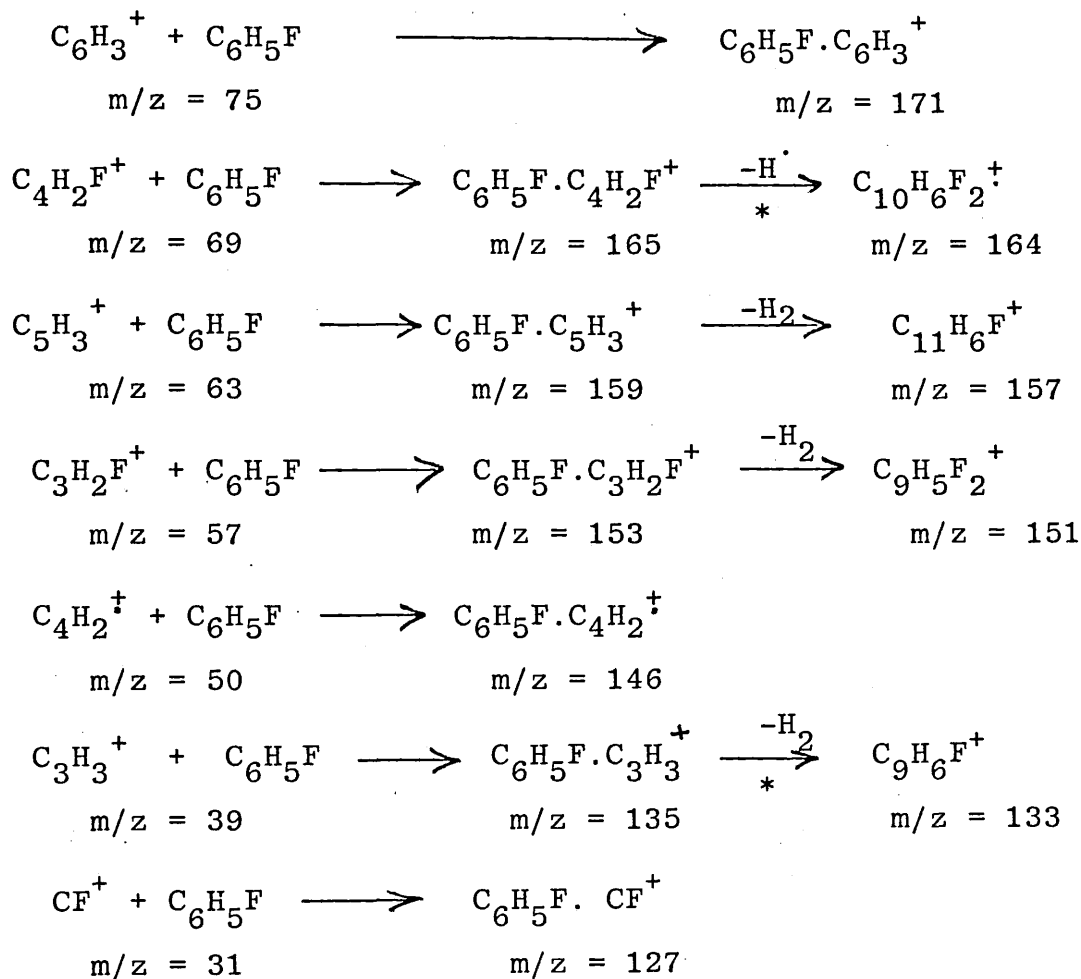
Variation of abundance of primary ion  $m/z = 75$  and cluster ion  $m/z = 171$ , with ion-source fluorobenzene pressure.



This and postulated pathways for the formation of the other principal cluster ions are given in scheme (4.2). The ions with  $m/z = 133$  and  $164$  which result from fragmentation of the cluster ion  $m/z = 135$  and  $165$  have relative abundances considerably in excess of their precursors, presumably owing to their greater stability. The observed cluster ions may be visualised as similar to the Wheland intermediate, and the collision activated complex to the transition state, in electrophilic substitution of aromatic rings. Fluorine deactivates aromatic rings to electrophilic substitution through the negative inductive effect, raising the energy barrier for the formation of the first transition state. It is not surprising that the degree of cluster formation in fluorobenzene reagent gas is small, and results in primarily a mono-ionic plasma at 0.2 Torr. However the degree of clustering in chlorobenzene, which has been suggested as a suitable reagent gas for ionization of aromatic compounds in hydrocarbon mixtures,<sup>123</sup> is considerably greater at the same pressure. This is as expected since chlorobenzene is less deactivating towards aromatic substitution. Therefore fluorobenzene reagent gas is to be favoured over chlorobenzene since the reaction of only one ion needs to be considered in kinetic studies.

Interestingly the differences in rates of reaction of the ions  $C_3H_3^+$  and  $C_3H_2F^+$  may well result from  $C_3H_3^+$  possessing the particularly stable cyclopropenium structure and the greater reactivity of  $C_3H_2F^+$ ,

SCHEME 4.2    FORMATION OF CLUSTER IONS IN FLUOROBENZENE  
REAGENT GAS.



\* Denotes observation of fragmentation of a metastable ion in support of the transition.

lack of such structure through the strongly electron withdrawing fluorine atom preventing delocalisation of positive charge in a cyclic structure.

However the values of the rate coefficients given in Table (3.5) should be viewed with caution, for the reasons given in Section (1.2). Additionally, since the large fluorobenzene molecules will be difficult to pump from the region between the ion-exit slit and the analyser entrance slit the pressure of neutral in the ion acceleration region may be considerable. Under such conditions the possibility of collision dissociation of cluster ions is greatly increased. Recently Illies and Meisels<sup>124</sup> have suggested that such processes occur in high pressure mass spectrometry. They attributed an observed "low mass tail" on  $N_2^+$  ion peaks to  $N_2^+$  resulting from collision dissociation of  $N_4^+$  in the acceleration region of their mass spectrometer. The magnitude of this tailing was observed to increase with pressure. Spectra recorded in the current study showed a small amount of tailing on the low mass side of the fluorobenzene molecular ion peak, see Figure (4.5), but no tailing of other ions was observed. Therefore some collision dissociation of the cluster ions results in formation of  $C_6H_5F^+$ . Collision dissociation outside the ion-source results in errors in measured rate coefficients. However it is hoped that the magnitudes of rate coefficients still indicate the relative reactivities of the various primary ions.

In addition to the above cluster reactions, on increasing the sensitivity of the mass spectrometer cluster ions whose  $m/z$  values suggested they contained two fluorobenzene molecules were observed. These ions and plausible pathways for their formation are illustrated in Scheme (4.3). However the presence of these cluster ions little affects the reagent gas plasma since their relative abundances ( $<0.005\%$  total ion-current) are an order of magnitude lower than clusters containing one fluorobenzene molecule.

An unfortunate consequence of the small variations in ion-currents above 0.05 Torr was limited ability to determine ion-source pressures with sufficient accuracy from reagent gas spectra. However suitable operating conditions for chemical ionization are attained by maximising the portion of the total ion-current carried by the molecular ion.

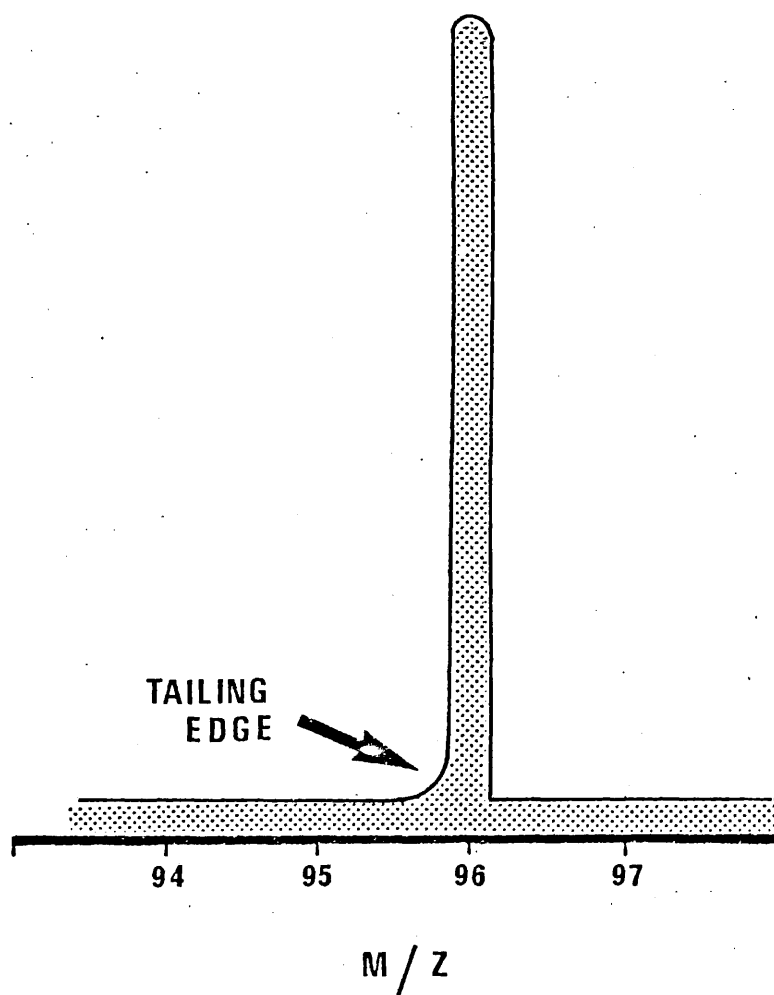
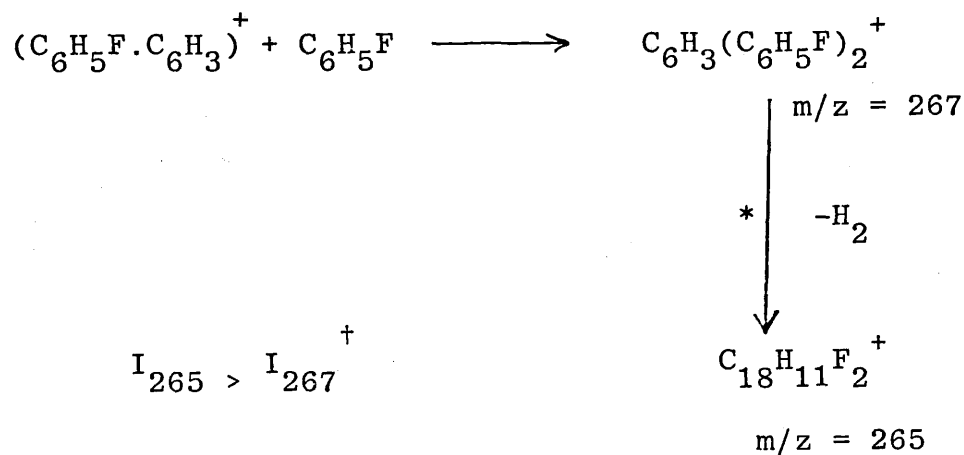
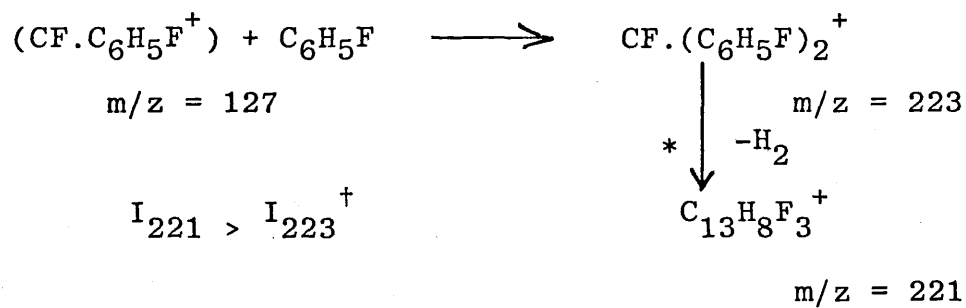


**FIG. (4.5)**

Tailing of ion abundance profile of peak  $m/z = 96$  resulting from collision dissociation of cluster ions in the vicinity of the ion-source exit slit.

SCHEME 4.3     CLUSTER IONS CONTAINING TWO FLUOROBENZENE  
MOLECULES.



\* Denotes observation of fragmentation of a metastable ion.

†  $I_n$  = Relative abundance of ion  $m/z = n$ .

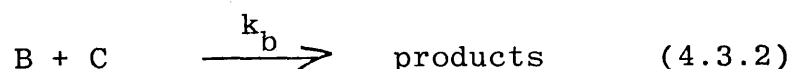
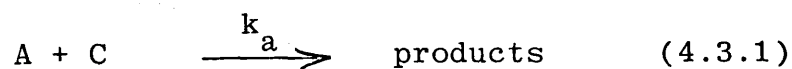
#### 4.3.2 Difluoronated benzenes

The mechanism of reaction of primary ions is assumed to be the same as that developed for fluorobenzene and this is borne out by similar variations in ion abundances with pressure. However it is of interest that decrease in cluster ion abundances above 0.15 Torr is more pronounced in difluorobenzenes. It is assumed that such reductions result from formation of higher order cluster ions. Since primary ion abundances continue to decrease and no increase in other low mass ions was observed, post source collision dissociation may be discounted from causing the reduction in cluster ions. The observation that p-difluorobenzene plasma has the highest relative abundance of molecular ion is also in agreement with the proposed mechanism. Being the most deactivated to electrophilic substitution lower cluster ion abundances are expected. M-difluorobenzene, the least deactivated, displays the lowest molecular ion relative abundance.

Unfortunately the values obtained for disappearance rate coefficients for primary ions in the different reagent gases are less easily rationalised. One might expect reaction with m-difluorobenzene to be more facile but although this is the case for many ions several display the opposite. It seems likely that primary ions of the same m/z resulting from different precursors (i.e. o, m, p difluorobenzenes) will possess different quantities of internal energy. Such would result in different reactivities. Also it is fair to

say that since the relative abundance of the primary ions is small the accuracy of measurement and subsequent rate coefficient determinations is low.

In Section (3.1.3.2) it was proposed that the ion-current recorded when focusing ions of mass to charge ratio ( $m/z$ ) 75 results from the two ions  $C_6H_3^+$  and  $C_3H.F_2^+$  in *o*- and *m*-difluorobenzene. The kinetic plot of  $\log(I_{75}/\Sigma I)$  against  $P^2$ , Figure (4.6) may be sub-divided into two lines A and B. In the first region, A, which has a larger negative gradient, the relative abundance of both ions decreases. In region B, one ion is considered to have reacted to completion while the abundance of the other, less reactive ion, continues to decrease. For the concurrent reactions of two ions A and B with a neutral C



The rates of disappearance of A and B are given by

$$\frac{-d[A]}{dt} = k_a [A][C]$$

$$\frac{-d[B]}{dt} = k_b [B][C]$$

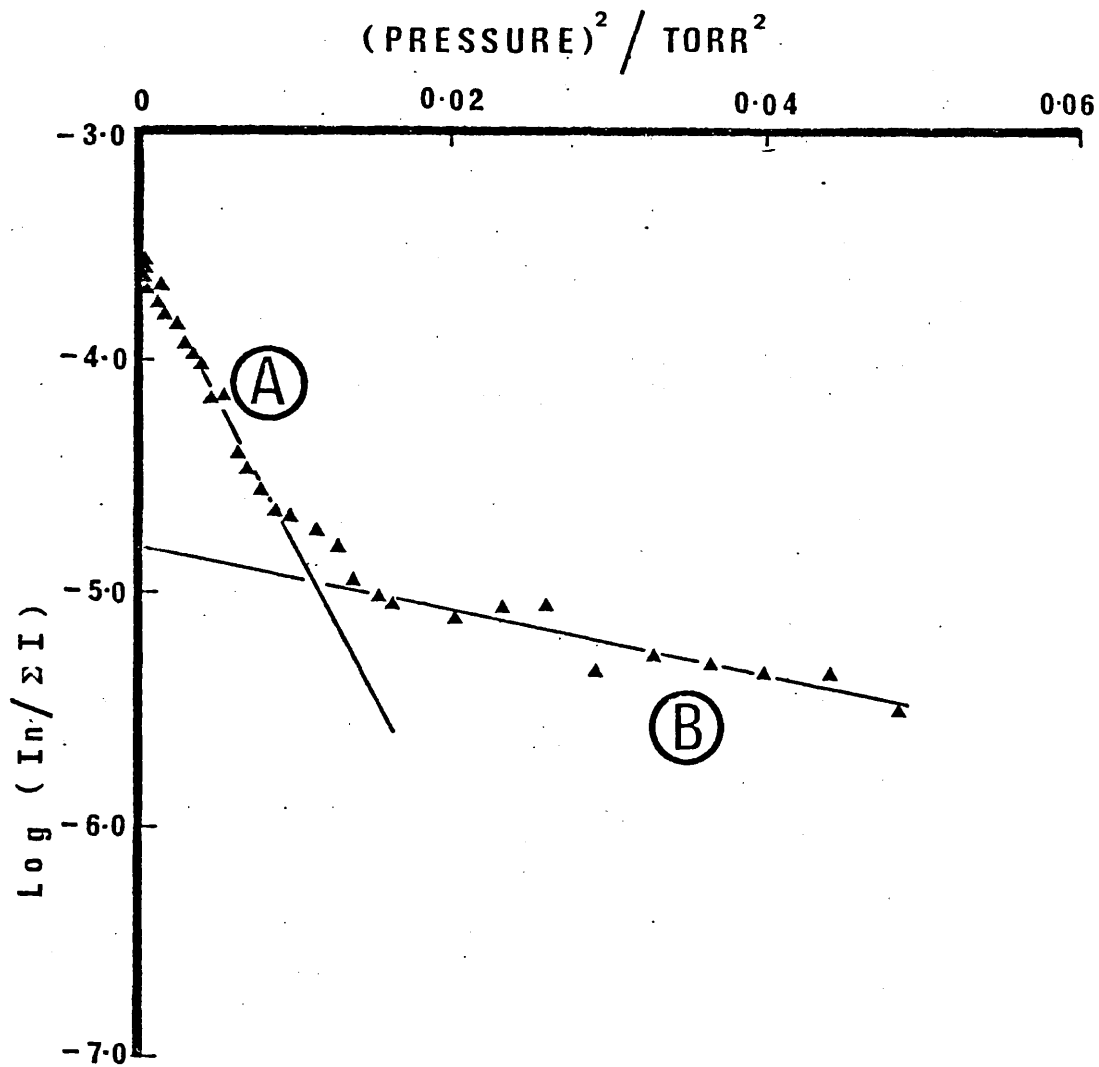
and the rate equations are

$$\ln \frac{A_0}{A} = k_a P c \tau$$

$$\frac{B_0}{B} = k_b P c \tau$$

since A and B gave the same nominal mass the mean residence time of each is identical,  $\tau$ .  $A, B, A_0, B_0$  are



**FIG. (4.6 )**

Kinetic plot for reaction of two ionic species with the same mass to charge ratio but different rates of reaction.

the relative ion currents at pressure  $P_c$  and  $P_c < 10^{-5}$

Thus

$$A + B = A_0 e^{-k_a P_c \tau} + B_0 e^{-k_b P_c \tau} \quad (4.3.3)$$

and rearranging (4.3.3) yields

$$(A + B) = (A_0 + B_0) e^{-k_a P_c \tau} - B_0 (e^{-k_a P_c \tau} - e^{-k_b P_c \tau}) \quad (4.3.4)$$

if  $k_a \gg k_b$

$$A + B = B_0 e^{-k_b P_c \tau} \quad (4.3.5)$$

and

$$\log (A + B) = \ln B_0 - k_b P_c \tau \quad (4.3.6)$$

and thus  $k_b = (1.39 \pm 0.31) \times 10^{-11} \text{ cm}^3 \text{ molec}^{-1} \text{ s}^{-1}$  and  $B_0 = 0.008$  are obtained from the gradient and intersect of line B in Figure (4.6). Now equation (4.3.4)

may be written as

$$\log \{ (A + B) - B_0 e^{-k_b P_c \tau} \} = -k_a P_c \tau + \ln A_0 \quad (4.3.7)$$

and hence  $k_a = 14.8 \times 10^{-11}$  and  $A_0 = 0.003$

evaluated, the gradient and intersect of a plot of  $\log \{ (A + B) - B_0 e^{-k_b P_c \tau} \}$  against  $P^2$ . The faster reaction is assumed to be that of  $C_6H_3^+$  and the value of rate coefficient obtained compares well with those found for other fluorinated benzenes. The value of  $k_b$  is much slower as might be expected for  $C_3HF_2^+$  which may well possess the cyclopropenium structure.

In conclusion a more monoionic plasma is obtained with p-difluorobenzene and the IP (9.15 eV) is lower than that of fluorobenzene (9.19 eV)<sup>111</sup>. Thus

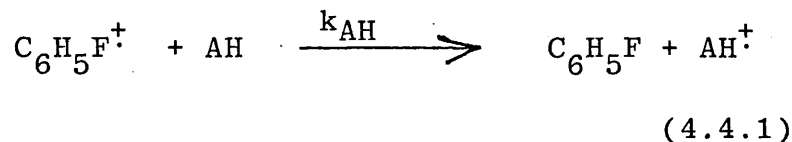
this may well be a more suitable reagent than fluorobenzene for preferential ionization of aromatic components of hydrocarbon mixtures. However, the higher cost and lower purity of commercially available p-difluorobenzene is likely to deter people from its use.

Once again the variation in primary ion relative abundances was too small to facilitate ion-source pressure determination directly from the reagent gas plasma.

4.4 SIGNIFICANCE OF RELATIVE RATES OF REACTION OF FLUOROBENZENE REAGENT GAS MOLECULAR ION ( $C_6H_5F^+$ ) WITH A VARIETY OF AROMATIC COMPOUNDS.

The magnitudes of rate coefficients for ion-molecule reactions of  $C_6H_5F^+$  with aromatic compounds are of academic interest in furthering knowledge of ion-chemistry, in addition to their practical importance to the analyst using fluorobenzene reagent gas for quantitative analysis of aromatic components in hydrocarbon mixtures.

For the general reaction



where AH represents an aromatic compound and k is the reaction rate coefficient, the rate of disappearance of reactant ion  $C_6H_5F^+$  is given by

$$-d \frac{[C_6H_5F^+]}{dt} = k [C_6H_5F^+][AH] \quad (4.4.2)$$

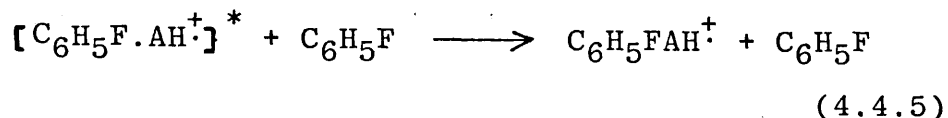
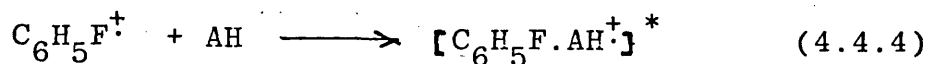
Using arguments similar to those stated in Section (3.1.1), the relative abundance ( $I_{96}/\Sigma I$ ) and the pressure of aromatic sample  $P_{AH}$  are used as measures of  $C_6H_5F^+$  and AH concentration respectively, Equation (4.4.2) becomes

$$\log \frac{I_{96}}{\Sigma I} = -k_{AH} N_{96} P_{AH} + \log \frac{I_{96}^0}{\Sigma I^0} \quad (4.4.3)$$

where  $(I_{96}^0/\Sigma I^0)$  is the relative abundance of  $C_6H_5F^+$  when  $P_{AH} = 0$ ,  $\tau_{96}$  the residence time of the fluorobenzene molecular ion estimated from ion-mobilities and  $N$  a factor for converting sample pressure (Torr) to number density (molecules  $cm^{-3}$ ). Thus if the kinetics of reaction (4.4.1) are in agreement with equation (4.4.2) then a semi logarithmic plot of the relative abundance of  $C_6H_5F^+$  against the pressure of aromatic sample should be a straight line. Such a plot for reaction of fluorobenzene with methylbenzene is given in Figure (4.7). The plot is clearly linear over the pressure range 0 - 4 mTorr, and the rate coefficient was readily obtained from the gradient and is recorded in Table (4.8). From examination of Figure (4.7) it is evident that the value of  $\log (I_{96}^0/\Sigma I^0)$  obtained from the intersect of the best straight line, through the experimental data, differs noticeably from that obtained experimentally from the mass spectrum of the reagent gas at 0.2 Torr. The calculated value of  $\log (I_{96}^0/\Sigma I^0)$  is more negative indicating a lower relative abundance of  $C_6H_5F^+$  than that measured experimentally. Such an observation suggests that reaction of  $C_6H_5F^+$  with aromatic compounds at pressures  $< 0.2$  m Torr is noticeably faster than at higher pressures, ca. 0.2 - 4 m Torr. This is highly unlikely since fast ion-molecule reactions, such as charge exchange, do not require a second collision to proceed to products and therefore the rate coefficients of such reactions are

independent of sample concentration. It seems more likely that the discrepancy between experimental and calculated values of  $\log(I_{96}^0/\Sigma I)$  arises from under-estimation of sample pressures. This is not unreasonable since the precision in measurement of sample pressure decreased with pressure. At sample pressures greater than 4.0m Torr a departure from linearity in plots of  $\log(I_{96}/\Sigma I)$  against  $P_{AH}$  was observed for most of the compounds studied. At higher sample pressures a decrease in gradient was observed. Such departure normally occurred when the observed relative abundance of  $C_6H_5F^+$  dropped below 15% of the total ion-current. A plausible explanation for such behaviour is that some sample ions possess sufficient excess internal energy to ionize fluorobenzene, in an endothermic reaction, before they exit the source. This would increase the relative abundance of fluorobenzene molecular ions and appear as a reduction in their reaction rate. This would become most pronounced at high sample molecular ion relative abundances as observed.

In addition to charge exchange, other workers have reported observation of association reactions<sup>125</sup> between aromatic ions and molecules. Such reactions (equations (4.4.4), (4.4.5)) require a second collision of the collision complex  $[C_6H_5F.AH^+]^*$  with fluorobenzene.



If the life time of the collision complex is very short and the overall pressure low then the probability of collision stabilisation is very small. In the current studies no ions, with mass to charge ratios, characteristic of association ions were observed. Here the life time is probably ca.  $10^{-7}$  s.

The reactions of many other aromatic compounds, with fluorobenzene, were studied and the rate coefficients, obtained from the gradients of plots similar to Figure (4.7) are recorded in Tables (4.8) and (4.9). In all cases, the pressure range for which  $\log(I_{96}/\Sigma I)$  plotted against  $P_{\text{AH}}$  is linear, the ionization potential of AH and the A.D.O. collision capture rate coefficient for reaction (4.4.1) are appended. The low volatility of ethylnaphthalene resulted in sample introduction problems leading to a large scatter in data which precluded evaluation of a rate coefficient.

To date few rate coefficients for charge exchange reactions between aromatic compounds have been published. Since the ionization potential (IP) of benzene, 9.24 eV,<sup>111</sup> is close to that of fluorobenzene, 9.20 eV,<sup>111</sup> the heats of charge exchange

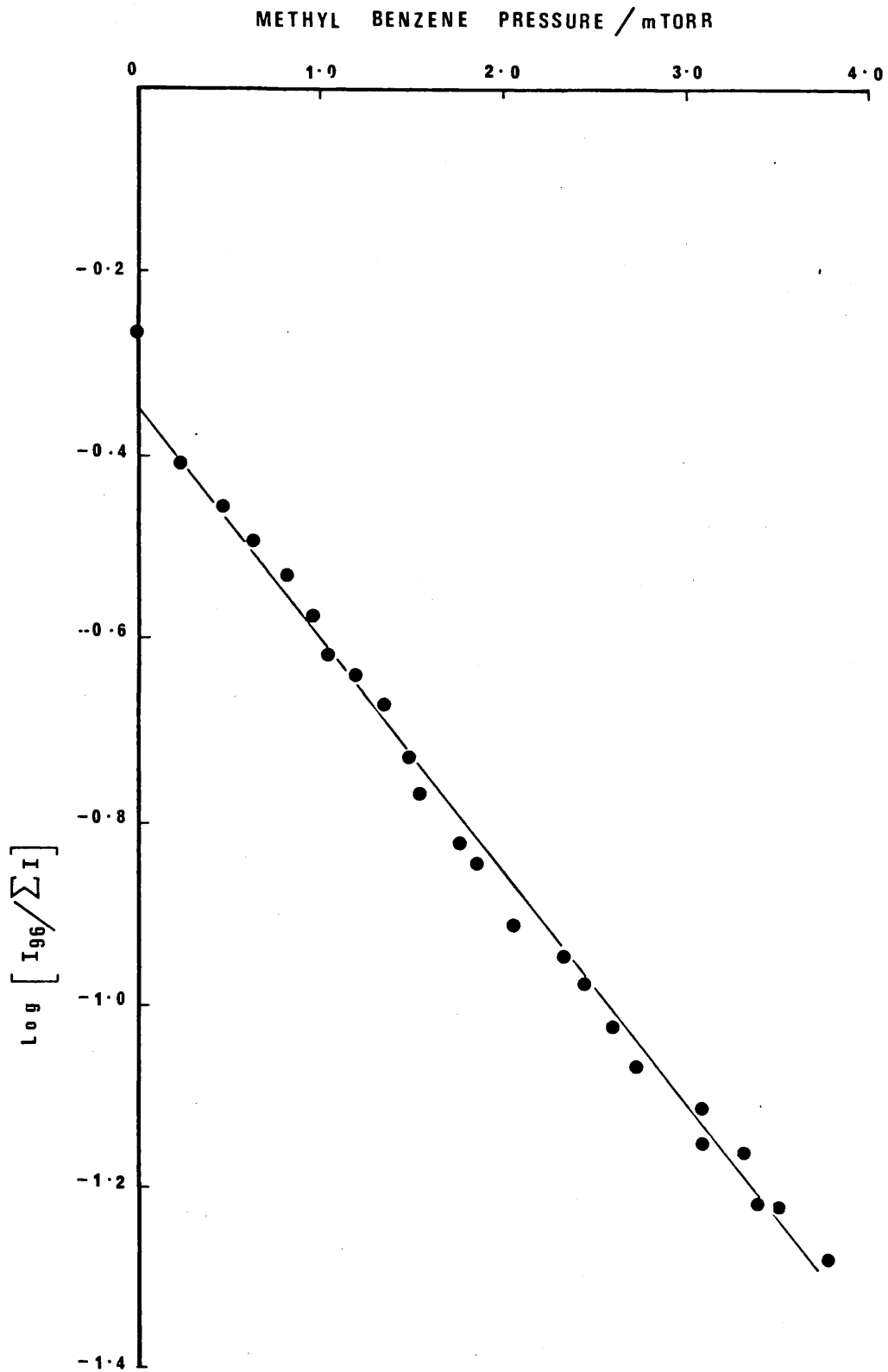


FIG. (4.7)

Kinetic plot for reaction of fluorobenzene molecular-ion with methylbenzene.



TABLE 4.8 Rate coefficients for reaction of  $C_6H_5F^+$  with alkyl benzenes

SAMPLE	Rate coefficient $\times 10^{-10}/\text{cm}^3 \text{ molec}^{-1} \text{ s}^{-1}$	Pressure range for which kinetics hold (m Torr)	ADO collision capture rate constant $\times 10^{-10}/\text{cm}^3$ $\text{molec}^{-1} \text{ s}^{-1}$	Sample ionization potential/ eV	Collision efficiency $k_{\text{exp}}/k_{\text{ADO}}$
1-Pentylbenzene	$13.88 \pm 0.68$	0 - 4.4	-	-	-
n-Butylbenzene	$11.18 \pm 0.80$ $12.90 \pm 1.38$	0.07 - 5.5 0.0 - 4.0	13.2	8.69 <sup>†</sup>	0.91
n-Propylbenzene	$17.52 \pm 2.32$	0.0 - 3.0	12.7	8.72 <sup>†</sup>	1.38
iso-Propylbenzene	$17.54 \pm 1.30$	0.0 - 3.0	12.7	8.69 <sup>†</sup>	1.38
1,3,5-Trimethylbenzene	$13.68 \pm 0.80$	0.0 - 3.0	12.7	8.40 <sup>†</sup>	1.08
n-Ethylbenzene	$14.08 \pm 0.56$	0.3 - 3.0	12.7	8.76 <sup>†</sup>	1.16
1,2 Dimethylbenzene	$14.34 \pm 0.26$	0.0 - 3.0	12.7	8.56 <sup>†</sup>	1.13
1,3 Dimethylbenzene	$17.48 \pm 0.62$	0.2 - 2.9	12.5	8.56 <sup>†</sup>	1.40
1,4 Dimethylbenzene	$12.18 \pm 0.44$	0.3 - 2.9	12.4	8.45 <sup>†</sup>	0.98
Methylbenzene	$11.88 \pm 0.4$	0.2 - 3.8	12.0	8.82 <sup>†</sup>	0.99

<sup>†</sup> Values taken from Ref. 17

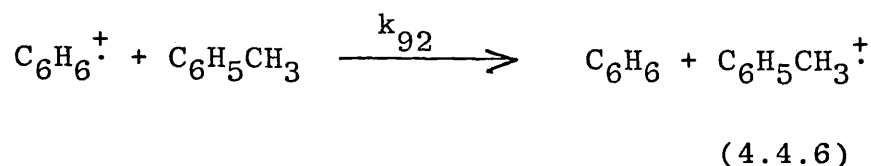
TABLE 4.9 Rate coefficients for reaction of  $C_6H_5F^+$  with other aromatic compounds

SAMPLE	Rate coefficients $\times 10^{-10}/\text{cm}^3 \text{ molec}^{-1} \text{ s}^{-1}$	Pressure range for which kinetics hold (m Torr)	ADO collision capture rate constant $\times 10^{-10}/\text{cm}^3$ $\text{molec}^{-1} \text{ s}^{-1}$	Sample ionization potential/ eV	Collision efficiency $k_{\text{exp}}/k_{\text{ADO}}$
2,5-Dimethylthiophene	$8.07 \pm 1.00$	0 - 4.0	12.3	$8.10^{\dagger}$	0.66
2-Methylthiophene	$11.12 \pm 0.78$	0 - 3.0	12.3	8.14 <sup>†</sup>	0.90
Thiophene	$8.48 \pm 0.60$	0 - 4.0	11.7	8.87 <sup>†</sup>	0.72
2-Methylfuran	$17.04 \pm 1.36$	0 - 3.0	11.6	8.39 <sup>†</sup>	1.47
Furan	$8.80 \pm 0.30$	0 - 4.5	11.1	8.89 <sup>†</sup>	0.79
1-Methylnaphthalene	$18.92 \pm 1.42$	0 - 2.0	13.2	7.96 <sup>†</sup>	1.43
Cyclohexylbenzene	$12.66 \pm 0.74$	0 - 3.5	12.7		0.996
Benzene	No reaction			9.24 <sup>†</sup>	
1-Chloro-2 fluorobenzene	No reaction			9.16 <sup>†</sup>	
1-Chloro-3 fluorobenzene	No reaction			9.21 <sup>†</sup>	

<sup>†</sup> Values from Ref. 17

<sup>‡</sup> Values from Ref. 111

reactions of the benzene molecular ion,  $C_6H_6^+$ , with various aromatic compounds will be similar to those if  $C_6H_5F^+$  were the reactant. Consequently the values of rate coefficients for reaction of  $C_6H_6^+$  with various aromatics are a good reference for the current study, e.g. the reaction of  $C_6H_6^+$  with methylbenzene,  $IP = 8.82 \text{ eV}^{111}$ .



has  $\Delta H \sim 42 \text{ kJmol}^{-1}$  compared to  $37 \text{ kJmol}^{-1}$  for a similar reaction of fluorobenzene. Meot-Ner and Field<sup>126</sup> have determined  $k_{92} = 13 \times 10^{-10} \text{ cm}^3 \text{ molec}^{-1} \text{ s}^{-1}$  at 445K using a pulsed source high pressure mass spectrometer. Therefore the values of  $11 - 17.5 \times 10^{-10} \text{ cm}^3 \text{ molec}^{-1} \text{ s}^{-1}$  obtained for reaction of fluorobenzene with various alkyl, Table (4.8), and cycloalkyl benzenes, Table (4.9), are of the order expected. Current theory of ion-molecule reactions<sup>56</sup> suggests that fast charge transfer reactions proceed via a direct reaction of reactant ion and neutral sample, and that every collision should result in charge exchange, provided the reaction is exothermic. Therefore the rate of such reactions should correspond to the collision capture rate. This may be calculated using the "average angle dipole orientation" theory (ADO)<sup>45</sup> and it is of interest to compare the experimentally determined rates of

---

<sup>†</sup> Values calculated using ionisation energies taken from Ref.(111)

reaction with calculated collision capture coefficients. Moet-Ner and Field<sup>126</sup> conducted such a comparison for a variety of reactions between aromatic compounds. Although most of their experimental rate coefficients were 7 - 20% greater than those calculated using ADO theory, (e.g. for reaction (4.4.6) at 570K they found  $k_{\text{exp}}=14 \times 10^{-10}$  and  $k_{\text{ADO}}=13 \times 10^{-10} \text{ cm}^3 \text{ molec}^{-1} \text{ s}^{-1}$ ) they concluded that charge exchange reactions between aromatic compounds do proceed at the collision rate. Similarly in the current study most of the experimental rate coefficients are greater than those calculated from ADO theory. Some workers have suggested an electron jump mechanism<sup>127</sup> to explain collision efficiencies ( $k_{\text{exp}}/k_{\text{ADO}}$ ) greater than unity. However the opinion of Ausloos, Eyler and Lias<sup>128</sup> seems preferable: that charge transfer reactions should proceed no faster than the collision rate. Obviously one has to assume that ADO theory does indeed estimate the true collision capture rate. The more recent AADO<sup>46</sup> theory, which includes a term for the conservation of angular momentum during collision, predicts collision capture rates for ions with polar molecules ~10% in excess of ADO values. Bowers, Su and Su<sup>46</sup> in their paper discussing AADO theory indicate that energy conservation during a collision should also be considered. Therefore considering the inadequacies of ADO theory and for the reasons stated in Section (1.2), the current experimental values may be in error by as much as a factor of two, the agreement between experimental and theoretical values is excellent.

In an earlier publication<sup>129</sup> it was suggested that the relative reactivity of fluorobenzene molecular-ion depends upon the difference in ionization

energy  $\Delta IE$  between the aromatic compound and fluorobenzene namely the exothermicity\* of the reaction. Figure (4.8) shows the variation in observed rate coefficient with  $\Delta IE$ . Although there is considerable scatter the general trend is that reaction rates do appear to increase with  $\Delta IE$ . However, it is more correct to compare collision efficiency with reaction exothermicity, since many of the compounds with low ionization potentials have higher molecular polarizabilities and thus are expected to yield higher collision capture rate coefficients. Figure (4.9) shows the variation of collision efficiency with  $\Delta IE$  for the compounds studied and it is clear that with two exceptions, namely 2-methyl and 2,5-dimethyl thiophene, collision efficiency increased with  $\Delta IE$ . Such behaviour, and the apparent unreactivity of 1-chloro-2-fluorobenzene,  $IE = 9.16 \text{ eV}$ ,<sup>111</sup> some 0.04 eV less than fluorobenzene, suggests the existence of some small energy barrier to charge exchange under the conditions used. This is clearly contrary to current theory which dictates that no energy barrier exists in charge exchange reactions. Alternatively the lower reactivities of some compounds may result from a poor match of their electronic energy levels with those of fluorobenzene. It is known that the presence of a favourable transition, i.e. a large "Franck Condon Factor", between a compound ground state and the accessible electronic states of its molecular ion, results in higher collision efficiencies. The absence

---

\* (i)  $\Delta IE = IE_{C_6H_5F} - IE_{SAMPLE}$

(ii) Recombination energy of sample ions should also be considered but experimental values were not available for all the materials studied.

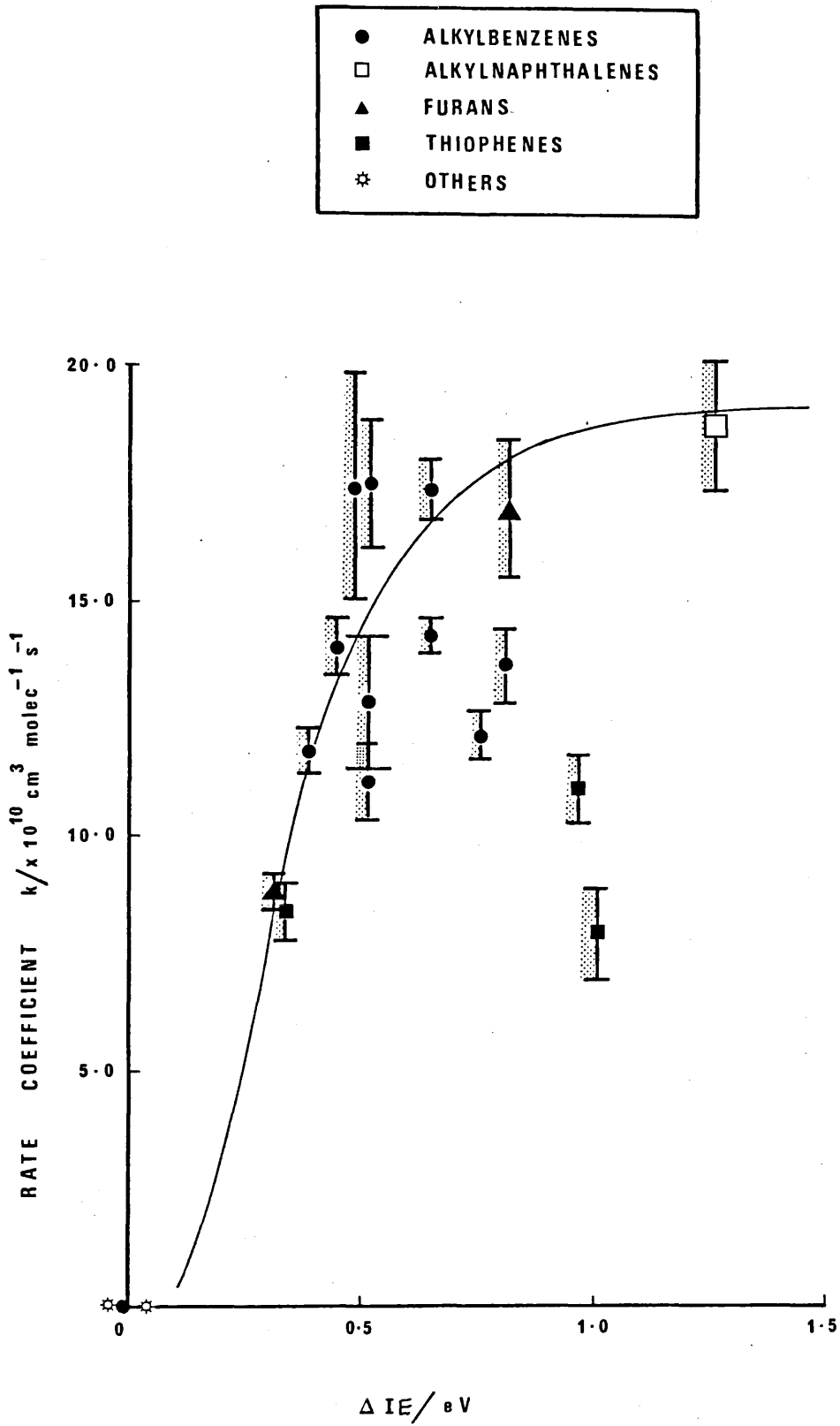


FIG. (4.8)

Variation in rate coefficient for reaction of fluorobenzene molecular-ion with various aromatic compounds as a function of difference in ionization energy.

1	Me Bz	9	1, 3, 5, Tri Me Bz
2	n-Et Bz	10	FURAN
3	n-Pr Bz	11	2 Me FURAN
4	iso-Pr Bz	12	THIOPHENE
5	n-Bu Bz	13	2 Me Thio
6	1, 2 Di Me Bz	14	2, 5 Di Me Thio
7	1, 3 Di Me Bz	15	1- Me Naph
8	1, 4 Di Me Bz	16	1-Cl-2F Bz

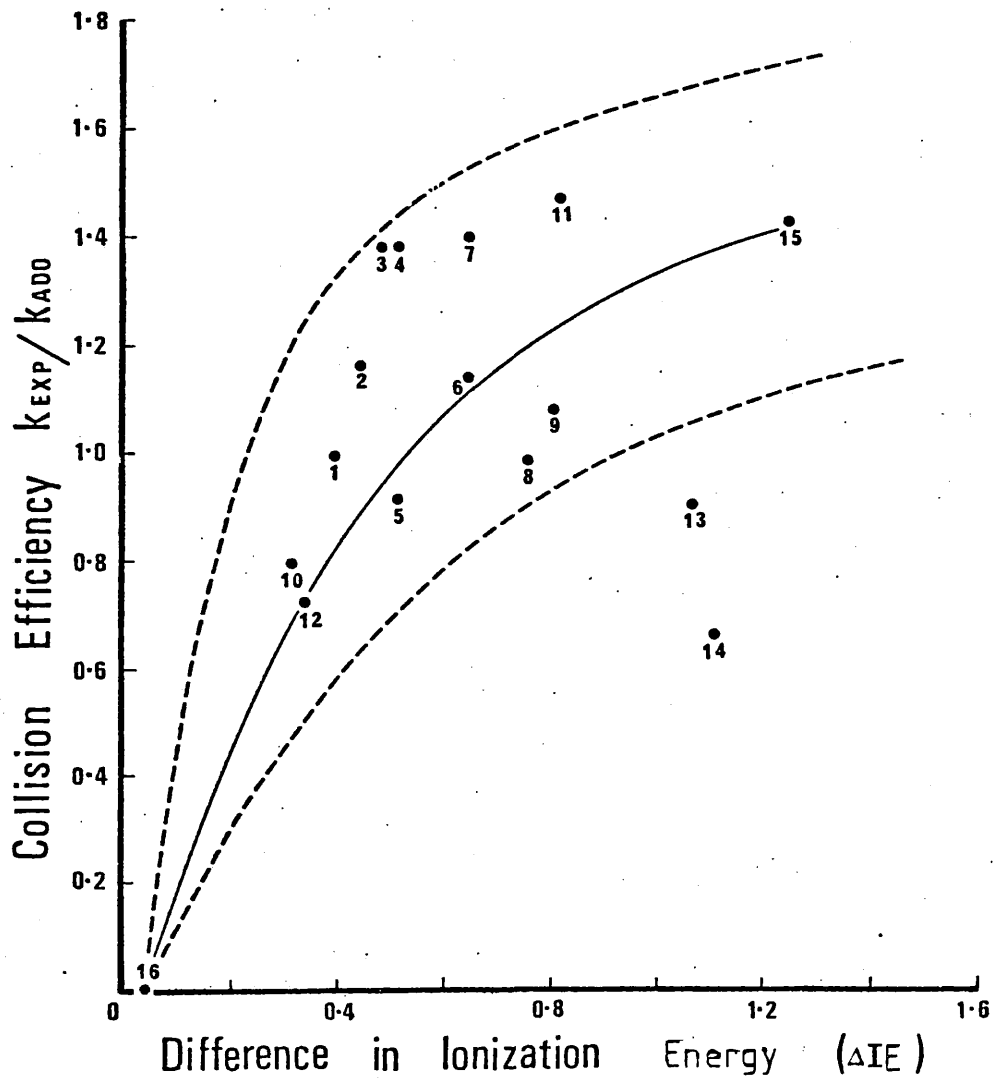


FIG. ( 4.9 )

of such transitions is believed to result in slower reaction.<sup>121,130</sup> Clearly there is a need to study the reactions of fluorobenzene molecular ion at thermal energies and in the absence of electric fields, since these could also considerably effect reaction rates.

Since it appears that most reactions proceed here with observed efficiencies greater than unity, these high rates may well result from an underestimation of the ion-source residence time of  $C_6H_5F^+$ . This highlights the chief problem of determining rate coefficients using a continuous extraction ion-source. However such an underestimation would not affect the relative magnitudes of reactivities with different compounds. Therefore, the scatter in reaction efficiency of ~15% for compounds with ionization potentials (IP) less than 8.5 eV, excluding 2-methyl and 2,5 dimethylthiophene, will be unchanged by an incorrect ion source residence time. Allowing for this scatter the rates of reaction of compounds with  $IP > 8.5$  eV follow the collision rate. Larger aromatic molecules, with molecular masses greater than 250 Daltons, may be expected to exhibit little variation in molecular polarizability or dipole moment with carbon number and thus only small changes in collision capture rate coefficients are expected. Therefore for a variation in relative molecular mass of ca. 200 Daltons, the variation in rate of reaction with  $C_6H_5F^+$  may be small. Thus if the response of the electron multiplier, used for ion detection, were independent of ion mass, then sensitivities for different aromatic compounds to



a first approximation should be identical within  $\pm 15\%$ .

Clearly from the data so far obtained the above are bold claims, and the determination of rates of reaction of  $C_6H_5F^+$  with a far greater number of aromatic compounds, particularly those with higher molecular masses (e.g. naphthalenes), is urgently required. Also the anomalous rate coefficients obtained for alkylated thiophenes requires further investigation. The determination of rate coefficients for naphthalenes and higher boiling alkylbenzenes was prevented by sample introduction problems but with improved instrumentation this problem could be alleviated.

In conclusion fluorobenzene positive ion chemical ionization (CI) mass spectrometry has one clear advantage over negative ion chemical ionization (NCI), e.g.  $OH^-NCI$ , for quantitation in that reaction rates and hence relative sensitivities appear to be independent of chemical structure. This is not the case for  $OH^-NCI$  where reactivity depends on the ease of removal of an  $\alpha$ -proton from the aromatic molecule, which varies considerably with structure, <sup>91</sup>e.g. t-butylbenzene is ionised by fluorobenzene but not using  $OH^-NCI$ .

Chlorobenzene also used in positive chemical ionization mass spectrometry of aromatic components of hydrocarbon mixtures is believed to possess similar reaction properties to fluorobenzene. Unfortunately no study of the kinetics of reactions of  $C_6H_5Cl^+$  and the other prominent ions in the chlorobenzene plasma with aromatic compounds

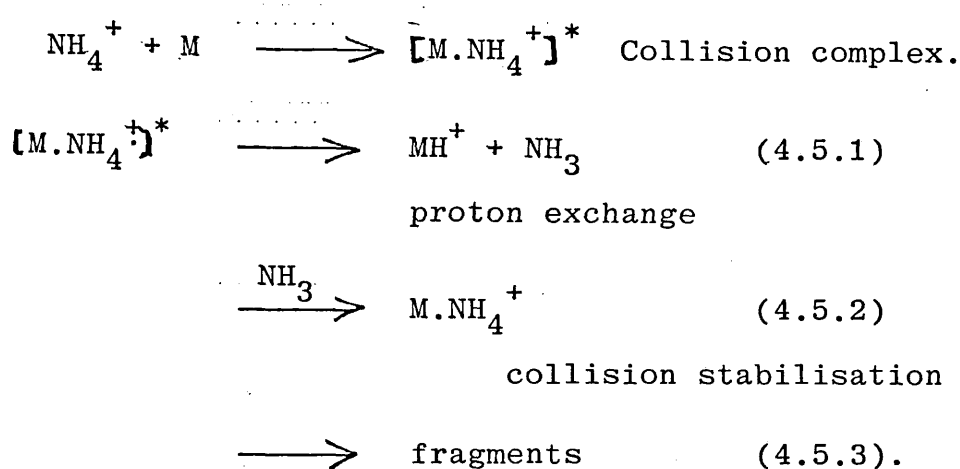
has been reported to date. Such a study would be particularly interesting for comparison of reaction rates with those of fluorobenzene.

4.5 INFORMATION GAINED FROM CHEMICAL  
IONIZATION MASS SPECTROMETRIC ANALYSIS  
OF LUBRICATING OILS AND A COMPARISON WITH  
THAT OBTAINED BY OTHER ANALYTICAL METHODS.

4.5.1 Ester base oils

Although ammonia chemical ionization has already been conducted on many esters including some ester based lubricants<sup>131</sup>, so far it has only been of pure compounds or in the case of mixtures after some prior separation, e.g. by GLC.<sup>131</sup> Additionally ester fluids are often hydrolysed and derivatised<sup>26</sup> prior to such analyses to provide more information regarding their chemical structure, or to improve the determination of complex mixtures. However, such methods are time consuming and the aim of the current study has been to evaluate chemical ionization as a tool for direct analysis of the total sample without any need for prior hydrolysis, derivatization or separation. Such a method would considerably reduce labour costs in an analytical laboratory.

As indicated in Section (4.2) for ion-source ammonia pressure of 0.2 - 0.6 Torr the reagent gas ions are principally  $\text{NH}_4^+$  and  $\text{NH}_4.\text{NH}_3^+$ . The relative proportions of each varying with pressure. These may react with sample molecules by formation of a collision complex which then either dissociates (4.5.1) and (4.5.3), or is collision stabilised by a neutral ammonia molecule (4.5.2).



The pathway followed after formation of the collision complex depends to a large extent on the relative proton affinities (PA's) of the sample and ammonia (see Section ( 1.3 )). Esters having proton affinities slightly less than ammonia, means that proton transfer would be endothermic and little sample ionization would be expected via this pathway. By considering the ammonium ion an acid and the sample ester molecule (M) a base then the dissociation energy of (M ....  $[\text{HNH}_3]^+$ ) hydrogen bond would be expected to decrease with decreasing PA (M). Conversely the dissociation energy of the ( $[\text{MH}]^+ \dots \text{NH}_3$ ) hydrogen bond would decrease with increasing PA (M). Furthermore, the excess internal energy initially present in the  $[\text{M.NH}_4]^+ *$  complex increases with PA (M), assuming there is a direct correspondence between PA (M) and ammonium ion affinity. For the esters studied PA (M) (ca.  $858 \text{ kJmol}^{-1}$ )<sup>133</sup> is only slightly less than that of ammonia ( $866 \text{ kJmol}^{-1}$ )<sup>134</sup> and although the dissociation energy of the (M... $[\text{HNH}_3]^+$ ) hydrogen bond will be less than that of ( $[\text{MH}]^+ \dots \text{NH}_3$ ) the difference will be small. Therefore,

although dissociation to the starting materials will be preferred, some formation of  $MH^+$  may be expected.

Additionally since  $\Delta H$  solvation  $\sim T\Delta S$  solvation the  $[M.NH_4]^+$  complex is expected to possess little excess energy, provided the energies of the  $NH_4^+$  ions are near thermal, and therefore have a noticeable lifetime (ca.  $10^{-7}$  sec.). During such time collisions with neutral  $NH_3$  molecules would result in further stabilisation, leading to a longer lived complex  $M.NH_4^+$  which would be detected by the mass spectrometer. In the current study at low ammonia pressures (ca. 0.2 Torr), collision rate is low, considerable quantities (ca. 25% of the sample ion-current) of  $MH^+$  ions were detected and many of these result from fragmentation of  $M.NH_4^+$ . Further when using higher ammonia pressures (ca. 0.7 Torr), the probability of  $[M.NH_4]^+$  collisions is far greater and very few  $MH^+$  ions were detected (ca. 2% of the sample ion-current). These results support the above proposed mechanism for reaction of  $NH_4^+$  with esters and imply that the half life for the  $[M.NH_4]^+$  complex may well be of the order of the mean ion-source residence time at 0.2 Torr (viz  $5 \times 10^{-6}$  sec).

Thus by use of relatively high (ca. 0.7 Torr) ammonia pressures simple spectra consisting almost entirely of  $M.NH_4^+$  ions were readily generated. It is particularly interesting that even less fragmentation of  $M.NH_4^+$  ions of the neopentyl polyol esters (> 96% of the sample ion current due to  $M.NH_4^+$  ions) was observed than for similar molecular

weight esters of dicarbocyclic acids (e.g. 86% of sample ion current due to  $M.NH_4^+$  ions). The greater stability of neopentyl polyol ester  $M.NH_4^+$  ions may result from the ammonium ion partially bonding to more than one carbonyl function. The greater delocalization of charge achieved may result in a reduction of excess energy in the initial complex. Such a reduction would be expected to increase both the lifetime of the complex and the possibility of collision stabilization.

Although the aim of almost monoionic sample spectra is realised at high reagent gas pressure it is gained at a price, namely a reduction in sensitivity. The higher source pressures were found to lead to a noticeable increase in pressure in the vacuum chamber surrounding the source. Since ions are required to pass through this region after exiting the source and prior to entering the analyser, any reduction in mean free path, due to increased gas pressures, will result in an increased loss of ions by discharge and collision dissociation, leading to an overall reduction in sensitivity. Such effects were observed in the current study, the sensitivity at 0.7 Torr being an order of magnitude lower than that obtained at 0.2 Torr. However the sensitivity obtained at 0.7 Torr was quite sufficient for the analysis of the quantities of ester material (typically 50 $\mu$ g) introduced via the solid probe.

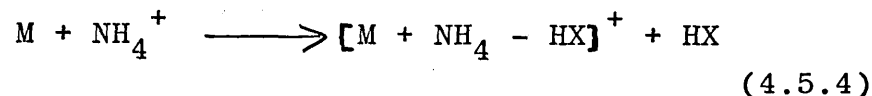
Since the isomeric nature of the alkyl groups in ester lubricating fluids are not normally known

prior to analysis and only relative molecular masses can be determined in ammonia CI, it was important to establish that the degree of branching did not drastically affect either sensitivity or stability of the  $M.NH_4^+$  ions. Analysis of various acid esters of 2-ethyl hexanol, a bulk industrial chemical often used in lubricant ester production, indicated that branching at the second carbon little affected sensitivity or fragmentation. However spectra obtained for bis(2-nonyl)hexanedioate appear to indicate that branching at the alcoholic carbon (C-2) does result in an increase in fragmentation, illustrated by the high relative abundance of  $((M + NH_4) - R)^+$  ions. Such increases may result from the methyl group destabilising the  $M.NH_4^+$  ion by steric hinderance. Obviously the presence of an ester with branching of the alkyl chain at the alcoholic carbon will result in a reduction in precision. However the problem will be minimal in fluids where either small or large proportions of secondary alcohols are used in ester preparation, and only when near equal quantities of secondary alcohols are used will precision be severely impaired.

For similar reasons esters of acids with carbonylic function separated by different numbers (n) of methylene units were studied. Little change in the amount of fragmentation was observed, an increase in n often resulted in an increase of  $(M.NH_4)^+$  relative abundances. (See Table (3.9)). Additionally the possibility of a

change in fragmentation pathways with  $n$ , similar to that observed by Weinkam and Gal<sup>115</sup> was investigated.

Particular attention was paid to the ability of  $\text{NH}_4^+$  to react via substitution,<sup>134,135</sup> e.g. (4.5.4), reactions.



Such reactions require a good leaving group, X, and are enhanced by the presence of electron donating groups attached to the same carbon as X. The reaction observed by Weinkam and Gal for methyl esters is similar but the  $\text{CH}_3\text{-O}$  group is replaced by  $\text{NH}_2$  and a hydrogen added to the carboxyl oxygen. They proposed a concerted mechanism, see Scheme (3.1) Section (3.2.1.1), which may be compared to hydrolysis but  $\text{NH}_4^+$  being the reactant rather than  $\text{H}_3\text{O}^+$ . Also they noted that small relative abundances (ca. 3% of the total sample ion current, when using ammonia at 0.3 Torr) of the product  $[\text{M} + \text{NH}_4 - \text{ROH}]^+$  ions were produced. Additionally they noted that for "ammonolysis" to occur,  $n$  should be greater than or equal to 4. In the current study although ions with  $m/z$  consistent with  $[\text{M} + \text{NH}_4 - \text{HOR}]^+$  were observed for esters with  $n=4$ , e.g. 0.4% of the sample ion-current for bis(2-ethylhexyl)hexane-dioate evidence for formation of such ions via loss of ROH from  $[\text{M}.\text{NH}_4]^+$  ions was only observed for  $n > 4$ . This may be a consequence of the low stability of intermediates in Scheme (3.1) when  $n=4$  precluded this pathway. However data obtained for



esters of higher  $n$  would appear to indicate that the length of alcoholic alkyl chain does not greatly impede substitution reactions in dibasic acid esters.

However, with the ability to assign both daughter and parent ions, using modern "metastable-mapping" techniques, the above fragmentation pathways could be readily verified or disproved. Such analysis was not carried out since the prime interest of the current study was to eliminate fragmentation and since the necessary equipment was not readily available. An appropriate investigation would be a useful adjunct to this work.

Since the ultimate aim was to obtain quantitative as well as qualitative data the effect of molecular size, branching of alcoholic alkyl groups, and the value of  $n$ , (as defined above), on sensitivity needed to be evaluated. Several factors should be considered in such an evaluation. First, ADO theory predicts that increased molecular size<sup>45</sup> should result in an increase in collision capture rate coefficients. Thus the rate of reaction of  $\text{NH}_4^+$  with  $M$  and the quantity of  $M.\text{NH}_4^+$  ions so produced for a given quantity of  $M$  is expected to increase with the mass of  $M$ . Secondly, mass spectrometer sensitivity is known to decrease with increasing ion mass. Finally, the effect of the lower volatility and high temperature required to volatilize higher mass molecules from the solid probe into the ion-source must be considered.

In Section (3.2.1.2) it was shown that very

little variation in relative sensitivities with compound molecular mass was observed provided the sample volatility was not so low that losses occurred during introduction of the probe into the ion-source. Additionally good reproducibility and a relative accuracy of  $\pm 3\%$  per component in an ester mixture was demonstrated. The accuracy obtained was better than expected and, considering the crudeness of the analytical method was excellent.

The analysis of an authentic sample, the blending component 'A' was simple and required the recording of spectra during volatilization, ~6 mins, at both high (ca. 0.6 Torr) and low (ca. 0.2 Torr) ammonia pressures. Reproducibility between two separate analyses of the sample was good. The molecular mass, type of ester, i.e. dibasic acid ester, number of methylene groups in the acidic moiety, and quantity of each component were readily determined. The ester type was easily deduced since esters of dibasic acids, 2-ethyl-2(hydroxymethyl)-propane-1,3-diol and 2,2,bis-(hydroxymethyl)-propane-1,3 diol have discrete masses. Additionally the type of dibasic acid was readily obtained from low pressure (0.2 Torr) ammonia CI by determining the mass of  $[M + H - 2R]^+$  ions, where R is the alcoholic alkyl group.

It is reasonable to compare the data obtained here to that which might have been obtained by other means. Molecular mass would normally be

estimated from capillary g.l.c. However the high boiling point and presence of isomers often makes total separation of components difficult. Once separation is achieved quantitation is relatively simple and the accuracy obtained is far greater than that achieved using ammonia CI mass spectrometry. The nature of esters, i.e. dibasic acid or neopentyl polyol cannot easily be determined by one method alone. Normally hydrolysis and further analysis of the acidic and alcoholic products is required. Ammonia CI obviously has much to offer in this area since ester type can be determined far quicker than by methods using hydrolysis.

Clearly although ammonia CI is not able to obtain as high an accuracy in quantitation as other methods the quantity of qualitative data obtained in a relative short time is impressive. Therefore although a definitive analysis may not be possible using ammonia CI the method is excellent for preliminary investigation of unknown ester fluids. It is hoped that it will rapidly find use in this important area.

#### 4.5.2 Hydrogenated polyalpha-olefin base oils.

Chemical ionization of low molecular mass hydrocarbons is well documented and a brief review can be found in Section (1.3). When analysing higher molecular weight compounds although considerable fragmentation is observed the  $(M-H)^+$  ions are readily discernable in the spectra of synthetic hydrocarbon mixtures, see Figure (3.24).

Using the mass of the observed  $(M-H)^+$  ion the carbon numbers of the alkane components of base oils were readily obtained, see Table (3.18). Since the components were known to result from polymerisation of alkenes it is of interest to speculate whether the alkenes used in their preparation can be deduced from the carbon number of the oligomers. In the case of SHC-2, two oligomers of carbon numbers 20 and 30 were observed, suggesting that they have been prepared from decenes. However not all the oils studied contained oligomers of a single alkene. The base oil SHC-5 contains oligomers with carbon numbers 28, 30, 32, 42, 44, 46, 48 and therefore cannot result from the polymerisation of a single alkene. Neither would the blending of two base oils, prepared from two alkenes having different carbon numbers give the above distribution of components. However a co-polymerisation of  $C_{14}$  and  $C_{16}$  alkenes would result in the following oligomers:

$$C_{28} = 2 \times C_{14}, \quad C_{30} = C_{16} + C_{14}, \quad C_{32} = 2 \times C_{16},$$

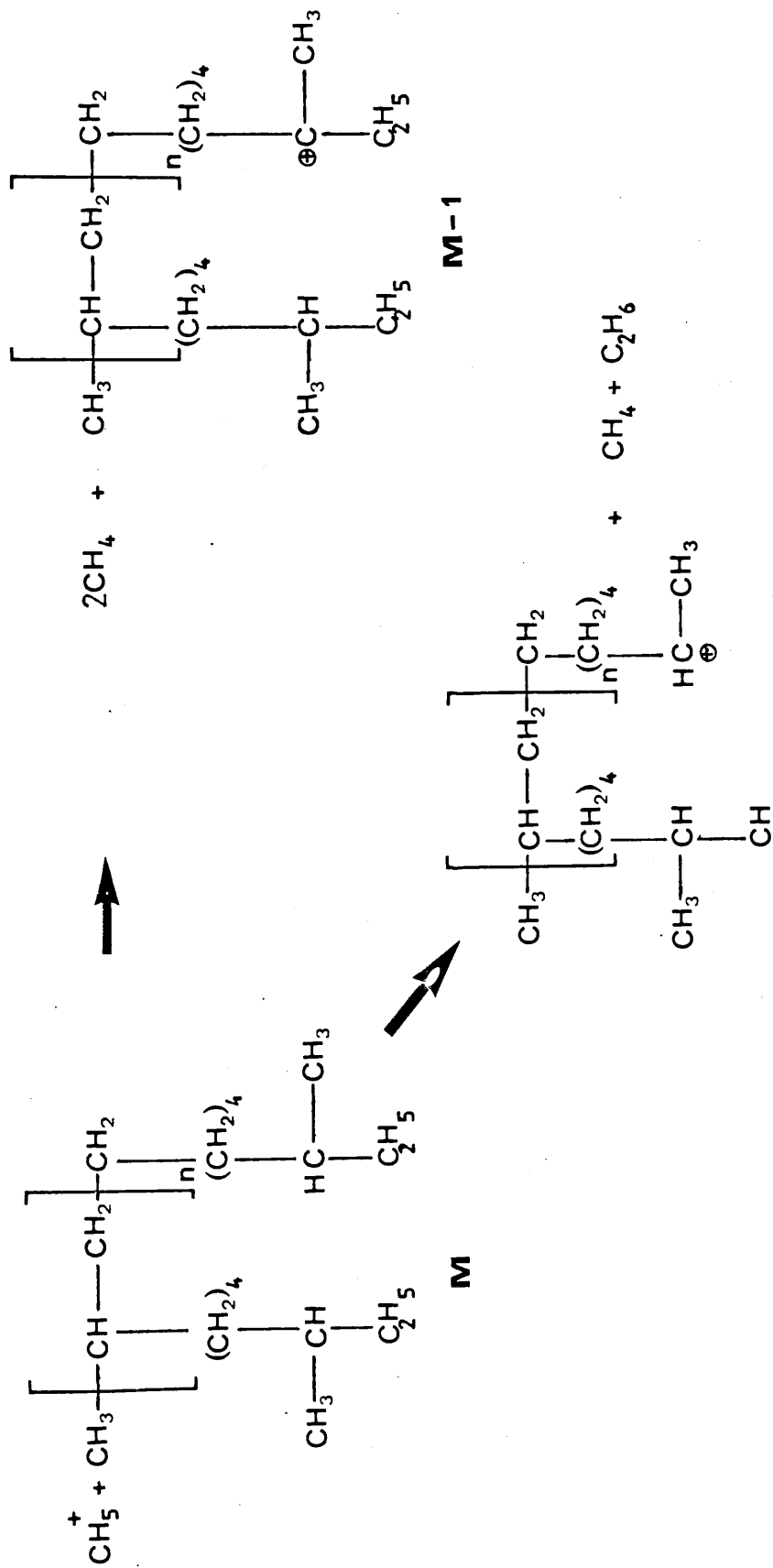
$$C_{42} = 3 \times C_{14}, \quad C_{44} = C_{16} + 2 \times C_{14}, \quad C_{46} = 2 \times C_{16} + C_{14}$$

$$\text{and } C_{48} = 3 \times C_{16}.$$

It is possible therefore, from the CI spectrum, to give a reasonable indication of the alkene or alkenes used to prepare the base oil and to distinguish whether the fluid is a blend or co-polymer. Table (4.10) lists possible origins of the fluids studied. However assignment of parent alkenes becomes difficult when more than one is used with carbon number < 6, e.g. SHC-16-19.

As stated in Section (1.3), fragment ions resulting from either the loss of  $\text{CH}_3 \cdot$  or  $-(\text{CH}_2)_{n-3}-\text{CH}_3$ , (where n is the number of carbons in the parent alkene), should be the most abundant since these will produce secondary carbonium ions. However some base oils give  $(\text{M}-\text{C}_2\text{H}_5)^+$  ions that are more abundant than  $(\text{M}-\text{CH}_3)^+$ . Scheme (4.4) gives the structure and possible fragmentation of oligomers derived from the polymerisation of 7-methyl non-1-ene. Howard, McDaniel, Nelson and Blomquist<sup>25</sup> have demonstrated that fragmentation by  $\alpha$ -cleavage at a methyl branch is particularly facile. This would result in abundant  $(\text{M}-\text{C}_2\text{H}_5)^+$  ions. Therefore it is possible that the base oils SHC 20,21,22,23 were prepared from 7-methyl-non-1-ene. Another particularly interesting oil is SHC-1, a hydrogenated polybutene, whose mass spectrum shows particularly abundant  $(\text{M}-\text{CH}_3)^+$  ions. See Table (3.19).

SCHEME 4.4 Fragmentation of poly-7-methyl-non-1-ene.

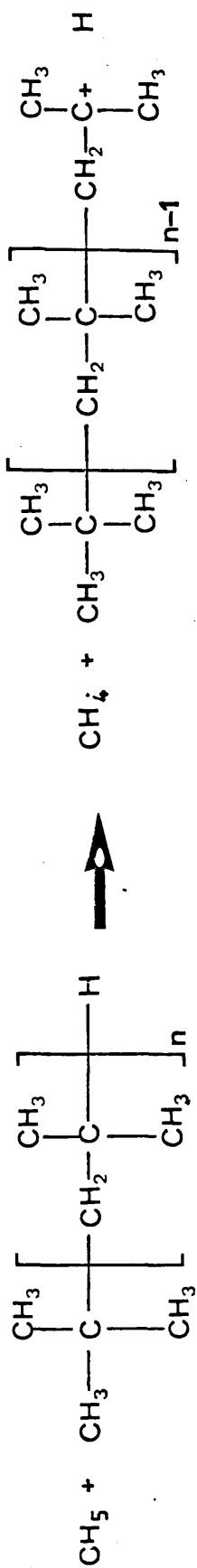


As seen in Scheme (4.5) poly-2-methyl-prop-1-ene is expected to exhibit abundant  $(M-CH_3)^+$  ions owing to its high 'density' of methyl branches.

When hydrogenated polyalphaolefins are analysed by gas chromatography quantitative data is easily obtained. Unfortunately under the conditions used in the methane CI study the relative ion-currents of  $(M-H)^+$  ions are low, (often < 10% of the total ion current) the greater part of the ion-current being due to fragment ions, the intensities of which vary with molecular structure. Quantitation by monitoring a particular ion for each component, as demonstrated in the ammonia CI of esters, was not possible. Methane spectra of insect derived cuticular alkanes,<sup>25</sup> show little fragmentation, at ion-source pressures ~ 0.5 Torr. Operation at pressures greater than 0.25 Torr was not possible in this work since it resulted in considerable reduction in sensitivity of the mass spectrometer, for the reasons given in Section (4.5.1). Therefore although both the molecular mass and parent alkene structure of hydrogenated polyalphaolefins was obtainable the method could not be used to produce quantitative data.

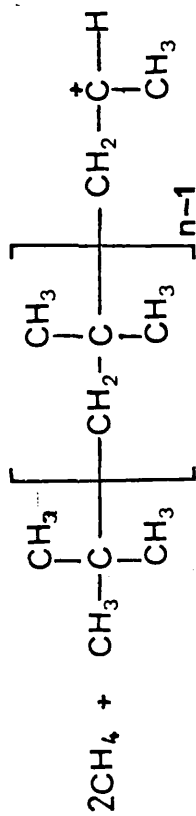
In order to reduce the fragmentation a lower energy transferring species than  $CH_5^+$  is required.  $NO^+$  formed by the ionization of nitric oxide has this characteristic. Hunt and Harvey<sup>71</sup> showed that the energy of hydride transfer between  $NO^+$ , produced in  $NO/N_2$

SCHEME 4.5 Fragmentation of poly-2-methyl-prop-1-ene.



**M**

**M-1**



**M-15**



TABLE 4.10 (A)

Structural information gained from methane chemical ionization mass spectrometry of hydrogenated polyalpha-olefin base oils.

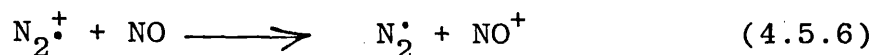
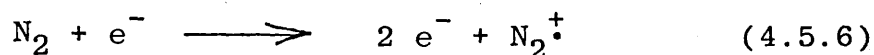
Base oil	Carbon number of principal components	Alkene(s) polymerised	Special notes
SHC-1	C <sub>20</sub> , C <sub>24</sub> , C <sub>28</sub> , C <sub>32</sub>	C <sub>4</sub> alkene	Very high relative abundance of (M-15) ions observed. May arise from 2-methyl-prop-1-ene
SHC-2	C <sub>30</sub> little C <sub>20</sub>	Dec-1-ene	
SHC-3	C <sub>30</sub> , C <sub>40</sub>	Dec-1-ene	
SHC-4	C <sub>30</sub> , C <sub>40</sub>	Dec-1-ene	
SHC-5	C <sub>42</sub> , C <sub>44</sub> , C <sub>46</sub> little C <sub>28</sub> , C <sub>30</sub> , C <sub>32</sub> , C <sub>48</sub>	C <sub>14</sub> and C <sub>16</sub> alkenes	Carbon number of ions observed indicates a co-polymer of C <sub>14</sub> and C <sub>16</sub> alkene similar to SHC-5.
SHC-6	C <sub>42</sub> , C <sub>44</sub> , little C <sub>48</sub>	C <sub>16</sub> , C <sub>14</sub>	
SHC-7	C <sub>24</sub> , C <sub>32</sub>	Oct-1-ene	
SHC-8	C <sub>24</sub> , C <sub>32</sub> , C <sub>40</sub>	Oct-1-ene	
SHC-9	C <sub>20</sub>	Dec-1-ene	
SHC-10	C <sub>30</sub>	Dec-1-ene	
SHC-11	C <sub>30</sub> , C <sub>40</sub>	Dec-1-ene	
SHC-12	C <sub>40</sub>	Dec-1-ene	
SHC-13	C <sub>24</sub> , C <sub>32</sub>	Oct-1-ene	



TABLE 4.10 (C) Structural information gained from methane chemical ionization mass spectrometry of hydrogenated polyalpha-olefin base oils.

Base oil	Carbon number of principal components	Alkene(s) polymerised	Special notes
SHC-24	)	)	)
SHC-25	)	)	)
SHC-26	)	)	)
	Even carbon number		Unlikely that origin was alkenes
	C <sub>20</sub> - C <sub>40</sub>		)
SHC-27	C <sub>24</sub> , C <sub>32</sub>	Oct-1-ene	)
SHC-28	C <sub>30</sub> , C <sub>40</sub>	Dec-1-ene	)
SHC-29	C <sub>30</sub> , C <sub>40</sub>	Dec-1-ene	)

mixture, by the reactions given in equations (4.5.5) and (4.5.6), was considerably less ( $\sim 110 \text{ kJ mol}^{-1}$ ) than for



reaction of  $\text{CH}_5^+$ . The near zero enthalpy of reaction means little excess internal energy is given to the resulting  $(\text{M-H})^+$  ion. Accordingly little fragmentation occurred, e.g.  $\text{C}_{10}\text{H}_{21}^+$ ; more than 80% of the sample ion-current is carried by this ion. In this study  $\text{NO}/\text{N}_2$  reagent gas was used at the same ion-source pressure as previously used for methane, viz 0.2 Torr. A dramatic reduction in fragmentation, whilst monitoring sensitivity was observed. See Section (3.2.2.3). The possibility of obtaining semi-quantitative data in a manner similar to that used for the ester fluids could now be realised. It is necessary however to overcome the problem of both setting the  $\text{NO}:\text{N}_2$  partial pressure ratio and determining the total ion-source pressure in the absence of an ion-source pressure gauge. Additionally, although the rates of reaction of  $\text{CH}_5^+$  with alkanes have been extensively studied,<sup>136</sup> very few rate coefficients for reaction of  $\text{NO}^+$  with organic compounds have been obtained. Clearly a greater understanding of ion-molecule reactions between  $\text{NO}^+$  and hydrocarbons is required, to ascertain whether reaction rates and thus CI sensitivities are structure dependent. Then true quantitation should be

achieved.

One concludes that at present, gas chromatography should be used if absolute quantitation of known materials is required. Methane CIMS provides information regarding molecular mass and parent alkene structure and NO/N<sub>2</sub> CIMS can give molecular mass and some semi-quantitative data.

#### 4.5.3 Synthetic aromatic hydrocarbon lubricants

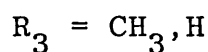
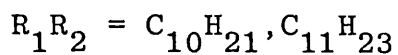
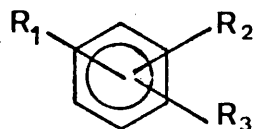
These fluids are typically prepared by polymerisation of simple aromatic hydrocarbons. The resulting fluids have found use in large electrical transformers as coolants. Their use in automotive lubricants is limited and thus only small quantities are produced. It is probably for these reasons that little information on their analysis is found in the literature. Therefore each fluid has to be treated as a complete unknown and analysis by a variety of techniques is often required to obtain a structural picture.

Since the material is known to be aromatic, the molecular mass of components should be readily obtainable from fluorobenzene chemical ionization mass spectrometry using methods similar to those described for ester analysis, see Section (3.2.1). Reaction of fluorobenzene with aromatic compounds has been shown to produce only molecular ions and sensitivities are expected to be practically independent of structure (see Section (4.4)). Accordingly the mass and relative abundance of the ions in Tables (3.21.1) and (3.21.2) will correspond to those of the aromatic components present. They are grouped according to their probable structures, see Scheme (4.6).

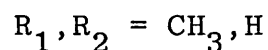
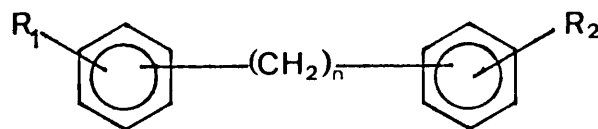
The principal component of fluid SAH2 has mass 236 which can correspond to diphenylcyclohexane. A compound of mass 312 also observed, similarly can

SCHEME 4.6 Chemical structures of synthetic aromatic lubricant components.

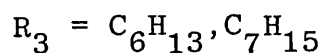
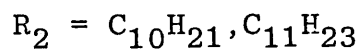
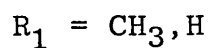
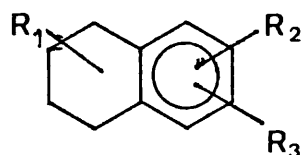
(A) Alkylbenzenes



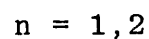
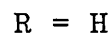
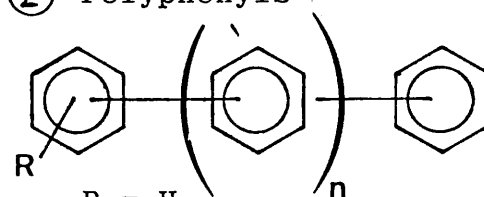
(B) Diphenylalkanes



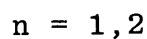
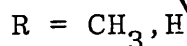
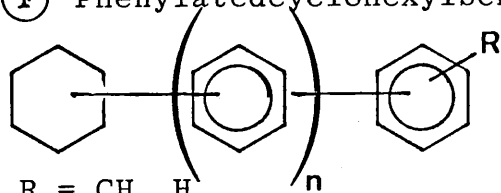
(C) Alkyltetrahydronaphthalenes



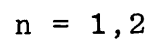
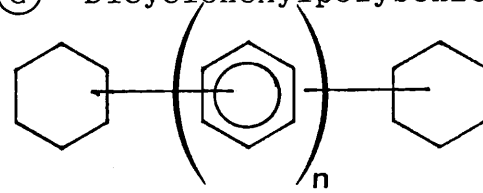
(E) Polyphenyls



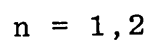
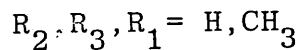
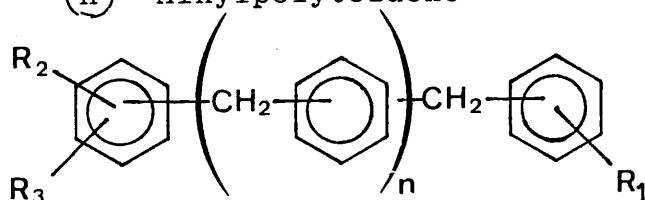
(F) Phenylatedcyclohexylbenzene



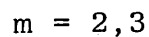
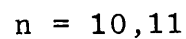
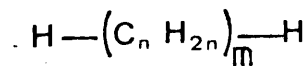
(G) Dicyclohexylpolybenzer



(H) Alkylpolytoluene



(D) Alkanes



correspond to cyclohexyl phenyl-phenylbenzene. The other components have masses characteristic of polyphenyls (structure E) and dicyclohexyl-polyphenyls (structure G), which are likely impurities from the preparation of diphenylcyclohexane.

SAH2 has components with molecular masses expected for compounds resulting from the polymerisation of toluene having small quantities of benzene and xylenes as impurities, see structure H, Scheme (4.6).

Some synthetic aromatic fluids are prepared by alkylation of benzene and toluene. Often alkenes are utilised for such preparations resulting in production of long chain alkanes as by-products. These would not have been ionized by fluorobenzene so each fluid was also analysed by NO/N<sub>2</sub> chemical ionization mass spectrometry. The NO<sup>+</sup> ion generated in NO/N<sub>2</sub> reagent gas reacts with aromatic hydrocarbons by charge transfer and aliphatic compounds by hydride transfer giving ions that are easily distinguishable by their odd masses, provided they do not contain odd numbers of nitrogen atoms. Only fluid SAH1 was found to contain alkanes. See Table (3.20). These had carbon numbers of 20, 21, 22 and 30. By arguments similar to those used in the assignment of hydrogenated polyalphaolefin monomers, section (4.5.2), the alkanes observed in SAH1 probably result from polymerisation of decene and undecene. From the fluorobenzene spectra the principal aromatic components of



SAH1, structure A, Table (3.20), have those masses expected for benzene and toluene poly-alkylated by decene and undecene. The other aromatic components, structures B and C, Scheme (4.6), are plausible by-products of alkene alkylation of benzene and toluene.

Thus the molecular mass, possible structure and relative abundance of the components in synthetic aromatic fluids were relatively easily determined from a combination of fluorobenzene and NO/N<sub>2</sub> chemical ionization mass spectrometry. The accuracy of quantitation is limited by the same constraints as already discussed for the analysis of both esters, (4.5.1) and hydrogenated poly-alphaolefins, (4.5.2). Additionally their synthetic origin may be postulated. The three fluids were independently analysed<sup>‡</sup> by more conventional methods when the same structural conclusions were reached. However for this far greater time and effort were required. The short analysis time for the CI analysis, ca 20 mins, and its simplicity makes it ideal for a quick initial inspection of an unknown fluid. The method also demonstrates the value of discriminatory ionization of compounds of different chemical types for the simplification of direct mass spectrometric analysis of unknown mixtures.

---

<sup>‡</sup> Private communication with Burmah Castrol Company.

#### 4.5.4 Mineral oil analysis

Over the years a great deal of effort has been expended developing methods for the analysis of aromatic components in hydrocarbon mixtures. This is because aromatic material can drastically affect both physical and chemical properties of the hydrocarbon fluid. Viscosity, additive solubility, rubber compatibility and pour point are affected by the type of aromatic material present. Additionally, the total aromatic content affects thermal and oxidation stability of the fluid. High aromatic contents are detrimental. Therefore determination of both total aromatic content and compound type is required.

In the current study fluorobenzene chemical ionization has been utilised for the analysis of aromatics without prior separation. The initial results gained are encouraging with good reproducibility of quantitative and qualitative data. Other mass spectrometric methods have been used in the past, notably electron impact,<sup>16</sup> but such analysis requires prior separation of the aromatic components by liquid chromatography. Qualitative data has been acquired for hydrocarbon fluids<sup>91,137</sup> with a variety of boiling ranges using negative chemical ionization by  $\text{OH}^-$  ions generated from  $\text{N}_2\text{O}$  and low boiling hydrocarbons, e.g.  $\text{CH}_4$  or hexane. Unfortunately extension of this mass spectrometric method to provide quantitative data is not possible since response depends strongly on structural type. To date quantitation by chemical ionization has been limited to low boiling

fluids e.g. gas oils<sup>18,123</sup> and gasolines. In these studies samples were dissolved in chlorobenzene and introduced to the source via a batch inlet system. The solvent then acts as the reagent gas. When using chlorobenzene reagent gas in such a manner sample ionization results from several reagent gas ions, and there is always the possibility of different ions reacting preferentially with compounds of different types. No kinetic studies to evaluate this have been reported.

In the analysis reported here a constant source pressure of fluorobenzene was maintained resulting in an essentially monoionic plasma. Kinetic studies (4.4) have shown that, at least for alkyl benzenes, reactivity is expected to be independent of structure. Very low sample partial pressures were used to alleviate both possibilities of cascade type ionization, which has been observed when using cyclohexane reagent gas<sup>18</sup>, matrix effects leading to increased fragmentation, and to avoid reagent gas plasma saturation resulting in sensitivity changes. The possibility of the latter occurring was indicated by reductions in rates of reaction of the reagent gas ion  $C_6H_5F^+$  with samples at partial pressures greater than 4 m Torr, see Section (4.4).

Lubricant oils were volatilized into the source from the solids sample probe using a linear temperature gradient while spectra were continually

recorded. This results in a variation of total ion-current with time due to the volatilization profile of the sample. Schrank, Grigsby and Scheppelle<sup>138</sup> observed changes in mass spectrometer sensitivity with total ion-current. In order to maintain quantitation they used a feed back loop between the total ion current and the probe heater controller such that volatilization occurred at such a rate as to produce a constant total ion-current. In the present study it was felt that only limited control of volatilization rate would be achieved by such a feed back system. Accordingly, use was made of the low intensity ion,  $m/z=247$ , in the reagent gas plasma, which did not react with the sample, to correct sample ion-current for changes in mass spectrometer sensitivity.

To facilitate quantitation it was necessary to add a standard to the lubricant. Although it has been shown that sample independent standards<sup>139</sup> may be used in CIMS, in the current study an aromatic compound was required. Triphenylbenzene was chosen since it was readily available, had a mass greater than 300 Daltons (near to the mass range of lubricants ca. >280 Daltons) and its mass of 306 Daltons did not coincide with those of the major aromatic components, namely alkyl- and cycloalkylbenzenes. Although its use was found to be perfectly satisfactory for low boiling lubricants such as MIN.1, see Section (3.2.4), it was unsatisfactory for use with higher boiling fluids, e.g. MIN.2. This was manifest by low values for aromatic

contents of such fluids. In the case of MIN.2 the triphenylbenzene distilled from the probe prior to the sample rather than during sample vaporization. Clearly there is a need for several higher boiling standards to ensure good quantitation. Additionally standard mixtures should be examined to further evaluate the quantitation potential of the method.

Tentative structural assignments may be made based on the 'z' value, see Section (3.2.4) but only when the concentration of heteroaromatics is low. This is normally the case in lubricating fluids which are refined oils. However, should heteroaromatic compounds detection be specifically required or their concentration become significant, ca. >4% of aromatics, then other reagent gases which specifically ionize heteroaromatics should be sought. The concentration of such compounds so determined could then be subtracted from the fluorobenzene "total aromatic mass spectrum" to produce quantitative data on non-heteroaromatics. To date no such reagent gas exists for the specific analysis of e.g. sulphur heterocycles. Analysis of these is of particular importance to the lubricant industry owing to the adverse effect they have on lubricant life.

See Section (1.1).

However molecular mass distribution currently obtained using fluorobenzene is very useful in distinguishing different lubricants, as illustrated by MIN.1 and MIN.2 in Figure (3.28). Not only is the

boiling range difference clearly seen, in good agreement with results obtained from simulated distillation, but also the proportions of alkyl and cycloalkylbenzene are seen to be markedly different.

High pressure liquid chromatography (HPLC) is routinely used for the determination of both total aromatic content of hydrocarbon fluids and evaluation of relative proportions of polycyclic compounds. However it cannot provide the detailed information determined using fluorobenzene CIMS. Therefore once the quantitative approach has been more fully defined both by further kinetic studies and analysis of standard mixtures, data at least as good as that obtained in low voltage, low resolution EI mass spectrometry will be obtained but without the need for preconcentration of the aromatic compounds.

APPENDICESAPPENDIX IPolarizabilities and dipole moments of organic molecules.

Dipole moments and polarizabilities used in the estimation of: (a) ion-source residence times, by the ion mobility (equation (3.1.9), Section (3.1.1)), and (b) collision capture rate coefficients by ADO (averaged dipole orientation) theory<sup>45</sup> are given below.

Values of dipole moments for compounds in the gas phase were taken from tables. Where gas phase data was not available the phase or solution solvent in which determinations were made is appended.

Values of molecular polarizabilities were taken from tables.<sup>141,142</sup> Where experimental values were not available estimates were made from the Lippincott  $\delta$ -function potential.<sup>140</sup>

Compound name	Dipole moment † μD/ Debyes	Molecular polarizability	
		cal ‡ / Å <sup>3</sup>	expt
Iso-butane			8.14 <sup>a</sup>
Methylcyclopentane		10.85	11.03 <sup>a</sup>
Methylcyclohexane		12.66	12.80 <sup>a</sup>
Ammonia			2.26 <sup>b</sup>
Flurobenzene		10.23	9.86 <sup>b</sup>
Di-fluorobenzene		10.21	9.80 <sup>b</sup>
Benzene	0.02 (liq.)	10.29	10.32 <sup>a</sup>
Methylbenzene	0.37 (liq.)	12.07	10.26 <sup>a</sup>
Ethylbenzene	0.54 (CCl <sub>4</sub> soln.)	13.86	-
1,2 Dimethylbenzene	0.56 (benzene soln.)	} 13.86	14.2 <sup>a</sup>
1,3 Dimethylbenzene	0.35 ( " " )		
1,4 Dimethylbenzene	0.0		
n-Propylbenzene	0.36 (liq.)	} 15.66	-
iso-Propylbenzene	0.40 (liq.)		-
1,3,5 Trimethylbenzene	0.0		15.94 <sup>b</sup>
n-Butylbenzene	-	17.47	-
sec-Butylbenzene	-	17.47	-
iso-Butylbenzene	0.52 (benzene soln.)	17.47	-
n-Pentylbenzene	-	19.26	-
Cyclobenzylbenzene	0.62 (benzene soln.)	20.40	-

† Values taken from tables (Dig Dielect 1972, 1974, 1976).

‡ Calculated using Lippincott δ-function potentials (Ref.140)

a Values taken from tables (Ref.141).

b Values from work of Denbigh (Ref.142).



Compound name	Dipole moment <sup>†</sup> μD/ Debyes	Molecular polarizability	
		cal <sup>‡</sup> / Å <sup>3</sup>	expt.
Hexamethylbenzene	0.0	21.06	21.48 <sup>b</sup>
Thiophene	0.55	10.60	-
2-Methylthiophene	0.67	12.34	-
2,5 Dimethylthiophene	0.51	14.10	-
Furan	0.72 (benzene soln.)	7.23	7.23 <sup>b</sup>
2-Methylfuran	0.65	9.03	-
3-Methylfuran	1.03	-	-
2,5 Dimethylfuran	-	10.83	-
Napthalene	-	16.50	17.48 <sup>b</sup>
1-Methylnaphthalene	0.48 {Cyclobenzene}	12.28	-
2-Methylnaphthalene	0.45 { soln. }	-	-

<sup>†</sup> Values taken from tables (Dig Dielect 1972, 1974, 1976).

<sup>‡</sup> Calculated using Lippincott δ-function potentials (Ref.140)

a Values taken from tables (Ref.141).

b Values from work of Denbigh (Ref.142).

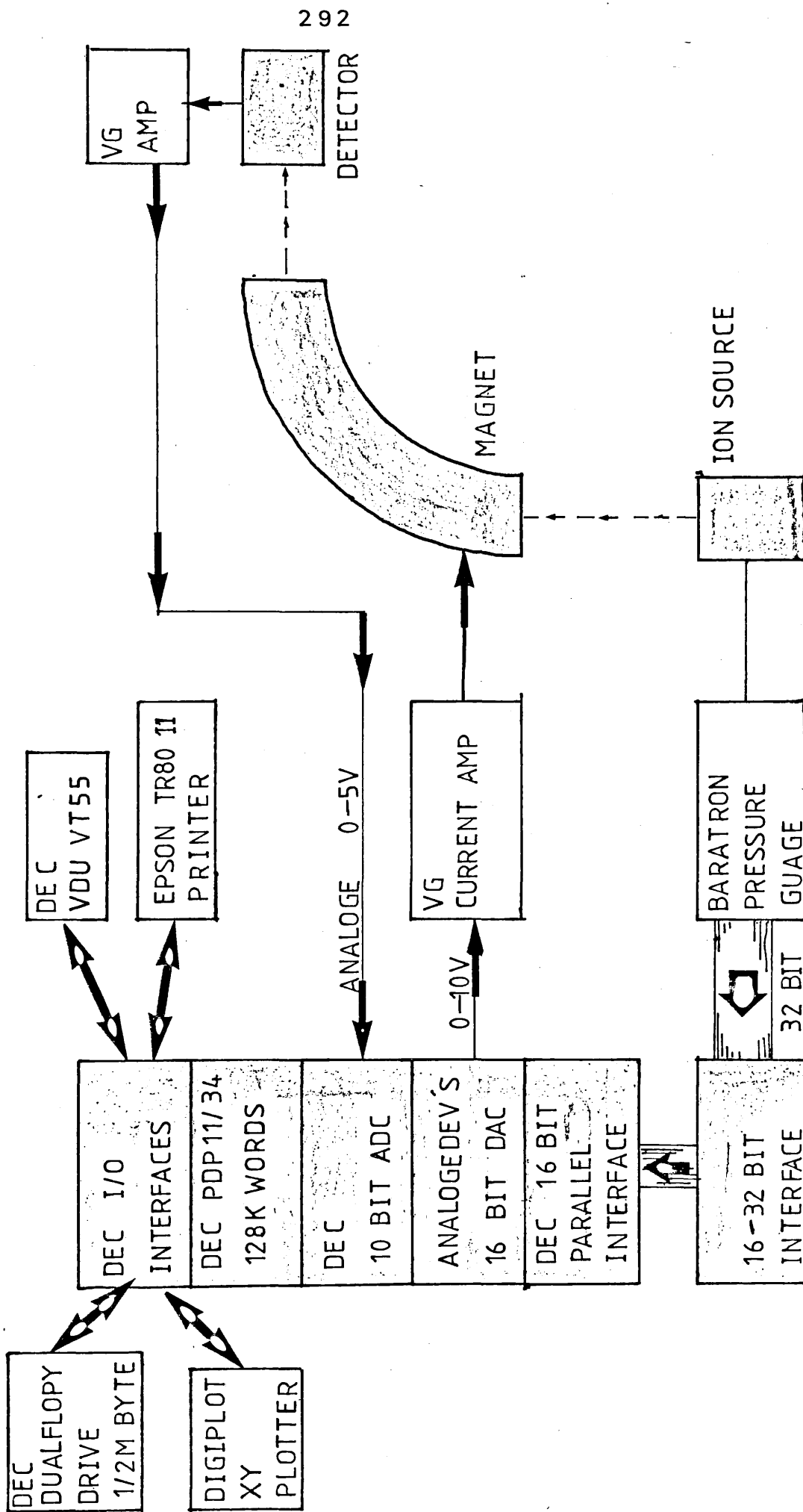
APPENDIX IIThe computer data system.

The hardware components of the system are given in Figure (II.1). The control software enabled the following:-

- Real time: - digital scan control
- data collection and peak thresholding
- Inter-scan: - peak area and mass calculation
- mass and intensity reporting
- Display/Hard copy - total ion-current plot
- reconstructed ion-current plots
- mass spectra plots
- tabulated spectra
- averaged spectra plot/table
- Long term data storage
- Direct ion-source pressure measurement

The user interacts with the system via a simple monitor program (written in FORTRAN IV) which facilitates control of: scan rate, scan start mass, signal threshold, data processing and data storage. Real time control and data acquisition is performed by routines written in machine code (MACRO-11). The scan mode used is exponential down. Data is collected at a digitisation rate of 30 kHz. Other routines (also written in FORTRAN IV) facilitate manipulation and display of the mass spectra data. A list of the commands available is given below.

**FIGURE (5.11.1) Computer Data System: HARDWARE**



The software was written by the author.

#### DATA SYSTEM CONTROL COMMANDS

Scan and acquisition commands

SS = set scan speed

AV = set accelerating voltage

LM = set last mass

RN = set number of scans

TH = set threshold value

Data storage

SN = no data stored

SD = temporary store only

ST = raw digital data stored

PE = mass/abundance data stored

Data processing

PN = no processing

PS = mass calculated

PA = mass/abundance found

PC = Time/area data found

Utilities

SE = list control parameters

CF = edit/create calibration file

CA = auto calibration

RT = Enter data manipulation routines

HP = Help file

Data manipulation

These commands can be activated by a single key on a secondary key pad of the VDU.

Display/Plot total ion current

Plot/Display reconstructed ion-current

Plot/Display mass spectra

List mass spectra number x to number y.

Average mass spectra between number  $x_1$  and  $y_1$

Plot/Display/List average mass spectra

Help Display.

APPENDIX IIIChemical and spectroscopic data of esters prepared as standards for ammonia CIMS.

Carbon and hydrogen elemental analysis was conducted on all compounds. The values obtained are given in Table (III.1).

All compounds were analysed by NMR and Infrared spectrometry. The data obtained from NMR is recorded in Table (III.2). The infrared spectra of the dibasic acid esters showed the same principal features, namely:

$\nu_{\max}$  (liquid) 2960(s) ( - CH<sub>3</sub> ), 2920(s) ( - CH<sub>2</sub> - ),  
2870(m) ( - CH - ), 1740(s) (saturated ester C=O),  
1465 (w) ( - CH<sub>2</sub> - ), 1380(w) ( - C - CH<sub>3</sub> ).

Similarly esters of the neopentyl polyols

2-ethyl-hydroxymethylpropane-1,3 diol and 2,2 bis(hydroxymethyl) propane-1,3 diol displayed:

$\nu_{\max}$  (liquid) 2960(s) ( - CH<sub>3</sub> ), 2940(s) ( - CH<sub>2</sub> - ),  
2880(m) ( - CH - ), 1740(vs) (saturated ester (C=O),  
1470(w) ( - CH<sub>2</sub> - ), 1380(w) (C - CH<sub>3</sub>), 1250(m), 1170(s)

(H -  $\begin{array}{c} \text{C} \\ | \\ \text{C} \\ | \\ \text{C} \end{array}$  - C - ).

TABLE III.1 Compound identity and elemental analysis

Identity	Compound name	Molecular formula	Found (%)	
			C	H
DBE-1	bis(2-ethylhexyl)hexanedioate	$C_{22}H_{42}O_4$	71.26 (71.31)	11.51 (11.42)
DBE-2	bis(2-ethylhexyl)heptanedioate	$C_{23}H_{44}O_4$	72.27 (71.83)	11.66 (11.53)
DBE-3	bis(2-ethylhexyl)octanedioate	$C_{24}H_{46}O_4$	72.63 (72.31)	11.75 (11.63)
DBE-4	bis(2-ethylhexyl)nonanedioate	$C_{25}H_{48}O_4$	72.78 (72.77)	11.83 (11.72)
DBE-5	bis(decyl)hexanedioate	$C_{26}H_{50}O_4$	73.61 (73.19)	11.91 (11.81)
DBE-6	bis(undecyl)hexanedioate	$C_{28}H_{54}O_4$	73.10 (73.95)	11.76 (11.97)
DBE-7	bis(dodecyl)hexanedioate	$C_{30}H_{58}O_4$	73.84 (74.64)	12.06 (12.11)
DBE-8	bis(nonane-2-ol)hexanedioate	$C_{24}H_{46}O_4$	(Requires) 73.05 (72.31)	11.86 (11.63)
TMPE-1	1,1,1-tris(pentylcarbonyloxymethyl)propane	$C_{21}H_{38}O_6$	(Calculated) 63.26 (65.26)	9.95 (9.91)
TMPE-2	1,1,1-tris(hexylcarbonyloxymethyl)propane	$C_{24}H_{44}O_6$	67.52 (67.26)	10.46 (10.35)

TABLE III.1 (continued)

Identity	Compound name	Molecular formula	Found (%)	
			C	H
TMPE-3	1,1,1-tris(heptylcarbonyloxymethyl)propane	$C_{27}H_{50}O_6$	69.30 (68.90)	10.96 (10.71)
TMPE-4	1,1,1-tris(octylcarbonyloxymethyl)propane	$C_{30}H_{56}O_6$	70.37 (70.27)	11.12 (11.01)
TMPE-5	1,1,1-tris(nonylcarbonyloxymethyl)propane	$C_{35}H_{62}O_6$	71.65 (71.44)	11.30 (11.26)
PE-1	1,3-propanediol 2,2 bis(pentylcarbonyloxymethyl)- dipentanoate	$C_{25}H_{44}O_8$	63.57 (63.53)	9.47 (9.38)
PE-2	1,3-propanediol 2,2 bis(hexylcarbonyloxymethyl)- dihexanoate	$C_{29}H_{52}O_8$	66.44 (65.88)	10.01 (9.91)
PE-3	1,3-propanediol 2,2 bis(heptylcarbonyloxymethyl)- diheptanoate	$C_{33}H_{60}O_8$	67.90 (67.77)	10.51 (10.34)
PE-4	1,3-propanediol 2,2 bis(octylcarbonyloxymethyl)- dioctanoate	$C_{37}H_{68}O_8$	69.44 (69.34)	10.77 (10.69)
PE-5	1,3-propanediol 2,2 bis(nonylcarbonyloxymethyl)- dinonanoate	$C_{41}H_{76}O_8$	70.89 (70.65)	11.15 (10.99)



TABLE III.2 50 MHz NMR Data

Compound ID	Solvent	Ref	$-\text{CH}_2-$	$-\text{CH}-$	$-\text{CH}_2-\text{C}(=\text{O})-\text{O}-$	$-\text{CH}_2-\text{O}-\text{C}(=\text{O})-$
TMPE-3	$\text{CDCl}_3$	TMS	$\delta$ 1.42 (26H, m)	-	$\delta$ 2.36 (6H, dist t, J6Hz)	$\delta$ 4.23 (6H, s)
TMPE-4	$\text{CDCl}_3$	TMS	$\delta$ 1.32 (32H, m)	-	$\delta$ 2.30 (6H, dist t, J6Hz)	$\delta$ 4.27 (6H, s)
TMPE-5	$\text{CDCl}_3$	TMS	$\delta$ 1.34 (38H, m)	-	$\delta$ 2.32 (6H, dist t, J5Hz)	$\delta$ 4.10 (6H, s)
PE-1	None	TMS	$\delta$ 1.52 (16H, m)	-	$\delta$ 2.32 (8H, dist t, J6Hz)	$\delta$ 4.22 (8H, s)
PE-2	None	TMS	$\delta$ 1.42 (24H, m)	-	$\delta$ 2.56 (8H, dist t, J6Hz)	$\delta$ 4.15 (8H, s)
PE-3	None	TMS	$\delta$ 1.42 (32H, m)	-	$\delta$ 2.36 (8H, dist t, J6Hz)	$\delta$ 4.14 (8H, s)
PE-4	None	TMS	$\delta$ 1.35 (40H, m)	-	$\delta$ 2.36 (8H, m)	$\delta$ 4.2 (8H, s)
PE-5	None	TMS	$\delta$ 1.32 (48H, m)	-	$\delta$ 2.5 (8H, m)	$\delta$ 4.25 (8H, s)
DBE-1	None	TMS	$\delta$ 1.32 (20H, m)	$\delta$ 1.6(2H, m)	$\delta$ 2.28 (4H, m)	$\delta$ 4.03(4H, d, J5Hz)
DBE-2	None	TMS	$\delta$ 1.31 (22H, m)	$\delta$ 1.44(2H, m)	(4H, dist, t, J5Hz)	(4H, d, J4Hz)
DBE-3	None	TMS	$\delta$ 1.35 ((26H, m)	$\delta$ 1.45	$\delta$ 2.25 (4H, dist t, J7Hz)	$\delta$ 4.03 (4H, d, J4Hz)

continued/

# See Table (III.1)

TABLE III.2 (continued)

Compound ID <sup>#</sup>	Solvent	Ref	-CH <sub>3</sub>	-CH <sub>2</sub> -	-CH-	-CH <sub>2</sub> -C(=O)-	-CH <sub>2</sub> -O-C(=O)-
DBE-4	None	TMS	δ 0.92 (12H, dist t, J5Hz)	δ 1.34 (28H, m)	δ 1.55	δ 2.24 (4H, dist t, J6Hz)	δ 4.04 (4H, d, J4Hz)
DBE-5	CCl <sub>4</sub>	TMS	δ 0.9 (6H, m)	δ 1.31 (36H, m)		δ 2.27 (4H, m)	δ 4.03 (4H, t, J6Hz)
DBE-6	CCl <sub>4</sub>	TMS	δ 0.88 (6H, m)	δ 1.34 (40H, m)		δ 2.28 (4H, m)	δ 4.06 (4H, t, J6Hz)
DBE-7	CDCl <sub>3</sub>	TMS	δ 0.88 (6H, dist t, J5Hz)	δ 1.33 (44H, m)		δ 2.34 (4H, dist t, J7Hz)	δ 4.12 (4H, t, J7Hz)
DBE-8	CDCl <sub>3</sub>	TMS	δ 0.88, δ 1.12 (12H, dist t, J6Hz)	δ 1.34 (28H, m)		δ 3.36 (2H, m)	δ 4.88 (4H, m)
TMPE-1	CDCl <sub>3</sub>	TMS	δ 0.96 (19H, m)	δ 1.48 (14H, m)		δ 2.36 (6H, m)	δ 4.14 (6H, s)
TMPE-2	CDCl <sub>3</sub>	TMS	δ 0.89 (12H, dist, t, J6Hz)	δ 1.34 (20H, m)		δ 2.27 (6H, dist t, J6Hz)	δ 4.05 (6H, s)

<sup>#</sup> See Table III.1

REFERENCES

1. Matthews, D.M., J. Am. Oil Chem. Soc., 56, 841A, (1979).
2. Freedman, P., Lubrication and friction. Sir Isaac Pitman and Son Ltd., London (1962).
3. Potter, R.I., in Society of automotive engineers proceedings of fuels and lubricants meeting. St Louis, Missouri (1976) p.7.
4. Byford, D.C. and Edgington, P.G., Erdoch Kohle, Erdgas, Petroleum 22, (11), 694, (1969)
5. Brennan, J.A., in Proceedings of symposium on Chemistry of synthetic lubricants and additives. (1970) p.827.
6. Sniegowski, P.J. ASLE Trans., 12, 273 (1969).
7. Fick, N.H., Sudbury, B., and Bradley, M.P.T. Anal. Chem. 53 (5), 94R-IRR, (1981).
8. Petroleum products and lubricants (1 -111) Annual book of ASTM standards (1980) Parts 23-25
9. Clutter, D.R., Petrakis, L., Stenger Jr., R.L., and Jensen, R.K., Anal. Chem., 44, 1395 (1972).
10. Ozubbo, R.S., Clugston, D.M. and Furlmsky, E., Anal. Chem. 53, 183 (1981).
11. Brandes, G., Brennst. Chem., 37, 263, (1956).
12. ASTM Methods D-1017. Ann. book ASTM standards, 23, (1980)
13. ASTM Methods D-1840 and D-2269. Ann book ASTM standards, 24, (1980).
14. ASTM Methods D-2786, D-2789, D-2425 Ann. book ASTM standards, 24, (1980).

15. Gallegos, E.J. et al., Anal.Chem., 39, 1833, (1967).
16. Lumpkin, H.E., Anal.Chem., 36, 2399 (1964).
17. Levin, R.D., Lias, S.G.; "Ionization Potential and Appearance Potential Measurements, 1971-1981", NSRDS-NBS Series No.71, (1982).
18. Sieck, L.Wayne, Anal.Chem., 51, 128 (1979).
19. Burke, P., Jennings, K.R., Morgan, R.P., and Gilchrist, C.A., Anal.Chem. 54, 1304, (1982).
20. Sieck, L.Wayne, Chem.Br., 16, 38 (1980).
21. ASTM Methods D-3710 and D-2887. Ann.book of ASTM standards (1980), Parts 24 and 25.
22. ASTM Methods D-76 and D-1160 Ann.book of ASTM standards (1980), Part 23.
23. Zeman, A., Zer.Anal.Chem., 310, 243 (1982).
24. Dnuska, F.I., J.Chromatog., 186, 259 (1979).
25. Howard, R.W., McDaniel, C.A., Nelson, D.R. and Blomquist, G.J., J.Chem.Ecol., 6, 609, (1980).
26. Stavinoha, L.L., Fodor, G.E., Newman, F.M., and Lestz, S.J., ASLE Trans., 21, 217 (1978).
27. Beynon, J.H., Mass Spectrometry and its applications to Organic Chemistry, Elsevier, Amsterdam (1960).
28. McFadden, W.H., Techniques of Combined Gas Chromatography/Mass spectrometry, Wiley-Interscience, New York (1972).
29. Dempster, A.J., Phil.Mag. 31, 438 (1916).
30. Hognes, T.R. and Lunn, E.G. Phys.Rev., 26, 44 (1925).

31. Smyth, H.D., Phys. Rev., 25, 452 (1925).
32. Smyth, H.D., Rev.Mod.Phys., 3, 347 (1931).
33. Hogness, T.E. and Harkness, R.W., Phys.Rev., 32, 784 (1928).
34. Eyring, H., Hirshfelder, J.O. and Taylor, H.S., J.Chem.Phys., 4, 479 (1936).
35. Stevenson, D.P., and Schissler, D.O., J.Chem.Phys., 29, 282 (1958).
36. Stevenson, D.P., and Schissler, D.O., J.Chem.Phys., 23, 1353 (1955).
37. Field, F.H., Franklin, J.L. and Lampe, F.W., J.Amer.Chem.Soc., 79, 2419 (1957).
38. Tal'roze, V.L., and Lyubimova, A.K., Dokl.Akad.Nauk, SSSR, 86, 909 (1952).
39. Munson, M.S.B., and Field, F.H., J.Amer.Chem.Soc., 87, 3294 (1965).
40. Munson, M.S.B., and Field, F.H., J.Amer.Chem.Soc., 87, 4242 (1965).
41. Munson, M.S.B., and Field, F.H., J.Amer.Chem.Soc., 88, 2621 (1966).
42. Field, F.H., and Lampe, F.W., J.Amer.Chem.Soc., 80, 5587 (1958).
43. Kebarle, P., NATO Adv.Study.Inst.Ser., Ser.B., B.6 (Interact.Ions.Mol.), Ausloos, P., Ed., Plenum Press, New York (1975) p.459.
44. Borkowski, R.P., and Ausloos P., J.Chem.Phys., 39, 818 (1963).

45. Su, T., and Bowers, M.T., J.Chem.Phys., 58, 3027 (1973).
46. Su, T., Su, E.C.F., and Bowers, M.T., J.Chem.Phys., 69, 2243 (1978).
47. Munson, M.S.B., Anal.Chem., 49, 772 (1977).
48. Jennings, K.R., in Gas Phase Ion Chemistry. Vol.II, Bowers, M.T., Ed., Academic press, London (1979). p.124.
49. Jennings, K.R., in Mass Spectrometry, Johnstone, R.W.A., Ed., (Special Periodical Reports) The Chemical Society, London (1977). Vol.4, p.203
50. Munson, M.S.B., NATO.Adv.Study Inst.Ser., Ser.B., B.6. (Interact. Ions.Mol), Ausloos, P., Ed., Plenum Press, New York (1975), p.505.
51. Meot-Ner, M., and Field, F.H., J.Chem.Phys., 64, 277 (1976).
52. Thesis. R.Walder. "Kinetics of some ion-molecule reactions associated with chemical ionization mass spectrometry". London (1979).
53. Rabinowitz, E., Trans.Faraday Soc., 33, 283 (1937).
54. Bohme, D.K., Dunkin, D.B., Fehsenfeld, F.C., and Ferguson, E.E., J.Chem.Phys., 49, 5201 (1968).
55. Meot-Ner, M., and Field, F.H., J.Amer.Chem.Soc., 97, 5339 (1975).
56. Meot-Ner(Mautner), M., in Gas Phase in Chem., Vol.1., Bowers, M.T., Ed., Academic press, London (1979). p.197-271.

57. Bohme, D.K., NATO Adv.Study Inst.Ser., Ser.B., B.40. (Kinet.Ion-Mol.React.) Ausloos, P., Ed., Plenum Press, New York (1979). p.323.
58. Ferguson, E.E., and Frank, A., Acc.Chem.Res., 14, 327 (1981).
59. Smith, D., and Adams, N.G., NATO Adv.Study Inst.Ser., Ser.B., B.40. (Kinet.Ion-Mol.React.), Ausloos, P., Ed., Plenum Press, New York (1979). p. 345.
60. Lias, S.G., and Ausloos, P., Ion-Molecule Reactions, American Chemical Society, Washington, D.C. (1975).
61. Laudenslager, J.B., NATO. Adv.Study.Inst.Ser., Ser.B., B.40 (Kinet.Ion-Mol.React.), Ausloos, P., Ed., Plenum press, New York (1979). p.405.
62. Tal'rose, V.L. and Frankevich, E.L., Zh.Fiz.Khim., 34, 2709 (1960).
63. Anders, L.R., Beauchamp, J.L., Dunbar, R.C., and Balderschwiler, J.D., J.Chem.Phys., 45, 1062 (1966).
64. Henschman, M., in Ion-Molecule Reactions, Vol.1., Franklin, J.L. Ed., Plenum press, New York (1972).
65. Fehsenfeld, F.C., Ferguson, E.E., and Schmeltekopf, A.L., J.Chem.Phys., 45, 1844 (1966).
66. Smith, D., and Adams, N.G., in Gas Phase Ion Chemistry, Bowers, M.T., Ed., Academic press, London (1979). p.2.
67. Field, F.H., Munson, M.S.B., and Becker, D.A., Adv.Chem.Ser., 58, 167 (1966).
68. Field, F.H., J.Amer.Chem.Soc., 90, 5649 (1968).

69. Field, F.H., and Munson, M.S.B., J.Amer.Chem.Soc., 89, 4272 (1967).
70. Field, F.H., and Munson, M.S.B., J.Amer.Chem.Soc., 89, 1047 (1967).
71. Hunt, D.F., and Harvey, T.M., Anal.Chem., 47, 1965 (1975).
72. Meot-Ner, M., and Field, F.H., J.Amer.Chem.Soc., 97, 5339 (1975).
73. Neilson, P.V., Bowers, M.T., Chau, M., Davidson, W.R., and Ave, D.H., J.Amer.Chem.Soc., 100, 3649 (1978).
74. Arshadi, M.R., and Futrell, J.H., J.Phys.Chem., 78, 1482 (1974).
75. Keough, T., and De Stefano, A.J., Org.Mass Spectrom., 16, 527 (1981).
76. Dougherty, R.C. et al., J.Org.Chem., 39, 451 (1974).
77. Dzidic, I., McCloskey, J.A., Org.Mass Spectrom., 6, 939 (1972).
78. Maquestiau, A., Flammarg, R., and Nielsen, L., Org.Mass Spectrom., 15, 376 (1980).
79. Weinkam, R.J., and Gal, J., Org.Mass Spectrom., 11, 197 (1976).
80. Vine, J., J.Chromatogr. 196, 415 (1980).
81. Buchanan, M.V., Anal.Chem., 54, 570 (1982).
82. Haegele, K.D., and Desiderio, D.M., Jr., J.Org.Chem., 39, 1078 (1974).
83. McCloskey, J.A., and Futrell, J.H., et al., J.Amer.Chem. Soc., 95, 5762 (1973).



84. Base, A.K., Fujiwara, H.P., Birendra, N., Lazara, E., and Spillert, C.R., Anal.Biochem., 89, 284 (1978).
85. Luijten, W.C.M.M., Onkenhout, W., and Thuijl, J. van., Org.Mass Spectrom., 15, 329 (1980).
86. Ryhage, R., and Brandenberger, H., Biomed. Mass Spectrom., 5, 615 (1978).
87. Guieze, J., Devant, G., and Loyaux, D. Int.J.Mass Spec. Ion Phys., 46, 313 (1983).
88. Karger, B.L., Petersen, B.A., Vouros, P., Colwell, L., Anal.Chem., 49, 1039 (1979).
89. Hunt, D.F., and Sethi, S.K., Acs.Symp.Ser. 1978, 70, (High Perform. Mass Spectrom. Chem.Appl.) D.150
90. Buchanan, M.V., Anal.Chem., 54, 570 (1982).
91. Burke, P., Jennings, K.R., Morgan, R.P., and Gilchrist, C.A., Anal.Chem., 54, 1304 (1982).
92. Morgan, R.P., Gilchrist, C.A., Jennings, K.R., and Gregor, I.K., Int.J.Mass Spec.Ion Phys., 46, 309 (1983).
93. Feagan, Jr.R.A., and Copenhagen, J.E., J.Amer Chem.Soc., 62, 869 (1940).
94. Reith, H. and Eckardt, H. Freiberger Forschugoh A250 39 (1962).
95. Murai, K. and Akazonie, A., et al., J.Oil Chem.Soc., 3, 2 (1954).
96. Itsikson, T.M., Rapoport, I.B., and Mikheen, V.A., Khim.Technol.Topl.Masel., 14 (4) 47 (1969).
97. Breusch, F.L., and Oguzer, M., Chem.Ber., 1511, (1955)
98. V.G.Analytical Ltd., Altrincham, Cheshire, England.
99. Comark Electronics Ltd., Rustington, Sussex, England.

100. La Lau, C., in Topics in Organic Mass Spectrometry, Burlingame, A.L., Ed., Wiley-Interscience, New York (1969), p.93.
101. S.E.Laboratories Ltd., Feltham, Middlesex, England.
102. MKS. Instruments Inc., 22 Third Avenue, Burlington, Massachusetts, U.S.A.
103. Digital Equipment Co., Maynard, Massachusetts, U.S.A.
104. Pyrofilm Corp., 60 South Jefferson Road, Whippany, New Jersey, U.S.A.
105. Futrell, J.H. and Wojeik, L.H., Rev.Sci.Instrum., 42, 244 (1971).
106. Illes, A.J., Bowers, M.T., and Meisels, G.G., Anal Chem., 53, 1551 (1981).
107. Patterson, G.N., in Molecular Flow of Gases, Wiley, New York, 1956.
108. Texas Instruments, T1 Model 144, Bedford, England.
109. Eurotherm Ltd., Faraday Close, Durrington, Worthing, Sussex, U.K.
110. Private communication with Field, F.H.
111. Rosenstock, H.M., Draxl, K., Steiner, B.W., Herron, J.T., J.Phys.Chem.Ref.Data, 6, (1977) Suppl. 1.
112. Vogel, A.I., J.Chem.Soc., 1809 (1948).
113. Majer, J.R., in Advances in Fluorine Chemistry, Vol.2. Ed. Stacey, M.; Tatlow, J.C.; Sharpe, A.G.; Butterworths, London 1961. P55.
114. McLaughlin, A.G.; Morrison, J.D., Traeger, J.C., Org Mass Spectrom., 13 (8), 483 (1978).

115. Weinkam, R.J., Gal, J., Org.Mass Spectrom., 11 (2) 188 (1976).
116. Hancock, R.A., Walder, R. Unpublished results.
117. Field, F.H., and Meot-Ner, M., J.Amer.Chem.Soc., 100, 1356 (1978).
118. Huntress, W.T. Jr., Pinizzotto, R.F.Jr., J.Chem.Phys., 59, 4742 (1973).
119. Su., T. and Bowers, M.T., Int.J.Mass Spec.Ion Phys., 17, 211 (1975).
120. Meisels, G.G., Palley, G.W.Jr., Illies, A.J., Anal.Chem., 52, 1797 (1980).
121. Laudenslager, J.B.; Huntress, Jr., W.T.; Bowers, M.T., J.Chem.Phys., 61, 4600 (1974).
122. Hancock, R.A., Hodges, M.G., Int.J.Mass Spec.Ion Phys., 46, 329 (1983).
123. Sieck, L. Wayne., Anal.Chem., 55, 38 (1983).
124. Illies, A.J., Meisels, G.G., J.Phys.Chem., 86, 1286 (1982).
125. Meot-Ner, M.; Hamlet, P.; Hunter, E.P.; Field, F.H., J.Amer.Chem.Soc., 100, 5466 (1978).
126. Meot-Ner, M., and Field, F.H., Chem.Phys.Lett., 44, 484 (1976).
127. Henschman, M. in Ion-Molecule Reactions, Ed. Franklin, J.L., Plenum Press, New York, 1972, Ch.5. P196.
128. Ausloos, P., Eyler, J.R., Lias, S.G., Chem.Phys.Lett. 30, 21 (1975).

129. Hancock, R.A. and Hodges, M.G., Int.J.Mass Spec.Ion Phys., 46, 317 (1983).
130. Bowers, M.T.; and Elle-man, D.D.; Chem.Phys.Let . 16, 486 (1972).
131. Zeman, A., Fresenius Z.Anal.Chem., 310, 243 (1982).
132. Long, J. and Munson, B., J.Amer.Chem.Soc., 95, 2427 (1973).
133. Walder, R., and Franklin, J.L., Int.J.Mass Spec.Ion Phys., 36, 85-112 (1980). "Proton affinities of neutral molecules".
134. Luijten, W.C., M.M.; Onkenhout, W.; Van Thuijl, J.; Org.Mass Spec. 15, 329 (1980).
135. Keough, T., and Destafano, A.J. Org.Mass Spectrom., 16(12), 527 (1981).
136. Sieck, L.Wayne., Lias, S.G., J.Phys.Chem.Ref.Data, 5, 1123 (1976).
137. Sieck, L.Wayne., Burke, P., Jennings, K.R., Anal Chem. 51, 2232 (1979).
138. Schrank, L.R., Grigsby, R.D., Scheppele, S.E., Anal.Chem., 54, 748 (1982).
139. Heresch, F., Schmid, E.R., Weiszbart, A., Biomed Mass Spec., 6, 566 (1979).
140. Lippincott, E.R., Stutman, J.M., J.Phys.Chem., 68, 2926 (1964).
141. Landolt, H.H., Bornstein, R., Atom and Molekulorphysick, Vol.1, (1951), p.1511-13.
142. Denbigh, K.G., Trans.Faraday Soc., 36, 936 (1940).

